Secondary Metabolites from Endophytic fungi derived from Traditional Medicinal Herbs: Drug Discovery, Diversity Enhancement, Structure Elucidation and Bioactivity

Inaugural-Dissertation

zur Erlangung des Doktorgrades
der Mathematisch-Naturwissenschaftlichen Fakultät

der Heinrich-Heine-Universität Düsseldorf

vorgelegt von

Nam Michael Tran-Cong

aus Düsseldorf

Düsseldorf, Oktober 2019

aus dem Institut für Pharmazeutische Biologie und Biotechnologie

der Heinrich-Heine-Universität Düsseldorf

Gedruckt mit der Genehmigung der
Mathematisch-Naturwissenschaftlichen Fakultät der

Heinrich-Heine-Universität Düsseldorf

Berichterstatter:

1. Prof. Dr. Dres. h.c. Peter Proksch

2. Prof. Dr. Rainer Kalscheuer

Tag der mündlichen Prüfung:

18.12.2019

Table of Contents

Abstract

Fungal natural products are an important source for drugs and drug discovery. This dissertation describes investigations of bioactive secondary metabolites from endophytic fungi aiming to find new potential lead compounds acting as anti-cancer compounds or as antimicrobials. Endophytic fungi are organisms which live in plants as symbionts and mainly support their hosts by contributing to their defence against herbivores or against facultative or obligate pathogens.

Talaromyces sp. and *Trichocladium* sp., two of the endophytic fungi described in this dissertation, were isolated from a traditional Vietnamese herbal plant *Houttuynia cordata.* Additionally, the third studied endophytic fungus *Coniothyrium* sp.was isolated from the medicinal plant *Quercus robur*.

This dissertation is divided into 8 chapters corresponding to three publications/manuscript drafts which are ready for submission or presently under review.

1. Project Antiplatelet compounds from the endophytic fungus Talaromyces sp.

"Twelve natural products obtained from the endophytic fungus *Talaromyces* sp. were studied for their effects on the aggregation of human platelets. All compounds featured an ortho-hydroxylated benzoic acid moiety reminiscent of salicylic acid. Among the different metabolites the mycotoxin altenusin proved to be the most promising inhibitor of collagen induced thrombozyte aggregation with an IC50 value of 29.6 μM. In contrast to earlier reports by other groups, our in vitro assays indicated no inhibition of cyclooxygenases, but rather modulation of peroxisome proliferator-activated receptors (PPARs) as the most plausible target of altenusin. Comparison of altenusin with the known PPAR modulator magnolol and molecular docking studies indicated binding of altenusin to the magnolol binding pocket of PPARγ. These results complement earlier reports of altenusin binding to closely related farsenoid X receptors and showcase the importance of PPARs as relevant targets for inhibition of thrombozyte aggregation.", abstract taken from draft

2. Project Expanding the metabolic profile of the endophytic fungus Trichocladium sp.

"The endophytic fungus *Trichocladium* sp. isolated from roots of *Houttuynia cordata* was cultured on solid rice medium, yielding a new amidepsine derivative (**1**) and a new reduced spiro azaphilone derivative (**3**) together with eight known compounds (**4–11**). Co-cultivation of *Trichocladium* sp. with *Bacillus subtilis* resulted in induction of a further new compound (**2**) and a 10-fold increase of **11** compared to the axenic fungal culture. Moreover, when the fungus was cultivated on peas instead of rice, a new sesquiterpene derivative (**13**) and two known compounds (**12** and **14**) were obtained. Addition of 2% tryptophan to rice medium led to the isolation of a new bismacrolactone (**15**). The structures of the new compounds were elucidated by HRESIMS, 1D and 2D NMR as well as by comparison with the literature. A combination of TDDFT-ECD, TDDFT-SOR, DFT-VCD and DFT-

NMR calculations were applied to determine the absolute and relative configurations of **13** and **15**. Compounds **7**, **11** and **15** exhibited strong cytotoxicity against the L5178Y mouse lymphoma cell line with IC_{50} values of 0.3, 0.5 and 0.2 mM, respectively.", (Tran-Cong et al., 2019)

3. Project Furoic Acid Derivatives from the Endophytic Fungus Coniothyrium sp.

„The endophytic fungus *Coniothyrium* sp. was isolated from leaves of *Quercus robur*. Fermentation of this fungus on solid rice medium yielded two new furoic acid derivatives (**1** and **2**) and two additional known compounds. The structures of the new compounds were determined by extensive analysis of 1D and 2D NMR spectra as well as HRMS data. All isolated compounds were tested for their cytotoxicity but proved to be inactive." , (Tran-Cong et al., 2020)

Zusammenfassung

Naturstoffe aus Pilzen spielen eine große Rolle als Arzneistoffe und für die Entwickung von neuen Medikamenten. Diese vorliegende Disseration befasst sich mit Sekundärstoffen aus endophytischen Pilzen, um neue potenzielle Leitstrukturen gegen Tumore oder Mikroorganismen zu finden. Endophytische Pilze sind Organismen, welche in Pflanzen leben und ihre Wirte in der Abwehr von Fraßfeinden oder mikrobiellen Pathogenen unterstützen.

Zwei der untersuchten endophytischen Pilze, welche in dieser vorliegenden Dissertation behandelt werden, wurden aus der traditionellen vietnamesischen Heilpflanze *Houttuynia cordata* isoliert: *Talaromyces sp*. and *Trichocladium sp.* Ein anderer endophytischer Pilz wurde aus einer anderen traditionellen Heilpflanze isoliert: *Quercus robur*.

Diese vorliegende Dissertation wurden in Kapitel eingeteilt, welche drei vorbereitete bzw. bereits publizierte Manuskripte beinhaltet.

1. Thrombozytenaggregationshemmende Stoffe aus dem endophytischem Pilz *Talaromyces* sp.

Der endophytische Pilz *Talaromyces* sp. wurde aus den Wurzeln einer vietnamesischen Heilpflanze namens *Houttuynia cordata* isoliert. Zwölf Verbindungen wurden aus der Reisfermentation des Pilzes erhalten. Alle Verbindungen besitzen eine ortho-Hydroxybenzoesäure-Grundstruktur. Durch die strukturelle Ähnlichkeit der Verbindungen **1** – **12** mit dem bekannten Thrombozytenaggregationshemmer Salicylsäure wurde vermutet, dass die isolierten Verbindungen diese Aktivität ebenfalls besitzen. Unter den isolierten Verbindungen besaß Altenusin mit einem IC_{50} Wert von 51,6 µM gegen humane Thrombozyten die beste aggregationshemmende Wirkung. Im Gegensatz zu anderen Gruppen zeigten die durchgeführten *in vitro* Assays keine Hemmung des Enzyms Cyclooxygenase durch Altenusin, sondern wiesen auf eine Modulation der Peroxisomal Proliferierenden Rezeptoren (PPAR) hin, die zur Aggregationshemmung führt. Anschließende vergleichende Untersuchungen von Altenusin mit dem bekannten PPAR Modulator Magnolol und Docking Studien deuten darauf hin, dass Altenusin auch an PPARgamma bindet. Diese Ergebnisse ergänzen vorausgegangene Berichte, welche Altenusin als Farsenoid X Rezeptor Modulator beschrieben. Farsenoid X Rezeptoren und PPAR Rezeptoren sind eng miteinander verwandt, sodass auch PPARs ein bedeutsames Target für Thrombozytenaggregation sind.

2. Projekt Erweiterung des Metabolitenprofils des endophytischen Pilzes *Trichocladium* sp.

Der endophytische Pilz, *Trichocladium* sp., der aus den Wurzeln der Pflanze *Houttuynia cordata* isoliertwurde, wurde auf Reismediumkultiviert. Die chromatographische Aufarbeitung ergab ein neues Amidepsin Derivat (**1**) und ein neues reduziertes Azaphilon-Derivat **(3),** zusammen mit acht bekannten Verbindungen (**4-11**). Cocultivierung des Pilzes mit dem Bakterium *Bacillus subtilis* resultierte in der Isolation von einem weiteren neuen Naturstoff und in einer 10-fach erhöhten Ausbeute von Verbindung **11** Vergleich zu Kontrollkulturen. Darüber hinaus führten Kultivierungsversuche auf Erbsen anstatt auf Reis zur Isolation von einem neuen Sesquiterpen (**13**) und zwei bekannten Verbindungen. Nachdem 2% L-Tryptophan zum Reismedium hinzugegeben worden war, führte dies zur Isolation eines neuen Bismakrolaktons (**15**). Die Strukturen der neuen Naturstoffe wurden mittels HRESIMS, 1D und 2D NMR sowie mittels Vergleichen mit der Literatur bestimmt. Eine Kombination von TDDFT-ECD, TDDFT-SOR, DFT-VCD und DFT-NMR wurde angewendet, um sowohl die relative als auch die absolute Konfiguration von Verbindungen **13** und **15** zu bestimmen. Die Verbindungen **7**, **11** und **15** zeigten eine starke Zytotoxizität gegen L5178Y Maus Lymphom Zellen mit IC_{50} Werten von jeweils 0,3, 0,5 und 0,2 µM. (Tran-Cong et al., 2019)

3. Furanoylsäure – Derivate aus dem endophytischem Pilz *Coniothyrium* sp.

Der endophytische Pilz *Coniothyrium* sp. wurde aus den Blättern der Eiche *Quercus robur* isoliert. Reisfermentation des Pilzes führte zur Isolierung von zwei neuen Furanoylsäurenderivaten (**1** und **2**) und zwei bekannten Verbindungen. Die Strukturen der neuen Verbindungen wurden mittels 1D und 2D NMR als auch mit HRESIMS bestimmt. Alle isolierten Verbindungen wurden auf deren Zytotoxizität getestet, zeigten aber keine Aktivität.

1. Introduction

Natural products and their derivatives have been used for medicinal purposes for millennia. Several examples can be dated back to the beginning of history. (Patridge et al., 2016) Morphine, a widely used analgesic drug, has been used for a long period of time and is still in use today. Its clay tablet dated back to the Sumerian time can be seen as one of the world's oldest records of medicinal prescriptions. (Norn et al., 2005) In particular, the ancient Greek Minoan as well as the Egyptian culture used poppy as a pain reliever. Furthermore, it has been reported that the oils of *Cedrus* (cedar), *Cupressus sempervirens*, *Glycyrrhiza glabra*, *Commiphora* species as well as *Papaver somniferum* were used since ancient times and can be dated back to 2,600 BC. (Cragg, Newman, 2001) Natural products and their derivatives have thus played an important role in drug discovery and have often acted as lead structures. (Harvey, 2008, Katz, Baltz, 2016, Pascolutti, Quinn, 2014)

Until the end of 2013, the FDA has approved a total of 547 natural products and natural product derived compounds. (Butler et al., 2014) One third of them are non-mammalian natural products and biochemical natural products. Around 9.8% of the FDA approved new molecular entities (NME) are natural products that have not been structurally modified such as taxol. (Butler et al., 2014) These unmodified natural products offer a platform for further modifications. However, due to their toxicity or adverse effects they are often replaced by derivatives which are safer to use (Patridge et al., 2016) showing the importance of natural products as lead structures in drug discovery. Natural products used directly as active pharmaceutical ingredients (API) or as precursors for partial synthesis can be isolated from plants, bacteria or fungi and from animals such as cone snails (Olivera et al., 1985) or e.g. venomous lizards *Heloderma suspectum*, known as the "Gila monster". (Hoshino et al., 1984) However, total synthesis of natural products is also possible reducing exploitation from nature such as for ziconotide, a peptide derived from the toxin of the cone snail *Conus magus (Olivera et al., 1985, Venoms to Drugs: Venom as a Source for the Development of Human Therapeutics, 2015)* which is produced via a stepwise linear solid-phase-process synthesis strategy on a kg scale with a yield of approximately 20 %. Ziconotide is used to treat chronical pain. (Venoms to Drugs: Venom as a Source for the Development of Human Therapeutics, 2015)

Natural products are classified into two main groups. Compounds which are present in all cells and are needed for survival, metabolism and reproduction, are known as primary metabolites. High molecular weight polymers such as cellulose, lignins or proteins are considered to be primary metabolites (J.R. Hanson, 2003) . However, secondary metabolites are not directly involved in crucial metabolic processes but are usually characteristic for certain species. They often have an impact on other species e.g. for attraction of insects, chemical defence etc. (Stone, Williams, 1992, Traxler, Kolter, 2015). Because of their limited distribution among certain species, secondary metabolites can be used for the chemotaxonomic determination of a species, genus or family. (J.R. Hanson, 2003).

Chemotaxonomy uses results from a chemical analysis of one or more compounds from an organism. (M.T. Madigan, T. D. Brock, 2013) . In particular, it allows the chemical profiling of fungal species such as *Alternaria, Aspergillus* etc. (Frisvad et al., 2008). It can also be combined with plant taxonomy to classify higher plants (Hegnauer, 1986). Secondary metabolites can be categorized according to their biosynthesis as polyketides, fatty acids, terpenoids, steroids, phenylpropanoids, alkaloids, specialized amino acids, peptides and specialized carbohydrates. (J.R. Hanson, 2003)

1.1. Polyketides

The biosynthetic pathway of polyketides is based on acetyl-CoA. Acetyl-CoA is derived for example from glycolysis and is mainly used in the citric acid cycle for energy production in form of reducing equivalents. (Akram, 2014) Polyketide biosynthesis is conducted stepwise by a multifunctional enzyme complex which is called polyketide synthases. (Hopwood, 1997) By condensation of an acetyl-CoA (C2-Unit) and malonyl-CoA unit (C3-Unit), one carboxyl function is lost and a beta-keto functional group is formed simultaneously. The term polyketide was defined by Collie. (Collie, 1907) (Hertweck, 2009) In general, polyketides can be roughly divided into two sub structural groups: complex and aromatic polyketides. (Hertweck, 2009) Erythromycin, a well-established antibiotic synthesized by *Saccharopolyspora eryhtraea* (Oliynyk et al., 2007), is an example for a natural polyketide which has been used for more than five decades. (Bunch, Mcguire, 1953)

1.2. Fatty acids

The biosynthesis of fatty acids is closely related to the biosynthesis of polyketides (Hertweck, 2009) . Fatty acids consist of a carboxylic acid and an aliphatic carbon chain. The aliphatic carbon chain can be unsaturated or saturated. (Tvrzicka et al., 2011)

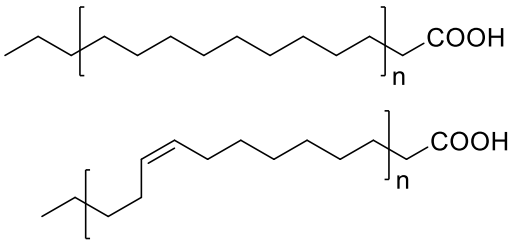

Figure 1 examples for an unsaturated and a saturated fatty acid

The immunomodulating drug fingolimod (Gilenya®) used for multiple sclerosis therapy (Kappos et al., 2010) is a derivative of myriocin, a natural serine palmitoyltransferase inhibitor, which belongs to the subclass sphingolipids. (Harrison et al., 2018) Biosynthesis of sphingolipids is proposed to be derived from fatty acids such as palmitoyl-CoA. (Harrison et al., 2018)

1.3. Terpenoids

Fungal terpenoids are derived from isopentenyldiphosphate (IPP) and dimethylallyl diphosphate (DMAPP) (Schmidt-Dannert, 2015) both containing five carbon atoms respectively. The precursor for isopentenyldiphosphate (IPP) and dimethylallyl diphosphate (DMAPP) is often acetyl-CoA, which itself is derived from glycolysis or by fatty acid degradation. Plant derived terpenoids can also be derived from two pathways: Cytosolic mevalonic pathway or methylerythritol phosphate in plastids. (Tholl, 2015)

Terpenoids contain numbers of carbon atoms that can be divided by five as IPP and/or DMAPP react with each other or themselves in a so called head to tail reaction or tail to tail reaction. (Oldfield, Lin, 2012) Depending on the number of carbon atoms terpenoids are divided into monoterpenes (C10), sesquiterpenes (C15), diterpenes (C20), sesterterpenes (C25), triterpenes (C30) etc. Many terpenoids are biologically active and therefore pharmacologically interesting. (Wang et al., 2005) For example, the essential oil of thyme leaves, whose main composition is of terpenes, is used to treat productive cough or in general respiratory tract infections

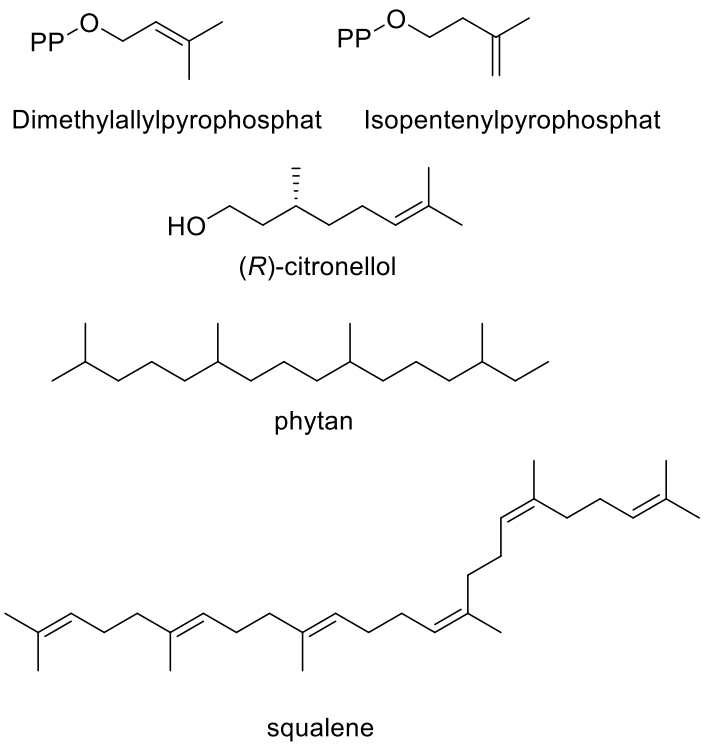

Figure 2 Different terpenoids are shown. Dimethylallylpyrophosphat and isopentenylpyrophosphat are core units of terpenoid biosynthesis. Citronellol is a monoterpene, phytan a diterpene and squalene is a triterpene. Components from essential oils are mostly terpenes such as the thyme's essential oil. Essential oils from thyme leaves are used to treat productive cough or in general respiratory tract infections.

1.4. Alkaloids

Alkaloids are a heterogeneous group that can be divided into various subclasses. About 12,000 different alkaloids are known from plants. (Ziegler, Facchini, 2008) They are derived from amino acids and can be classified into subclasses depending on the type of the amino acid. In general, alkaloids include a nitrogen containing heterocycle and in most cases a basic nitrogen atom. There are exceptions to this as the nitrogen atom can be exocyclic as in e.g. ephedrine and paclitaxel. One of the most prominent alkaloids is morphine obtained from *Papaver somniferum* or opium poppy. (Norn et al., 2005)

1.5. Steroids

Steroids are derived from the mevalonic terpene pathway starting from six connected isoprene units forming the C30-unit squalene. (Dempsey, 1974) The type of steroid produced by a certain organism is often specific e.g. plant cells synthesize the so called phyto-sterols, fungal cells synthesize ergosterol and animals synthetize cholesterol. These primary metabolites increase the fluidity of cell membranes and walls. (Abe, Hiraki, 2009, Jain, 1975).

1.6. Amino acids/Peptides

Amino acids contain at least one basic amino function and one carboxylic moiety belonging to primary metabolism as well as serving as precursors for secondary metabolites. Some amino acids play a major role such as neurotransmitters, semiochemicals or building blocks for proteins needed for primary metabolism or hormones such as insulin. Peptides, as secondary metabolites, often serve for instance as defence or for hunting such as mentioned before for the cone snail toxins. Vancomycin, produced by *Amycolatopsis orientalis* (Zmijewski, Milton J., Jr., Briggs, 1989), is a glycopeptide that is used against problematic microbial infections.

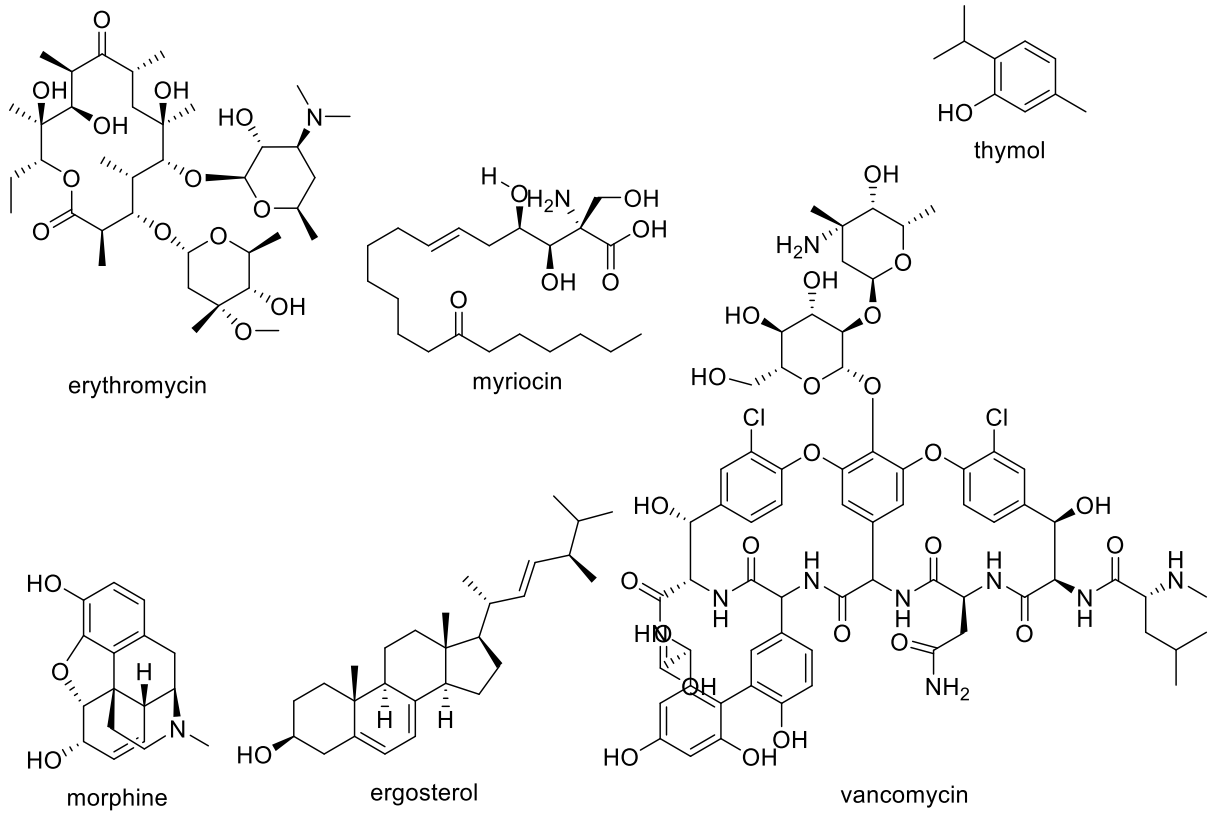

Figure 3 Natural products mentioned in the categories above as examples for different compound classes

2. Natural products from plants and fungi; sources for new molecular entities

Nearly 22% of the new molecular entities are derived from fungi (Patridge et al., 2016) which are thus an interesting resource for drugs discovery.

In 1929, the first beta lactam antibiotic penicillin was discovered by Alexander Fleming (Fleming, 1929) He was awarded the Nobel prize in medicine along with Florey and Chain in 1945. (Bennett, Chung, 2001) From then on, fungal secondary metabolites began to attract the attention of scientists for natural products discovery. Penicillin had become “the paradigm for natural products drugs discovery”. (Bennett, Chung, 2001) Its structure as penicillamine hydrochloride was fully elucidated via X-Ray analysis in 1942 (Glusker, 1994) but only published later by Crowfoot et al. in 1949. (Crowfoot et al., 2015) Penicillin’s ring system is formed by a L – cysteine and L-valine unit by the enzyme iso – Penicillin-N synthase (IPNS). (Baldwin, Abraham, 1988) This enzyme needs Fe^{3+}, ascorbate and molecular oxygen as co-substrates. (Baldwin, Abraham, 1988) Furthermore, it was shown that culturing conditions such as airflow, stirring speed, pH, temperature etc. have an impact on the overall yield of penicillin. (Vardar, Lilly, 1982) Various derivatives have been developed from penicillin starting from penicillin V, the first orally acid stable penicillin. (Ernst, Hans, 1956) Methicillin was the first penicillinase stable penicillin. (Walker, SR, Walker, 2012) Ampicillin, a broad-spectrum antibiotic, was approved in 1962. (Acred et al., 1962) It is worth to mention that penicillin G is the parent substance

for other penicillins. The history of penicillin antibiotics is a significant example of a well-established use of a fungal metabolite in medicine as well as of a lead compound used for further modifications such as amoxicillin.

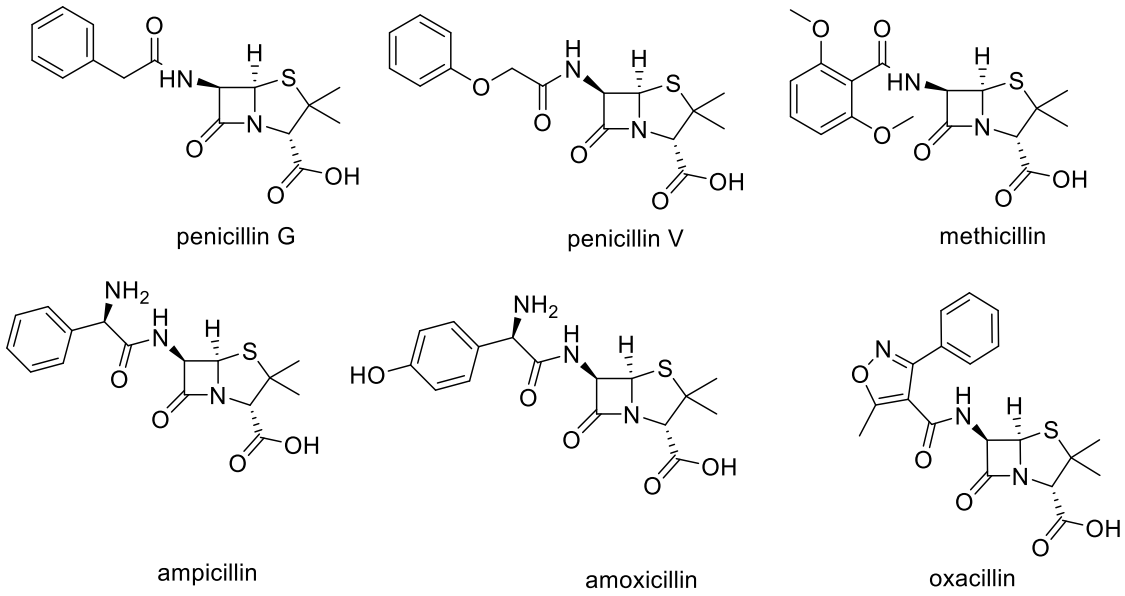

Figure 4 Penicillin and its derivatives.

2.1. Sources of fungi

Fungi can be found everywhere. (Christensen, 1989) Because of their presence in different ecosystems, fungi have developed different strategies to survive in e.g. soil, sea water, lichens, plants, animals or under extreme conditions like black smokers or in the deep sea. The different climatic zones have direct and indirect effects on plants as well as on fungal diversity. (Tedersoo et al., 2014) Due to their diversity, fungi offer a great opportunity to discover unknown bioactive natural products which can serve as lead structures For example, natural products such as penicillin G which is used against syphilis (Sukthankar, 2014) and griseofulvin used against nail infections (Roberts, 1994), can be used directly without any modificarions. Furthermore, a high fungal diversity including unculturable strains can be found in tropical and subtropical areas. The total number of fungi is estimated to be approximately 5.1 million species. (Blackwell, 2011) This number offers great opportunities for drug discovery.

Extreme living conditions such as mangroves with their fluctuating salt concentrations, arid regions and deep sea due the high water pressure or nutrition poor soils can offer interesting fungi. These fungi have got a high impact on the biological diversity of a given habitat and in case of endophytes on the ability of their hosts to increase fitness and stress tolerance. (Rodriguez et al., 2009)

The endophytic fungus *Penicillium brocae*, isolated from fresh tissue of the marine mangrove plant *Avicennia marina* in Hainan, China, yielded six new cytotoxic bisthiodiketopiperazine derivatives namely brocazines A-F. Fermentation of this fungus was conducted on PDA medium at 28°C for 4 days.

Brocazine A and B exhibited cytotoxicity against SW480 tumor cell lines with an IC_{50} of 2.0 and 1.2 µM, respectively. Brocazine F exhibited strong cytotoxicity against DU145 and NCI-H460 cells with IC_{50} values of 1.7 and 0.89 µM, respectively. (Meng et al., 2014)

When the same fungus was cultivated on Czapek medium, the extracts yielded four new diketopiperazine alkaloids namely spirobrocazine A-C and brocazine G. Brocazine G exhibited potent activity against A2780 and also against A2780 cisplatin resistant tumor cell lines with IC_{50} values of 664 and 661 nM, respectively. (Meng et al., 2016) suggesting that changing media is a good approach to enhance diversity of compounds. This topic is further described in the OSMAC section.

Deep see derived fungi or marine derived fungi are also great sources for bioactive natural products. Halimide, an aromatic alkaloid, was first isolated following fermentation of the marine fungus *Aspergillus* sp. CNC139 collected from waters off the Philippine Islands. (William Fenical,Paul R. Jensen,Xing C. Cheng. Halimide, a cytotoxic marine natural product, and derivatives thereof. US6069146A) Its mechanism of action relies on the inhibition of the polymerization of tubulin by binding to a region between α and β tubulin. This region is located next to the colchicine binding site. Further studies on plinabulin, a synthetic analogue of halimide, revealed that it is able to disrupt tumor vascularization leading to the idea of combination of chemotherapeutics e.g. with docetaxel against non-small cell lung cancer.

From a deep ocean sediment sample collected at a depth 5,080 m, the marine fungus *Penicillium* sp. was isolated. Sea-water-based-culture PDB media were used for its fermentation. This led to the isolation of four new alkaloids two of which exhibited a diketopiperazine moiety. The other two were meleagrin analogs. However, the new compounds were inactive against HL-60 cell lines compared to the known compound meleagrin. Meleagrin exhibited IC_{50} values of 6.7 and 2.7 µM against HL-60 and A-549, respectively. (Du et al., 2010)

Traditional medicinal herbs can also be an interesting source for obtaining new interesting fungal endophytes from which many bioactive compounds can be isolated. Well established medicinal herbs such as *Quercus robur* and *Ranuculus sceleratius* are promising sources to obtain undescribed endophytic fungi and/or fungi which are producing interesting natural products. In particular, undescribed endophytic fungi are interesting because their extracts provide a higher probability to isolate new natural products.

Kowalski et al. isolated from the same species of *Quercus* an undescribed fungus *Cryptosporiopsis radicicola* sp. .(Kowalski, Bartnik, 1995) Also oak pathogenic fungi are interesting to isolate and determine. From an infected cork oak, *Quercus suber*, the plant pathogenic fungus *Diplodia mutila* was isolated. Work up of its liquid culture led to the isolation of diplopyrone, a new phytotoxic tetrahydropyranpyran-2-one. (Evidente et al., 2003) The cultivation of the undescribed coprophilous

fungus *Niesslia* sp. , isolated from horse dung in Texas, USA., with SMYA – media afforded two new antifungal wortmannin derivatives, namely wortmannin C and D. (Dischler et al., 2019)

The previously mentioned examples demonstrated that well-known medicinal plants can also provide undescribed endophytic fungi yielding new natural product candidates for drug discovery.

2.2. Silent Gene Clusters

In fungi and bacteria not all gene clusters are always active. During cultivation under laboratory conditions, only some genes that encode for secondary metabolites are active. After sequencing fungal genomes, it became clear that a high percentage of secondary metabolite gene clusters are kept silent. The fungal metabolism reacts to different environmental conditions. (Grimaldi et al., 2006) In order to activate silent gene clusters, several strategies have been developed such as OSMAC, co-cultivation, epigenetic and genetic modification. Similar fungal genes are grouped like other eukaryotic genes in gene clusters. (Nierman et al., 2005)

2.3. OSMAC

The term OSMAC is an acronym for "**O**ne **S**train **Ma**ny **C**ompounds". This term was first introduced by Fuchser and Zeeck in 1997. (Fuchser, ZEECK, 1997) As in the case of Zeeck *et al*. such changes can include altering the media type, the physical properties such as static or stirring conditions, or the atmosphere such as overpressure. (Daletos, G., Ebrahim, W., Ancheeva, E., El-Neketi, M., Lin, WH., Proksch, P., 2017) It emphasizes how a single strain can produce different compounds when cultivated under different fermentation conditions. Changes in fermentation conditions include different parameters such as temperature, media type, media composition and aeration. By altering the culturing conditions of the fungus *Aspergillus ochraceus,* three new 10-membered lactones were isolated that had not been detectable in control cultures. Therefore, Fuchser and Zeeck summarized their approach as an "alternative method to enhance metabolite diversity" (…) and termed it as "one strain many compounds". (Fuchser, ZEECK, 1997) Moreover, the OSMAC approach was applied with *Streptomyces sp.* and also proved to be successful in finding new natural products. (SCHIEWE, ZEECK, 1999) UV – radiation can also be used as a modification of cultivation as Bode et al. have demonstrated. (Bode et al., 2000) Additionally, Vardar et al. have experienced similar findings by changing culturing conditions in penicillin production by fungi. (Vardar, Lilly, 1982) These consecutive approaches demonstrated that small changes in cultivation parameters result in diversification or enhancement of secondary metabolites production.

Cultivation of the endophytic fungus *Fusarium tricinctum* on solid rice medium that had been supplemented with fruit and vegetable juices led to the discovery of a new natural product, fusarielin J, which was not detectable when the fungus was grown on rice medium without juices. In addition, two known compounds namely fusarielin A and B were isolated. Fusarielin J exhibited cytotoxicity against human ovarian cancer A2780 cells with an IC_{50} value of 12.5 µM. (Hemphill et al., 2017) Moreover, small changes such as using distilled water instead of tap water for the preparation of PDB medium (potato dextrose broth) in cultivating the fungus *Paraphaeosphaeria quadriseptata* resulted in the isolation of six new secondary metabolites. (Paranagama et al., 2007)

2.4. Co-cultivation

Under normal lab conditions microorganisms are cultivated axenically. This often results in silencing of biogenetic gene clusters. (Burstein et al., 1965) Co-cultivation can be applied to simulate interactions (quorum sensing, siderophores, etc.) between microorganisms which also happen in nature. (Bertrand et al., 2014, Marmann et al., 2014, Netzker et al., 2015) This may lead on one hand to an increase or decrease of secondary metabolites or enhance the production of new natural products which are not detectable under axenic laboratory conditions. Thus, co-cultivation mimics microbial competition which takes place under natural conditions.

2.5. Epigenetic modification

Epigenetic modification is an approach to trigger silent gene clusters without manipulating the DNA in order to induce secondary metabolites production.

Generally, the targets for an epigenetic modification approach are commonly histone deacetylases, or DNA methyl transferases. Therefore, inhibitors are used and grouped into two classes: Histone deacetylase inhibitors (HDAC) like trichostatin A (TSA) and suberoylanilide hydroxamic acid (SAHA) and DNA methyl transferase inhibitors like 5 – azacytidine (5-AC) as well as aza-2'-deoxcytidine (decitabine). (Williams et al., 2008)

Cultivation of the endophytic fungus *Chaetomium* sp. with the epigenetic modifiers suberoylanilide hydroxamic acid and 5-azacytidine led to an upregulation of two benzophenone derivatives. One of the benzophenone derivatives namely SB238569 exhibited strong cytotoxicity against the mouse lymphoma cell line L5178Y with an IC_{50} value of 1 µM. (Akone et al., 2016)

3. Drug Discovery Process

Whenever compounds are promising as future drug candidates, they are submitted to pre-clinical studies followed by clinical studies with patients. On the one hand academia can proceed with drug development at least with regard to the preclinical phase, on the other hand drug development especially during clinical evaluation is an expensive and time costing project (Adams, van Brantner, 2006) which can last more than 10 years and will cost more than 500 Million Euro. (Abrantes-Metz et al., 2004) (DiMasi et al., 2003) The next section gives an example on the topic of drug development.

Drug development is divided into four phases including the preclinical development. Drug discovery is the step, which is located before the preclinical phase. There is also no guarantee that an active compound is not abandoned due to unexpected adverse effects. Overall analysis revealed that the success rate of new molecular entities was 6.2% demonstrating also that 93.8% of studies failed (Mullard, 2016). On the one hand the responsible pharmaceutical company, which is developing the drug, can stop clinical studies, or the medical agency monitoring clinical trials can order to stop further development. In Germany, the Arzneimittelgesetz (Drug Law) was reformed after the Contergan® crisis in 1961 and 1978. (Wille, Schönhöfer, 2002) In the past, it had been necessary to confirm only quality and harmlessness. (Wille, Schönhöfer, 2002) Furthermore, there was no need for proving efficacy. For this reason, during the discovery of the adverse effects caused by of Contergan® on development of embryos, a demand for proving efficacy was introduced, too.

Drug Discovery phase includes the discovery, target finding including molecular modelling such as docking and scoring functions with virtual screening approach (Kitchen et al., 2004), as well as modifications for obtaining better physical – chemical properties. The importance of molecular modelling to predict and explore targets and binding solutions has increased. It allows for a better understanding of molecular properties and enables derivatization in order to enhance efficacy. (Tollenaere, 1996) This is known as lead structure optimization. *In-silico* virtual screening with appropriate efficient computer systems permits the screening of huge numbers of compounds, sorting them by chemical properties in order to reduce the numbers for *in-vitro* screening assays. Choosing the right docking model is crucial for the success and the accuracy of the approach. (Cross et al., 2009, Shoichet, 2004) Virtual screening combined with docking experiments can also lead to negative results. After bio- and toxicity assays as well as animal testing were conducted with no sign of severe necrosis in cell studies, phase I of clinical trials begins. Phase I includes a small number of healthy volunteers with the aim to investigate safety and kinetics in the human body. (Reilly et al., 2013) Phase II of clinical trials starts after Phase I but now patients, who carry the disease under investigation, are chosen to be tested. The aim is to check for efficacy and expand the knowledge about safety of the drug. (Simon, 1989) Phase III of clinical trials is used to confirm the results of Phase II; the difference being that Phase III includes far more patients than phase II. (Opal et al., 1997) After approval by the responsible agencies (FDA, EMA, etc.) phase IV starts after the market launch with the goal of continuing to observe safety

related issues such as to identify side effects which have not been found in the preceding clinical studies, on the other hand to identify possible new indications for the drug. (Suvarna, 2010)

At present plinabulin, an anticancer agent of fungal origin which goes back to the lead structure halimide, has reached clinical phase III. Eight studies are listed on *clinicaltrials.gov* of which one was terminated, two were completed, two are still ongoing but recruiting subjects has been finished and three are still recruiting (status from 4:36 pm, 2019/04/30). One study with the code: "DUBLIN-3" (NCT02504489) is labeled as Phase III with the indication small cell lung cancer.

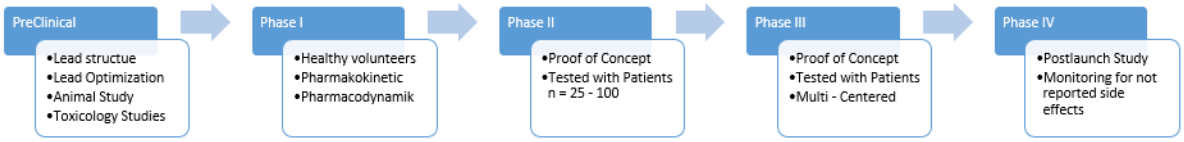

Figure 5 Simplified scheme of a typical clinical trial

4. Aim of this study/thesis

As mentioned above, fungi are promising sources to obtain novel and bioactive natural products. The aim of this study is to investigate bioactive secondary metabolites from promising endophytic fungi as potential lead structures against pathogenic microorganisms or cancer. Hitherto undescribed or less investigated endophytic fungi are also interesting due their potential of containing new secondary metabolites. The fungi are selected due to screening results of an in-house spectral library containing secondary metabolites based on UV and LC-MSspectra. In order to expand the metabolic pattern of these fungi in the search for new natural products, different cultivation methods such as the One Strain Many Compounds (OSMAC) approach by changing media or by applying different soil derived bacteria such as *Streptomyces lividans* and *Bacillus subtilis* for co-cultivation are used. In particular, fungal metabolites are isolated, structurally elucidated and analyzed for their biological activities. New compounds are evaluated regarding their antibiotic and cytotoxic activity.

Two endophytic fungal strains, *Talaromyce*s sp. and *Trichocladium* sp., isolated from a traditional Vietnamese medicinal plant *Houttuynia cordata* (*Sauraceae*) and an undescribed *Coniothyrium* sp., obtained from the leaves of the medicinal plant *Quercus robur* were chosen for this dissertation.

5. Publication 1 - The mycotoxin altenusin is a platelet aggregation inhibitor

Ready to submit

The Mycotoxin Altenusin is a Platelet Aggregation Inhibitor

Nam Michael Tran-Cong,[a] Thomas Hohlfeld,[b]* Michele Bonus,[c] Marian Frank,[a] Holger Gohlke,[c,d]* Zhen Liu,[a] and Peter Proksch[a]*

[a]*Institute for Pharmaceutical Biology and Biotechnology, Heinrich-Heine-University Düsseldorf, Düsseldorf, Germany;* [b]*Institute of Pharmacology and Clinical Pharmacology, University Hospital, Düsseldorf, Germany;* [c]*Institute for Pharmaceutical Chemistry and Medical Chemistry, Heinrich-Heine-University Düsseldorf, Düsseldorf, Germany;* [d] *John von Neumann Institute for Computing (NIC), Jülich Supercomputing Centre (JSC) & Institute for Complex Systems - Structural Biochemistry (ICS 6), Forschungszentrum Jülich GmbH, Wilhelm-Johnen-Straße, 52425 Jülich, Germany*

Correspondence details: Thomas Hohlfeld, Institute for Pharmacology and Clinical Pharmacology, University Hospital, Heinrich-Heine-University Düsseldorf, Moorenstr. 5, 40225, Düsseldorf. Email: hohlfeld@uni-duesseldorf.de ; Holger Gohlke, Institute for Pharmaceutical and Mecinal Chemistry, Universitätstraße 1, 40225, Düsseldorf. Email: gohlke@hhu.de ; Peter Proksch, Institute for Pharmaceutical Biology and Biotechnology, Heinrich-Heine-University Düsseldorf, Universitätsstraße 1, 40225, Düsseldorf. Email: proksch@hhu.de

The Mycotoxin Altenusin is a Platelet Aggregation Inhibitor

Twelve natural products obtained from the endophytic fungus *Talaromyces* sp. were studied for their effects on the aggregation of human platelets. All compounds featured an ortho-hydroxylated benzoic acid moiety reminiscent of salicylic acid. Among the different metabolites the mycotoxin altenusin proved to be the most promising inhibitor of collagen induced platelet aggregation with an IC_{50} value of 23.31 µM. In contrast to earlier reports by other groups, our *in vitro* assays indicated no inhibition of cyclooxygenases, but rather modulation of peroxisome proliferator-activated receptors (PPARs) as the most plausible target of altenusin. Comparison of altenusin with the known PPAR modulator magnolol and molecular docking studies indicated binding of altenusin to the magnolol binding pocket of PPARγ. These results complement earlier reports of altenusin binding to closely related farsenoid X receptors and showcase the importance of PPARs as relevant targets for inhibition of platelet aggregation.

Keywords: endophytic fungus; Talaromyces sp.; antiplatelet; PPAR.

Introduction

Fungi of the genus *Talaromyces* (*Trichocomaceae)* occur as molds e.g. on food products [1, 2], as human pathogens (especially *Talaromyces marneffei* which causes infections in patients with HIV [3-5]), as air borne fungi[6] or as endophytes in various host plants.[7-10] In this study we isolated several natural products (NPs) (**1** – **12**) from the endophytic fungus *Talaromyces* sp. obtained from the traditional South East Asian medicinal plant *Huoutuniya cordata.* All compounds (**1** – **12**) feature an ortho-hydroxyl-benzoic acid moiety similar to the known antiplatelet agent salicylic acid, which prompted us to investigate these natural products with regard to inhibition of platelet aggregation. Using light transmission aggregometry, we demonstrated that three of the isolated compounds **(5, 7** and **9)** exhibited platelet inhibition albeit not by inhibiting COX enzymes as reported earlier[2]. Altenusin (**9**) proved to be the best inhibitor among the analyzed compounds. Its average IC_{50} value was 23.31 µM which is comparable to ibuprofen[11] and indometacin, two analgesic drugs known for their inhibition of platelet aggregation.[12] Altenusin (**9**) had already previously shown interesting pharmacological properties. Several studies reported this compound as a myosin light chain kinase inhibitor[13] as well as an inhibitor of other protein kinases.[14] Furthermore, altenusin was shown to be an activator of farsenoid X receptors (FXRs)[15] which belong to a class of nuclear receptors (NRs), which can also exhibit non-genomic effects.[16, 17] These NRs were recently discovered in platelets, where they display a promising target for inhibiting platelet aggregation.[18, 19] In this study we provide evidence for the peroxisome proliferator-activated receptor (PPARγ) as the most likely target of altenusin (**9**). Peroxisome proliferator-activated receptors (PPARs) are another group of NR that are present in platelets[20] and likewise play an important role for the function of platelets through non-genomic effects. Our results on the mode of action of altenusin (**9**) with

regard to platelet inhibition showcase the importance of fungal secondary metabolites as sources for future drug design.

[Figure 1 near here]

[Figure 2 near here]

Materials and Methods

Plant Material

Houttuynia cordata was raised from commercially available (Dehner, Germany) seeds and was grown in a local garden at Willich (Germany). The identity of the plants used in this study was confirmed by M.S. Appelhans, curator of the herbarium of Goettingen University (GOET). A voucher specimen of *Houttuynia cordata* (HC-HHU) has been deposited at the Goettingen University Herbarium (GOET)."

Materials

Following used reagents with corresponding seller are listed:

Acectylsalicylic acid (ASS), Bayer, Leverkusen; Adenosine diphosphate (ADP), Sigma-Aldrich; Agar, Sigma Aldrich; Arachidonic acid (AA), Natutech, Frankfurt; Chloramphenicol, Sigma Aldrich; Cicaprost, Bayer, Bergkamen; Collagen (Typ I), Horm, Nycomed, Munich; DMSO, Sigma Aldrich; EDTA (Titriplex III®), Merck Darmstadt; Ethanol, Sigma Aldrich; Ibuprofen, Sigma-Aldrich; Indometacin, Luitpold Pharma; Maltextract, Sigma Aldrich; Magnolol, Sigma Aldrich; Methanol, Sigma Aldrich; n-Hexane, Sigma Aldrich; NaOH, Merck Darmstadt; Prostaglandin E1; Sigma-Aldrich; Silica gel, Merck Darmstadt; Sodiumcitrate, Merck Darmstadt; Thiobarbituric acid (TBA), Sigma Aldrich, Thrombin, Nobis, D- Endingen;

Isolation and Identification of Fungal Strain

Sterilized demineralized water was used two times to wash fresh roots of *H. cordata* in order to remove remaining soil. The roots were then surface sterilized with 70% ethanol for 1 min, and cut into small pieces (around 1 cm × 1 cm × 1 cm) using a flame sterilized blade. These pieces were put on malt agar plates (15 g/L malt extract, 15 g/L agar, and

0.2 g/L chloramphenicol in demineralized water, pH 7.4–7.8 adjusted with sodium hydroxide and hydrochloric acid solution 1 M), and then incubated at room temperature for several days. The fungus was transferred to fresh agar plates using the streaking and dilution method until a pure fungal strain was obtained. The purified fungus was later transferred to solid rice medium for fermentation. The identification of the fungus was performed by polymerase chain reaction amplification and Sanger sequencing of the 5.8S ribosomal RNA gene including the internal transcribed spacer region and subsequent basic local alignment search tool search according to the previously described protocol.[21] Sequence data were submitted to GenBank under accession number MN577410. A deep-frozen sample of the fungal strain (No.HCR-3) is kept in the Institute of Pharmaceutical Biology and Biotechnology, Heinrich-Heine University, Düsseldorf, Germany.

Cultivation

Fermentation of the fungus was conducted in 1L Erlenmeyer flasks on solid rice medium (autoclaved 100 g rice (*Oryza* Milchreis) and 110 ml demineralized water) at 20°C under static condition. After 21 days, flasks were soaked overnight in 600 ml ethyl acetate each. The rice was cut into small pieces and shaken for 8 hours at 150rpm. The ethyl acetate extract was filtered through a paper filter and evaporated to dryness at low pressure to yield the crude extract

Isolation and Identification of Compounds 1 – 12

The crude fungal extract (3.32 g) was firstly separated by liquid/liquid separation to yield three main fractions: *n*-hexane fraction (1.2 g), methanol fraction (1.58 g) and water fraction (0.38 g). The methanol fraction was next subjected to a vacuum liquid chromatography (VLC) column using a step gradient of *n*-hexane/ethyl acetate and then

methanol to yield six VLC fractions. All fractions were further separated via a Sephadex LH20 column with methanol as mobile phase. Some subfractions were further purified by semipreparative high-performance liquid chromatography (HPLC) with methanol/water (0.01% formic acid) as mobile phase. The structures of the compounds were elucidated with 1D-NMR, 2D-NMR, mass spectroscopy and comparison with the literature.

Blood Samples

Blood samples were collected from 6 different donors, who gave their written informed consent prior to donating blood. All donors were healthy and did not take nonsteroidal anti-inflammatory drugs (NSAIDs) during the last two weeks. The study was conducted under the guidelines of Helsinki Declaration for Human Research with approval from the institutional ethical review board (local study number 6103R). Fresh blood samples were collected in vacutainers containing 0.14M sodium citrate and centrifuged with 1000 rotations per minutes with a centrifuge for 10 mins. Platelet-rich plasma (PRP) was extracted without taking any erythrocytes and transferred into 10 ml tubes. Thereof 1 ml PRP was taken and centrifuged at room temperature with 14000 rotations per minutes.

Platelet Aggregation

Aggregation of platelets was induced by one of the following stimuli: thrombin, ADP (adenosine diphosphate) , AA (arachidonic acid) or collagen. Measurements were performed by turbidimetry on a Labor APACT, Labor Biomedical Technologies, Ahrensburg, Germany according, to the method of Born.[22-24]

50 µl of sample or 50 µl ASS (500 µM or 150 µM, control) or 30µM (50µl) ibuprofen, DMSO as control (50µl) was added to 200 µl PRP and incubated for 4 min in

a heating block adjusted at 37°C. The combined sample was stirred for 2 min and aggregation was induced by adding collagen, AA, ADP. Aggregation was stopped 4 min later by adding 4µl 50µM indometacin and 15µl (77mM) EDTA, stirred for additional 30 seconds and transferred into Eppendorf cups. The samples were centrifuged for 12000 R/min for 10 mins. The retrieved supernatants were frozen at -20°C for determination of TXA_2 by an indirect assay of malondialdehyde (MDA). Due to the usage of dimethyl sulfoxide (DMSO) as a solvent, DMSO was used together with the stimulus as a control.

MDA with Arachidonic Acid stimulated Platelets

150µl supernatant centrifuged for 15000 RPM from platelet aggregation were added to 150µl thiobarbituric acid (TBA) and incubated for 30 mins at 70°C. After 10 min incubation at room temperature, 80µl of each prepared sample was transferred into a 96 well plate and the fluorescence measured at 555 nm.

Moreover, a commercially available enzyme-linked immunosorbent assay (ELISA) kit (No.50120, Cayman Chemicals, AnnArbor, MI, USA) was used for determination of TXB_2 levels. Known TX concentrations were used for validation by adding defined TX concentrations in blood plasma. Platelet thromboxane synthesis was indirectly measured by malondialdehyde formation, conducted on an Ascent spectrofluorometer to obtain TXA_2 synthase activity[25] (Labsystems, Helsinki,Finland). In human platelets, the COX-dependent bioconversion of arachidonic acid to thromboxanes produces malondialdehyde (MDA) as a side product of the spontaneous degradation of prostagladin endoperoxides.[26, 27]

In order to perform these tests ethical authorization was requested and granted in 29.09.2017 containing following requirements. The subjects must be healthy and must have fully agreed to the study (especially taking blood samples) and should not take

NSAIDs for at least 14 days. Because of no clinical intervention no further requirements were needed.

Platelet-rich plasma was put into vials. Positive controls were prepared before starting with the regular measurement of the compounds.

Spectroscopic and Chromatographic Procedures

Optical rotations were measured on a PerkinElmer-241 MC polarimeter (PerkinElmer, Watham, USA). NMR data of the natural products were obtained with a Bruker ARX 300 or AVANCE DMX 600 NMR spectrometers.

Mass spectra were obtained from a Finnigan LCQ Deca XP mass spectrometer (Thermo, Bremen, Germany) while high resolution mass spectra were recorded on a FTHRMS-Orbitrap (Thermo, Bremen, Germany) mass spectrometer. A Dionex P580 system was used in combination with a diode array detector (UVD340S) (Thermo Scientific, Germering, Germany) and an Eurosphere 10 C18 column (125 × 4mm) (Knauer, Berlin, Germany) for HPLC analysis and recording UV spectra. Semipreparative HPLC was conducted on a Lachrom-Merck Hitachi system (pump L7100, UV detector L7400) (Merck, Darmstadt, Germany) and a Eurosphere 100 C_{18} column (300 × 8 mm) (Knauer, Berlin, Germany). Sephadex-LH20 (Sigma-Aldrich, Steinheim, Germany) and silica gel 60M (0.04–0.063 mm) (Merck, Darmstadt, Germany) were used as stationary phases for column chromatography. Thin-layer chromatography plates precoated with silica gel 60 F254 (Merck, Darmstadt, Germany) were used for monitoring separation. For spectroscopic measurements spectral grade solvents were used.

GraphPad Prism® 6 (GraphPad software Inc, San Diego, CA, USA) and IBM SPSS© (New York, NY, USA) were used for IC_{50} calculations.

Identification and Preparation of suitable PPAR-Γ Structures for Ensemble Docking

Given that PPAR-γ offers multiple binding regions for agonists and that these binding regions are conformationally heterogeneous[28], we pursued an ensemble docking approach to identify the most suitable structure for predicting the binding mode of Altenusin. To this end, we considered all structures of ligand-bound human PPAR-γ with a resolution ≤ 2 Å available in the RCSB Protein Data Bank (PDB[29]), but excluded structures in which PPAR-γ was bound to organometallic compounds. This pre-filtering step led to 38 complex structures, each bound to one or more ligands (Supplementary Tab. 1). Using the Protein Preparation Wizard[30] implemented in the Maestro GUI of the Schrödinger Suite of programs (Schrödinger Release 2018-1: *Maestro*, Schrödinger, LLC, New York, NY, 2018; *Protein Preparation Wizard*; *Epik*, Schrödinger, LLC, New York, NY, 2016; *Impact*, Schrödinger, LLC, New York, NY, 2016; *Prime*, Schrödinger, LLC, New York, NY, 2018), we pre-processed the deposited biological units of all 39 complex structures by assigning bond orders, adding hydrogen atoms, automatically identifying disulfide bonds, converting selenomethionines to methionines, removing water molecules more than 5.0 Å away from ligand molecules, calculating protonation states for ligands at pH 7.4, and adding missing side chains when necessary. Whenever alternative conformational states for ligand molecules or amino acid residues were detected, we committed to the state with the highest crystallographic occupancy; in the cases where the occupancy of two available states was 0.5 each, we committed to the first deposited state. Following these initial preparation steps, we removed all duplicate chains from structures for which a dimer was deposited as a biological unit, removed the Steroid Receptor Coactivator from all structures in which it was co-crystallized, and deleted all remaining small molecule entities that were not ligands of PPAR-γ. After assigning protonation states to aspartate, glutamate, histidine and lysine, tautomeric states to

histidine, and flip states to asparagine, glutamine and histidine according to pH 7.4 using the PROPKA[31, 32] implementation in the Protein Preparation Wizard, we removed all remaining water molecules from the structures. In structures for which a neutral state for K367 was predicted by PROPKA, we transformed this residue back to the charged state, since the conformational heterogeneity of this residue in the different structures contradicts a stabilizing effect of the neutral form. Lastly, we aligned all structures to the structure with the PDB ID 2FVJ using the Protein Structure Alignment module implemented in the Schrodinger Suite.

Docking of Altenusin to the Structural Ensemble of Human PPAR-Γ

We generated the three-dimensional structure of altenusin using the Maestro GUI and predicted possible protonation states at pH 7.4 ± 2.0 with the LigPrep module (default settings, Schrödinger Release 2018-1: *LigPrep*, Schrödinger, LLC, New York, NY, 2018); this resulted in a single state with a charged carboxylate group, which we used for the subsequent docking experiment. We generated the grid(s) for docking with GlideSP[33, 34] individually by defining the grid center via the centroid of the respective bound ligand(s) in the 38 complex structures from above. The inner and outer box sizes were set to 10.0 Å and 26.0 Å, respectively. Van der Waals scaling factors and partial charge cutoffs for the receptor and ligand atoms were left at their default values of 1.00/0.25 (receptor) and 0.80/0.15 (ligand), respectively. For each complex, we considered only the docking pose with the lowest docking score for evaluation.

Results and Discussion

Twelve natural products (**1** – **12**) which included mitorubrinol[35] (**1**), mitorubrinic acid[36] (**2**), secopenicillide A [37] (**3**), purpactin F[38]·[39] (**4**), secopenicillide B[37] (**5**), deoxyfunicone[40] (**6**), purpactin C [41] (**7**), bacillisporin B[42] (**8**), altenusin[13] (**9**), djalonensone [43] (**10**), alternariol[44] (**11**) and HCRS3-VHE7525-S32-45-3[45] (**12**) (Figure **2**) were isolated from the endophytic fungus *Talaromyces* sp. All compounds feature an ortho-hydroxylated benzoic acid moiety reminiscent of the known platelet aggregation inhibitor salicylic acid.

Due to the fact that salicylic acid is a COX-I and COX-II inhibitor[46], we suspected binding of the analyzed natural products to COX enzymes due to their structural similarity to the former compound. This prompted us to perform platelet aggregation experiments with compounds **1** – **12** with platelets taken from healthy human donors. Secopenicillide A **(3),** purpactin C **(7)** and altenusin **(9)** each inhibited platelet aggregation at an initial concentration of 100 µM (**SI:** S6, S5 and S2), whereas the remaining compounds were inactive **(SI: S2-S6)**. After this initial screening experiment, we aimed to increase the conclusivenessof the obtained *in vitro* data by analyzing the effects of the active compounds on platelets derived from four rather than one individual donors.

Secopenicillide A **(3),** purpactin C **(7)** and altenusin **(9)** all displayed platelet aggregation inhibition in this second experiment regardless of the analyzed individual plasma samples, even though clear differences with regard to the individual compounds became visible. As a first inducer of platelet aggregation, collagen was added to the plasma samples alongside with the investigated inhibitors (Figure 3). Purpactin C **(7)** and secopenicillide A **(3)** exhibited only minimal inhibition of platelet aggregation in this experiment when tested at a concentration of 100 µM and were thus excluded from further tests. Altenusin **(9)** on the other hand was a better inhibitor with an IC_{50} value of 23.31

µM and was thus selected for further experiments directed to the potential target of this compound.

[Figure 3 near here]

Our first suspected target of altenusin (**9**) was cyclooxygenase I (COX-I) since inhibition of cyclooxygenase II (COX-II) activity with IC_{50} values of 30 µM had been reported recently for this compound.[2] COX-I is the predominantly occurring COX enzyme in platelets. Arachidonic acid was added to platelets as a stimulus for platelet aggregation in presence of the suspected COX-I inhibitor altenusin (**9**), (Figure 4A). A colorimetric quantification of MDA produced by platelets can be used as readout for COX-I activity[47]. However, no significant changes in MDA concentrations were detected for platelets that had been induced by arachidonic acid in presence of altenusin (**9**) vs. induced platelets in the absence of compound **9** (Fig. 4A). As these results contradicted our initial hypothesis that altenusin (**9**) acts as a COX inhibitor, we performed further experiments using an ELISA thromboxane assay that employed the more stable TXA_2-analogue TXB_2.[48] No significant inhibition of TXB_2 formation was observed in presence of altenusin (**9**) (Fig. 4B), which confirmed our earlier results from the MDA assay. Thus, our initial hypothesis that altenusin (**9**) acts on platelets as a COX inhibitor had to be discarded pointing to other pathways (Fig. 1) as targets for altenusin.

[Figure 4 near here]

[Figure 5 near here]

In further experiments, aggregation assays with altenusin (**9**) were performed that focused on the ADP receptor P2Y12, the thrombin receptor PAR1 or the thromboxane receptor TXA2R as alternative targets of compound **9**. In these experiments either ADP, the thrombin receptor activated peptide or the prostaglandin I_2 analogue cicaprost, a

prostacyclin analogue acting as an inhibitor of platelet function[49, 50] were used for aggregation experiments in the presence of the inhibitor altenusin. Cicaprost blocked platelets that had been induced with arachidonic acid. Altenusin (**9**), however, was unable to inhibit platelet aggregation in the presence of all of the latter stimuli (SI: S9-S12), thus excluding the corresponding pathways as possible targets of the compound.

These findings taken together with a recent patent describing the interaction of altenusin with PPARβ and γ receptors via a binding affinity assay[51] put the peroxisome proliferator-activated receptors (PPARs)[52] into the focus of our study on the potential target of altenusin (**9**) in platelets. Molecular docking experiments were conducted with altenusin (**9**). The known PPARγ inhibitor magnolol was included into these docking studies due to its structural similarity to altenusin (**9**). Magnolol is a biphenyl compound originally discovered in the plant *Magnolia officinalis*. As the original study that discovered magnolol as a PPARγ inhibitor had used washed platelets[20], we followed this protocol in our study and used washed platelets for platelet aggregation experiments assays.[20] In these experiments the PPAR inhibitor magnolol as well as altenusin showed a concentration-dependent inhibition of platelet aggregation. Whereas the IC_{50} value of magnolol amounted to 1.1 µM (table 1), altenusin (**9**) was less active and exhibited an IC_{50} value of 23.3 µM. Platelet aggregation inhibition of magnolol is known to be caused by modulation of PPARs-β/γ[20]

[Table 1 near here] [Figure 6 near here]

The binding mode predicted for Altenusin strongly differs depending on the receptor structure (Supplementary Fig. 1). For each of the three “arms” in the Y-shaped binding region of PPAR-γ (as described by Xu et al.[53] and Jang et al.[28, 54]), the docking algorithm found at least one binding mode (Fig. 1A, Supplementary Fig. 1): 14

binding modes in arm 1, a single binding mode in arm 2, and 23 binding modes in arm 3 (Supplementary Fig. 1, 2). However, the average docking score in arm 1 (mean: -7.11 ± 0.16 kcal mol^{-1}) is significantly lower than the average docking score in arm 3 (mean: -6.51 ± 0.10 kcal mol^{-1}, $t(35) = 3.44$, $p = 0.0015$), indicating that arm 1 is more likely to be the binding site of Altenusin. There, the docking score for the best docking solution identified – which we consider the most probable binding mode of Altenusin – is -8.14 kcal mol^{-1}. The predicted binding site is formed by residues in helices h3, h5, h7, h10, and h12, where Altenusin is stabilized by hydrogen bonds to residues ^{h3}S317, ^{h5}H351, ^{h5}Y355, ^{h7}K395, and ^{h12}Y501, a salt bridge with ^{h7}K395, and π-π stacking with ^{h10}H477 (Fig. 1B); the remaining residues in this pocket form a sufficiently large hydrophobic surface to accommodate the biphenyl, methyl, and methoxy substituents (Fig. 1B). Notably, the predicted binding site of Altenusin overlaps with the known binding site of the structurally similar agonist Magnolol (PDB ID: 3R5N[55]), but is not identical (Fig. 1B, inset). This difference in binding mode can likely be attributed to the carboxylate group in Altenusin, which strongly stabilizes its bound conformation through a salt bridge with ^{h7}K395, whereas Magnolol is predominantly stabilized by hydrophobic interactions and π-π stacking. Altenusin, similar to other PPAR-γ agonists, may directly stabilize the active conformation of h12 via a hydrogen bond to ^{h12}Y501 and hydrophobic interactions with ^{h12}L497 (Fig. 1B). Note that h12 in all of the 38 receptor structures used for docking was in the active conformation and that all receptor structures were bound to an agonist. In summary, these results corroborate the hypothesis that Altenusin binds to arm 1 of the PPAR-g binding site and may thereby act as a PPAR-γ agonist.

[Figure 7 near here]

With the molecular docking studies information together with the binding affinity assay of altenusin towards PPAR described by Micikas *et al.*[51] in hand, the following derivation can be given:

When considering the structural similarity of altenusin (**9**) to magnolol, both featuring a biphenyl system, combined with the similar assay results of all PPAR inhibitors and our modelling experiments with PPAR, it is feasible to assume a similar mode of action for altenusin as for magnolol (**9**).

In conclusion, our findings establish the mycotoxin altenusin (**9**) for the first time as a platelet inhibitor. Molecular docking experiments suggest that the platelet inhibition of altenusin is due to binding to PPAR-β/γ receptors as previously shown for the structurally similar platelet inhibitor magnolol. For the first time, we are confirming earlier binding affinity assays[51] and complementing closely related FXR binding mode studies.[15] Based on our experiments and on earlier reports, we suspect that the mode of action of altenusin (**9**) in platelets is based on the modulation of non-genomic PPAR-β/γ effects. FXR effects may also be involved, as FXR binding affinity for altenusin (**9**) has been reported in liver cells.[15] Whether altenusin (**9**) exerts its aggregation inhibition effects as a dual mode ligand remains to be seen, as we were not able to exclude simultaneous binding to PPAR and FXR. Dual action ligands modulating FXR as well as PPAR exist[56, 57], pointing out why PPAR and FXR should not be treated completely separately regarding platelet functions. However, because this is the first study on effects of altenusin on platelets and non-genomic PPAR/FXR effects in platelets have not been investigated so far, further research is required.

Acknowledgments

This study was funded by the Deutsche Forschungsgemeinschaft (DFG, German Research Foundation) – 270650915 (Research Training Group GRK 2158, TP1c to P.P. and TP4a to H.G.). We are grateful for computational support by the "Zentrum für Informations und Medientechnologie" at the Heinrich-Heine-Universität Düsseldorf and the computing time provided by the John von Neumann Institute for Computing (NIC) to H.G. on the supercomputer JUWELS at Jülich Supercomputing Centre (JSC) (user ID: HKF7). Funding by Deutsche Forschungsgemeinschaft (DFG) (INST 208/704-1 FUGG) to purchase the hybrid computer cluster used in this study is gratefully acknowledged. Further support by the Manchot Foundation to P. P. is gratefully acknowledged. We wish to thank Mrs. Kirsten Bartkowski (Institute for Pharmacology and Clinical Pharmacology) for conducting the experiments. We furthermore wish to thank Dr. Marc Appelhans (Department of Systematics, Biodiversity and Evolution of Plants with Herbarium, Göttingen University, Germany) for identification of the plant material.

Declaration of Interest statement

The authors declare no conflict of interest.

References

[1] Tournas V. Heat-resistant fungi of importance to the food and beverage industry. Crit Rev Microbiol 1994;20:243-263. Epub 1994/01/01.
[2] Chen Y, Chen R, Xu J, Tian Y, Xu J, Liu Y. Two New Altenusin/Thiazole Hybrids and a New Benzothiazole Derivative from the Marine Sponge-Derived Fungus Alternaria sp. SCSIOS02F49. Molecules 2018;23:2844. Epub 2018/11/06.
[3] Chan JF, Lau SK, Yuen KY, Woo PC. Talaromyces (Penicillium) marneffei infection in non-HIV-infected patients. Emerg Microbes Infect 2016;5:e19. Epub 2016/03/10.
[4] Supparatpinyo K, Chiewchanvit S, Hirunsri P, Uthammachai C, Nelson KE, Sirisanthana T. Penicillium marneffei infection in patients infected with human immunodeficiency virus. Clinical infectious diseases 1992;14:871-874.
[5] Ustianowski AP, Sieu TP, Day JN. Penicillium marneffei infection in HIV. Current Opinion in Infectious Diseases 2008;21:31-36.
[6] Visagie CM, Hirooka Y, Tanney JB, Whitfield E, Mwange K, Meijer M, Amend AS, Seifert KA, Samson RA. Aspergillus, Penicillium and Talaromyces isolated from house dust samples collected around the world. Stud Mycol 2014;78:63-139. Epub 2014/12/11.
[7] Li H, Huang H, Shao C, Huang H, Jiang J, Zhu X, Liu Y, Liu L, Lu Y, Li M, et al. Cytotoxic norsesquiterpene peroxides from the endophytic fungus Talaromyces flavus isolated from the mangrove plant Sonneratia apetala. J Nat Prod 2011;74:1230-1235. Epub 2011/05/07.
[8] Liu F, Cai XL, Yang H, Xia XK, Guo ZY, Yuan J, Li MF, She ZG, Lin YC. The bioactive metabolites of the mangrove endophytic fungus Talaromyces sp. ZH-154 isolated from Kandelia candel (L.) Druce. Planta Med 2010;76:185-189. Epub 2009/08/12.
[9] Zhao JW, Yang ZD, Zhou SY, Yang LJ, Sun JH, Yao XJ, Shu ZM, Li S. Wortmannine F and G, two new pyranones from Talaromyces wortmannii LGT-4, the endophytic fungus of Tripterygium wilfordii. Phytochemistry Letters 2019;29:115-118.
[10] Bara R, Aly AH, Pretsch A, Wray V, Wang B, Proksch P, Debbab A. Antibiotically active metabolites from Talaromyces wortmannii, an endophyte of Aloe vera. J Antibiot (Tokyo) 2013;66:491-493. Epub 2013/05/17.
[11] Villanueva M, Heckenberger R, Strobach H, Palmer M, Schror K. Equipotent inhibition by R(-)-, S(+)- and racemic ibuprofen of human polymorphonuclear cell function in vitro. Br J Clin Pharmacol 1993;35:235-242. Epub 1993/03/01.
[12] Rainsford KD. 1999. Ibuprofen: A critical bibliographic review: CRC Press.
[13] Nakanishi S, Toki S, Saitoh Y, Tsukuda E, Kawahara K, Ando K, Matsuda Y. Isolation of myosin light chain kinase inhibitors from microorganisms: dehydroaltenusin, altenusin, atrovenetinone, and cyclooctasulfur. Biosci Biotechnol Biochem 1995;59:1333-1335. Epub 1995/07/01.
[14] Aly A, Ebel R, Edrada R, Wray V, Kubbutat M, Proksch P. Protein Kinase Inhibitors from the Endophytic Fungus Alternaria sp. isolated from Polygonum senegalense Growing in Egypt. Planta Medica 2009;75:PE55.
[15] Zheng Z, Zhao Z, Li S, Lu X, Jiang M, Lin J, An Y, Xie Y, Xu M, Shen W. Altenusin, a nonsteroidal microbial metabolite, attenuates nonalcoholic fatty liver disease by activating the farnesoid X receptor. Mol Pharmacol 2017;92:425-436.
[16] Matsubara T, Li F, Gonzalez FJ. FXR signaling in the enterohepatic system. Molecular and cellular endocrinology 2013;368:17-29.

[17] Gronemeyer H, Gustafsson J-Å, Laudet V. Principles for modulation of the nuclear receptor superfamily. Nature Reviews Drug Discovery 2004;3:950-964.
[18] Unsworth AJ, Bye AP, Tannetta DS, Desborough MJ, Kriek N, Sage T, Allan HE, Crescente M, Yaqoob P, Warner TD. Farnesoid X receptor and liver X receptor ligands initiate formation of coated platelets. Arteriosclerosis, thrombosis, and vascular biology 2017;37:1482-1493.
[19] Moraes LA, Unsworth AJ, Vaiyapuri S, Ali MS, Sasikumar P, Sage T, Flora GD, Bye AP, Kriek N, Dorchies E. Farnesoid X receptor and its ligands inhibit the function of platelets. Arteriosclerosis, thrombosis, and vascular biology 2016;36:2324-2333.
[20] Shih CY, Chou TC. The antiplatelet activity of magnolol is mediated by PPAR-beta/gamma. Biochem Pharmacol 2012;84:793-803. Epub 2012/07/04.
[21] Kjer J, Debbab A, Aly AH, Proksch P. Methods for isolation of marine-derived endophytic fungi and their bioactive secondary products. Nature Protocols 2010;5:479-490.
[22] Michal F, Born G. Effect of the rapid shape change of platelets on the transmission and scattering of light through plasma. Nature New Biology 1971;231:220.
[23] Born G, HUME M. Effects of the numbers and sizes of platelet aggregates on the optical density of plasma. Nature 1967;215:1027.
[24] Born G. Observations on the change in shape of blood platelets brought about by adenosine diphosphate. The Journal of physiology 1970;209:487-511.
[25] Dannhardt G, Flemmer L, Hartmann RW, Kleber A, Schulze E. Spectrofluorimetric Quantification of Malondialdehyde for Evaluation of Cyclooxygenase-1/Thromboxane Synthase Inhibition. Archiv der Pharmazie: An International Journal Pharmaceutical and Medicinal Chemistry 1998;331:359-364.
[26] Diczfalusy U, Falardeau P, Hammarström S. Conversion of prostaglandin endoperoxides to C17-hydroxy acids catalyzed by human platelet thromboxane synthase. Febs Letters 1977;84:271-274.
[27] Plastaras JP, Guengerich FP, Nebert DW, Marnett LJ. Xenobiotic-metabolizing cytochromes P450 convert prostaglandin endoperoxide to hydroxyheptadecatrienoic acid and the mutagen, malondialdehyde. Journal of Biological Chemistry 2000;275:11784-11790.
[28] Jang JY, Koh M, Bae H, An DR, Im HN, Kim HS, Yoon JY, Yoon H-J, Han BW, Park SB, et al. Structural basis for differential activities of enantiomeric PPARgamma agonists: Binding of S35 to the alternate site. Biochim Biophys Acta 2017;1865:674-681. Epub 2017/03/28.
[29] Burley SK, Berman HM, Bhikadiya C, Bi C, Chen L, Di Costanzo L, Christie C, Dalenberg K, Duarte JM, Dutta S, et al. RCSB Protein Data Bank: biological macromolecular structures enabling research and education in fundamental biology, biomedicine, biotechnology and energy. Nucleic Acids Res 2019;47:D464-D474. Epub 2018/10/26.
[30] Sastry GM, Adzhigirey M, Day T, Annabhimoju R, Sherman W. Protein and ligand preparation: parameters, protocols, and influence on virtual screening enrichments. J Comput-Aided Mol Des 2013;27:221-234. Epub 2013/04/13.
[31] Rostkowski M, Olsson MHM, Søndergaard CR, Jensen JH. Graphical analysis of pH-dependent properties of proteins predicted using PROPKA. BMC Struct Biol 2011;11:6.
[32] Olsson MHM, Søndergaard CR, Rostkowski M, Jensen JH. PROPKA3: Consistent Treatment of Internal and Surface Residues in Empirical pKa Predictions. J Chem Theory Comput 2011;7:525-537.

[33] Friesner RA, Banks JL, Murphy RB, Halgren TA, Klicic JJ, Mainz DT, Repasky MP, Knoll EH, Shelley M, Perry JK, et al. Glide: a new approach for rapid, accurate docking and scoring. 1. Method and assessment of docking accuracy. J Med Chem 2004;47:1739-1749. Epub 2004/03/19.
[34] Halgren TA, Murphy RB, Friesner RA, Beard HS, Frye LL, Pollard WT, Banks JL. Glide: a new approach for rapid, accurate docking and scoring. 2. Enrichment factors in database screening. J Med Chem 2004;47:1750-1759. Epub 2004/03/19.
[35] Büchi G, White J, Wogan G. The structures of mitorubrin and mitorubrinol. Journal of the American Chemical Society 1965;87:3484-3489.
[36] Marsini MA, Gowin KM, Pettus TR. Total synthesis of (+/-)-mitorubrinic acid. Org Lett 2006;8:3481-3483. Epub 2006/07/28.
[37] Komai SI, Hosoe T, Itabashi T, Nozawa K, Yaguchi T, Fukushima K, Kawai KI. New penicillide derivatives isolated from Penicillium simplicissimum. J Nat Med 2006;60:185-190. Epub 2006/07/01.
[38] Shao Z-GS, Wang C-Y. 1) On p. 443, line 9 should read as follows: Three new diphenyl ether derivatives, purpactins D–F (1–3, resp.), together with six known 2) On p. 443, line 32 should read as follows: purpactins D–F (1–3, resp.), together with six known analogs, 4–9. All isolated. CHEMISTRY & BIODIVERSITY 2015;12:1130.
[39] Chen M, Han L, Shao CL, She ZG, Wang CY. Erratum: bioactive diphenyl ether derivatives from a gorgonian-derived fungus Talaromyces sp. Chem Biodivers 2015;12:1130. Epub 2015/07/15.
[40] Sassa T, Nukina M, Suzuki Y. Deoxyfunicone, a new γ-pyrone metabolite from a resorcylide-producing fungus (Penicillium sp.). Agricultural and biological chemistry 1991;55:2415-2416.
[41] Nishida H, Tomoda H, Cao J, Okuda S, Omura S. Purpactins, new inhibitors of acyl-CoA:cholesterol acyltransferase produced by Penicillium purpurogenum. II. Structure elucidation of purpactins A, B and C. J Antibiot (Tokyo) 1991;44:144-151. Epub 1991/02/01.
[42] Yamazaki M, Okuyama E. Isolation and Structures of Oxaphenalenone Dimers from Talaromyces-Bacillosporus. Chemical & Pharmaceutical Bulletin 1980;28:3649-3655.
[43] Mao Z, Sun W, Fu L, Luo H, Lai D, Zhou L. Natural dibenzo-α-pyrones and their bioactivities. Molecules 2014;19:5088-5108.
[44] Zhang LH, Wang HW, Xu JY, Li J, Liu L. A new Secondary metabolites of the crinoid (Comanthina schlegeli) associated fungus Alternaria brassicae 93. Nat Prod Res 2016;30:2305-2310. Epub 2016/04/07.
[45] Sun TY, Kuang RQ, Chen GD, Qin SY, Wang CX, Hu D, Wu B, Liu XZ, Yao XS, Gao H. Three Pairs of New Isopentenyl Dibenzo[b,e]oxepinone Enantiomers from Talaromyces flavus, a Wetland Soil-Derived Fungus. Molecules 2016;21:1184. Epub 2016/09/13.
[46] Cryer B, Feldman M. Cyclooxygenase-1 and Cyclooxygenase-2 Selectivity of Widely Used Nonsteroidal Anti-Inflammatory Drugs. The American Journal of Medicine 1998;104:413-421.
[47] Ledergerber D, Hartmann R. Development of a screening assay for the in vitro evaluation of thromboxane A2 synthase inhibitors. Journal of enzyme inhibition 1995;9:253-261.
[48] Reinke M. Monitoring thromboxane in body fluids: a specific ELISA for 11-dehydrothromboxane B2 using a monoclonal antibody. American Journal of Physiology-Endocrinology and Metabolism 1992;262:E658-E662.

[49] Ashby B. Comparison of iloprost, cicaprost and prostacyclin effects on cyclic AMP metabolism in intact platelets. Prostaglandins 1992;43:255-261.
[50] Belch J, McLaren M, Lau C, Mackay I, Bancroft A, McEwen J, Thompson J. Cicaprost, an orally active prostacyclin analogue: its effects on platelet aggregation and skin blood flow in normal volunteers. British journal of clinical pharmacology 1993;35:643-647.
[51] MICIKAS SSCWMKFCSRJ, inventor. 2014. Amorfrutin analogs as ppargamma-modulators.
[52] Ray DM, Spinelli SL, O'Brien JJ, Blumberg N, Phipps RP. Platelets as a novel target for PPARgamma ligands : implications for inflammation, diabetes, and cardiovascular disease. BioDrugs 2006;20:231-241. Epub 2006/07/13.
[53] Xu HE, Lambert MH, Montana VG, Parks DJ, Blanchard SG, Brown PJ, Sternbach DD, Lehmann JM, Wisely GB, Willson TM, et al. Molecular recognition of fatty acids by peroxisome proliferator-activated receptors. Mol Cell 1999;3:397-403. Epub 1999/04/13.
[54] Jang JY, Kim H, Kim H-J, Suh SW, Park SB, Han BW. Structural basis for the inhibitory effects of a novel reversible covalent ligand on PPARgamma phosphorylation. Sci Rep 2019;9:11168. Epub 2019/08/03.
[55] Zhang H, Xu X, Chen L, Chen J, Hu L, Jiang H, Shen X. Molecular determinants of magnolol targeting both RXRalpha and PPARgamma. PLoS One 2011;6:e28253. Epub 2011/12/06.
[56] Merk D, Lamers C, Weber J, Flesch D, Gabler M, Proschak E, Schubert-Zsilavecz M. Anthranilic acid derivatives as nuclear receptor modulators—Development of novel PPAR selective and dual PPAR/FXR ligands. Bioorganic & Medicinal Chemistry 2015;23:499-514.
[57] Steri R, Schneider P, Klenner A, Rupp M, Kriegl JM, Schubert-Zsilavecz M, Schneider G. Target Profile Prediction: Cross-Activation of Peroxisome Proliferator-Activated Receptor (PPAR) and Farnesoid X Receptor (FXR). Molecular Informatics 2010;29:287-292.
[58] Barnes MJ, Knight CG, Farndale RW. The collagen-platelet interaction. Curr Opin Hematol 1998;5:314-320. Epub 1998/10/17.
[59] Fitzgerald GA. Mechanisms of Platelet Activation - Thromboxane-A2 as an Amplifying Signal for Other Agonists. American Journal of Cardiology 1991;68:B11-B15.
[60] Ali FY, Davidson SJ, Moraes LA, Traves SL, Paul-Clark M, Bishop-Bailey D, Warner TD, Mitchell JA. Role of nuclear receptor signaling in platelets: antithrombotic effects of PPARbeta. FASEB J 2006;20:326-328. Epub 2005/12/22.
[61] Fuentes E, Palomo I. Antiplatelet effects of natural bioactive compounds by multiple targets: Food and drug interactions. Journal of Functional Foods 2014;6:73-81.

Figure 1. Simplified overview on different pathways involved in platelet aggregation and their modulation by different natural products[52, 58-61] AA = arachidonic acid, ADP = adenosine diphosphate, COX = cyclooxygenase, GPVI-Fcr = glycoprotein VI receptor, LXR = liver X receptor, NP = natural product; $P2Y_{12}$ = purinergic G protein-coupled receptor, PAR1 = protease-activated receptor 1,, PPAR, peroxisome proliferated activated-receptor, TXA_2 = thromboxane A_2, TXA_2R = thromboxane A_2 receptor.

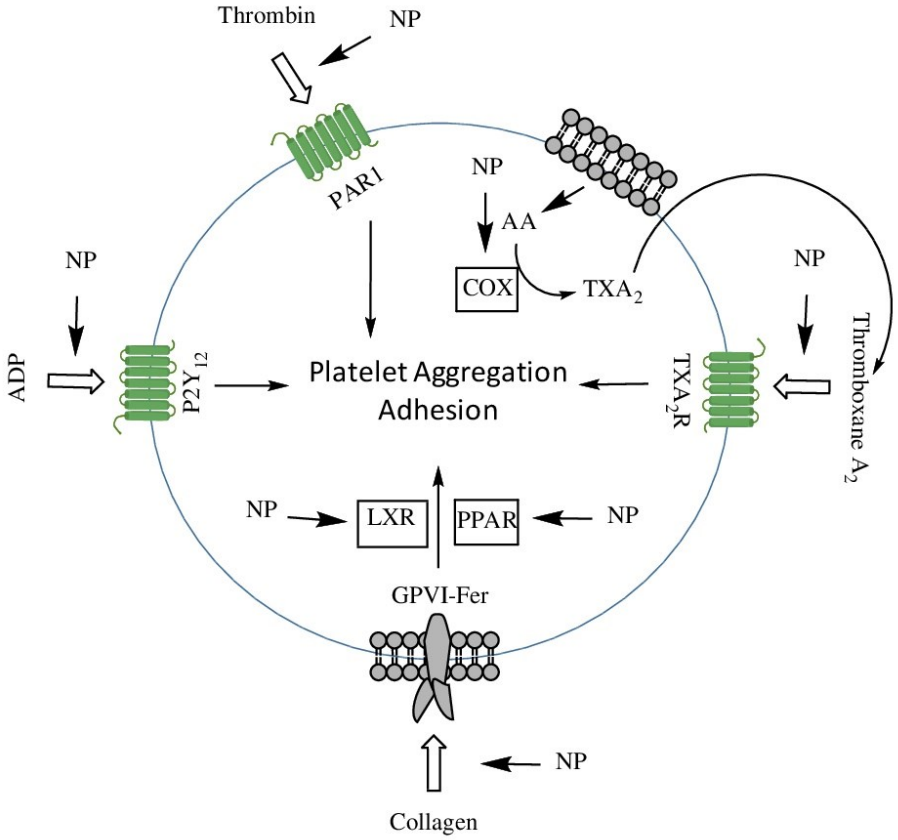

Figure 2. Structures of isolated compounds from *Talaromyces* sp.

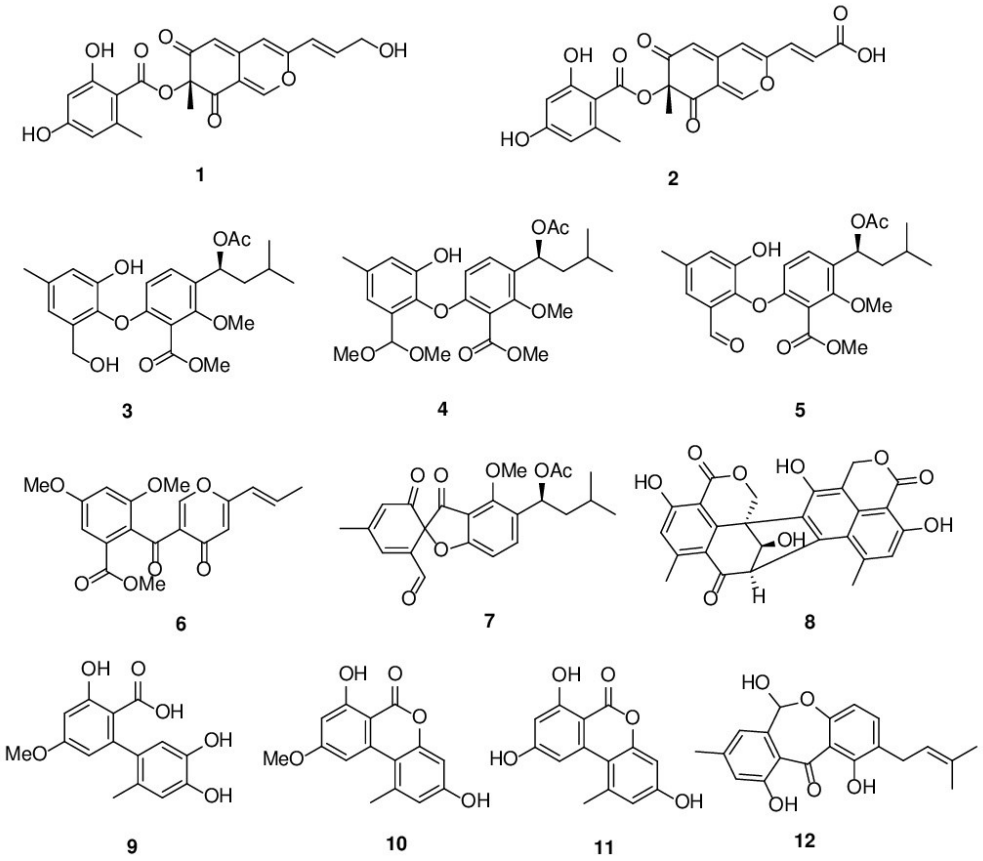

Figure 3. Aggregation studies were performed in PRP in the presence of altenusin (**9**). After 4 min of incubation with the compound, the sample (not shown) was stirred for 2 min. While the sample was stirring, it was analyzed for spontaneous aggregation. After 2 min, 3µg/ml collagen was added to the sample (arrow), followed by stirring for additional 4 min. All aggregation tests were conducted according to this protocol. Altenusin **(9)** inhibits collagen induced platelet aggregation at concentrations of 50µM (red) or 100µM (blue). Control aggregation without inhibitor (black). (See SI for full data)

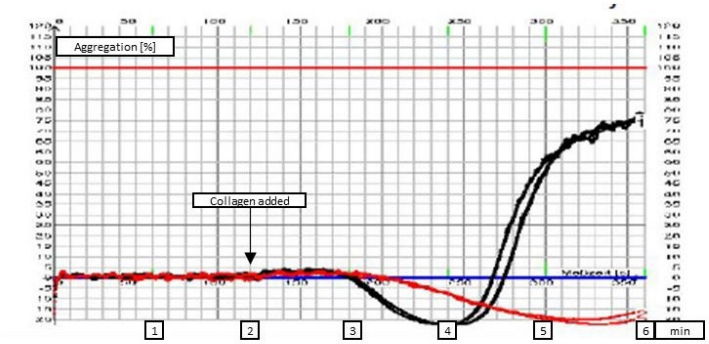

Figure 4. Altenusin aggregation results of platelets induced by 1mM ARA. Standard deviations between the samples were displayed as error bars.

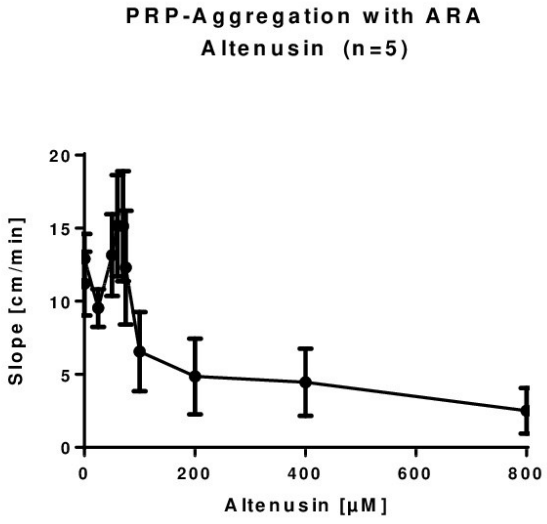

Figure 5. A) (n=5)Malondialdehyde (MDA) in platelet rich plasma following stimulation with arachidonic acid (1mM) -induced platelet aggregation. Aggregation was determined in presence of altenusin (**9**) at concentrations 0-800µM; **B**) (n=5) TXB2 – assay (ELISA) with arachidonic acid (1 mM)-stimulated platelets at altenusin (**9**) concentrations 0-400 µM. Standard deviations between the samples were displayed as error bars.

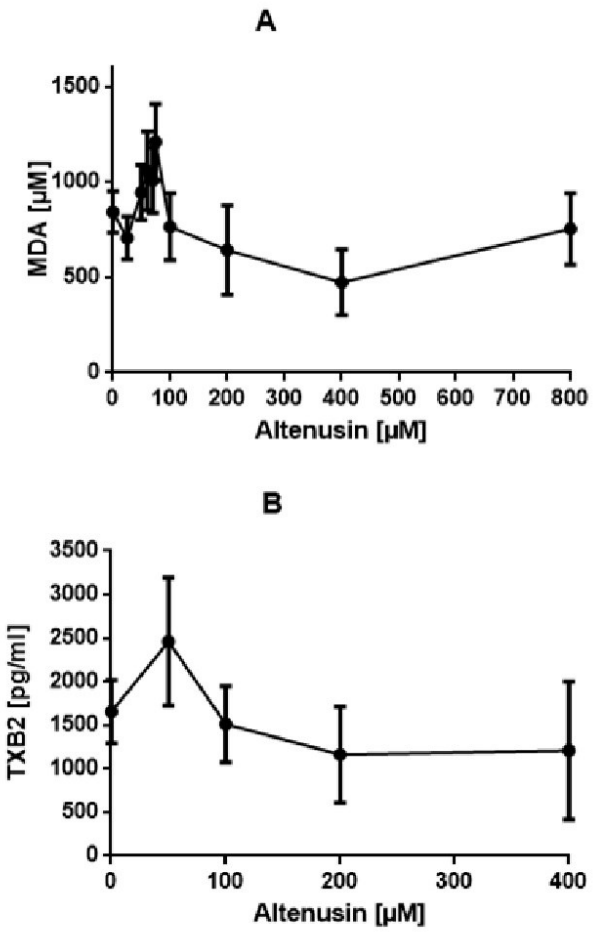

Figure 6. Platelet aggregation was induced in washed human platelets by addition of collagen. Compounds were added after 2 min and light transmission aggregometry was measured. Corresponding IC50 values are shown in table 1. Standard deviations between the samples were displayed as error bars. High standard deviations are due to individual blood donors.

From left to right: DMSO negative control (A), altenusin (9) (B), magnolol (C) for (n=5),

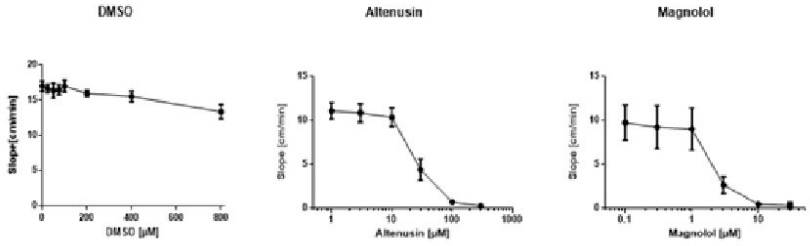

Table 1. IC_{50} values of the aggregation tests with washed platelets and standard deviations are shown (collagen induced).

Compound	IC_{50} µM
Magnolol	1.083
Altenusin	23.31

Figure 7. Predicted binding mode of Altenusin in human PPAR-γ. (A) Predicted binding modes of altenusin (sticks) in 38 PPAR-γ structures. The binding modes are colored from green (best docking score: -8.14 kcal mol^{-1}) to red (worst docking score: -5.50 kcal mol^{-1}). All protein structures are depicted as transparent ribbon diagrams, except 6DGL, which provided the best docking result and is depicted in cartoon representation. The Y-shaped binding pocket (transparent surface, colored according to the docking score of the bound ligands) consists of three "Arms" which are highlighted in the structure. (B) Predicted binding mode of altenusin (green sticks) in the receptor structure (6DGL) which provided the best docking score. Hydrogen bonds are depicted

as yellow dashed lines, salt bridges as violet dashed lines and π-π stacking interactions as blue dashed lines. Residues involved in polar interactions are depicted as grey sticks, residues that constitute the hydrophobic surface of the binding site are depicted as orange lines with orange surface.

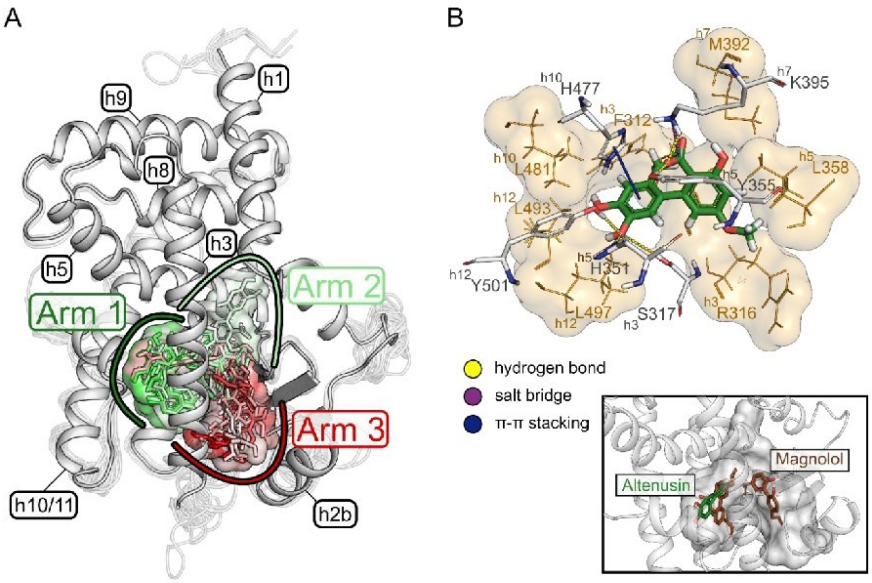

Supporting information

The Mycotoxin Altenusin is a Platelet Aggregation Inhibitor

Nam Michael Tran-Cong,[a] Thomas Hohlfeld,[b]* Michele Bonus,[c] Marian Frank,[a] Holger Gohlke,[c,d]* Zhen Liu,[a] and Peter Proksch[a]*

[a]*Institute for Pharmaceutical Biology and Biotechnology, Heinrich-Heine-University Düsseldorf, Düsseldorf, Germany;* [b]*Institute of Pharmacology and Clinical Pharmacology, University Hospital, Düsseldorf, Germany;* [c]*Institute for Pharmaceutical Chemistry and Medical Chemistry, Heinrich-Heine-University Düsseldorf, Düsseldorf, Germany;* [d] *John von Neumann Institute for Computing (NIC), Jülich Supercomputing Centre (JSC) & Institute for Complex Systems - Structural Biochemistry (ICS 6), Forschungszentrum Jülich GmbH, Wilhelm-Johnen-Straße, 52425 Jülich, Germany*

Correspondence details: Thomas Hohlfeld, Institute for Pharmacology and Clinical Pharmacology, University Hospital, Heinrich-Heine-University Düsseldorf, Moorenstr. 5, 40225, Düsseldorf. Email: hohlfeld@uni-duesseldorf.de ; Holger Gohlke, Institute for Pharmaceutical and Mecinal Chemistry, Universitätstraße 1, 40225, Düsseldorf. Email: gohlke@hhu.de ; Peter Proksch, Institute for Pharmaceutical Biology and Biotechnology, Heinrich-Heine-University Düsseldorf, Universitätsstraße 1, 40225, Düsseldorf. Email: proksch@hhu.de

Contents

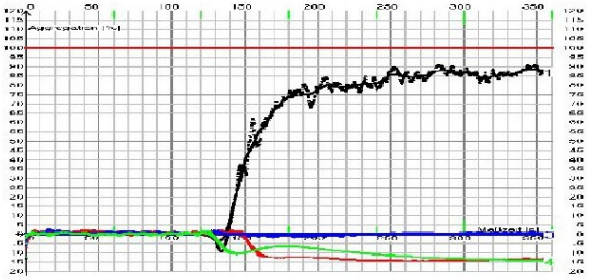

Nr.	Comment	Induced with	Agg. Max [%]	Agg. Slope [%/min]
EIA 19	**Control**	300µM AA	88.82	177.03
EIA 20	**30 µM ASS**	300µM AA	1.82	6.69
EIA 21	**100 µM ASS**	300µM AA	1.70	7.31
EIA 22	**30 µM Ibuprofene**	300µM AA	0.77	2.52

Figure S1. Light transmission aggrenometry results of acetylic acid and ibuprofen as used controls

Nr.	Induced with	Note	Agg. Max [%]	Agg. Slope [%/min]
EIA 59	500 µM AA	**Control**	92.52	212.74
EIA 60	500 µM AA	**100µM Altenusin**	1.70	3.91
EIA 61	500 µM AA	**100µM Alternariol**	93.83	195.47
EIA 62	500 µM AA	**100µM Bacillisporin**	95.23	194.81

Figure S2. Light transmission aggrenometry results of 100 µM altenusin, 100 µM alternariol and 100 µM bacillisporin.

			Agg.	Agg.
Nr.	Induced with	Note	Max [%]	Slope [%/min]
EIA63	500 µM AA	**Control**	90.44	204.20
EIA64	500 µM AA	**100µM Deoxyfunicone**	92.32	196.18
EIA65	500 µM AA	**100µM HCR-VHE7525-S3243-3**	91.12	181.26
EIA66	500 µM AA	**100µM Djalonensone**	91.01	199.58

Figure S3. Light transmission aggrenometry results of 100 µM deoxyfunicone, 100 µM HCR3-VHE7525-S32-42-3 and 100 µM Djalonensone

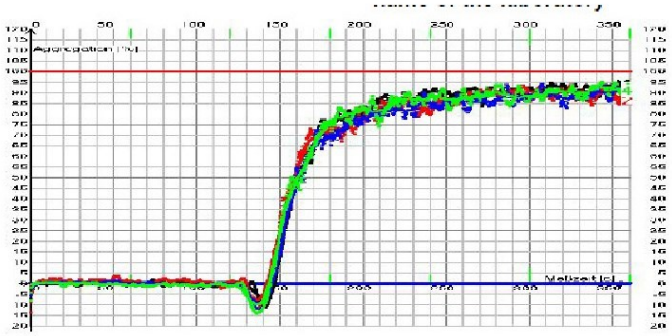

			Agg.	Agg.
Nr.	Induced with	Note	Max [%]	Slope [%/min]
EIA71	500 µM AA	**Control**	93.99	199.48
EIA72	500 µM AA	**100µM Mitorubrinol**	91.03	190.30
EIA73	500 µM AA	**100µM Mitorubrinic acid**	91.68	185.51
EIA75	500 µM AA	**100µM Secopenicillide B**	92.69	192.25

Figure S4. Light transmission aggrenometry results of 100 µM

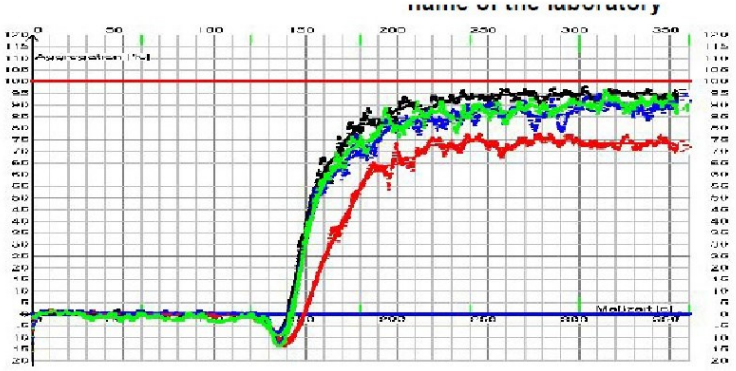

			Agg.	Agg.
Nr.	Induced with	Note	Max [%]	Slope [%/min]
EIA67	1 mM AA	**Control**	95.22	218.63
EIA68	1 mM AA	**100µM Purpactin C**	75.50	124.47
EIA69	1 mM AA	**100µM Purpactin F**	92.51	201.29
EIA70	1 mM AA	**100µM Mitorubrinol acetate**	92.35	210.54

Figure S5. Light transmission aggrenometry results of 100 µM

			Agg.	Agg.
Nr.	Induced with	Note	Max [%]	Slope [%/min]
EIA75	1 mM AA	**Control**	93.54	217.77
EIA76	1 mM AA	**100µM Secopenicillide A**	91.17	174.62

Figure S6. Light transmission aggrenometry results of 100 µM

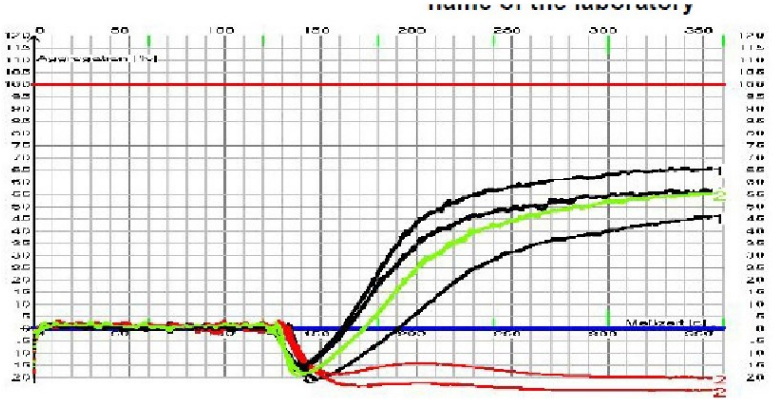

			Agg.	Agg.
Nr.	Induced with	Note	Max [%]	Slope [%/min]
1	1 mM AA	**Control**	45.98	39.38
2	1 mM AA	**50µM Altenusin**	1.79	1.61
3	1 mM AA	**Control**	56.80	65.49
4	1 mM AA	**50µM Altenusin**	2.30	10.04
5	1 mM AA	**Control**	65.61	74.90
6	1 mM AA	**5µM Altenusin**	55.52	55.62

Figure S7. Light transmission aggrenometry results of 50µM and 5µM altenusin

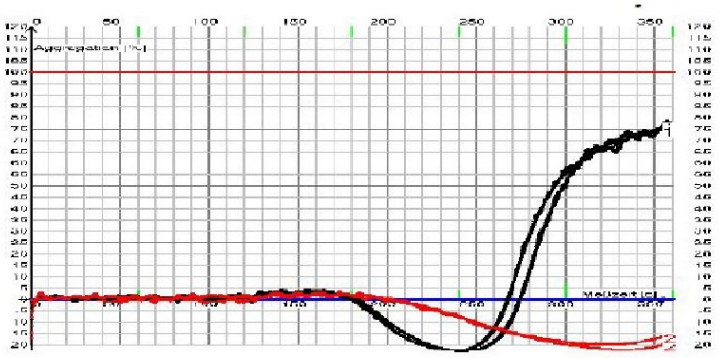

Nr.	Induced with	Note	Agg. Max [%]	Agg. Slope [%/min]
1	3µg/ml Collagen	**Control**	77.44	134.74
2	3µg/ml Collagen	**50µM Altenusin**	2.77	9.58
3	3µg/ml Collagen	**Control**	75.59	138.19
4	3µg/ml Collagen	**50µM Altenusin**	2.43	3.73

Figure S8. Light transmission aggrenometry results of 50µM altenusin with collagen for inducing platelet aggregation

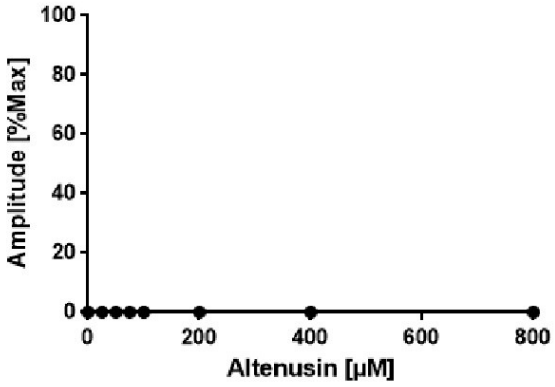

Figure S9. Different altenusin concentrations together with 100 nM cicaprost

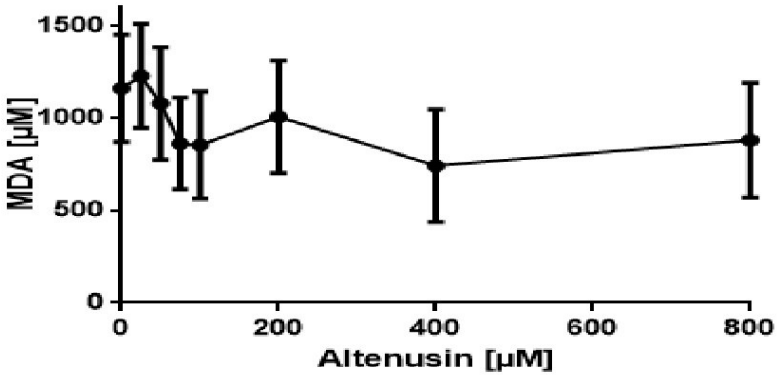

Figure S10. From supernatants of Figure S8. derived MDA – results. Error bars display standard deviation

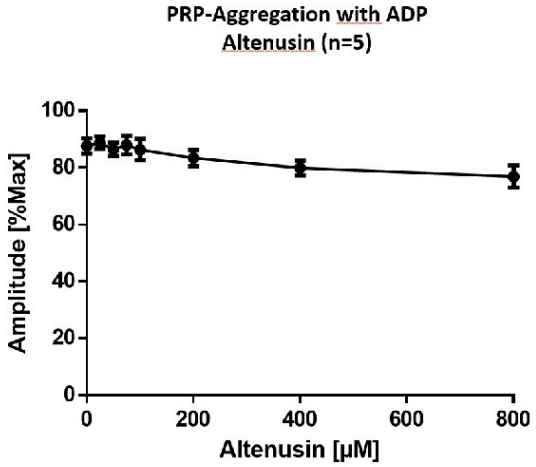

Figure S11. Different altenusin concentrations together with ADP. Error bars display standard deviation

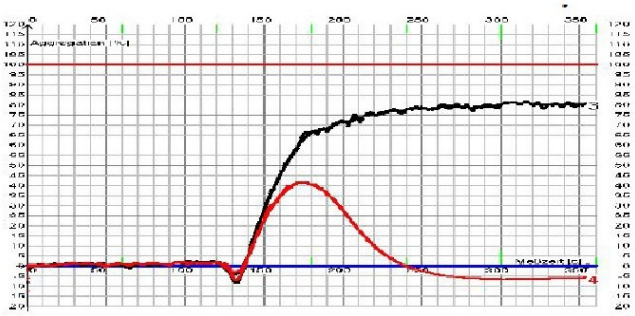

			Agg.	Agg.
Nr.	Comment	Note	Max [%]	Slope [%/min]
EIA 13	10µM TRAP,DMSO	**Control**	81.13	127.19
EIA 14	10µM TRAP,DMSO	**100µM Altenusin**	41.18	102.86

Figure S12. 100µM altenusin concentration together with 10µM TRAP

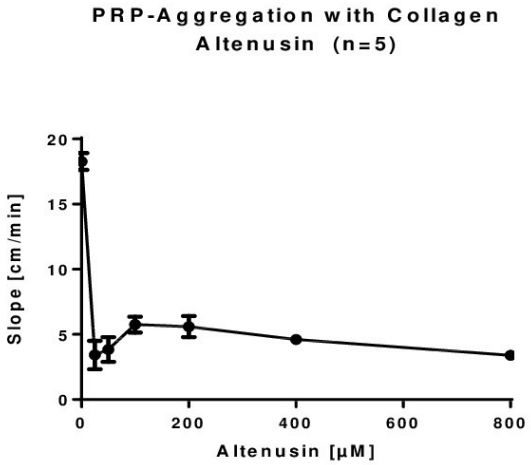

Figure S13. Dose response of collagen induced non washed platelets with altenusin. Error bars display standard deviation

Data of isolated compounds

Mitorubrinol (1): amorphous red solid; $[\alpha]_D$ = -255 (c 0.3, Methanol); UV (MeOH) λ_{max} 218, 262 , 344, 368 nm; ^{1}H NMR (300 MHz, CD_3OD) δ 8.20 (s, 1H), 6.75 (dt, J = 15.8, 4.3 Hz, 1H), 6.58 (s, 1H), 6.44 (dt, J = 15.2, 1.7 Hz, 2H), 6.28 (dd, J = 2.5, 0.8 Hz, 1H), 6.16 (d, J = 2.4 Hz, 1H), 5.67 (d, J = 1.2 Hz, 0H), 4.31 (dd, J = 4.4, 1.9 Hz, 2H), 2.67 (s, 8H), 2.61 (s, 3H), 1.66 (s, 3H); ESI *m/z* 398.9 $[M+H]^+$, 397.1 $[M+H]^-$.

Mitorubrinic acid (2): amorphous red solid; $[\alpha]_D$ = -150 (c 0.2, Methanol); UV (MeOH) λ_{max} 272, 350 nm; ^{1}H NMR (300 MHz, CD_3OD) δ 8.14 (s, 1H), 6.97 (d, J = 15.5 Hz, 5H), 6.72 (s, 1H), 6.61 (d, J = 15.7 Hz, 1H), 6.23 (d, J = 2.3 Hz, 1H), 6.12 (d, J = 2.4 Hz, 1H), 6.06 (q, J = 2.6 Hz, 2H), 2.56 (s, 4H), 1.61 (s, 3H); ESI *m/z* 434.7 $[M+Na]^+$, 410.8 $[M-H]^-$.

Secopenicillide A (3): oily liquid; $[\alpha]_D$ = -65 (c 0.7, $CDCl_3$); UV (MeOH) λ_{max} 216, 284 nm; ^{1}H NMR (600 MHz, $CDCl_3$) δ 7.25 (d, J = 8.9 Hz, 1H), 6.79 (t, J = 2.2 Hz, 2H), 6.52–6.46 (m, 1H), 6.10 (dd, J = 9.3, 4.5 Hz, 1H), 4.59 (s, 2H), 4.03 (d, J = 1.0 Hz, 3H), 3.95 (d, J = 1.0 Hz, 3H), 2.32 (s, 3H), 2.04 (d, J = 1.0 Hz, 3H), 1.74 (td, J = 9.1, 4.6 Hz, 1H), 1.61 (ddd, J = 8.2, 4.2, 1.5 Hz, 1H), 1.47 (ddd, J = 14.0, 8.3, 4.6 Hz, 1H), 0.94 (d, J = 1.9 Hz, 3H), 0.93 (d, J = 2.0 Hz, 3H); ESI *m/z* 443.0 $[M-H]^-$.

Purpactin F (4): oily liquid; $[\alpha]_D$ = -36 (c 0.7, $CDCl_3$); UV (MeOH) λ_{max} 210, 283 nm; ^{1}H NMR (600 MHz, CD_3OD) δ 10.14 (s, 1H), 7.32 (d, J = 8.8 Hz, 1H), 7.27 (d, J = 8.8 Hz, 1H), 7.21 (d, J = 2.1 Hz, 1H), 7.10 (d, J = 2.1 Hz, 1H), 6.88 (d, J = 2.1 Hz, 1H), 6.79 (d, J = 2.1 Hz, 1H), 6.39 – 6.30 (m, 2H), 6.12 (ddd, J = 8.4, 4.9, 3.1 Hz, 2H), 5.35 (s, 1H), 4.00 – 3.97 (m, 7H), 3.95 – 3.91 (m, 7H), 3.23 (d, J = 7.7 Hz, 6H), 2.36 (s, 3H), 2.32 (d, J = 1.7 Hz, 4H), 2.05 (d, J = 1.1 Hz, 8H), 1.79 (ddd, J = 14.1, 8.9, 5.5 Hz, 2H), 1.65 – 1.57 (m, 2H), 1.53 (dddd, J = 13.4, 8.3, 5.0, 3.5 Hz, 3H), 0.98 – 0.94 (m, 15H); ESI *m/z* 412.6 $[M+H]^+$.

Secopenicillid B (5): oily liquid; $[\alpha]_D$ = -54 (c 0.20, $CHCl_3$) ; UV (MeOH) λ_{max} 206, 282, 326 nm; ^{1}H NMR (600 MHz, CD_3OD) δ 10.14 (s, 1H), 7.32 (d, J = 8.8 Hz, 1H), 7.27 (d, J = 8.8 Hz, 1H), 7.21 (d, J = 2.1 Hz, 1H), 7.10 (d, J = 2.1 Hz, 1H), 6.88 (d, J = 2.1 Hz, 1H), 6.79 (d, J = 2.1 Hz, 1H), 6.39 – 6.30 (m, 2H), 6.12 (ddd, J = 8.4, 4.9, 3.1 Hz, 2H), 5.35 (s, 1H), 4.00 – 3.97 (m, 7H), 3.95 – 3.91 (m, 7H), 3.23 (d, J = 7.7 Hz, 6H), 2.36 (s, 3H), 2.32 (d, J = 1.7 Hz, 4H), 2.05 (d, J = 1.1 Hz, 8H), 1.79 (ddd, J = 14.1, 8.9, 5.5 Hz,

2H), 1.65 – 1.57 (m, 2H), 1.53 (dddd, J = 13.4, 8.3, 5.0, 3.5 Hz, 3H), 0.98 – 0.94 (m, 15H); ESI *m/z* 443.0 $[M-H]^+$.

Deoxyfunicone (6): amorphous pale solid; UV (MeOH) λ_{max} 206, 254, 326 nm; ^{1}H NMR (300 MHz, CD_3OD) δ 8.53 (s, 1H), 7.08 (d, J = 1.9 Hz, 1H), 6.82 (d, J = 2.2 Hz, 1H), 6.24 (s, 1H), 5.51 (s, 1H), 3.90 (s, 3H), 3.77 (d, J = 2.6 Hz, 6H), 3.37 (s, 2H), 2.00 – 1.93 (m, 3H), 1.06 – 0.83 (m, 1H); ESI *m/z* 359.1137 $[M+H]^+$.

Purpactin C (7): amorphous yellow solid; $[\alpha]_D$ = -55 (c 0.05, $CDCl_3$); UV (MeOH) λ_{max} 217, 271, 325 nm; ^{1}H NMR (600 MHz, $CDCl_3$) δ 9.50 (s, 1H), 7.64 (d, J = 8.6 Hz, 1H), 7.16 (d, J = 1.4 Hz, 1H), 6.92 (d, J = 8.6 Hz, 1H), 6.24 (d, J = 1.6 Hz, 1H), 4.03 (s, 3H), 2.31 (d, J = 1.6 Hz, 3H), 2.07 (s, 3H), 1.81 – 1.74 (m, 1H), 1.58 – 1.48 (m, 11H), 1.26 (d, J = 8.7 Hz, 3H), 0.94 (t, J = 6.6 Hz, 7H); ESI *m/z* 413.6 $[M+H]^+$.

Bacillisporin B (8): yellowish crystals; $[\alpha]_D$ = +45 (c 0.02, MeOH); UV (MeOH) λ_{max} 206, 231, 322 nm; ^{1}H NMR (300 MHz, DMSO-d_6) δ 11.99 (s, 1H), 11.86 (s, 1H), 9.96 (s, 1H), 6.96 (d, J = 0.9 Hz, 1H), 6.84 (d, J = 0.9 Hz, 1H), 6.23 (d, J = 4.9 Hz, 1H), 5.73 (d, J = 15.1 Hz, 1H), 5.64 (d, J = 15.1 Hz, 1H), 5.14 (d, J = 12.4 Hz, 1H), 4.98 (d, J = 12.3 Hz, 1H), 4.82 (d, J = 1.1 Hz, 1H), 4.77 (dd, J = 4.8, 1.0 Hz, 1H), 3.03 – 2.89 (m, 3H), 2.49 – 2.46 (m, 4H); ESI *m/z* 475.5 $[M+H]^+$.

Altenusin (9): amorphous solid; UV (MeOH) λ_{max} 256, 293 nm; ^{1}H NMR (300 MHz, DMSO-d_6) δ 6.59 (s, 1H), 6.48 (d, J = 2.4 Hz, 1H), 6.44 (d, J = 2.7 Hz, 1H), 6.17 (d, J = 2.8 Hz, 1H), 3.81 (d, J = 1.7 Hz, 3H), 1.91 (s, 3H); ESI *m/z* = 287.4 $[M+H^+]$

Djalonensone (10): amorphous solid; UV (MeOH) λ_{max} 204, 257 nm; ^{1}H NMR (600 MHz, DMSO-d_6) δ 11.85 (s, 1H), 8.45 (s, 2H), 7.26 (d, J = 2.2 Hz, 1H), 6.75 (d, J = 2.6 Hz, 1H), 6.68 (d, J = 2.6 Hz, 1H), 6.65 (d, J = 2.2 Hz, 1H), 3.93 (s, 3H), 2.76 (s, 3H); ESI *m/z* 273.4 $[M+H]^+$.

Alternariol (11): amorphous solid; UV (MeOH) λ_{max} 204, 255, 339 nm; ^{1}H NMR (600 MHz, DMSO-d_6) δ 11.77 (s, 1H), 10.39 (s, 1H), 7.22 (s, 1H), 6.72 (d, J = 2.6 Hz, 1H), 6.64 (d, J = 2.6 Hz, 1H), 6.33 (s, 1H), 2.71 (s, 3H); ESI *m/z* 259.5 $[M+H]^+$.

1,6,10-trihydroxy-8-methyl-2-(3-methylbut-2-en-1-yl)dibenzo[b,e]oxepin-11(6H)-one (12): yellowish crystals; $[\alpha]_D$ = not stable; UV (MeOH) λ_{max} 203, 282, 352 nm; ^{1}H NMR (600 MHz, $CDCl_3$) δ

13.61 (s, 1H), 11.60 – 11.42 (m, 1H), 7.32 (d, J = 8.2 Hz, 1H), 7.04 (d, J = 1.8 Hz, 1H), 6.89 (d, J = 1.7 Hz, 1H), 6.53 (dd, J = 8.1, 1.3 Hz, 1H), 6.13 (s, 1H), 5.31 (ddt, J = 7.3, 6.0, 1.5 Hz, 1H), 3.50 (d, J = 10.7 Hz, 1H), 3.33 (d, J = 7.4 Hz, 2H), 2.40 (d, J = 4.0 Hz, 4H), 1.76 (t, J = 1.3 Hz, 4H), 1.72 (s, 3H); ESI *m/z* 339.2 $[M-H]^+$.

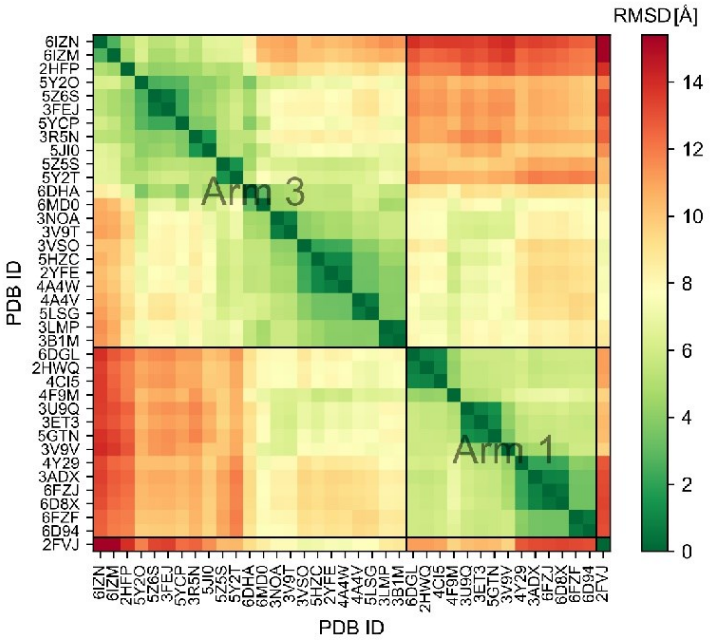

Figure S14. Structural deviations between the binding modes of Altenusin in PPAR-γ. Heatmap of the pairwise root-mean-square deviation (RMSD) of the atomic positions in the heavy atoms of Altenusin. RMSD values are colored from green (RMSD = 0 Å) over yellow (RMSD = 7.5 Å) to red (RMSD = 15 Å). The PDB IDs were ordered after RMSD-based k-Means clustering into three clusters (one for each arm of the binding site).

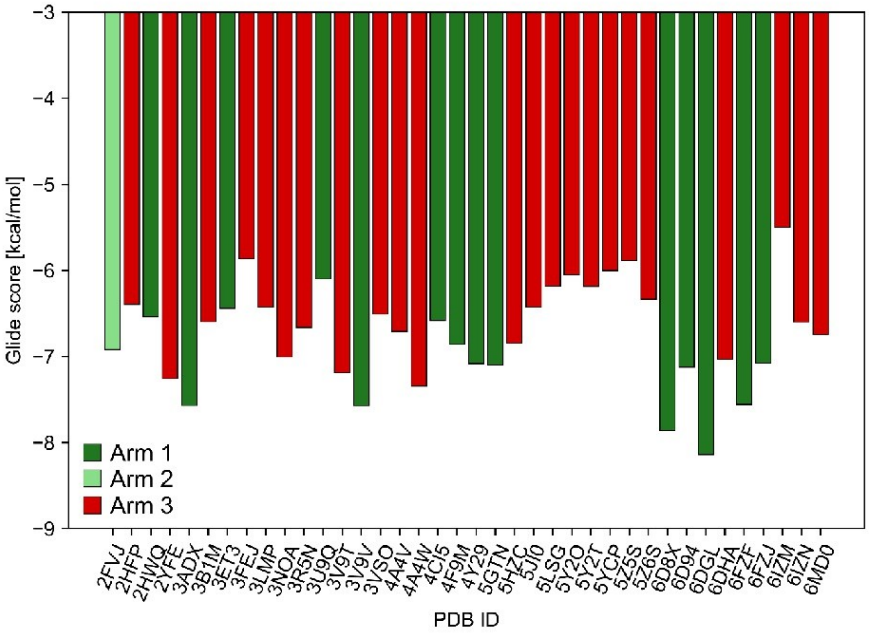

Figure S15. Docking scores of the binding modes of Altenusin in PPAR-γ. Glide scores for each predicted Altenusin-PPAR-γ complex. Bars are colored according to the location of the predicted binding site.

Supplementary Table 1. Structural ensemble of experimentally determined PPAR-γ complexes used for docking of Altenusin

PDB ID	Resolution[a]	Bound ligand(s)
2FVJ	1.99	RO0
2HFP	2.00	NSI
2HWQ	1.97	DRY
2YFE	2.00	YFE
3ADX	1.95	IMN, NRO
3B1M	1.60	KRC
3ET3	1.95	ET1
3FEJ	2.00	CTM
3LMP	1.90	CEK
3NOA	1.98	5BC
3R5N	2.00	MLO, MLO
3U9Q	1.52	DKA
3V9T	1.65	17L
3V9V	1.60	21L
3VSO	2.00	EK1
4A4V	2.00	YFD
4A4W	2.00	YFB
4CI5	1.77	Y1N
4F9M	1.90	FCM
4Y29	1.98	CTI
5GTN	1.85	Q35
5HZC	2.00	65W
5JI0	1.98	BRL, 9CR
5LSG	2.00	QZQ
5Y2O	1.80	8N6
5Y2T	1.70	8LX
5YCP	2.00	BRL
5Z5S	1.80	RTE
5Z6S	1.80	RTF
6D8X	1.90	EDK
6D94	1.90	EDK
6DGL	1.95	GEV
6DHA	1.88	GFV
6FZF	1.95	EDK
6FZJ	2.00	EDK
6IZM	1.80	B0X
6IZN	1.75	B1O
6MD0	1.95	OLA

[a] in Å

6. Publication 2 -Induction of Cryptic Metabolites of the Endophytic Fungus *Trichocladium* sp. through OSMAC and Co-Cultivation

Induction of Cryptic Metabolites of the Endophytic Fungus *Trichocladium sp.* through OSMAC and Co-Cultivation

Published in "Royal Society of Chemistry Advances"

N. M. Tran-Cong, A. Mándi, T. Kurtán, W. E. G. Müller, R. Kalscheuer, W. Lin, Z. Liu and P. Proksch, RSC Adv., 2019, 9, 27279 Published by The Royal Society of Chemistry.

RSC Advances

PAPER

View Article Online
View Journal | View Issue

Check for updates

Cite this: *RSC Adv.*, 2019, **9**, 27279

Induction of cryptic metabolites of the endophytic fungus *Trichocladium* sp. through OSMAC and co-cultivation†

Nam Michael Tran-Cong,[a] Attila Mándi,[b] Tibor Kurtán,[b] Werner E. G. Müller,[c] Rainer Kalscheuer,[a] Wenhan Lin,[d] Zhen Liu*[a] and Peter Proksch*[a]

Received 16th July 2019
Accepted 20th August 2019

DOI: 10.1039/c9ra05469c

rsc.li/rsc-advances

The endophytic fungus *Trichocladium* sp. isolated from roots of *Houttuynia cordata* was cultured on solid rice medium, yielding a new amidepsine derivative (**1**) and a new reduced spiro azaphilone derivative (**3**) together with eight known compounds (**4–11**). Co-cultivation of *Trichocladium* sp. with *Bacillus subtilis* resulted in induction of a further new compound (**2**) and a 10-fold increase of **11** compared to the axenic fungal culture. Moreover, when the fungus was cultivated on peas instead of rice, a new sesquiterpene derivative (**13**) and two known compounds (**12** and **14**) were obtained. Addition of 2% tryptophan to rice medium led to the isolation of a new bismacrolactone (**15**). The structures of the new compounds were elucidated by HRESIMS, 1D and 2D NMR as well as by comparison with the literature. A combination of TDDFT-ECD, TDDFT-SOR, DFT-VCD and DFT-NMR calculations were applied to determine the absolute and relative configurations of **13** and **15**. Compounds **7**, **11** and **15** exhibited strong cytotoxicity against the L5178Y mouse lymphoma cell line with IC_{50} values of 0.3, 0.5 and 0.2 μM, respectively.

Introduction

Paclitaxel, a well-known and widely used anti-cancer compound, was first isolated from the bark of *Taxus brevifolia* by Wani *et al.* in 1971.[1] Later in 1993, Stierle *et al.* discovered that the endophytic fungus *Taxomyces andreanae* from the yew tree is able to produce taxol and other taxane derivatives.[2] This sparked detailed investigations of natural products from endophytes which confirmed these organisms as a promising source of new bioactive compounds.[3] In continuation of our ongoing investigations on bioactive metabolites from fungi,[4–6] an endophytic fungus *Trichocladium* sp. was isolated from roots of the plant *Houttuynia cordata* known in Vietnam as "fish mint". Prior to renaming as *Trichocladium*, *Trichocladium* species have been listed in the literature under the genus *Humicola*.[7] Fungi of the genus *Trichocladium* have been reported to produce several bioactive secondary metabolites including inhibitors of serine proteases of the coagulation pathway, asterriquinones CT1, CT3 and CT4,[8] a cytotoxic phenolic tetralone, humicolone,[9] and inhibitors of human diacylglycerol acyltransferases (DGAT), amidepsines A–K.[10]

In this study, fermentation of *Trichocladium* sp. on solid rice medium yielded ten natural products (**1**, **3–11**) including two new compounds (**1** and **3**). Co-cultivation of *Trichocladium* sp. with *Bacillus subtilis* led to the production of a new compound (**2**) and a 10-fold increase of **11**. In addition, when the fungus was cultivated on peas instead of rice, a new sesquiterpene derivative (**13**) and two known compounds (**12** and **14**) that were not detected when the fungus was grown on rice medium were obtained. Compound **14** is a tryptophan derivative, inspiring us to add 2% tryptophan to rice medium in order to stimulate production of tryptophan derived compounds. Feeding of tryptophan led to the isolation of the new compound **15**, which represents a macrolide linked to an anthranilic acid moiety. The latter moiety is likely to be derived from feeding of tryptophan (Fig. 1).

Results and discussion

Compound **1** was obtained as pale yellow powder. Its molecular formula was determined as $C_{29}H_{27}NO_{13}$ by HREISMS, indicating seventeen degrees of unsaturation. The NMR data of **1** (Table 1) were similar to those of amidepsine J previously isolated from *Humicola* sp. FO-2942.[10] Six aromatic protons at δ_H

[a]*Institute of Pharmaceutical Biology and Biotechnology, Heinrich Heine University Düsseldorf, Universitätsstrasse 1, 40225 Düsseldorf, Germany. E-mail: zhenfeizi0@sina.com; proksch@uni-duesseldorf.de*

[b]*Department of Organic Chemistry, University of Debrecen, P. O. Box 400, H-4002 Debrecen, Hungary*

[c]*Institute of Physiological Chemistry, Universitätsmedizin der Johannes Gutenberg-Universität Mainz, 55128 Mainz, Germany*

[d]*State Key Laboratory of Natural and Biomimetic Drugs, Peking University, Beijing 100191, China*

† Electronic supplementary information (ESI) available: MS, 1D and 2D NMR spectra of compounds **1–3**, **13** and **15** as well as the results of Marfey's reaction and computational calculations. See DOI: 10.1039/c9ra05469c

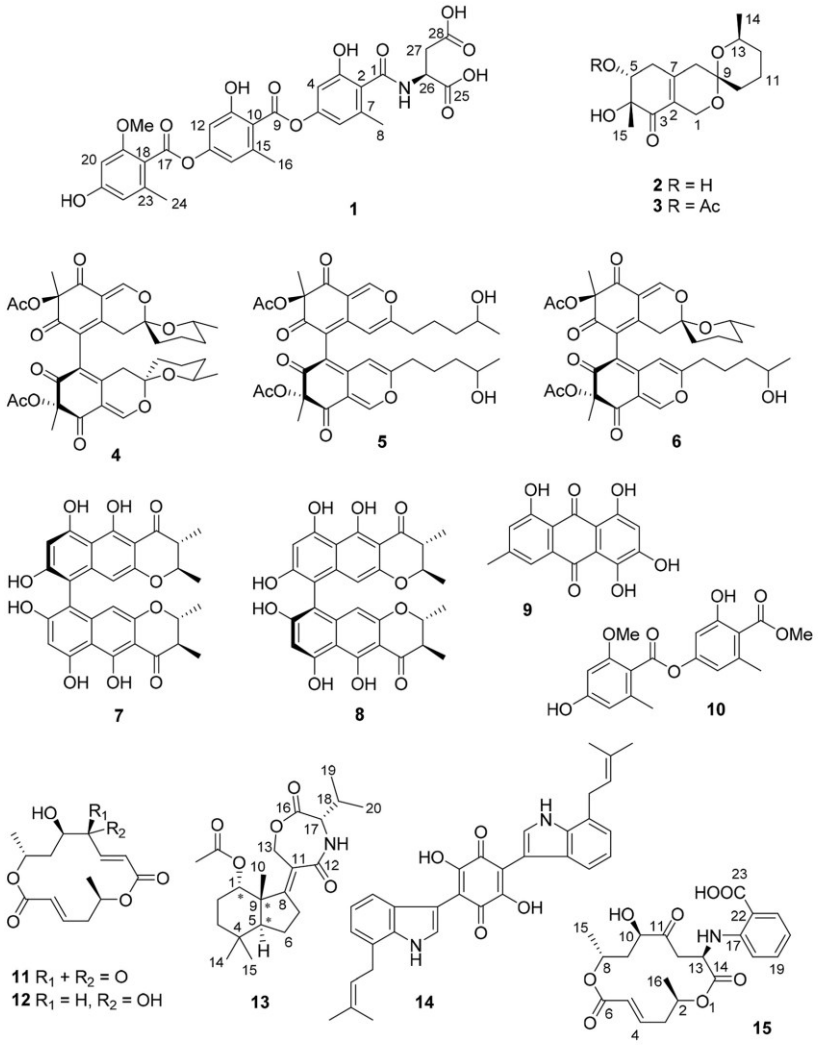

Fig. 1 Structures of isolated compounds from *Trichocladium* sp.

6.66 (H-12), 6.63 (H-14), 6.57 (H-4), 6.54 (H-6), 6.37 (H-20), and 6.31 (H-22) as well as three aromatic methyl groups at δ_H 2.37 (Me-16), 2.28 (Me-24), and 2.24 (Me-8) were observed. However, the NMR spectra of **1** showed signals of only one methoxy group at δ_C 55.8 and δ_H 3.79, instead of two methoxy groups as found for amidepsine J. The position of this methoxy group at C-19 was evident from the ROESY correlations between the protons of this methoxy group and H-20, and between H-20/21-OH (δ_H 9.96), 21-OH/H-22, H-22/Me-24. In addition, signals of a valine moiety were replaced by signals of an aspartic acid moiety (from C-25 to C-28) in **1**. The COSY correlations between 26-NH/H-26/H-27ab and the HMBC correlations from 26-NH to C-1 together with the ROESY correlation between 26-NH and Me-8 indicated the linkage between the aspartic acid moiety and C-1 through an amide bond. The absolute configuration of the aspartic acid moiety was determined after acid hydrolysis of **1** followed by Marfey's method which indicated that the aspartic acid moiety was present in the L-form. Thus, the structure of compound **1** was elucidated as shown, representing a new amidepsine derivative, for which a trivial name amidepsine L is proposed.

The molecular formula of **2** was determined as $C_{15}H_{22}O_5$ based on the HRESIMS data. The NMR data of **2** (Table 2) were

Table 1 ^{1}H and ^{13}C NMR data of compound **1**[a]

Position	δ_C, type[b]	δ_H (J in Hz)
1	166.4, C	
2	123.2, C	
3	155.1, C	
4	106.5, CH	6.57, d (2.1)
5	150.6, C	
6	113.4, CH	6.54, d (2.1)
7	137.7, C	
8	18.9, CH_3	2.24, s
9	165.8, C	
10	118.6, C	
11	156.1, C	
12	107.0, CH	6.66, d (2.0)
13	152.1, C	
14	114.1, CH	6.63, d (2.0)
15	137.8, C	
16	19.2, CH_3	2.37, s
17	165.7, C	
18	112.8, C	
19	158.5, C	
20	97.0, CH	6.37, d (2.0)
21	160.1, C	
22	109.1, CH	6.31, d (2.0)
23	138.0, C	
24	19.4, CH_3	2.28, s
25	172.6, C	
26	48.8, CH	4.69, dt (7.6, 6.6)
27	36.2, CH_2	2.78, dd (16.4, 6.6) 2.61, dd (16.4, 6.6)
28	171.8, C	
11-OH		10.44, s
19-OMe	55.8, CH_3	3.79, s
21-OH		9.96, s
26-NH		8.47, d (7.6)

[a] Measured in DMSO-d_6 (^{1}H at 300 MHz and ^{13}C at 75 MHz). [b] Data were extracted from the HSQC and HMBC spectra.

very similar to those of pestafolide A.[11] However, the smaller coupling constants between H-5 and H-6ab (both 3.5 Hz) in **2** compared to those in pestafolide A (10.0 and 5.8 Hz) suggested that the orientation of H-5 was different in **2**. This was further supported by the ROESY correlations between H-5 (δ_H 3.98)/Me-15 (δ_H 1.30), Me-15/H-6a (δ_H 2.70), and H-6a/H-5, indicating that these protons were on the same face of the cyclohexenone ring. The remaining substructure and stereochemistry of **2** were identical to those of pestafolide A as concluded after detailed analysis of the 2D NMR spectra of **2**. Thus, compound **2** was identified as 5-*epi*-pestafolide A.

Comparison of the ^{1}H and ^{13}C NMR data between **2** and **3** (Table 2) revealed the appearance of an additional acetoxy group (δ_C 170.5 and 21.1, δ_H 2.01) in **2**, which was also evident from the molecular formula of **3** ($C_{17}H_{24}O_6$) being 42 amu larger than that of **2**. The downfield-shifted H-5 signal (δ_H 5.29, dd, J = 3.6, 2.3 Hz) in **3** compared to that in **2** (δ_H 3.98, t, J = 3.5 Hz) suggested the location of this additional acetoxy group at C-5, which was confirmed by the HMBC correlation from H-5 to the carbonyl carbon of the acetoxy group. The coupling constants of H-5 were similar in **2** and **3**, indicating the same stereochemistry at C-5 for **2** and **3**. In conclusion, compound **3** was elucidated as 5-*O*-acetyl-*epi*-pestafolide A. Storage of **2** in EtOAc over one week did not yield **3** indicating that **3** is a true natural product and not an artifact arising from **2** during workup of the extract.

The remaining known compounds isolated from rice medium were identified as cochliodones A (**4**), E (**5**) and H (**6**),[12,13] chateochromin A (**7**),[14] ustilaginoidin D (**8**),[15] 5-hydroxyemodin (**9**),[16] methyl 2-*O*-methyllecanorate (**10**),[17] and colletoketol (**11**).[18–20]

In an OSMAC approach, the medium was changed from rice to peas. Investigation of the fungal culture on pea medium led to the isolation of colletodiol (**12**)[20] and asteriquinone CT4 (**14**)[8] as well as of a new compound (**13**).

Compound **13** was isolated as white amorphous powder. On the basis of the HRESIMS data, the molecular formula of **13** was established as $C_{22}H_{33}NO_5$ with seven degrees of unsaturation. The ^{1}H NMR spectrum (Table 3) of **13** exhibited six methyl groups at δ_H 1.88 (s, 1-OAc), 1.30 (s, Me-10), 1.03 (s, Me-14), 0.99 (s, Me-15), 0.97 (d, Me-20), and 0.95 (d, Me-19) as well as four oxygenated protons at δ_H 4.98 (t, H-1), 4.85 (dt, H-13a), 4.50 (ddd, H-13b), and 4.04 (d, H-17). The COSY correlations between H-1/H-2ab/H-3ab, and between H-5/H-6ab/H-7ab together with the HMBC correlations from Me-10 to C-1, C-5, C-8 and C-9, from Me-14 to C-3, C-4, C-5 and C-15, from H-7ab to C-8 and C-11, and from H-13ab to C-8, C-11 and C-12 established a bicyclic sesquiterpene skeleton (from C-1 to C-15) as shown (Fig. 2). In addition, the HMBC correlations from the protons of the methyl at δ_H 1.88 and H-1 to the carbonyl carbon at δ_C 173.4 indicated the location of an acetoxy group at C-1. The remaining signals suggested the presence of a valine moiety, which was confirmed by the COSY correlations between H-17/H-18/Me-19(20) and the HMBC correlations from H-17 and H-18 to C-16. The above substructures accounted for six degrees of unsaturation, suggesting the presence of an additional ring. In the HMBC spectrum, H-13ab showed correlations to C-16 while H-17 showed a correlation to C-12, indicating the linkage between the sesquiterpene moiety and the valine moiety through ester and amide bonds to form the third seven-membered ring. The relative configuration of the sesquiterpene part was assigned by coupling constants and NOE relationships. The large value of $^{2}J_{H\text{-}2a/H\text{-}3a}$ (13.8 Hz) and the small values of $^{2}J_{H\text{-}1/H\text{-}2a}$ and $^{2}J_{H\text{-}1/H\text{-}2b}$ (both 2.6 Hz) suggested *trans* diaxial orientation of H-2a (δ_H 2.07) and H-3a (δ_H 1.60) and equatorial orientation of H-1. Assuming that H-1 was on the β-face of the cyclohexane ring, H-2a and H-3b (δ_H 1.35) are suggested to be on the β-face of the ring whereas H-2b (δ_H 1.78) and H-3a are orientated on the α-face. The ROESY correlations from Me-10 to H-1, H-2a and Me-15 placed Me-10 on the β-face of the ring whereas the ROESY correlations from H-5 to H-3a and Me-14 placed H-5 on the α-face of the ring. After acid hydrolysis of **13** followed by Marfey's reaction, the valine moiety was determined to have L absolute configuration (17*S*).

In order to elucidate the absolute configuration of the other chirality centers in **13**, the solution TDDFT-ECD method was applied on the (1*S*,5*S*,9*S*,17*S*) and (1*R*,5*R*,9*R*,17*S*) stereoisomers.[21,22] The Merck Molecular Force Field (MMFF) conformational search resulted in 16 and 11 conformers in a 21 kJ mol^{-1}

Table 2 ^{1}H and ^{13}C NMR data of compound **2** and **3**

	2[a]		**3**[b]	
Position	δ_C, type	δ_H (J in Hz)	δ_C, type	δ_H (J in Hz)
1	58.1, CH_2	4.41, d (15.6) 4.01, d (15.6)	57.0, CH_2	4.55, d (15.8) 4.07, d (15.8)
2	127.7, C		126.9, C	
3	200.0, C		197.4, C	
4	77.2, C		74.1, C	
5	75.0, CH	3.98, t (3.5)	74.7, CH	5.29, dd (3.6, 2.3)
6	37.3, CH_2	2.70, dd (18.8, 3.5) 2.44, dd (18.8, 3.5)	34.3, CH_2	2.74, dd (19.5, 3.6) 2.47, dd (19.5, 2.3)
7	149.2, C		147.2, C	
8	41.8, CH_2	2.35, d (18.9) 2.11, d (18.9)	40.8, CH_2	2.30, d (18.9) 2.10, d (18.9)
9	96.4, C		94.9, C	
10	34.9, CH_2	1.69, m 1.54, m	33.8, CH_2	1.70, m 1.51, m
11	20.0, CH_2	1.92, m 1.62, m	18.9, CH_2	1.92, m 1.63, m
12	33.4, CH_2	1.62, m 1.20, m	32.2, CH_2	1.61, m 1.19, m
13	68.2, CH	3.80, m	66.9, CH	3.77, m
14	22.0, CH_3	1.08, d (6.3)	21.7, CH_3	1.09, d (6.4)
15	22.7, CH_3	1.30, s	23.7, CH_3	1.40, s
5-OAc			170.5, C	
			21.1, CH_3	2.01, s

[a] Measured in CD_3OD (^{1}H at 600 MHz and ^{13}C at 150 MHz). [b] Measured in $CDCl_3$ (^{1}H at 600 MHz and ^{13}C at 150 MHz).

Table 3 ^{1}H and ^{13}C NMR data of compound **13**[a]

Position	δ_C, type[b]	δ_H (J in Hz)
1	75.9, CH	4.98, t (2.6)
2	23.1, CH_2	2.07, dddd (15.2, 13.8, 4.2, 2.6) 1.78, dddd (15.2, 4.3, 2.6, 2.6)
3	36.2, CH_2	1.60, ddd (13.8, 13.8, 4.3) 1.35, ddd (13.8, 4.2, 2.6)
4	33.7, C	
5	46.6, CH	1.85, dd (12.6, 1.8)
6	18.8, CH_2	1.97, m 1.66, m
7	22.5, CH_2	2.35, m 2.11, m
8	170.3, C	
9	42.3, C	
10	21.3, CH_3	1.30, s
11	126.3, C	
12	172.4, C	
13	69.9, CH_2	4.85, dt (17.2, 2.8) 4.50, ddd (17.2, 3.6, 1.3)
14	33.6, CH_3	1.03, s
15	21.8, CH_3	0.99, s
16	171.7, C	
17	61.1, CH	4.04, d (7.1)
18	31.0, CH	2.02, m
19	19.5, CH_3	0.95, d (6.8)
20	19.1, CH_3	0.97, d (6.8)
1-OAc	173.4, C	
	22.0, CH_3	1.88, s

[a] Measured in CD_3OD (^{1}H at 600 MHz and ^{13}C at 150 MHz). [b] Data were extracted from the HSQC and HMBC spectra.

energy window, respectively, which were reoptimized separately at the B3LYP/6-31+G(d,p), the ωB97X/TZVP[23,24] PCM/MeCN, the CAM-B3LYP/TZVP[25] PCM/MeCN and the SOGGA11-X/TZVP[24,26] SMD/MeCN levels of theory. Interestingly, Boltzmann-averaged ECD spectra of both diastereomers computed for conformers over 1% Boltzmann-population at various levels of theory gave moderate to good mirror-image agreement with the experimental ECD spectrum of **13** indicating that the seven-membered ring with C-17 chirality center has the major contribution to the ECD spectrum[22] and suggested (17*R*) absolute configuration, opposite to that of the Marfey's analysis. However, while almost all low-energy conformers of (1*S*,5*S*,9*S*,17*S*)-**13** gave similarly mirror-image spectra to the experimental one, for (1*R*,5*R*,9*R*,17*S*)-**13** even highly populated conformers (and the lowest-energy ωB97X/TZVP PCM/MeCN one) gave moderate agreement with the measured ECD and the ratio of the Boltzmann-weights of conformers with congruent and mirror-image spectra is comparable at all applied levels of theory. Although some of the best performing DFT functionals were utilized as suggested by Bremond *et al.* in a recent study,[24] no combination of methods could be found, which would suggest the (1*R*,5*R*,9*R*,17*S*)-**13** absolute configuration. With the result of Marfey's analysis in hand, this demonstrated that the small difference in the two ensembles of conformers, having opposite ECD spectra, could not be predicted properly, which is the reason of the failure. Specific optical rotation (SOR) calculations were also performed for the CAM-B3LYP/TZVP PCM/MeOH conformers but resulting in

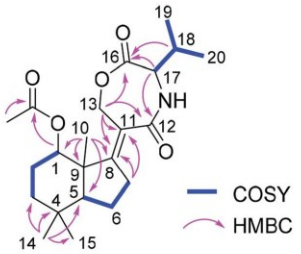

Fig. 2 COSY and key HMBC correlations of **13**.

similarly large negative average values with both levo- and dextrorotating low-energy conformers for both stereoisomers, which did not allow a solid assignment of the absolute configuration. The limited amount of **13** did not allow a VCD measurement. Thus, based on the Marfey's reaction and the ECD results, the structure of **13** was tentatively elucidated as shown, for which a trivial name humigriseamide is proposed.

Asteriquinone CT4 (**14**) is a dimeric tryptophan derivative. In rice approximately 8% of the dry weight consists of proteins whereas the tryptophan content amounts to approximately 1.7% of the total amino acid content.[27] Since peas are much richer in proteins compared to rice (20% *vs.* 8% of the dry weight), we assumed that a higher tryptophan content in peas might be responsible for the formation of **14** during the OSMAC experiment. To test this hypothesis, we added 2% tryptophan to the rice media in order to simulate an excess of tryptophan which resulted in the formation of compound **14** together with another new compound **15** and the known compounds anthranilic acid and *N*-formyl anthranilic acid.

Compound **15** has the molecular formula $C_{21}H_{25}NO_8$ as deduced from the HRESIMS data, corresponding to ten degrees of unsaturation. The ^{1}H and ^{13}C NMR data of **15** (Table 4) were similar to those of the co-isolated bismacrolactone colletoketol (**11**)[18–20] except for the disappearance of signals of the isolated double bond (C-12/C-13) and the presence of additional signals of one methine group (δ_C 49.8 and δ_H 4.57, CH-13), one methylene group (δ_C 41.8 and δ_H 3.16, 2.95, CH_2-12) and of four aromatic protons at δ_H 7.81 (H-21), 7.38 (H-19), 6.69 (H-18) and 6.64 (H-20) in **15**. An anthranilic acid moiety was established by the COSY correlations between H-18/H-19/H-20/H-21 and the HMBC correlations from H-19 to C-17 (δ_C 149.2) and from H-21 to C-17 and C-23 (δ_C 169.7) taking also into account the molecular formula of **15**. In addition, the COSY correlations between H_{ab}-12/H-13/13-NH along with the HMBC correlations from H-12ab to C-11 (δ_C 209.1) and C-14 (δ_C 172.3), from H-13 to C-11, C-14 and C-17, and from 13-NH to C-14 indicated the attachment of the anthranilic acid moiety at C-13 through an amide bond. Detailed analysis of the 2D NMR spectra of **15** revealed that the remaining substructure of **15** was identical to that of colletoketol (**11**). Thus, compound **15** was identified as 13-*N*-(2-carboxyphenyl)colletoketol. Based on the biogenetic relationship and similarity of coupling constants and NOE correlations between **11** and **15**, the stereochemistry at C-2, C-8 and C-10 in **15** was suggested to be identical to that in **11**, where the absolute configuration had been determined by X-ray analysis.[19] In order to confirm this and determine the absolute configuration of the additional C-13 chirality center, the experimental ECD, VCD, ^{13}C NMR chemical shifts and characteristic $^3J_{H,H}$ coupling constants were calculated for the stereoisomers (2*R*,8*R*,10*R*,13*R*)-**15** and (2*R*,8*R*,10*R*,13*S*)-**15**.[28]

Table 4 ^{1}H and ^{13}C NMR data of compound **15**[a]

Position	δ_C, type	δ_H (*J* in Hz)
2	71.2, CH	4.68, ddq (11.9, 2.7, 6.1)
3	37.1, CH_2	2.49, ddd (11.9, 8.0, 2.7)
		2.33, td (11.9, 8.0)
4	143.6, CH	6.67, dt (15.8, 8.0)
5	125.1, CH	5.77, d (15.8)
6	164.5, C	
8	65.2, CH	5.08, ddq (11.3, 1.9, 6.3)
9	38.4, CH_2	2.17, dd (14.2, 11.2)
		1.96, ddd (14.2, 7.5, 1.9)
10	73.0, CH	4.03, d (7.5)
11	209.1, C	
12	41.8, CH_2	3.16, dd (18.8, 6.0)
		2.95, dd (18.8, 2.0)
13	49.8, CH	4.57, ddd (7.1, 6.0, 2.0)
14	172.3, C	
15	20.0, CH_3	1.17, d (6.3)
16	20.5, CH_3	1.29, d (6.1)
17	149.2, C	
18	111.4, CH	6.69, br d (7.9)
19	134.5, CH	7.38, td (7.9, 1.6)
20	115.5, CH	6.64, br t (7.9)
21	131.9, CH	7.81, dd (7.9, 1.6)
22	111.2, C	
23	169.7, C	
13-NH		8.13, d (7.1)

[a] Measured in DMSO-d_6 (^{1}H at 600 MHz and ^{13}C at 150 MHz).

The MMFF conformational search of (2*R*,8*R*,10*R*,13*R*)-**15** and (2*R*,8*R*,10*R*,13*S*)-**15** resulted in 197 and 246 conformers, respectively, which were reoptimized at the B3LYP/6-31+G(d,p), the B3LYP/TZVP PCM/$CHCl_3$, the ωB97X/TZVP PCM/MeCN and the mPW1PW91/6-311+(2d,p) SMD/$CHCl_3$ levels of theory, separately. ^{13}C NMR shift calculations performed both at the mPW1PW91/6-311+(2d,p) *in vacuo* and the mPW1PW91/6-311+(2d,p) SMD/$CHCl_3$ levels for the B3LYP/6-31+G(d,p) conformers gave similar results for the two stereoisomers indicating no preference of any of the two diastereomers.[29,30] The ωB97X/TZVP PCM/MeCN conformers (>1%) of (2*R*,8*R*,10*R*,13*R*)-**15** and (2*R*,8*R*,10*R*,13*S*)-**15** showed different conformations for the macrolactone ring, which was also manifested in the dihedral angles $\omega_{H\text{-}13,C\text{-}13,C\text{-}12,H\text{-}12ab}$ and $\omega_{H\text{-}13,C\text{-}13,NH}$. Thus the coupling constants $^3J_{H\text{-}13,NH}$, $^3J_{H\text{-}12a,H\text{-}13}$ and $^3J_{H\text{-}12b,H\text{-}13}$ were selected for calculations, for which 7.1, 6.0 and 2.0 Hz values were measured, respectively. The computed coupling constants of (2*R*,8*R*,10*R*,13*R*)-**15** gave consistently better agreement with the experimental values than those of (2*R*,8*R*,10*R*,13*S*)-**15**, which had systematically larger values (Table 5). The largest and decisive difference could be observed for 6.0 Hz $^3J_{H\text{-}12a,H\text{-}13}$ experimental value, which was calculated 5.5 Hz for (2*R*,8*R*,10*R*,13*R*)-**15** and 11.2 Hz for (2*R*,8*R*,10*R*,13*S*)-

Table 5 Comparison of characteristic experimental and computed [mPW1PW91/6-311+G(2d,p)//B3LYP/6-31+G(d,p)] $^3J_{H,H}$ coupling constants of **15**

	$^3J_{H\text{-}13,NH}$	$^3J_{H\text{-}12a,H\text{-}13}$	$^3J_{H\text{-}12b,H\text{-}13}$
Experimental	7.1	6.0	2.0
(2*R*,8*R*,10*R*,13*R*)-**15**	8.6	5.5	2.9
(2*R*,8*R*,10*R*,13*S*)-**15**	9.2	11.2	4.1

15. H-13 and H-12a had *gauche* orientation in (2*R*,8*R*,10*R*,13*R*)-**15** with small $\omega_{H\text{-}13,C\text{-}13,C\text{-}12,H\text{-}12a}$ dihedral angles and coupling constants, while H-13 and H-12a had near *trans-periplanar* arrangement in the computed conformers of (2*R*,8*R*,10*R*,13*S*)-**15**, which gave rise to large coupling constant (11.2 Hz). The computed $^3J_{H,H}$ coupling constants clearly suggested that **15** has (2*R**,8*R**,10*R**,13*R**) relative configuration.

^{13}C NMR shifts were also computed for the mPW1PW91/6-311+(2d,p) SMD/$CHCl_3$ conformers at the same level and although this level gave worse agreement for both stereoisomers because of the rather limited number of compounds utilized for the NMR parameter generation,[31] it gave considerably better agreement for (2*R*,8*R*,10*R*,13*R*)-**15** than for (2*R*,8*R*,10*R*,13*S*)-**15** in line with the result of the coupling constant calculations. ECD calculations performed at various levels for the B3LYP/6-31+G(d,p) and the ωB97X/TZVP PCM/MeCN conformers gave similarly good agreement for both stereoisomers verifying the (2*R*,8*R*,10*R*) absolute configuration of the three stereocenters but giving no information about the C-10 chirality center (Fig. 3 and 4). However, with the combination of the (2*R**,8*R**,10*R**,13*R**) relative configuration from the coupling constants and (2*R*,8*R*,10*R*) absolute configuration from the ECD calculations allowed determining the (2*R*,8*R*,10*R*,13*R*) absolute configuration for **15**. VCD measurement and calculations were also carried out to check whether it can differentiate between the (2*R*,8*R*,10*R*,13*R*) and (2*R*,8*R*,10*R*,13*S*) stereoisomers independently from other methods (Fig. 5). VCD calculations performed on the B3LYP/TZVP PCM/$CHCl_3$ conformers at the same level gave acceptable agreement for both stereoisomers with a slight preference for the (2*R*,8*R*,10*R*,13*R*) stereoisomer. Similarity indexes (ESI†)[32] computed with the CDSpecTech package[33,34] gave considerably higher number (0.335 and a confidence level of 85.4%) for this stereoisomer than for (2*R*,8*R*,10*R*,13*S*)-**15** (0.128). Although this ESI† number is below the limit that Covington and Polavarapu suggested for a safe elucidation of configuration with VCD,[34] similarly to the ECD calculations it allowed determining the absolute configuration of **15** as (2*R*,8*R*,10*R*,13*R*) when combined with the result of the coupling constant calculations.

All compounds except for compounds **9** and **14** due to their low amounts were submitted to a cytotoxicity assay using the L5178Y mouse lymphoma cell line and to antimicrobial assay against *Mycobacterium tuberculosis*, *Staphylococcus aureus*,

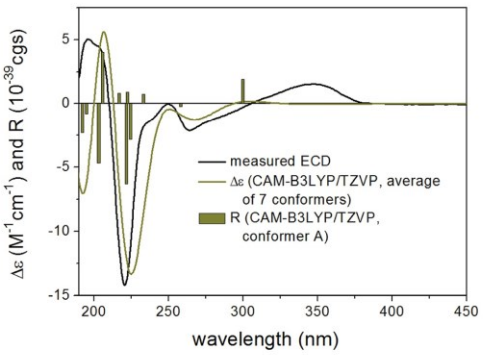

Fig. 4 Experimental ECD spectrum of **15** in MeCN compared with the Boltzmann-weighted CAM-B3LYP/TZVP PCM/MeCN ECD spectrum of (2*R*,8*R*,10*R*,13*S*)-**15**. Level of optimization: ωB97X/TZVP PCM/MeCN. Bars represent the rotatory strength values of the lowest-energy conformer.

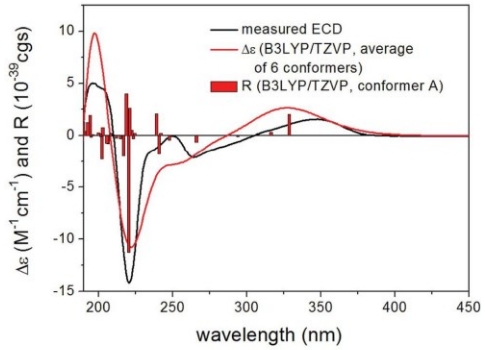

Fig. 3 Experimental ECD spectrum of **15** in MeCN compared with the Boltzmann-weighted B3LYP/TZVP PCM/MeCN ECD spectrum of (2*R*,8*R*,10*R*,13*R*)-**15**. Level of optimization: ωB97X/TZVP PCM/MeCN. Bars represent the rotatory strength values of the lowest-energy conformer.

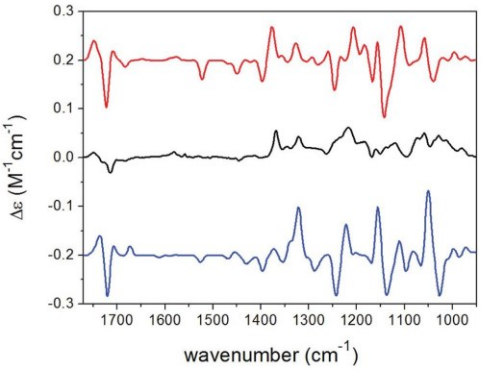

Fig. 5 Experimental VCD spectrum (black line) of **15** in $CDCl_3$ compared with the Boltzmann-weighted B3LYP/TZVP PCM/$CHCl_3$ VCD spectra of (2*R*,8*R*,10*R*,13*R*)-**15** (red line) and (2*R*,8*R*,10*R*,13*S*)-**15** (blue line).

Enterococcus faecalis, *Acinetobacter baumannii*, *Pseudomonas aeruginosa* and *Escherichia coli*. Chateochromin A (**7**), colletoketol (**11**) and the new compound **15** exhibited strong cytotoxicity with IC_{50} values of 0.3, 0.5 and 0.2 μM, respectively. Only chateochromin A (**7**) showed antibacterial activity against *E. faecalis* with an MIC value of 6.3 μM. The remaining compounds were inactive when tested at a dose of 10 μM.

In conclusion, an axenic fermentation of *Trichocladium* sp. on rice medium yielded ten natural products including two new compounds (**1** and **3**). Co-cultivation of the fungus with *B. subtilis* led to the production of a further new compound (**2**) and a 10-fold increase of **11**. The latter compound is known as a weak broad-spectrum antibiotic,[20] implying a possible defense reaction of the fungus against *B. subtilis*. A switch from solid rice to peas as medium for fungal cultivation resulted in the production of an additional new compound **13**, representing a sesquiterpene connected with an amino acid. In addition, a dimeric tryptophan derivative **14** was isolated. These results indicate that a protein rich medium such as peas induces the accumulation of different compounds compared to a carbohydrate rich medium like rice. Addition of tryptophan to the rice medium which was done trying to mimic the higher protein content of peas *vs.* rice caused the accumulation of the new compound **15** which in addition to colletoketol (**11**) includes anthranilic acid, the latter probably being a fungal biotransformation product of added tryptophan.[35]

Experimental section

General experimental procedures

Optical rotations were measured on a PerkinElmer-241 MC polarimeter. ECD spectra were recorded on a J-810 spectropolarimeter. VCD measurements were performed on a BioTools ChiralIR-2X spectrometer at a resolution of 4 cm^{-1} under ambient temperature for 18 × 3000 scans, respectively. Sample was dissolved in $CDCl_3$ at a concentration of 0.095 M (**15**), and the solution was placed in a 100 μm BaF_2 cell. NMR spectra were recorded on Bruker ARX 300 or AVANCE DMX 600 NMR spectrometers. Mass spectra were obtained from a Finnigan LCQ Deca XP mass spectrometer while high resolution mass spectra were recorded on a FTHRMS-Orbitrap (Thermo-Finnigan) mass spectrometer. A Dionex P580 system was used in combination with a diode array detector (UVD340S) and an Eurosphere 10 C_{18} column (125 × 4 mm) for HPLC analysis and recording UV spectra. Semi-preparative HPLC was conducted on a Lachrom-Merck Hitachi system (pump L7100, UV detector L7400, Eurospher 100 C_{18} column, 300 × 8 mm, Knauer Germany). Sephadex-LH20 and Merck MN silica gel 60M (0.04–0.063 mm) were used as stationary phases for column chromatography. TLC plates precoated with silica gel 60 F254 were used for monitoring separation. For spectroscopic measurements spectral grade solvents were used.

Fungal material

Houttuynia cordata was grown in a local garden at Willich, Germany. The identification of the plant used in this study was performed by Dr Marc Appelhans (Department of Systematics, Biodiversity and Evolution of Plants with Herbarium, Göttingen University). A voucher specimen of the plant (code GOET038305) has been deposited in Göttingen University Herbarium. Fresh roots were harvested in April 2016 and washed with sterilized water, surface sterilized with 70% ethanol for 1 min, and cut into small pieces (around 1 × 1 × 1 cm) using a flame sterilized blade. These pieces were put on malt agar plates (15 g L^{-1} malt extract, 15 g L^{-1} agar, and 0.2 g L^{-1} chloramphenicol in distilled water, pH 7.4–7.8 with sodium hydroxide or hydrochloric acid), and then incubated at room temperature for several days. A fungus that was growing out from the root segments was identified as *Trichocladium* sp. using a molecular protocol as described previously.[36] Sequence data were submitted to GenBank with the accession number MK241585. A voucher strain (code HCRSW) is kept in the Institute of Pharmaceutical Biology and Biotechnology, Heinrich-Heine University, Düsseldorf, Germany. After surface sterilization we also imprinted the surface sterilized roots on agar plates. Following incubation of these agar plates no fungal growth was detected which proofs that the fungus is an endophyte and not an exophyte.

Fermentation and co-cultivation

Fermentation of the fungus was conducted in 11 Erlenmeyer flasks on solid rice medium (100 g rice in 110 mL water followed by autoclaving) at 20 °C at static conditions. After 33 days each flask was extracted with 600 mL EtOAc. The rice medium was cut into small pieces and shaken for 8 hours followed by evaporation of EtOAc.

Co-cultivation experiment with *Bacillus subtilis* (ATCC168) was conducted on solid rice medium. A total of 15 flasks was prepared (5 axenic fungal cultures as controls, 5 co-cultures with bacteria and 5 axenic bacterial cultures as controls). After addition of 10 mL bacteria solution to each flask, the flasks were incubated at 30 °C for three days. Then a constant number of pieces from agar plates containing *Trichocladium* sp. were transferred to the co-culture flasks. All flasks were inoculated at 20 °C under static conditions. After 33 days 600 mL EtOAc was added to each flask in order to terminate the cultivation.

OSMAC experiments

In addition to rice, peas (*Pisum sativum*, from Müllers Mühle, Germany) were used as medium (100 g of peas in 110 mL of H_2O followed by autoclaving). The cultivation procedure was the same as described for cultivation on rice medium. For the feeding experiment using tryptophan, the rice medium was spiked with 2% tryptophan prior to autoclaving.

Extraction and isolation

The crude extract (12 g) obtained from axenic fungal rice cultures was subjected to silica gel vacuum liquid chromatography (VLC) using a step gradient of *n*-hexane/EtOAc and CH_2Cl_2/MeOH to give 11 fractions (V1–V11). Fraction V4 (4.6 g) was further fractionated by reversed phase vacuum liquid chromatography using a step gradient of H_2O and MeOH to yield 10 subfractions (V4RP1–V4PR10). Subfraction V4RP5 was subjected to

a Sephadex LH-20 column using MeOH as eluent followed by purification by semi-preparative HPLC using 55% MeOH–H_2O to give **1** (6.4 mg), **9** (1.2 mg) and **11** (4.5 mg). Following a similar procedure as described for V4RP5, **3** (2.4 mg) and **5** (5.2 mg) were isolated from subfraction V4RP6. Compounds **4** (5.4 mg) and **10** (6.4 mg) were isolated from subfraction V4RP7, while **8** (6.8 mg) was obtained from subfraction V4RP9. Compounds **6** (2.8 mg) and **7** (3.2 mg) were obtained from fractions V6 and V9, respectively, after separation by Sephadex LH-20 column chromatography with MeOH as eluent.

The chromatographic work up of the OSMAC extracts followed the same procedure as described for the axenic rice cultures. Silica gel vacuum liquid chromatography using a step gradient of *n*-hexane/EtOAc and CH_2Cl_2/MeOH was used for separation of the crude extracts obtained from co-cultivation, pea medium and rice medium with addition of tryptophan. A total of ten fractions (CV1–CV10) was obtained from the co-culture extract. Fraction CV4 (2.4 g) was separated by a Sephadex LH-20 column with MeOH as mobile phase followed by purification using semi-preparative HPLC with 45% MeOH–H_2O as eluting system to afford **2** (4.3 mg). The pea culture yielded nine subfractions (PV1–PV9) after VLC. Compounds **12** (6.4 mg) and **13** (5.4 mg) were isolated from fraction PV6, while **14** (0.5 mg) was obtained from fraction PV9 by semi-preprative HPLC using a gradient of MeOH–H_2O (from 10 : 90 to 90 : 10).

Fraction TV6 (854 mg) was obtained from rice medium after addition of tryptophan. The fraction was submitted to silica gel VLC and purified using reversed phase VLC and a step gradient of H_2O and MeOH to give **15** (22.5 mg).

Amidepsine L (1). Pale yellow powder; $[\alpha]_D$ = +50 (*c* 0.2, MeOH); UV (MeOH) λ_{max} 255 and 213 nm; ^{1}H and ^{13}C NMR data see Table 1; HRESIMS *m*/*z* 620.1370 $[M + Na]^+$ (calcd for $C_{29}H_{27}NO_{13}Na$, 620.1375).

5-Epi-pestafolide A (2). White amorphous solid; $[\alpha]_D = -55$ (*c* 0.05 CH_3OH); UV (MeOH) λ_{max} 248 nm; ^{1}H and ^{13}C NMR data see Table 2; HRESIMS *m*/*z* 283.1544 $[M + H]^+$ (calcd for $C_{15}H_{23}O_5$, 283.1540).

5-*O*-Acetyl-*epi*-pestafolide A (3). White amorphous solid; $[\alpha]_D$ = −51 (*c* 0.05 MeOH); UV (MeOH) λ_{max} 246 nm; ^{1}H and ^{13}C NMR data see Table 2; HRESIMS *m*/*z* 325.1651 $[M + H]^+$ (calcd for $C_{17}H_{25}O_6$, 325.1646).

Humigriseamide (13). White amorphous solid; $[\alpha]_D$ = +34 (*c* 0.05, MeOH); UV (MeOH) λ_{max} 216 nm; ECD (MeCN, λ [nm] ($\Delta\varepsilon$), *c* 0.128 mM): 289sh (+0.04), 243 (+0.47), 212 (−2.33), 191sh (−2.33); ^{1}H and ^{13}C NMR data see Table 3; HRESIMS *m*/*z* 392.2433 $[M + H]^+$ (calcd for $C_{22}H_{34}NO_5$, 392.2431).

13-*N*-(2-Carboxyphenyl)colletoketol (15). Light red oil; $[\alpha]_D$ = −50 (*c* 0.05, $CHCl_3$); UV (MeOH) λ_{max} 348, 252 and 214 nm; ECD (MeCN, λ [nm] ($\Delta\varepsilon$), *c* 0.075 mM): 348 (+1.56), 264 (−2.11), 237sh (−1.41), 220 (−14.20), 203sh (+4.49), 196 (+5.02); ^{1}H and ^{13}C NMR data see Table 4; HRESIMS *m*/*z* 420.1660 $[M + H]^+$ (calc. for $C_{21}H_{26}NO_8$ 420.1653).

Marfey's analysis

Marfey's analysis was conducted following a previously described protocol.[37] Acid hydrolysis of the isolated compounds **1** and **13** was conducted using 0.2 mg of each compound. After addition of 2 mL of 6 N HCl and incubation for 24 h at 110 °C, the acid was removed by drying under a nitrogen stream. 50 μL of each sample was treated with 100 μL of FDNPL (1% *N*-(5-fluoro-2,4-dinitrophenyl)-L-leucin amide) in acetone together with 20 μL 1 M $NaHCO_3$. Then the mixtures were incubated at 40 °C for 1 h under constant mixing. Next 10 μL of 2 N HCL was added to each vial followed by evaporation to dryness. For injection to HPLC, 1 mL MeOH was added to each vial. L- and D-amino acids which were used as standards were treated in the same manner. Analysis of the derivatized amino acids was performed by comparing their retention times with those of standards.

Computational methods

Mixed torsional/low-mode conformational searches were carried out by means of the Macromodel 10.8.011 software using the MMFF with an implicit solvent model for $CHCl_3$ applying a 21 kJ mol^{-1} energy window.[38] Geometry reoptimizations of the resultant conformers [B3LYP/6-31+G(d,p) level *in vacuo*, B3LYP/TZVP PCM/$CHCl_3$, ωB97X/TZVP and CAM-B3LYP/TZVP with PCM solvent model for MeCN, SOGGA11-X/TZVP SMD/MeCN and mPW1PW91/6-311+G(2d,p) SMD/$CHCl_3$] and DFT VCD, TDDFT ECD and SOR calculations were performed with Gaussian 09 for ECD and SOR using various functionals (B3LYP, BH&HLYP, CAM-B3LYP, PBE0) and the TZVP basis set with the same or no solvent model as in the preceding DFT optimization step.[39] ECD spectra were generated as the sum of Gaussians with 3000 cm^{-1} half-height widths, using dipole-velocity-computed rotational strengths.[40] VCD spectra were calculated with 8 cm^{-1} half-height width and scaled by a factor of 0.98.[41] Boltzmann distributions were estimated from the B3LYP, ωB97X, CAM-B3LYP, SOGGA11-X and mPW1PW91 energies. ESI† values were computed with the CDSpecTech 22.0 software package.[32–34] The MOLEKEL program was used for visualization of the results.[42]

Cytotoxicity assay

Cytotoxicity against the L51178Y mouse lymphoma cell line was measured using the MTT assay.[43] Kahalalide F and 0.1% ethylene glycol monomethyl ether in DMSO were used as positive and negative control, respectively.

Antimicrobial assay

Antimicrobial activity of the compounds was conducted using the microdilution method. Compounds were dissolved in DMSO and added to the broth. The resulting final DMSO concentration in the assay was 0.1%. The direct colony suspension method was employed for preparation of the inoculum, and MIC values for each strain were determined according to the recommendations of the Clinical and Laboratory Standards.[44] Two known antibiotics, ciprofloxacin and moxifloxacin (analytical standard, Sigma-Aldrich) were used as positive controls.

Conflicts of interest

There are no conflicts to declare.

Acknowledgements

This project was funded by the Deutsche Forschungsgemeinschaft (project number 270650915, GRK 2158). Further support by the Manchot Foundation to P. P. is gratefully acknowledged. The Hungarian authors were supported by the EU and co-financed by the European Regional Development Fund under the project GINOP-2.3.2-15-2016-00008. T. K. and A. M. thank the National Research, Development and Innovation Office (NKFI K120181 and PD121020). The Governmental Information-Technology Development Agency (KIFÜ) is acknowledged for CPU time. We furthermore wish to thank Dr Marc Appelhans (Department of Systematics, Biodiversity and Evolution of Plants with Herbarium, Göttingen University, Germany) for identification of the plant material.

References

1 M. C. Wani, H. L. Taylor, M. E. Wall, P. Coggon and A. T. McPhail, *J. Am. Chem. Soc.*, 1971, **93**, 2325–2327.
2 A. Stierle, G. Strobel and D. Stierle, *Science*, 1993, **260**, 214–216.
3 A. H. Aly, A. Debbab and P. Proksch, *Pharmazie*, 2013, **68**, 499–505.
4 S. Liu, H. Dai, G. Makhloufi, C. Heering, C. Janiak, R. Hartmann, A. Mándi, T. Kurtán, W. E. Müller, M. U. Kassack, W. Lin, Z. Liu and P. Proksch, *J. Nat. Prod.*, 2016, **79**, 2332–2340.
5 H. Wang, H. F. Dai, C. Heering, C. Janiak, W. H. Lin, R. S. Orfali, W. E. G. Müller, Z. Liu and P. Proksch, *RSC Adv.*, 2016, **6**, 81685–81693.
6 H. Wang, P. M. Eze, S. P. Höfert, C. Janiak, R. Hartmann, F. B. C. Okoye, C. O. Esimone, R. S. Orfali, H. F. Dai, Z. Liu and P. Proksch, *RSC Adv.*, 2018, **8**, 7863–7872.
7 X. W. Wang, F. Y. Yang, M. Meijer, B. Kraak, B. D. Sun, Y. L. Jiang, Y. M. Wu, F. Y. Bai, K. A. Seifert, P. W. Crous, R. A. Samson and J. Houbraken, *Stud. Mycol.*, 2018, **93**, 65–153.
8 U. Mocek, L. Schultz, T. Buchan, C. Baek, L. Fretto, J. Nzerem, L. Sehl and U. Sinha, *J. Antibiot.*, 1996, **49**, 854–859.
9 D. Laurent, G. Guella, I. Mancini, M. F. Roquebert, F. Farinole and F. Pietra, *Tetrahedron*, 2002, **58**, 9163–9167.
10 J. Inokoshi, Y. Takagi, R. Uchida, R. Masuma, S. Omura and H. Tomoda, *J. Antibiot.*, 2010, **63**, 9–16.
11 G. Ding, S. Liu, L. Guo, Y. Zhou and Y. Che, *J. Nat. Prod.*, 2008, **71**, 615–618.
12 N. Phonkerd, S. Kanokmedhakul, K. Kanokmedhakul, K. Soytong, S. Prabpai and P. Kongsearee, *Tetrahedron*, 2008, **64**, 9636–9645.
13 F. X. Yu, Y. Chen, Y. H. Yang and P. J. Zhao, *Phytochem. Lett.*, 2016, **16**, 263–267.
14 K. Koyama, S. Natori and Y. Iitaka, *Chem. Pharm. Bull.*, 1987, **35**, 4049–4055.
15 K. Koyama and S. Natori, *Chem. Pharm. Bull.*, 1988, **36**, 146–152.
16 N. Morooka, S. Nakano, N. Itoi and Y. Ueno, *Agric. Biol. Chem.*, 1990, **54**, 1247–1252.
17 J. Elix and L. Lajide, *Aust. J. Chem.*, 1981, **34**, 2005–2011.
18 J. MacMillan and T. J. Simpson, *J. Chem. Soc., Perkin Trans. 1*, 1973, 1487–1493.
19 U. Höller, A. D. Wright, G. M. König and P. G. Jones, *Acta Crystallogr., Sect. C: Cryst. Struct. Commun.*, 1999, **55**, 1310–1313.
20 T. J. Hunter and G. A. O'Doherty, *Org. Lett.*, 2002, **4**, 4447–4450.
21 S. Superchi, P. Scafato, M. Gorecki and G. Pescitelli, *Curr. Med. Chem.*, 2018, **25**, 287–320.
22 A. Mándi, I. W. Mudianta, T. Kurtán and M. J. Garson, *J. Nat. Prod.*, 2015, **78**, 2051–2056.
23 J. D. Chai and M. Head-Gordon, *J. Chem. Phys.*, 2008, **128**, 084106.
24 É. Brémond, M. Savarese, N. Q. Su, Á. J. Pérez-Jiménez, X. Xu, J. C. Sancho-García and C. Adamo, *J. Chem. Theory Comput.*, 2016, **12**, 459–465.
25 T. Yanai, D. P. Tew and N. C. Handy, *Chem. Phys. Lett.*, 2004, **393**, 51–57.
26 R. Peverati and D. G. Truhlar, *J. Chem. Phys.*, 2011, **135**, 191102.
27 V. W. Padhye and D. K. Salunkhe, *Cereal Chem.*, 1979, **56**, 389–393.
28 A. Mándi and T. Kurtán, *Nat. Prod. Rep.*, 2019, **36**, 889–918.
29 M. W. Lodewyk, M. R. Siebert and D. J. Tantillo, *Chem. Rev.*, 2012, **112**, 1839–1862.
30 CHESHIRE CCAT, *The Chemical Shift Repository for computed NMR scaling factors*, http://cheshirenmr.info/index.htm.
31 S. Qiu, E. de Gussem, K. A. Tehrani, S. Sergeyev, P. Bultinck and W. Herrebout, *J. Med. Chem.*, 2013, **56**, 8903–8914.
32 E. Debie, E. de Gussem, R. K. Dukor, W. Herrebout, L. A. Nafie and P. Bultinck, *ChemPhysChem*, 2011, **12**, 1542–1549.
33 C. L. Covington and P. L. Polavarapu, *CDSpecTech: Computer programs for calculating similarity measures of comparison between experimental and calculated dissymmetry factors and circular intensity differentials, version 22.0*, 2017, https://sites.google.com/site/cdspectech1/.
34 C. L. Covington and P. L. Polavarapu, *Chirality*, 2017, **29**, 178–192.
35 C. K. Wat and G. H. N. Towers, in *Biochemistry of plant phenolics. Recent advances in phytochemistry*, ed. T. Swain, J. B. Harbone and C. F. Van Sumere, Springer, Boston, MA, 1979, vol 12, Metabolism of the aromatic amino acids by fungi, pp. 371–432.
36 J. Kjer, A. Debbab, A. H. Aly and P. Proksch, *Nat. Protoc.*, 2010, **5**, 479–490.
37 P. Marfey, *Carlsberg Res. Commun.*, 1984, **49**, 591.
38 *MacroModel*, Schrödinger, LLC, 2015, https://www.schrodinger.com/MacroModel.

39 M. J. Frisch, G. W. Trucks, H. B. Schlegel, G. E. Scuseria, M. A. Robb, J. R. Cheeseman, G. Scalmani, V. Barone, B. Mennucci, G. A. Petersson, H. Nakatsuji, M. Caricato, X. Li, H. P. Hratchian, A. F. Izmaylov, J. Bloino, G. Zheng, J. L. Sonnenberg, M. Hada, M. Ehara, K. Toyota, R. Fukuda, J. Hasegawa, M. Ishida, T. Nakajima, Y. Honda, O. Kitao, H. Nakai, T. Vreven, J. A. Montgomery Jr, J. E. Peralta, F. Ogliaro, M. Bearpark, J. J. Heyd, E. Brothers, K. N. Kudin, V. N. Staroverov, R. Kobayashi, J. Normand, K. Raghavachari, A. Rendell, J. C. Burant, S. S. Iyengar, J. Tomasi, M. Cossi, N. Rega, J. M. Millam, M. Klene, J. E. Knox, J. B. Cross, V. Bakken, C. Adamo, J. Jaramillo, R. Gomperts, R. E. Stratmann, O. Yazyev, A. J. Austin, R. Cammi, C. Pomelli, J. W. Ochterski, R. L. Martin, K. Morokuma, V. G. Zakrzewski, G. A. Voth, P. Salvador, J. J. Dannenberg, S. Dapprich, A. D. Daniels, Ö. Farkas, J. B. Foresman, J. V. Ortiz, J. Cioslowski and D. J. Fox, *Gaussian 09 (Revision E.01)*, Gaussian, Inc., Wallingford, CT, 2013.
40 P. J. Stephens and N. Harada, *Chirality*, 2010, **22**, 229–233.
41 A. Mándi, M. M. Swamy, T. Taniguchi, M. Anetai and K. Monde, *Chirality*, 2016, **28**, 453–459.
42 U. Varetto, *MOLEKEL 5.4*, Swiss National Supercomputing Centre, Manno, Switzerland, 2009.
43 M. Ashour, R. Edrada, R. Ebel, V. Wray, W. Watjen, K. Padmakumar, W. E. Muller, W. H. Lin and P. Proksch, *J. Nat. Prod.*, 2006, **69**, 1547–1553.
44 CLSI, *Methods for Dilution Antimicrobial Susceptibility Tests for Bacteria That Grow Aerobically*, Approved Standard Ninth ed. CLSI document M07-A9, Clinical and Laboratory Standards Institute, Wayne, PA, 2012.

Supporting Information

Induction of Cryptic Metabolites of the Endophytic Fungus *Trichocladium* sp. through OSMAC and Co-Cultivation

Nam Michael Tran-Cong,[a] Attila Mándi,[b] Tibor Kurtán,[b] Werner E.G. Müller,[c] Rainer Kalscheuer,[a] Wenhan Lin,[d] Zhen Liu,[a,*] Peter Proksch[a,*]

[a]Institute of Pharmaceutical Biology and Biotechnology, Heinrich Heine University Düsseldorf, Universitätsstrasse 1, 40225 Düsseldorf, Germany

[b]Department of Organic Chemistry, University of Debrecen, P.O. Box 400, H-4002 Debrecen, Hungary

[c]Institute of Physiological Chemistry, Universitätsmedizin der Johannes Gutenberg-Universität Mainz, 55128 Mainz, Germany

[d]State Key Laboratory of Natural and Biomimetic Drugs, Peking University, Beijing 100191, China

Disclaimer : This version (supporting information) **does not** contain information about cartesian coordinates (see **Table S4.** , **Table S5.** and **Table S6**. For full supporting information please see DOI: 10.1039/c9ra05469c

Supporting Information

Induction of Cryptic Metabolites of the Endophytic Fungus *Trichocladium* sp. through OSMAC and Co-Cultivation

Nam Michael Tran-Cong,[a] Attila Mándi,[b] Tibor Kurtán,[b] Werner E.G. Müller,[c] Rainer Kalscheuer,[a] Wenhan Lin,[d] Zhen Liu,[a,*] Peter Proksch[a,*]

[a]Institute of Pharmaceutical Biology and Biotechnology, Heinrich Heine University Düsseldorf, Universitätsstrasse 1, 40225 Düsseldorf,

[b]Department of Organic Chemistry, University of Debrecen, P.O. Box 400, H-4002 Debrecen, Hungary

[c]Institute of Physiological Chemistry, Universitätsmedizin der Johannes Gutenberg-Universität Mainz, 55128 Mainz, Germany

[d]State Key Laboratory of Natural and Biomimetic Drugs, Peking University, Beijing 100191, China

Contents

Acquisition Parameter

Source Type	ESI	Ion Polarity	Positive	Set Nebulizer	0.3 Bar
Focus	Not active	Set Capillary	4000 V	Set Dry Heater	180 °C
Scan Begin	50 m/z	Set End Plate Offset	-500 V	Set Dry Gas	4.0 l/min
Scan End	1500 m/z	Set Collision Cell RF	600.0 Vpp	Set Divert Valve	Source

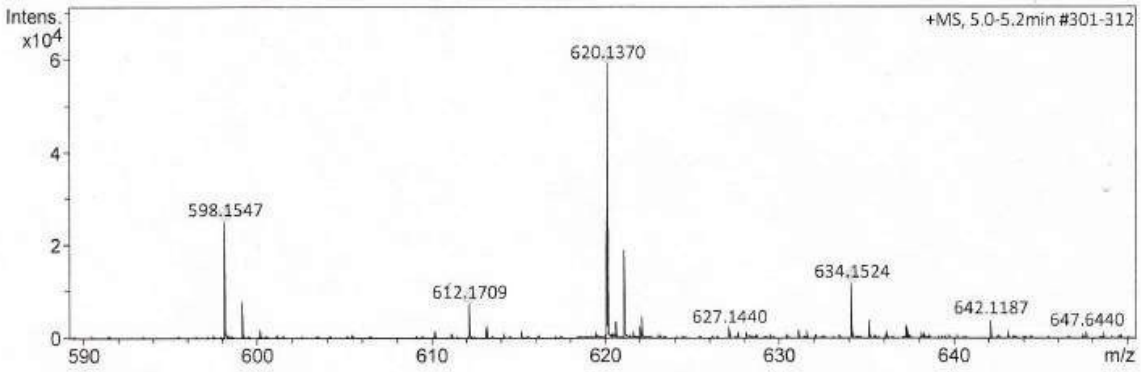

Meas. m/z	#	Ion Formula	m/z	err [ppm]	mSigma	# mSigma	Score	rdb	e⁻ Conf	N-Rule
598.1547	1	C29H28NO13	598.1555	1.4	5.5	1	79.18	16.5	even	ok
	2	C28H25N5NaO9	598.1544	-0.4	7.9	2	100.00	18.5	even	ok
	3	C26H20N11O7	598.1542	-0.9	9.2	3	85.80	22.5	even	ok
	4	C29H21N9NaO5	598.1558	1.8	18.2	4	53.46	23.5	even	ok
	5	C27H16N15O3	598.1555	1.3	18.5	5	62.10	27.5	even	ok
	6	C42H20N3O2	598.1550	0.5	77.5	6	13.51	34.5	even	ok
612.1709	1	C30H30NO13	612.1712	0.4	101.9	1	100.00	16.5	even	ok
	2	C29H27N5NaO9	612.1701	-1.3	103.9	2	68.12	18.5	even	ok
	3	C30H23N9NaO5	612.1714	0.8	104.6	3	77.28	23.5	even	ok
	4	C27H22N11O7	612.1698	-1.8	105.2	4	54.64	22.5	even	ok
	5	C28H18N15O3	612.1712	0.4	105.9	5	82.58	27.5	even	ok
	6	C43H22N3O2	612.1707	-0.4	117.2	6	45.44	34.5	even	ok
620.1370	1	C29H27NNaO13	620.1375	0.8	2.1	1	89.08	16.5	even	ok
	2	C27H22N7O11	620.1372	0.3	2.8	2	100.00	20.5	even	ok
	3	C26H19N11NaO7	620.1361	-1.4	6.8	3	67.71	22.5	even	ok
	4	C24H14N17O5	620.1358	-1.8	8.8	4	55.64	26.5	even	ok
	5	C26H26N3O15	620.1358	-1.8	10.3	5	54.47	15.5	even	ok
	6	C27H15N15NaO3	620.1375	0.8	15.8	6	69.74	27.5	even	ok
	7	C25H10N21O	620.1372	0.3	16.4	7	78.09	31.5	even	ok
	8	C40H14N9	620.1367	-0.5	74.4	8	13.70	38.5	even	ok
	9	C42H19N3NaO2	620.1369	-0.0	75.4	9	14.85	34.5	even	ok

Figure S1. The HRESIMS of compound **1**

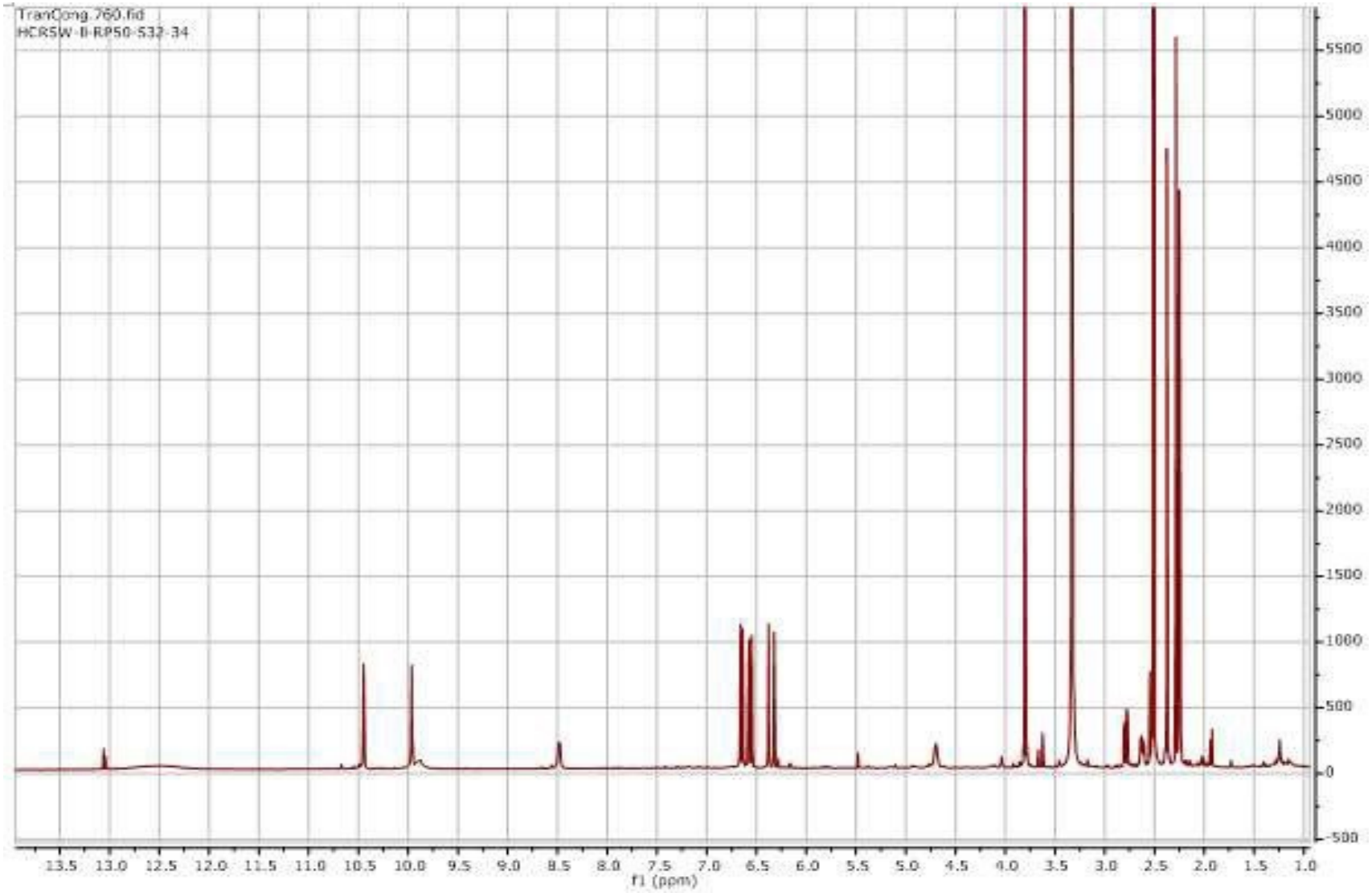

Figure S2. The ^{1}H NMR (600 MHz, DMSO-d_6) spectrum of compound **1**

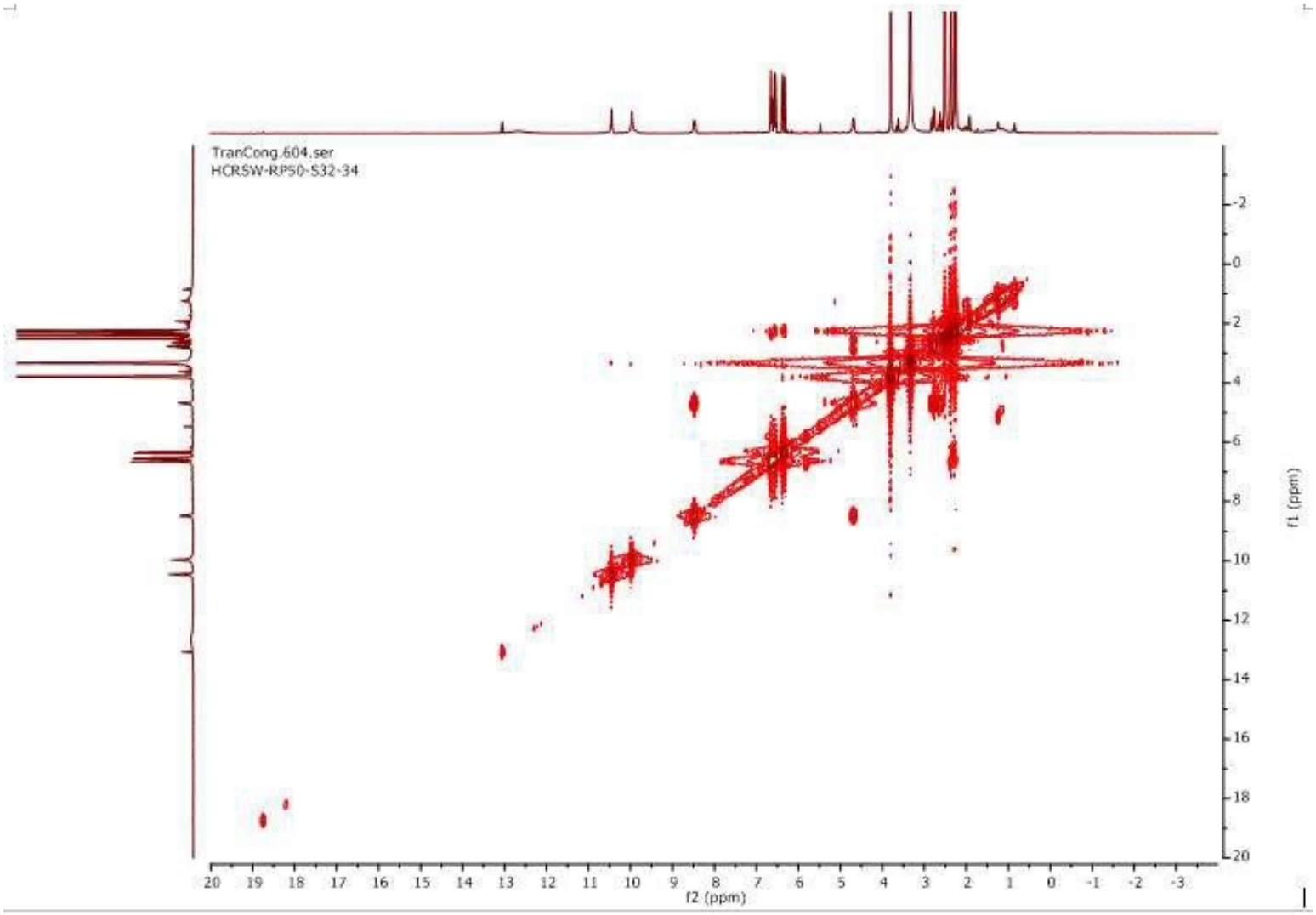

Figure S3. The COSY (300 MHz, DMSO-d_6) spectrum of compound **1**

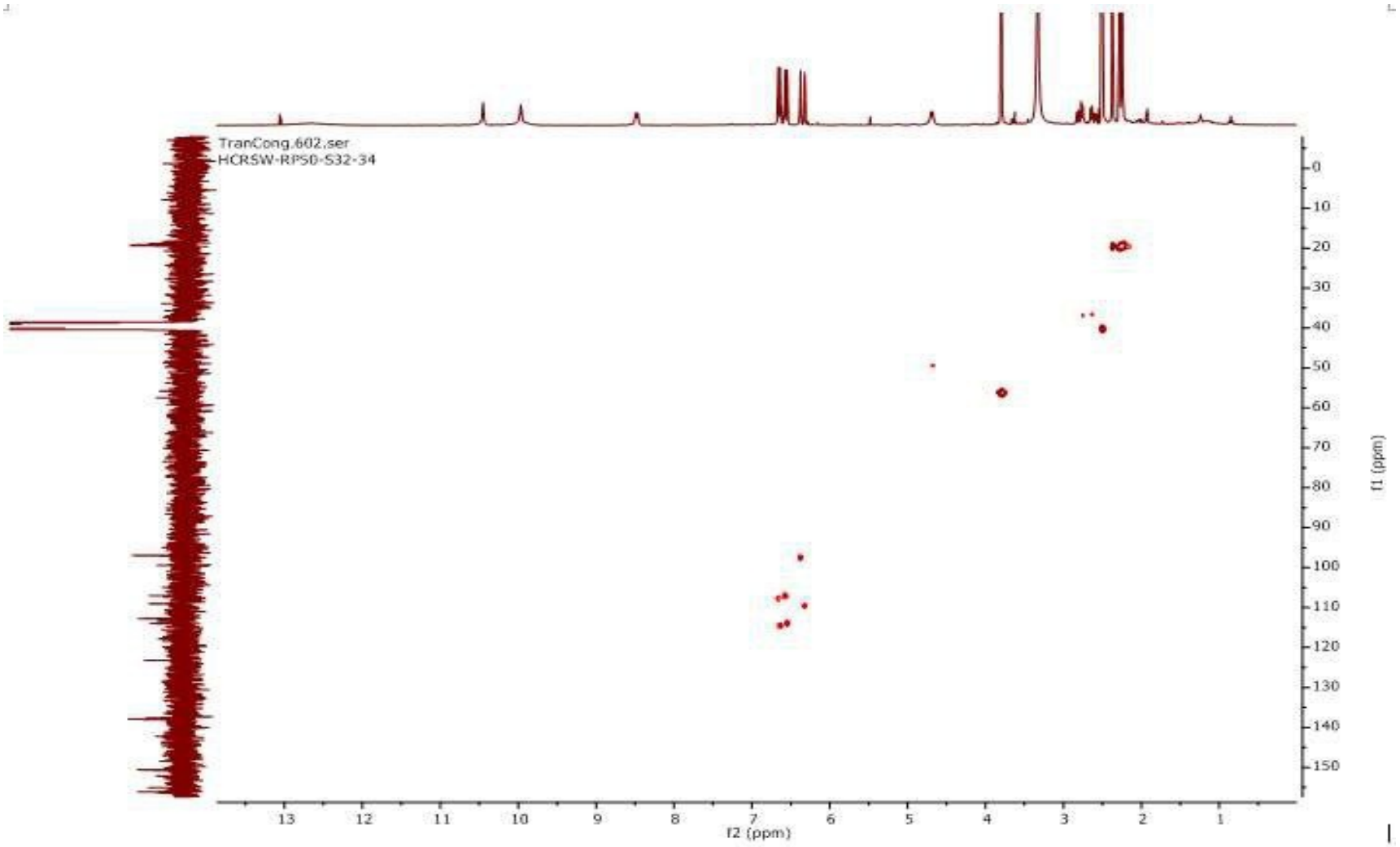

Figure S4. The HSQC (300 MHz, DMSO-d_6) spectrum of compound **1**

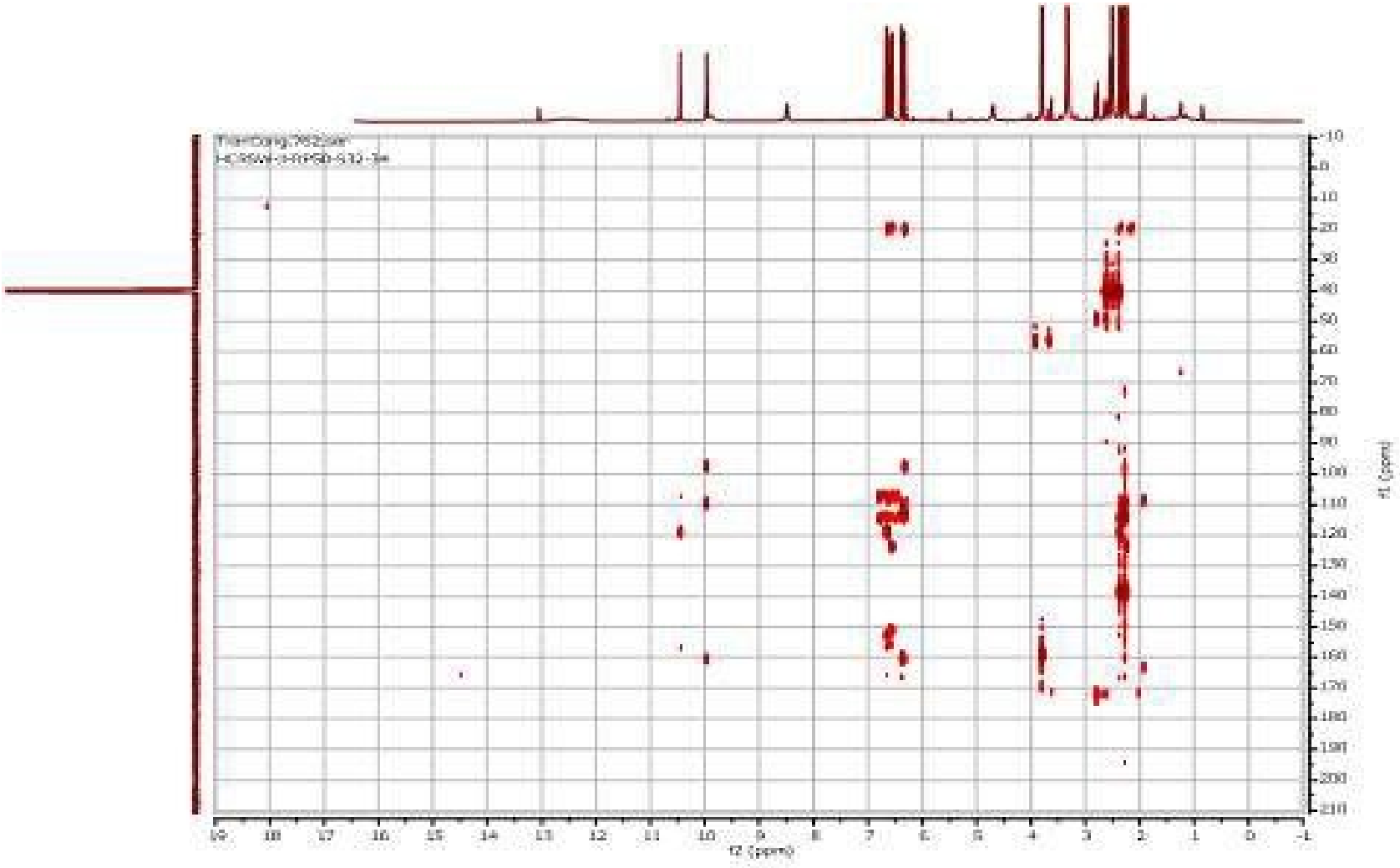

Figure S5. The HMBC (600MHz, DMSO-d_6) spectrum of compound **1**

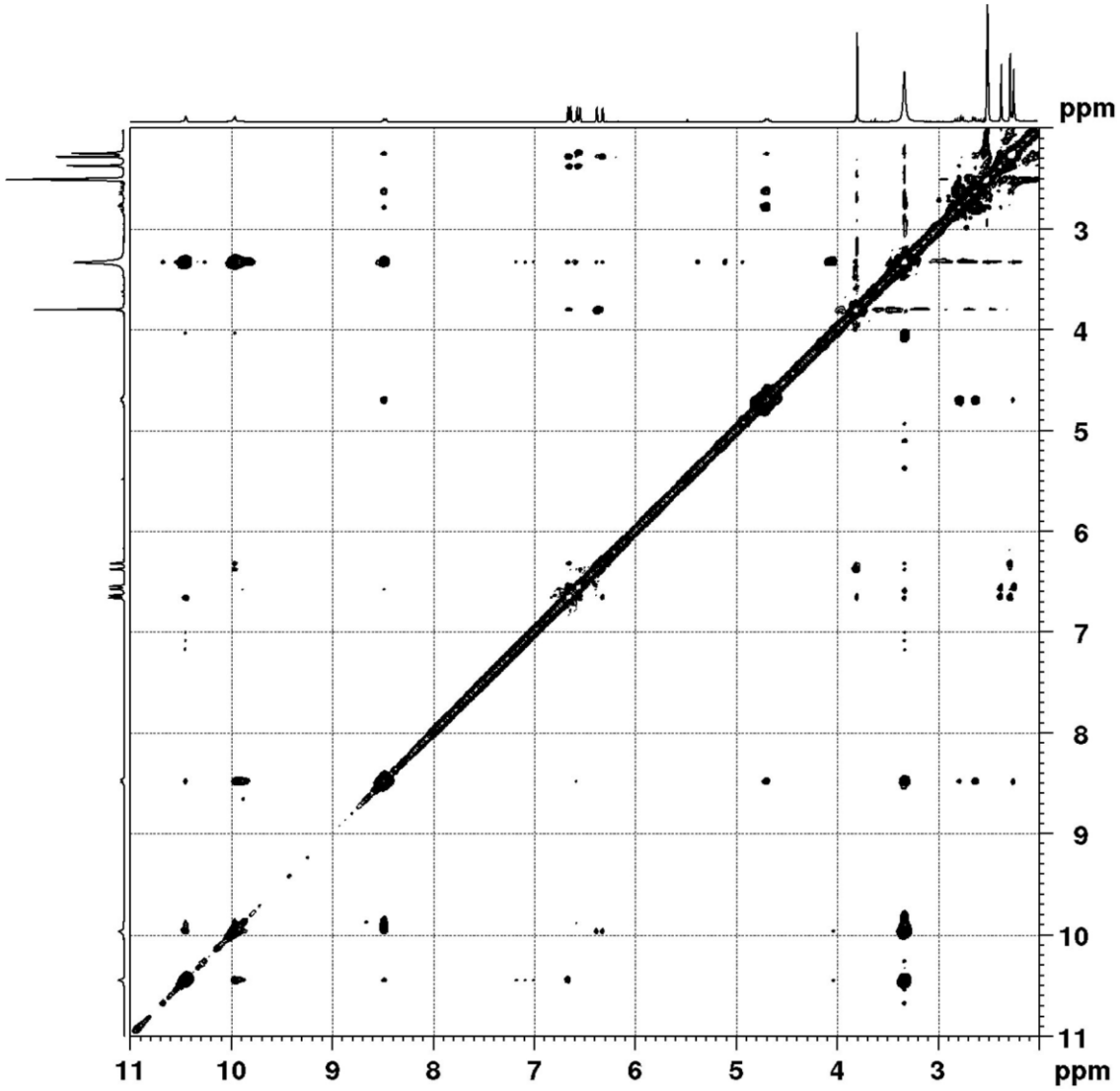

Figure S6. The ROESY (600MHz, DMSO-d_6) spectrum of compound **1**

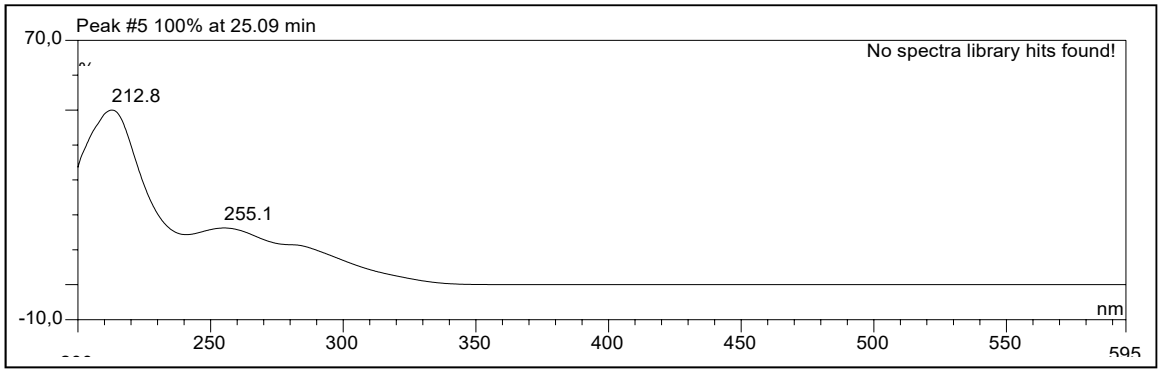

Figure S7. The UV spectrum of compound **1**

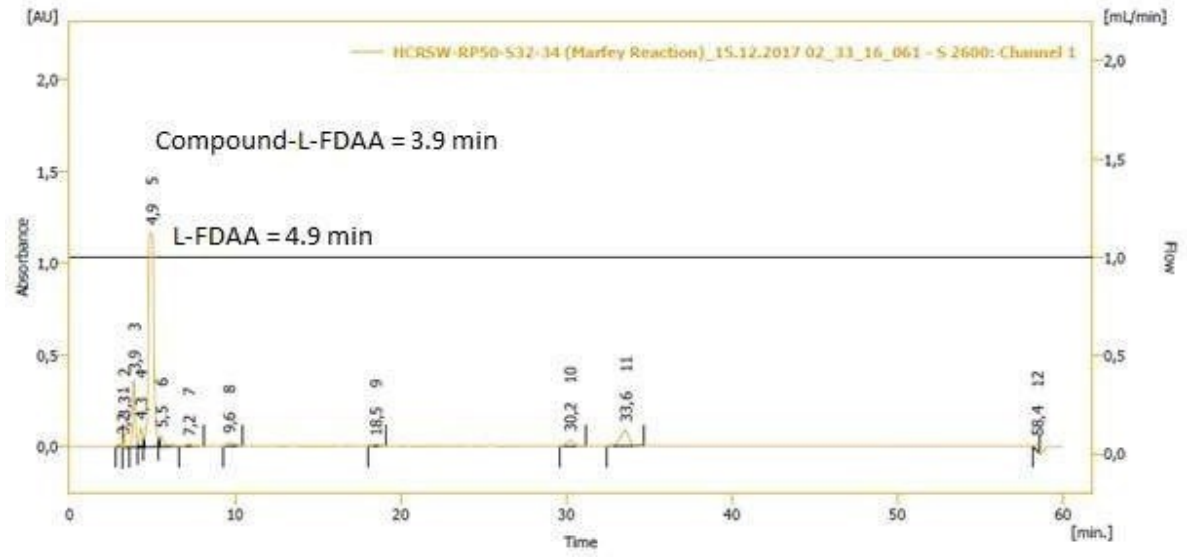

Figure S8. The HPLC chromatogram of compound **1** with L-FDAA for Marfey's method

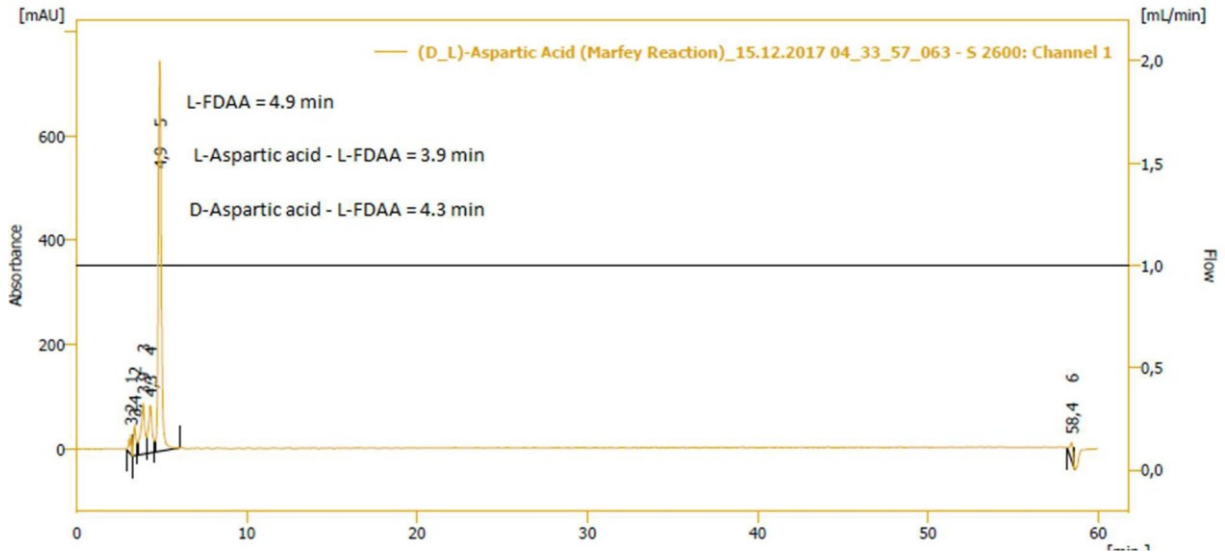

Figure S9. The HPLC chromatogram of DL-aspartic acid with L-FDAA for Marfey's method

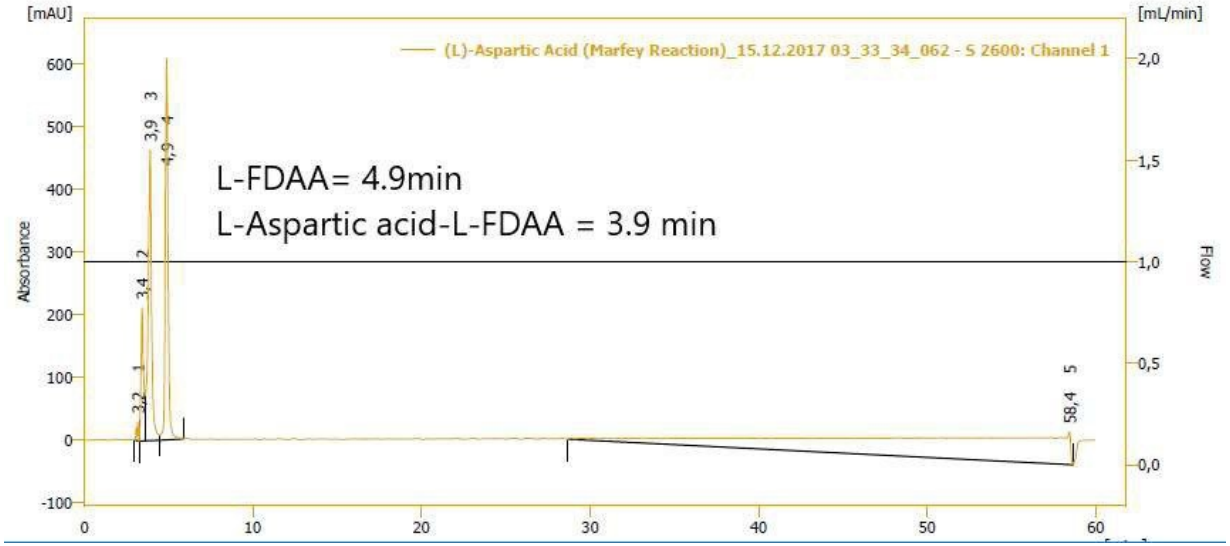

Figure S10. The HPLC chromatogram of L-aspartic acid with L-FDAA for Marfey's method

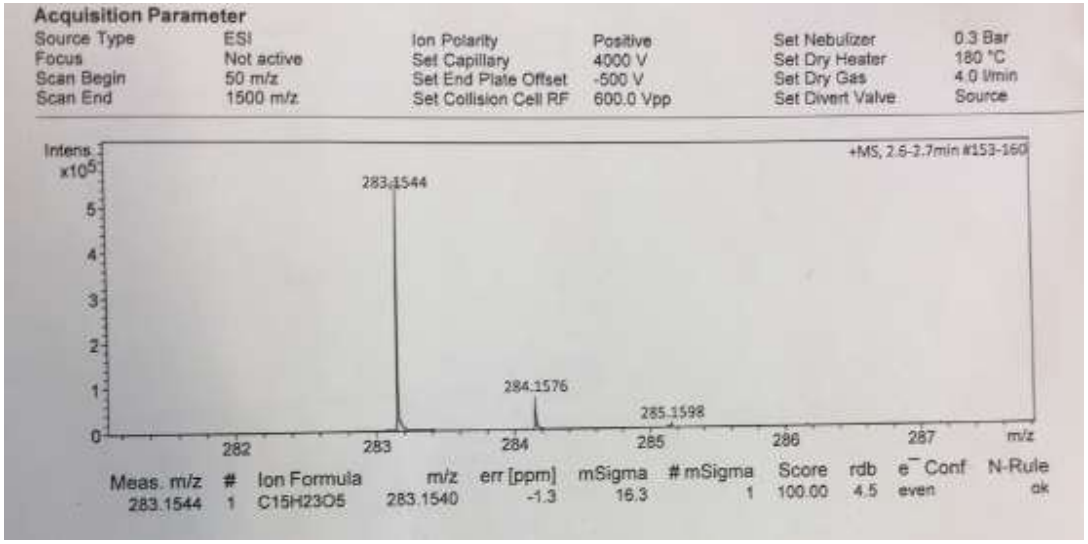

Figure S11. The HRESIMS of compound **2**

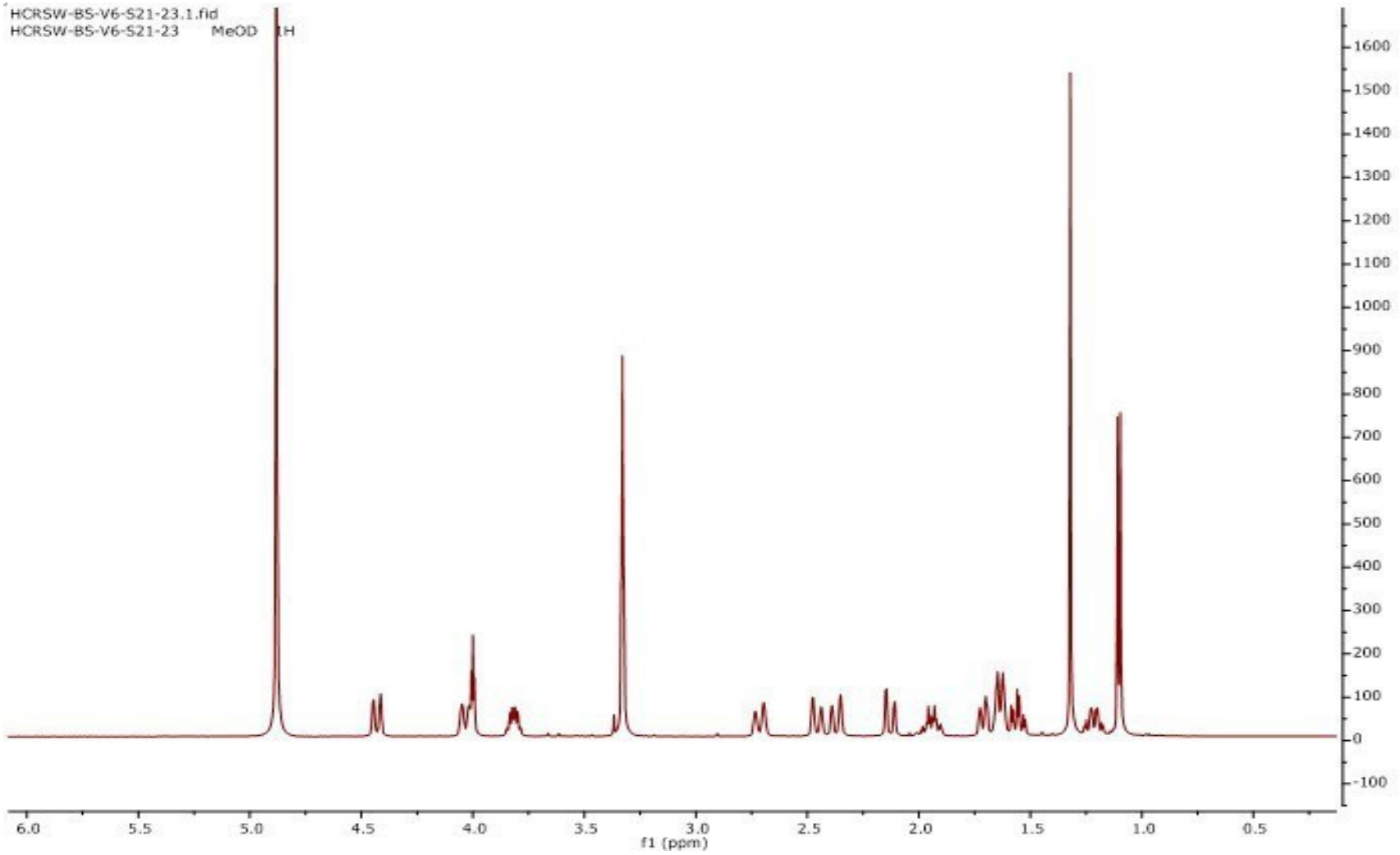

Figure S12. The ^{1}H NMR (500 MHz, CD_3OD) spectrum of compound **2**

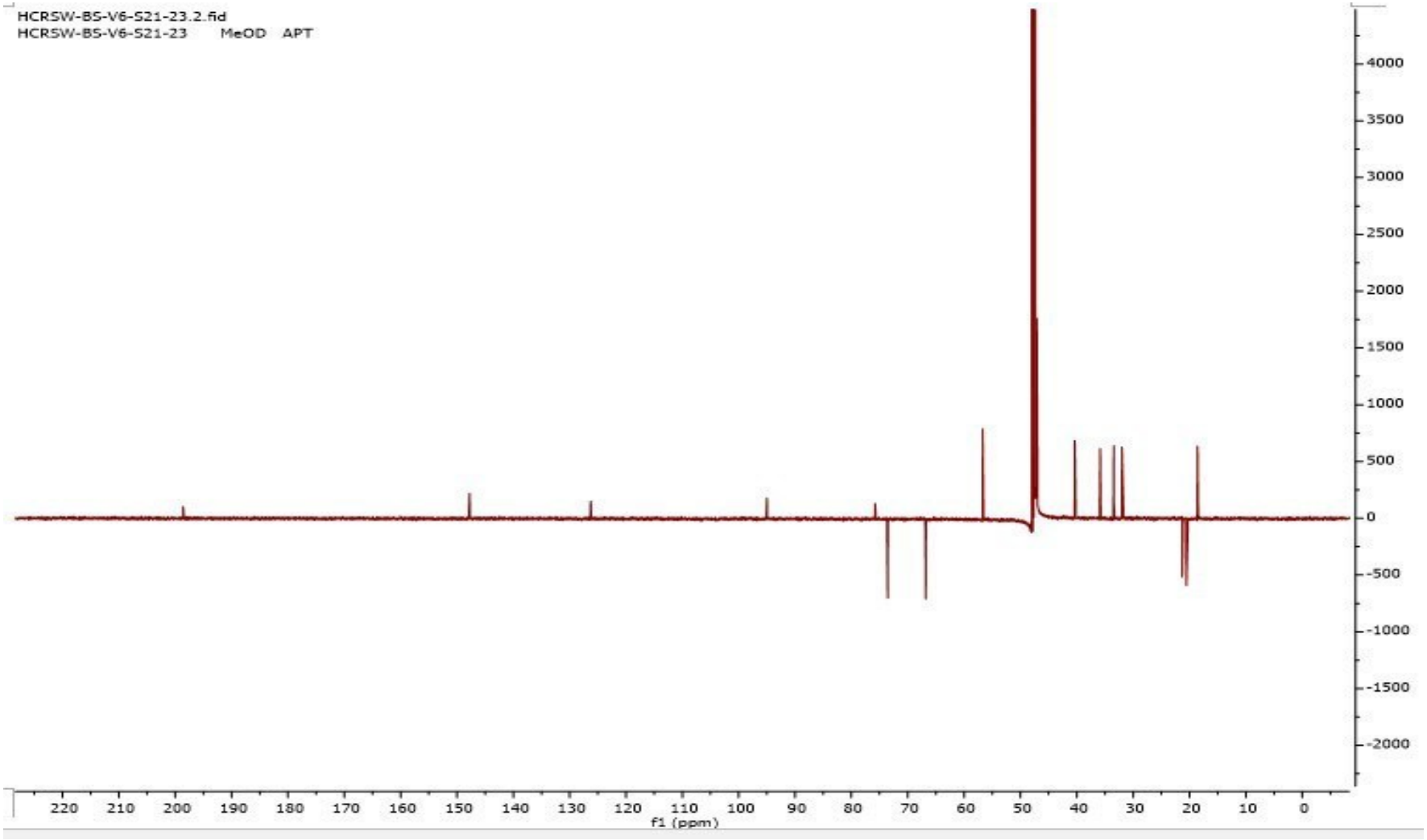

Figure S13. The ^{13}C NMR (125 MHz, CD_3OD) spectrum of compound **2**

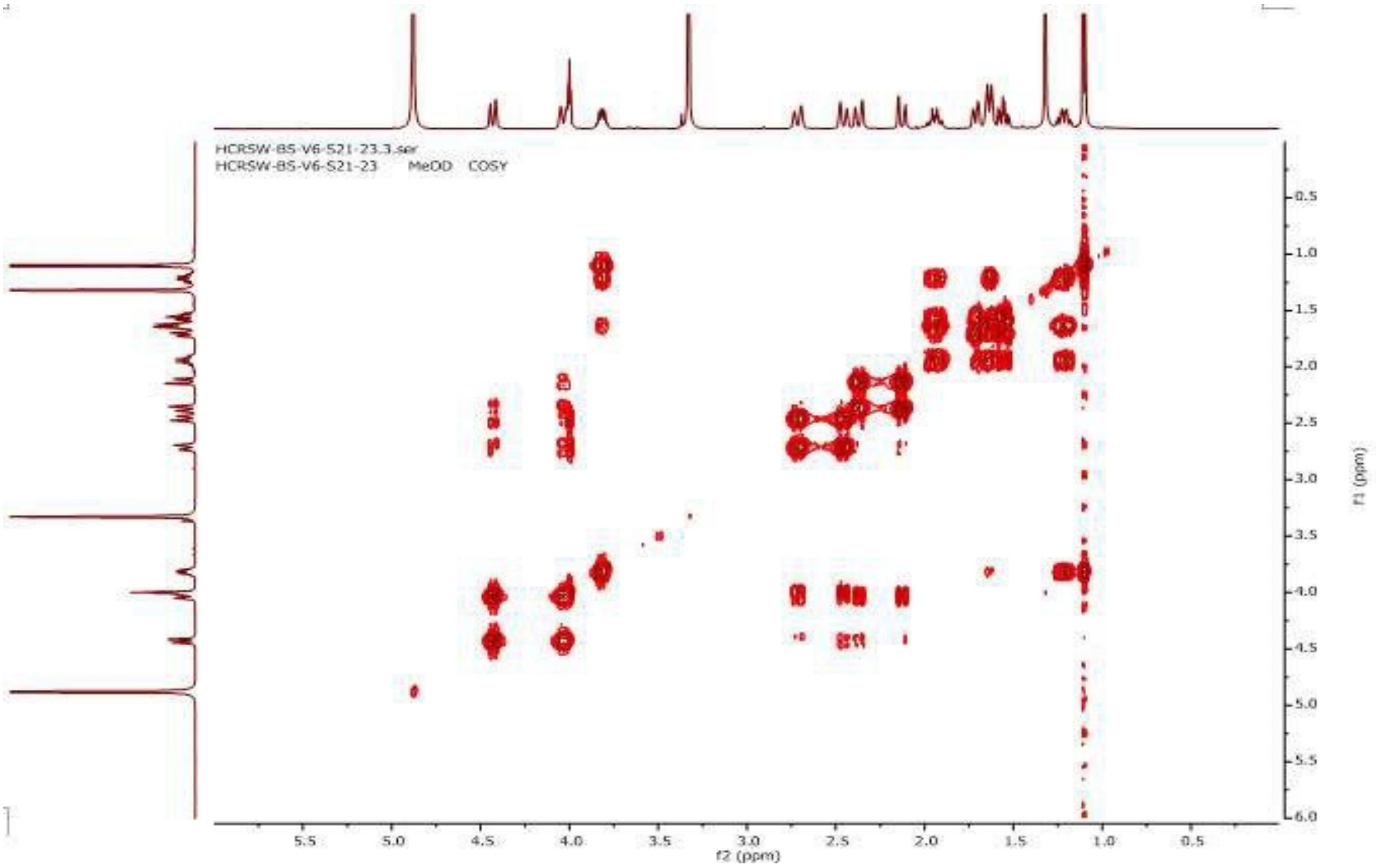

Figure S14. The COSY (500 MHz, CD_3OD) spectrum of compound **2**

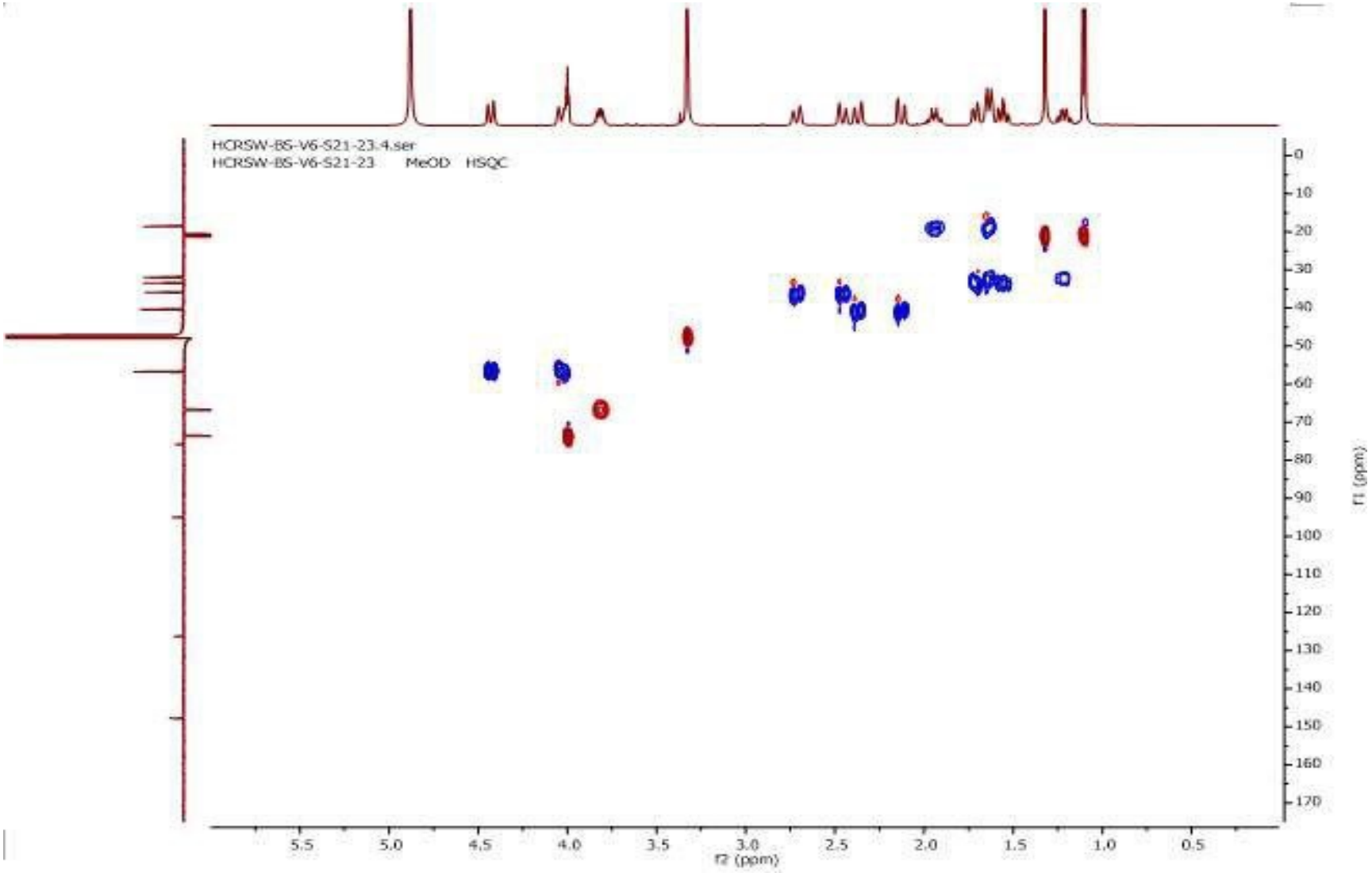

Figure S15. The HSQC (500 MHz, CD_3OD) spectrum of compound **2**

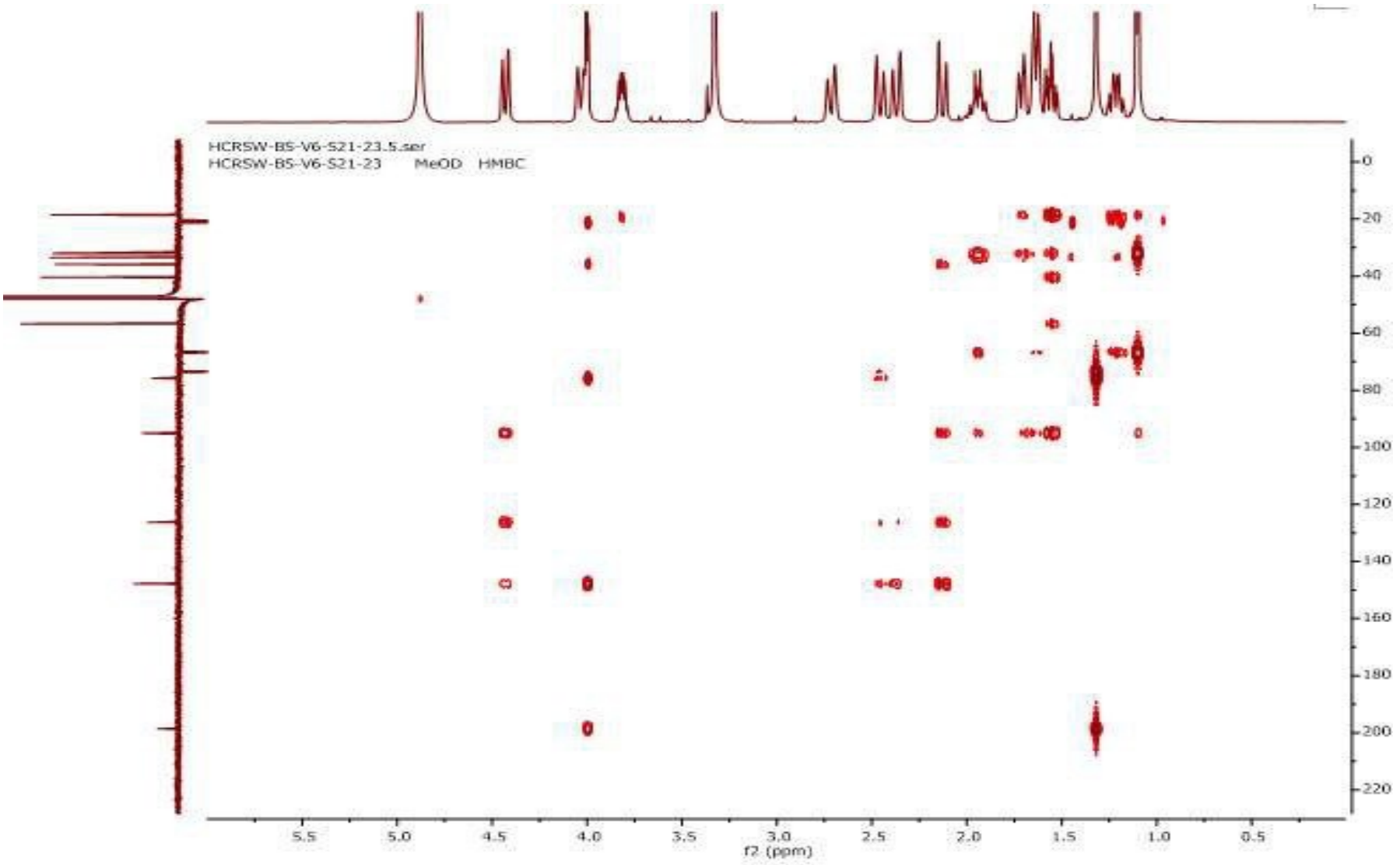

Figure S16. The HMBC (500 MHz, CD_3OD) spectrum of compound **2**

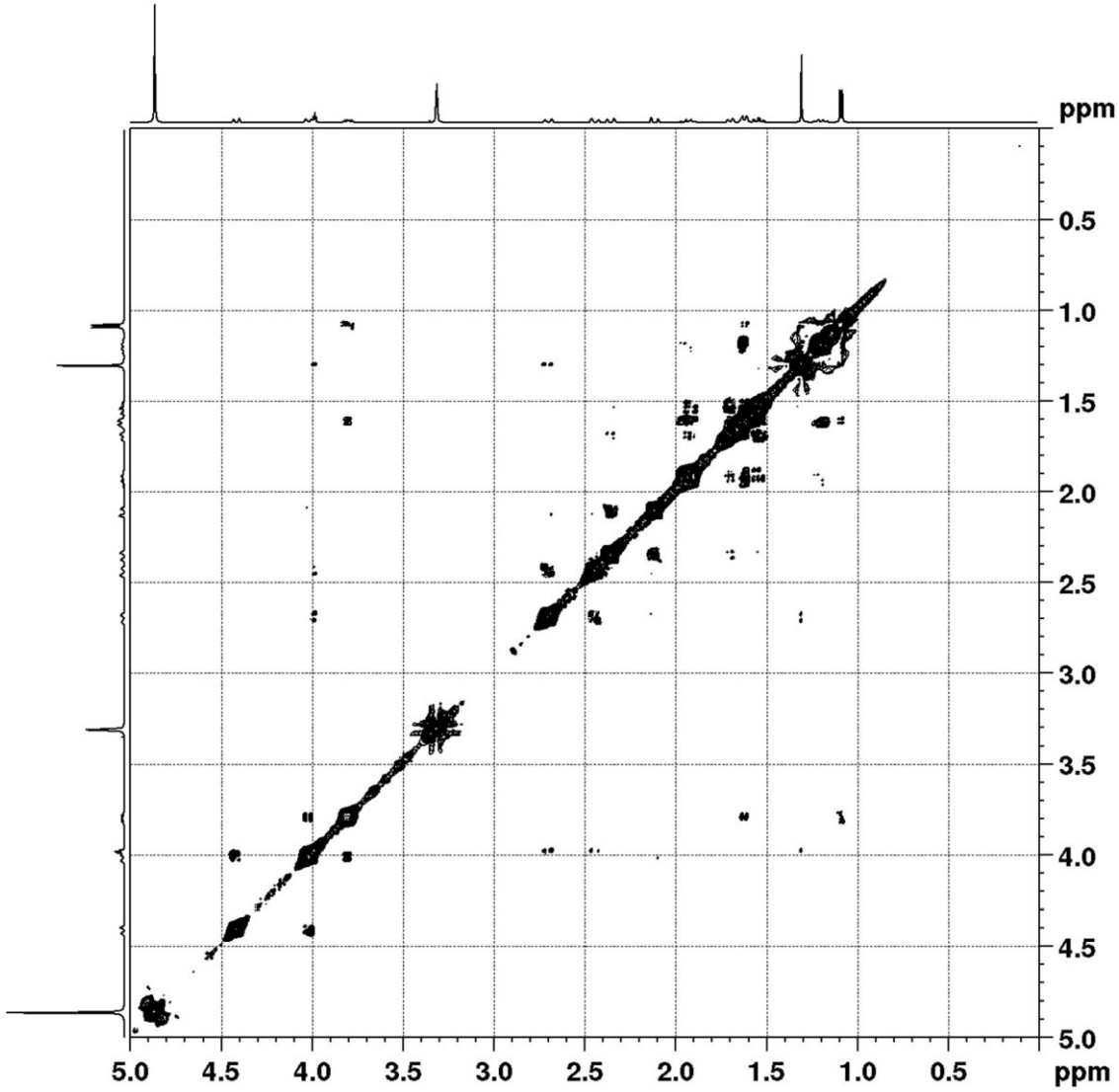

Figure S17. The ROESY (500 MHz, CD_3OD) spectrum of compound **2**

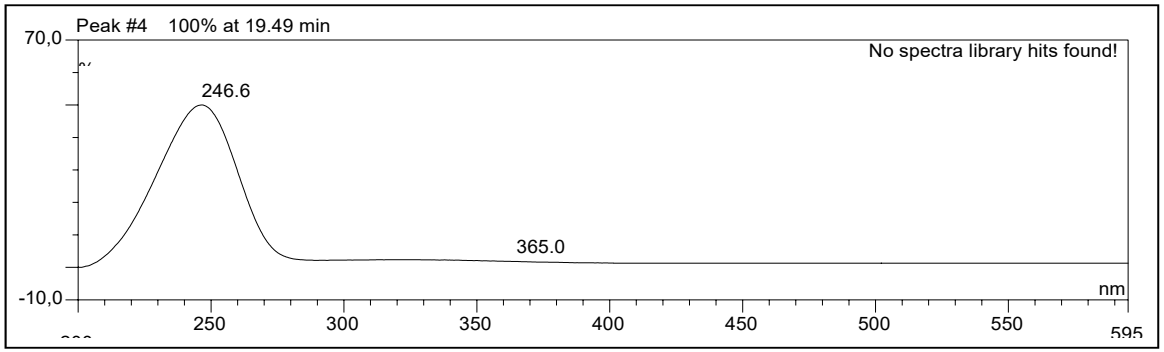

Figure S18. The UV spectrum of compound **2**

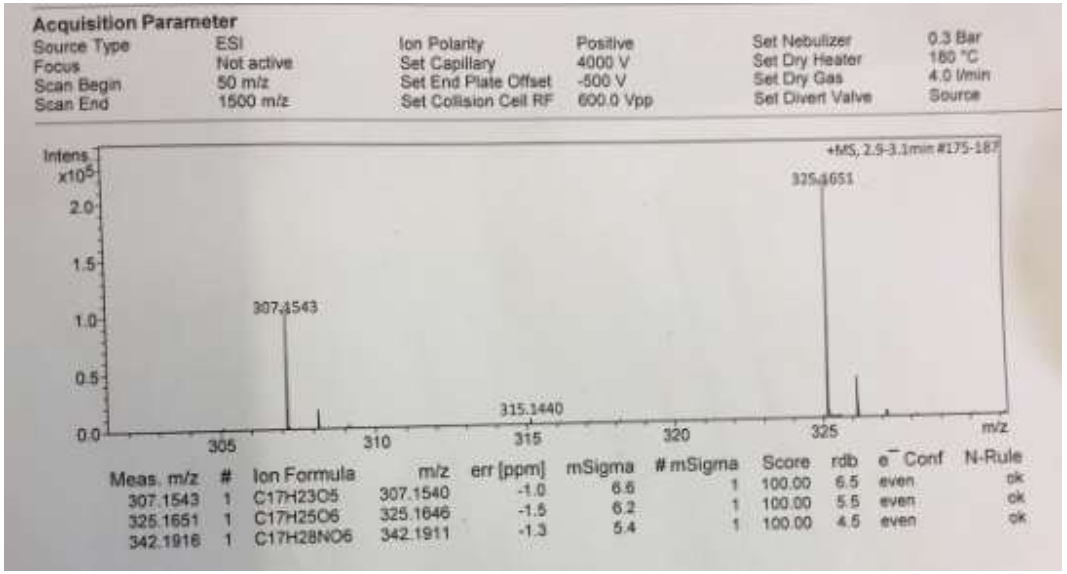

Figure S19. The HRESIMS of compound **3**

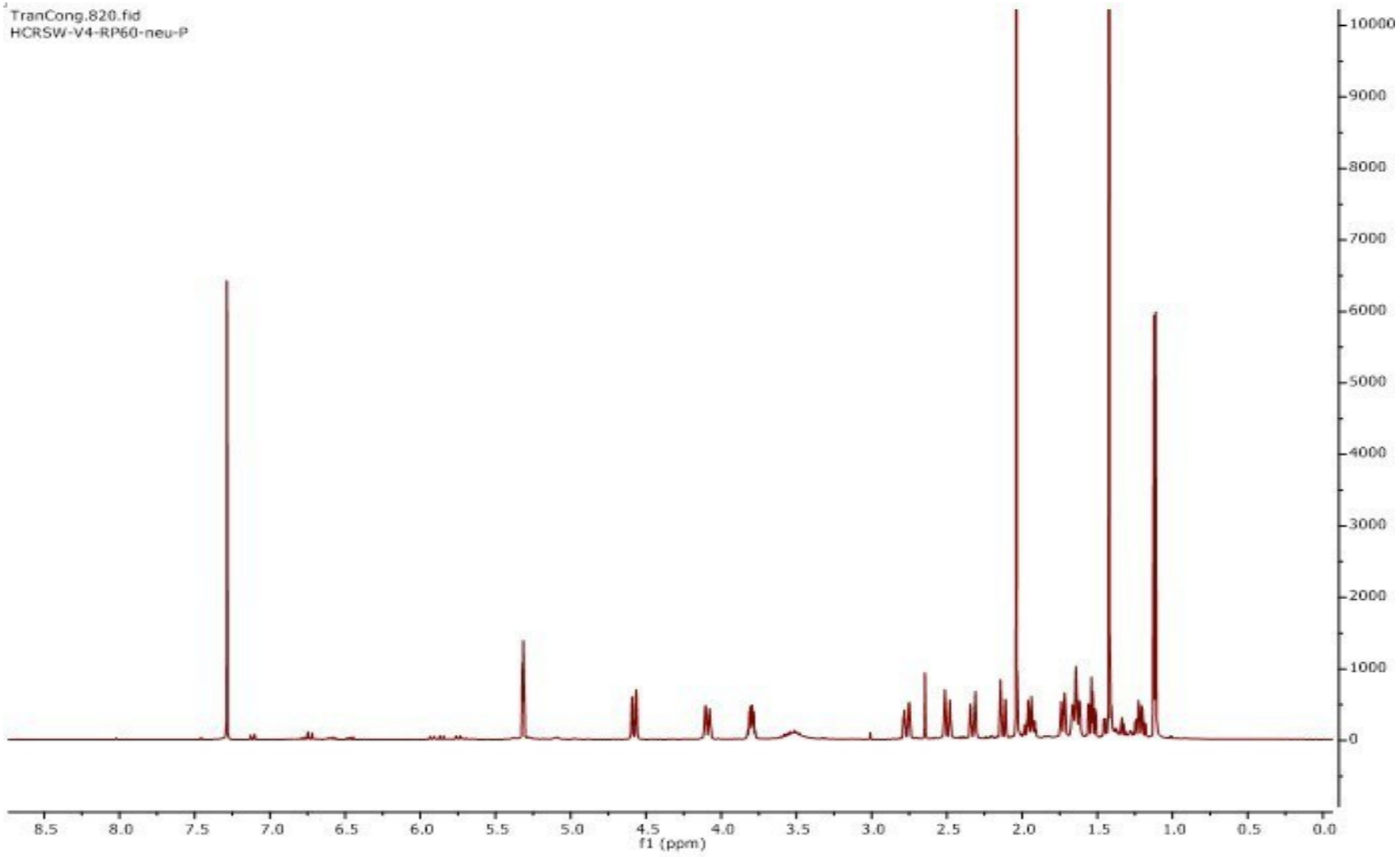

Figure S20. The ^{1}H NMR (600 MHz, $CDCl_3$) spectrum of compound **3**

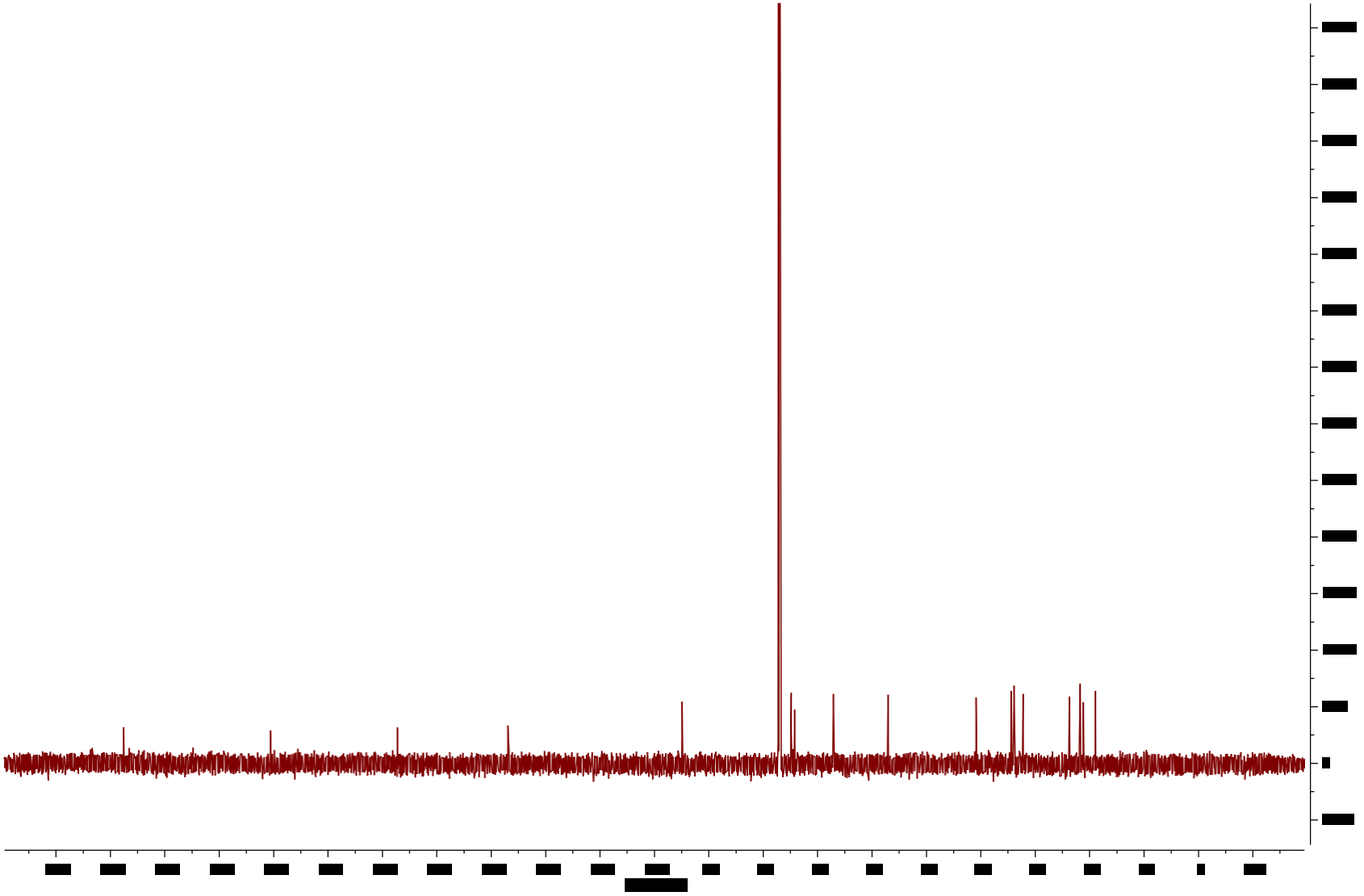

Figure S21. The ^{13}C NMR (150 MHz, $CDCl_3$) spectrum of compound **3**

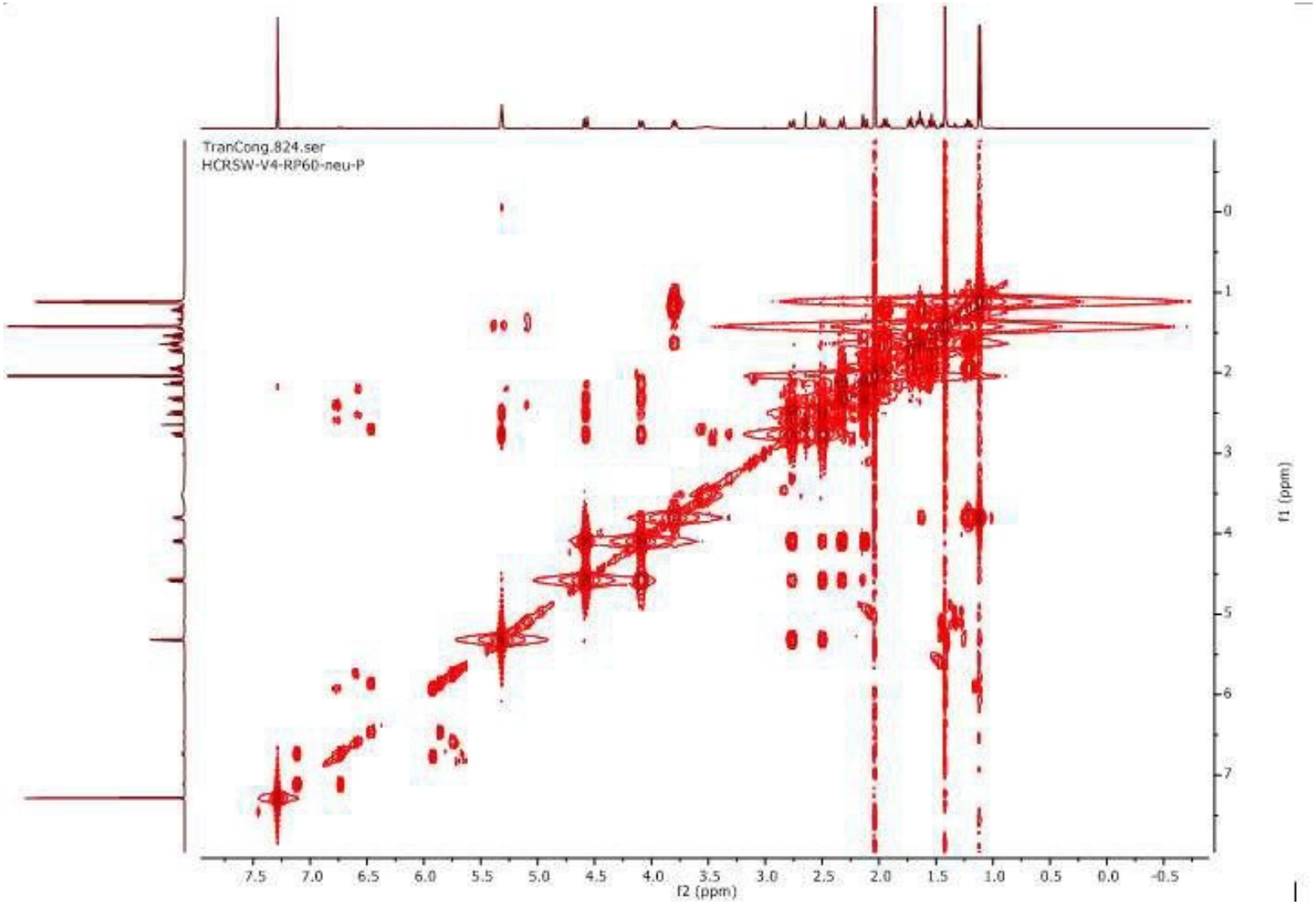

Figure S22. The COSY (600 MHz, $CDCl_3$) spectrum of compound **3**

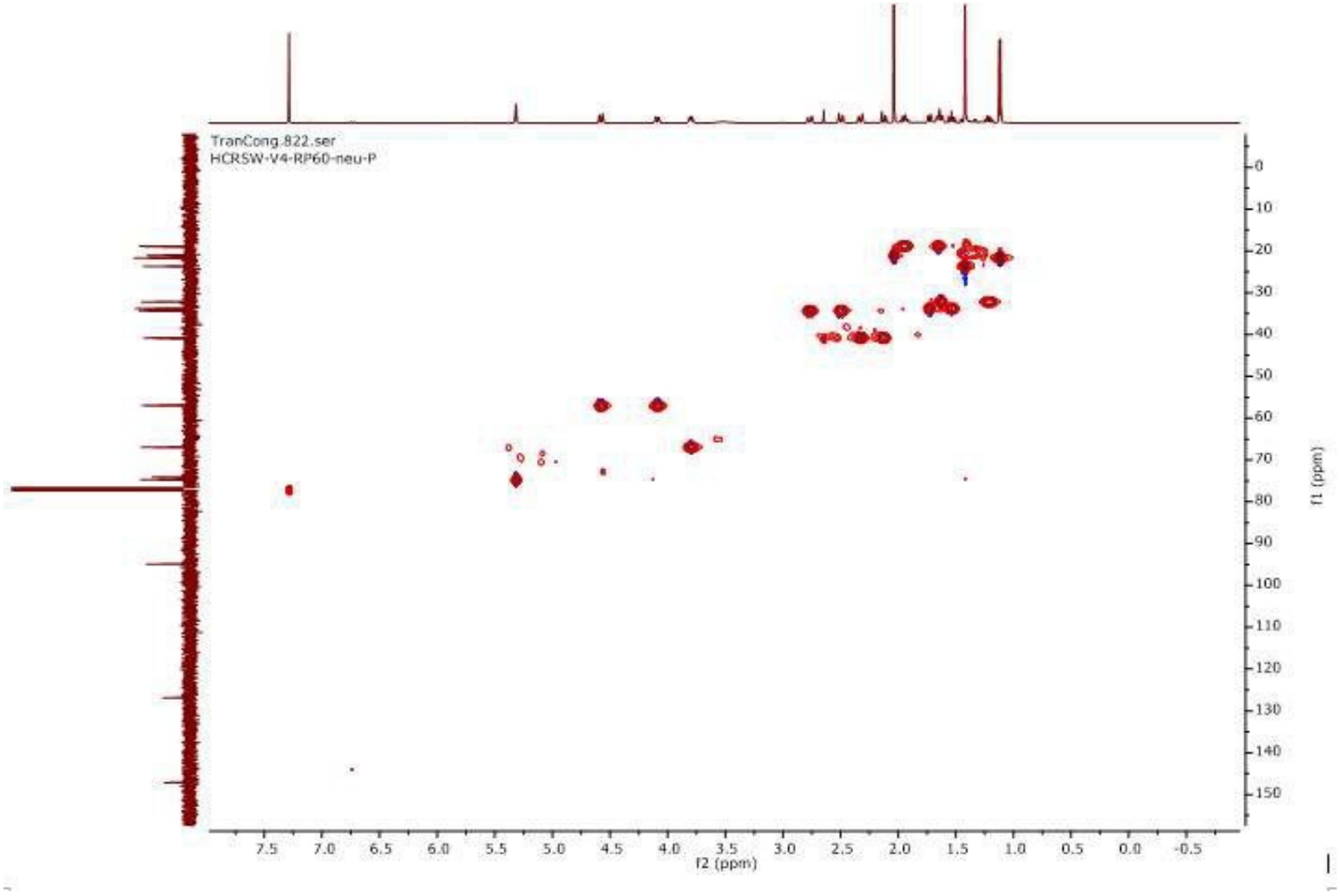

Figure S23. The HSQC (600 MHz, $CDCl_3$) spectrum of compound **3**

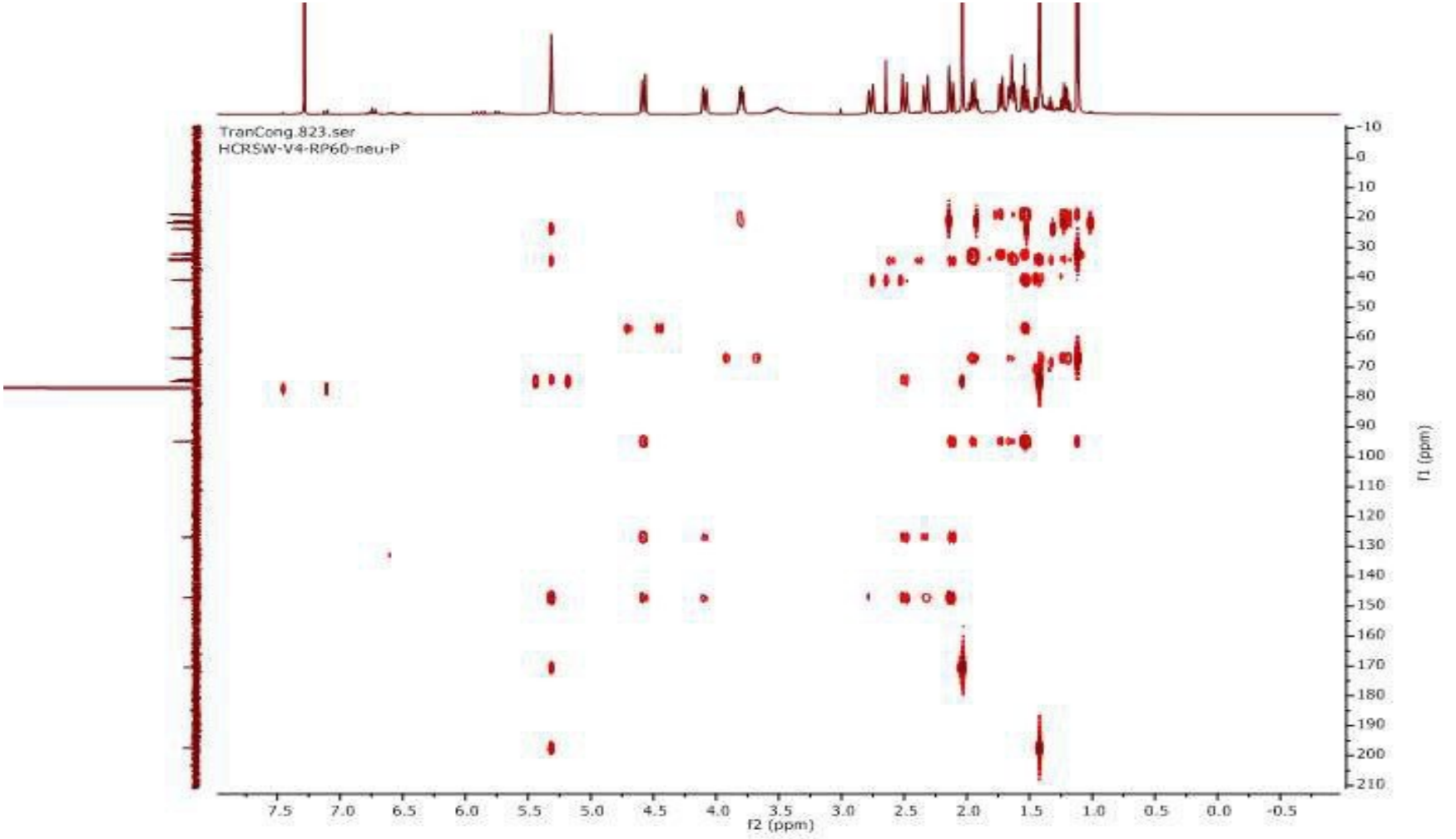

Figure S24. The HMBC (600 MHz, $CDCl_3$) spectrum of compound **3**

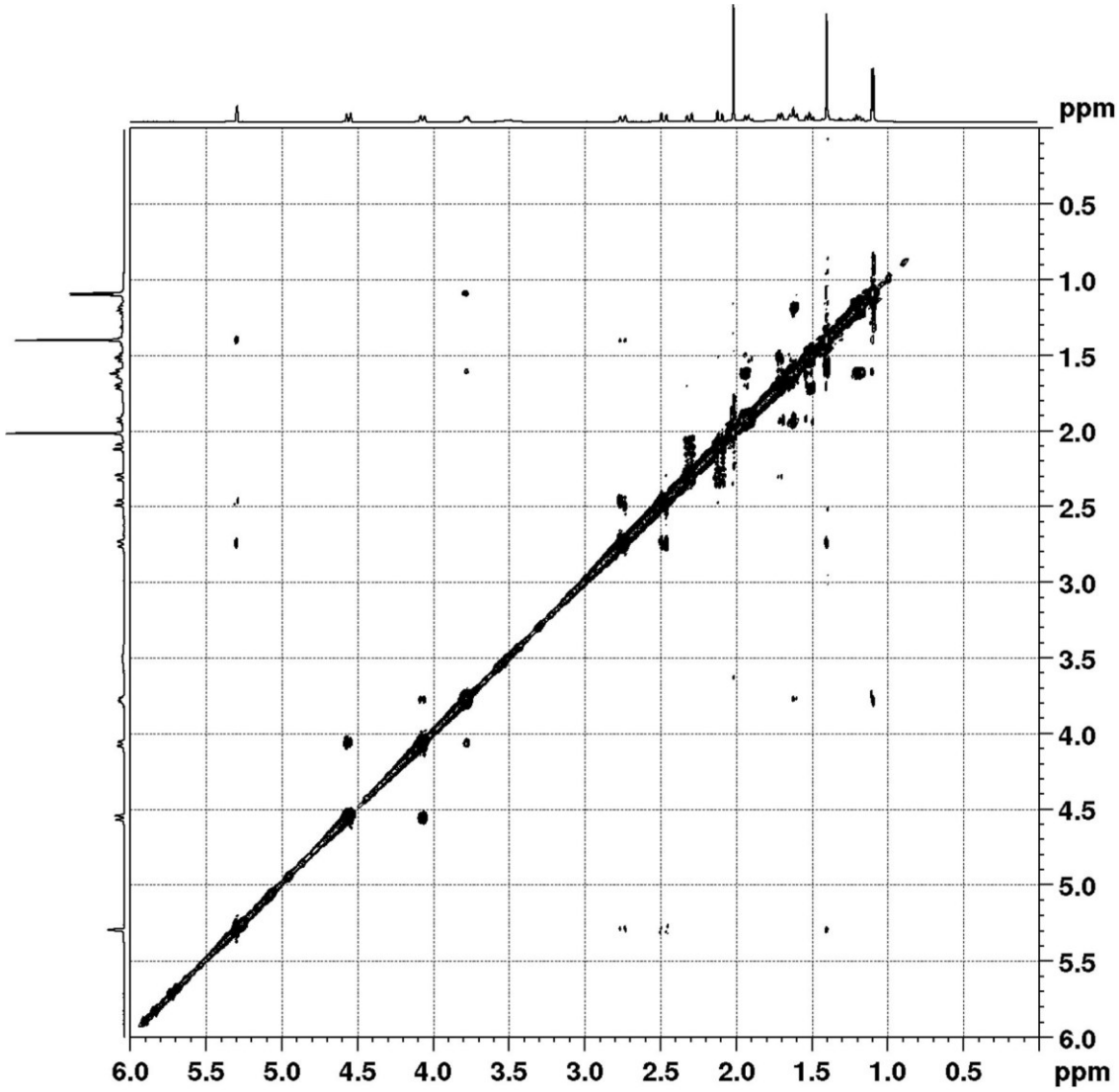

Figure S25. The ROESY (600 MHz, $CDCl_3$) spectrum of compound **3**

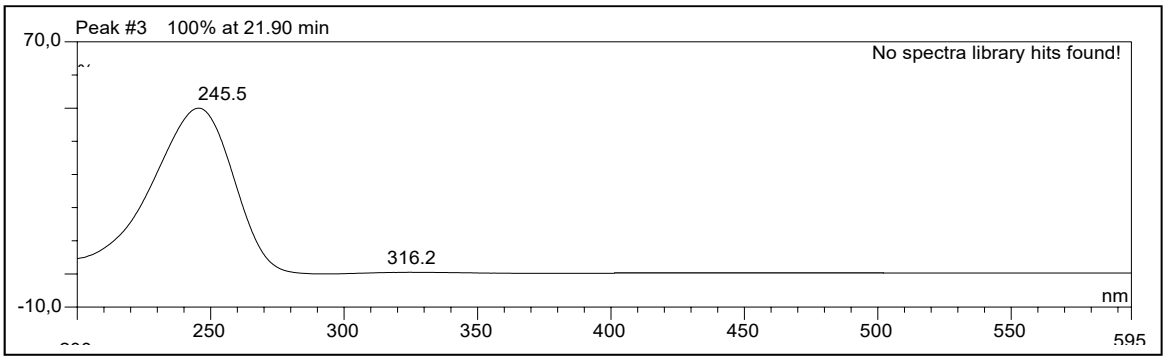

Figure S26. The UV spectrum of compound **3**

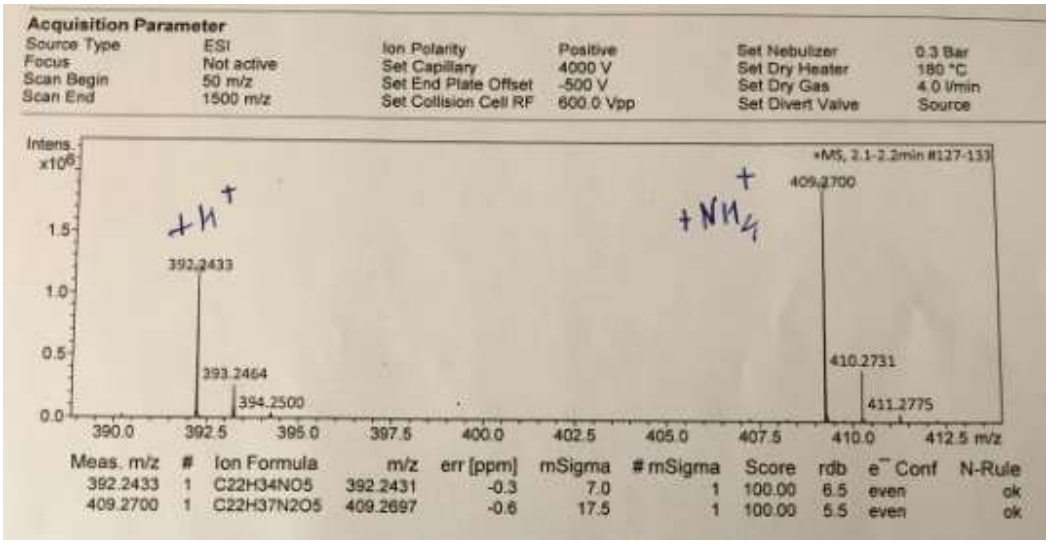

Figure S27. The HRESIMS of compound **13**

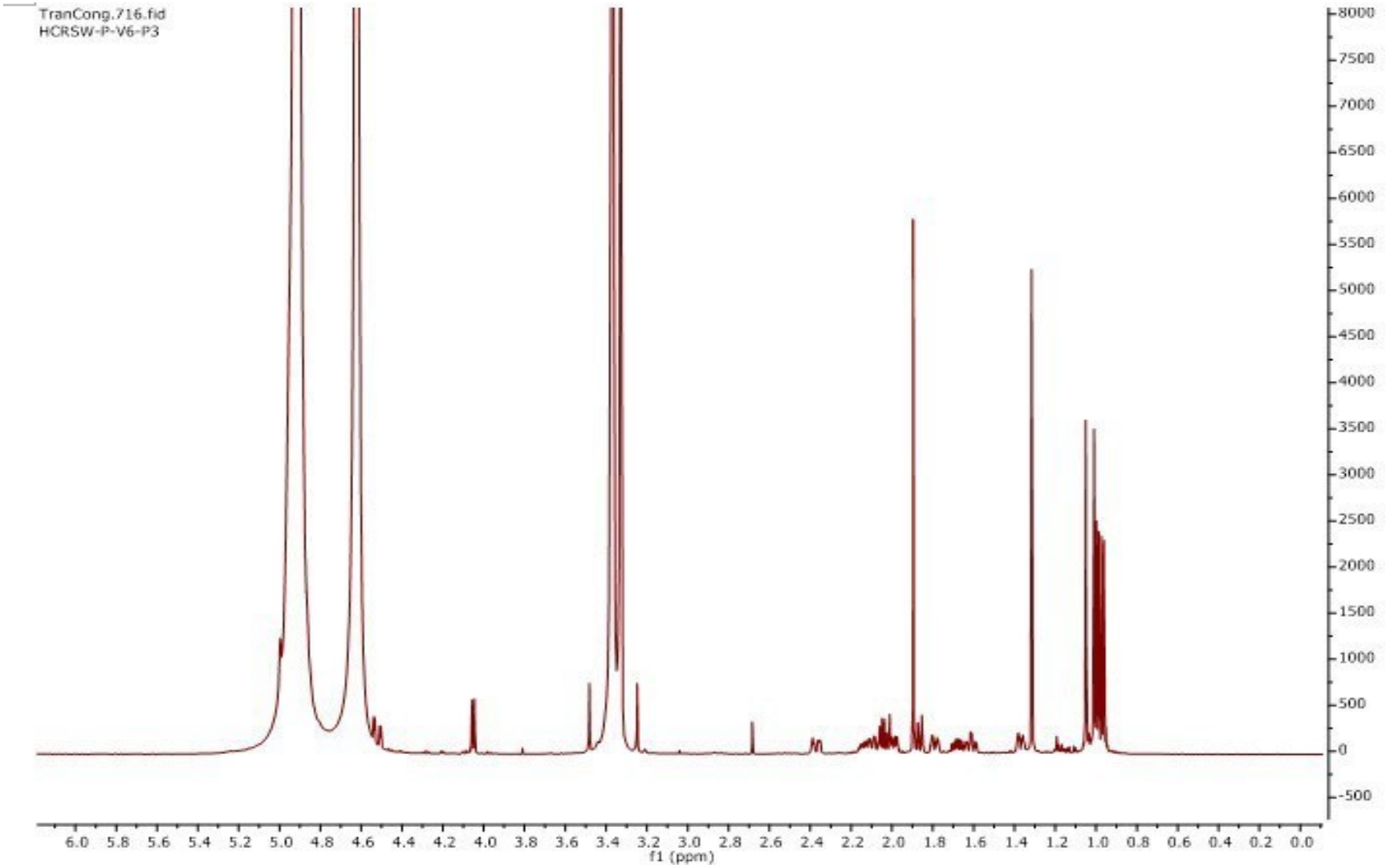

Figure S28. The ^{1}H NMR (600 MHz, CD_3OD) spectrum of compound **13**

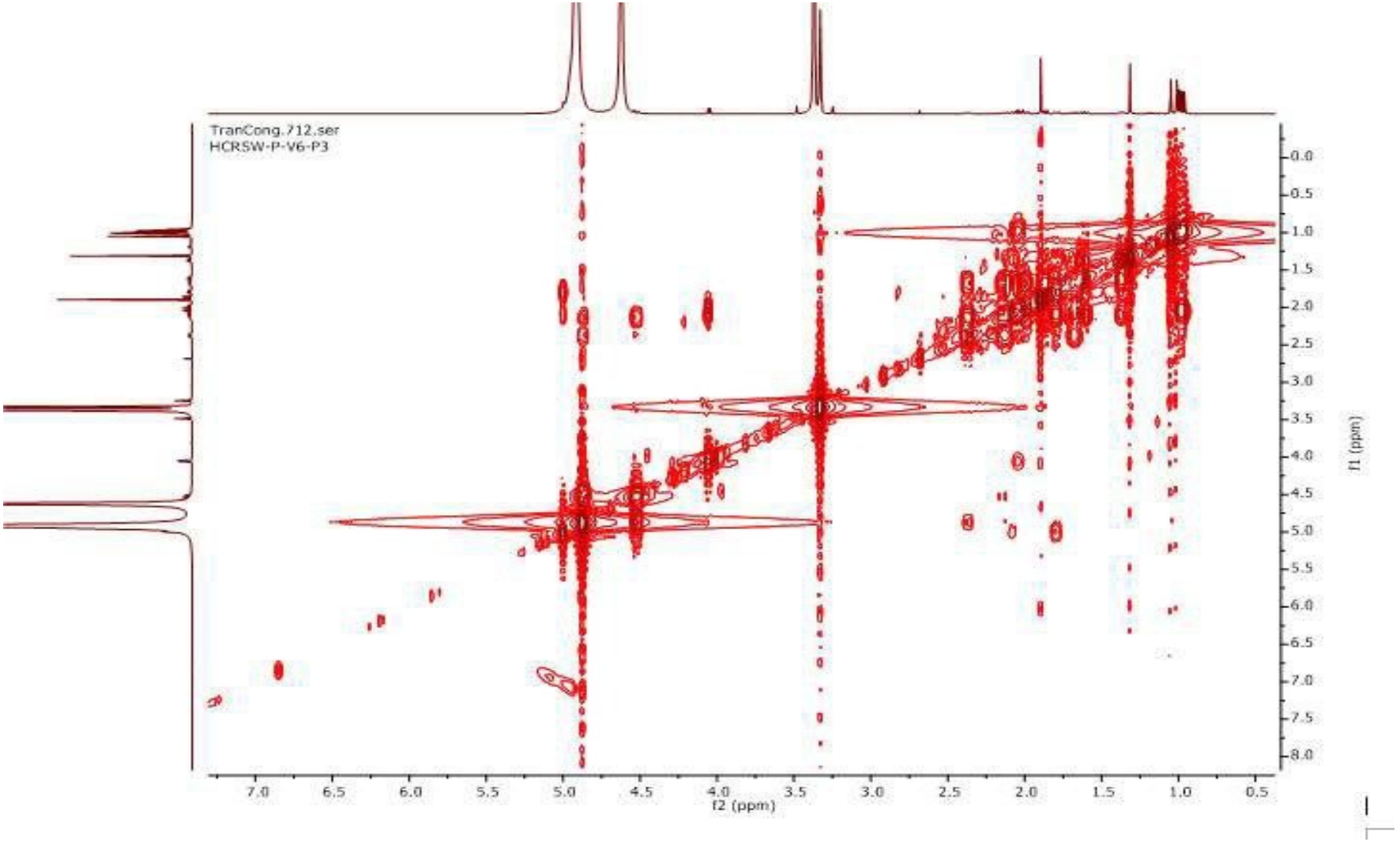

Figure S29. The COSY (600 MHz, CH_3OD) spectrum of compound **13**

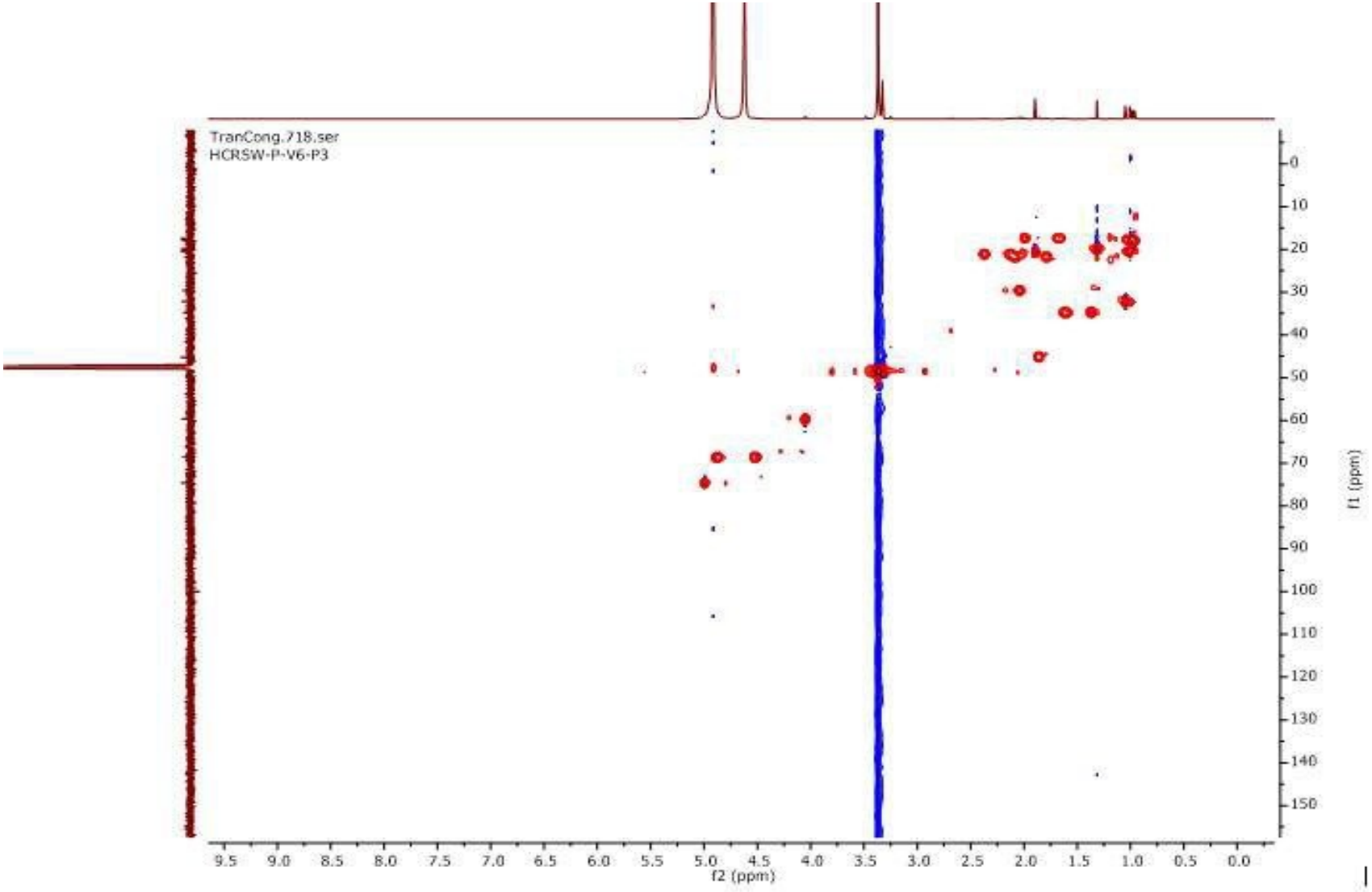

Figure S30. The HSQC (600 MHz, CD_3OD) spectrum of compound **13**

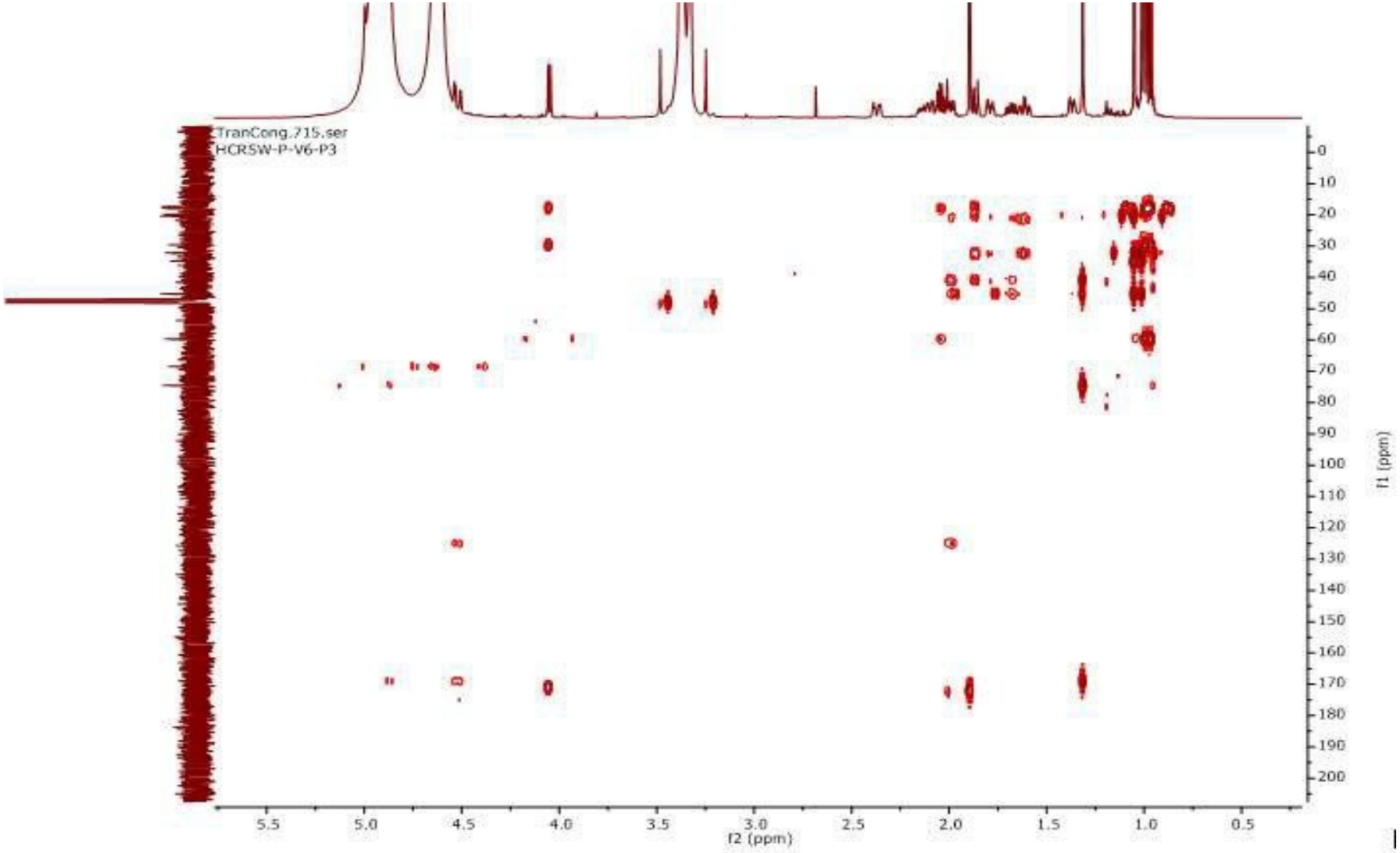

Figure S31. The HMBC (600 MHz, CD_3OD) spectrum of compound **13**

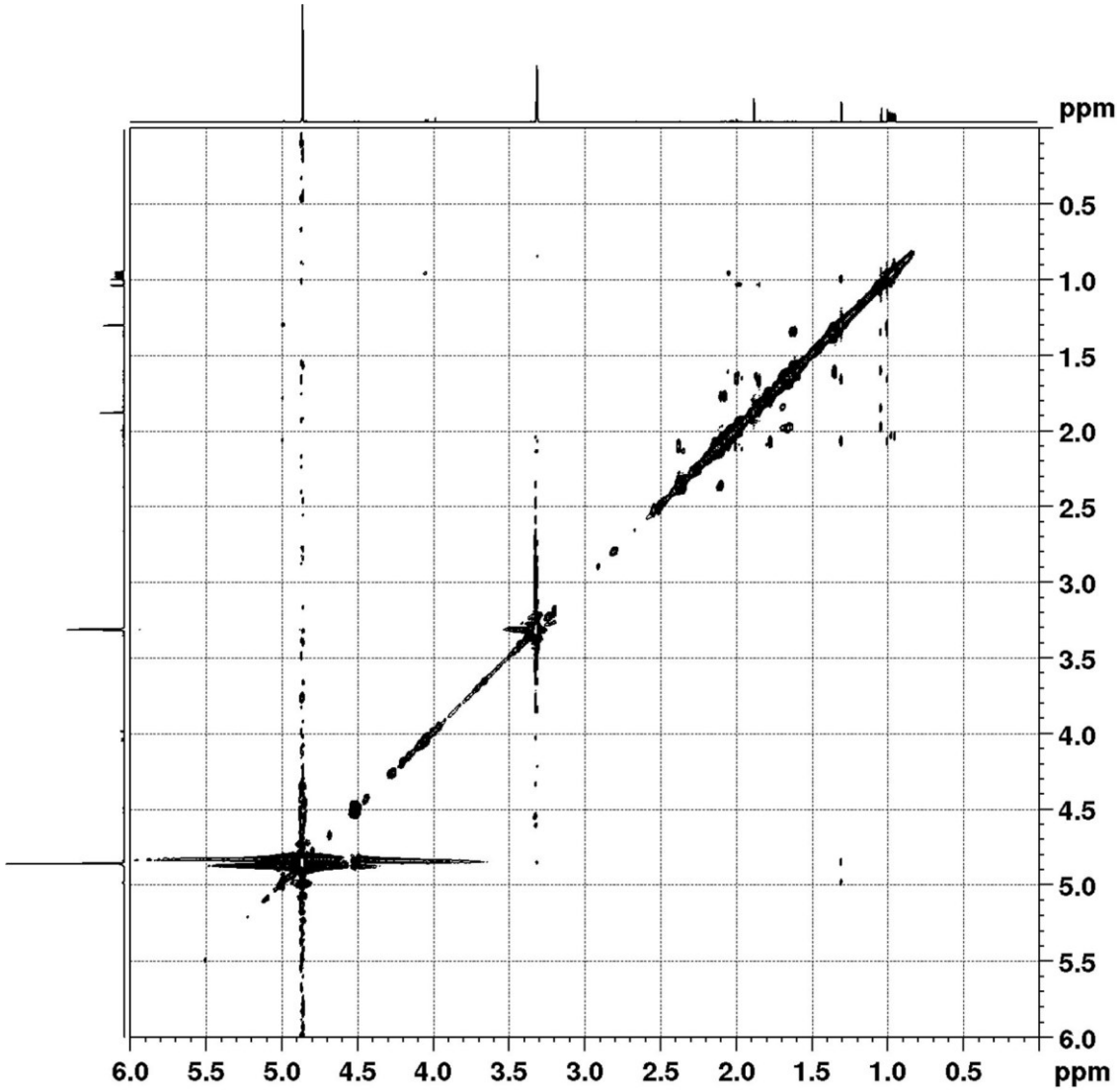

Figure S32. The ROESY (600 MHz, CD_3OD) spectrum of compound **13**

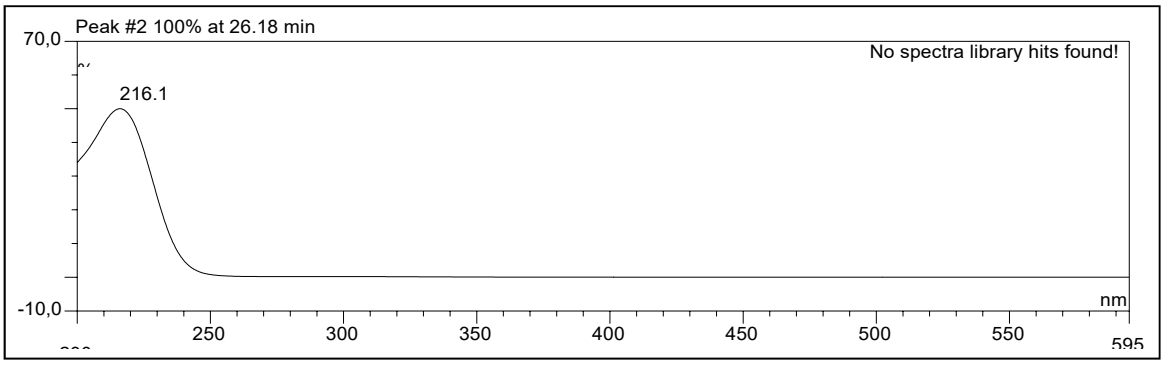

Figure S33. The UV spectrum of compound **13**

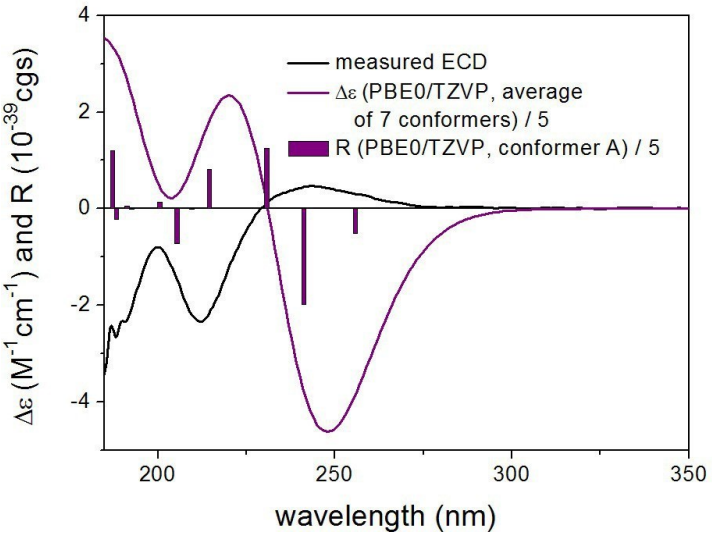

Figure S34. Experimental ECD spectrum of **13** in MeCN compared with the Boltzmann-weighted PBE0/TZVP SMD/MeCN ECD spectrum of (1*S*,5*S*,9*S*,17*S*)-**13**. Level of optimization: SOGGA11-X/TZVP SMD/MeCN. Bars represent the rotatory strength values of the lowest-energy conformer.

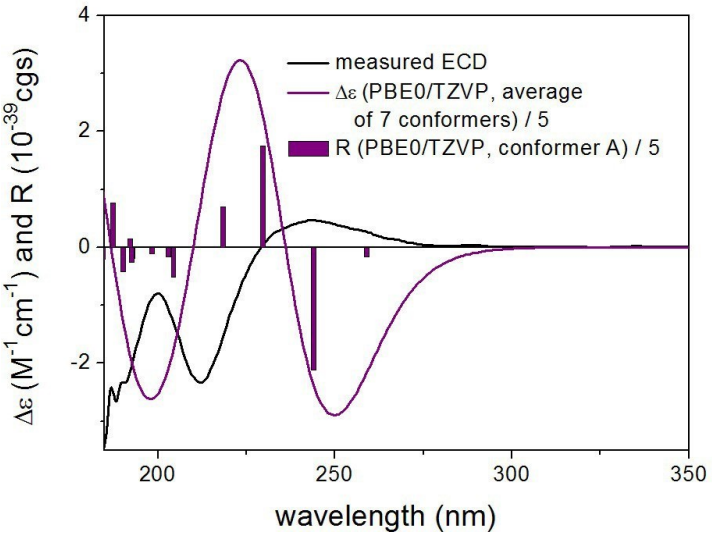

Figure S35. Experimental ECD spectrum of **13** in MeCN compared with the Boltzmann-weighted PBE0/TZVP SMD/MeCN ECD spectrum of (1*R*,5*R*,9*R*,17*S*)-**13**. Level of optimization: SOGGA11-X/TZVP SMD/MeCN. Bars represent the rotatory strength values of the lowest-energy conformer.

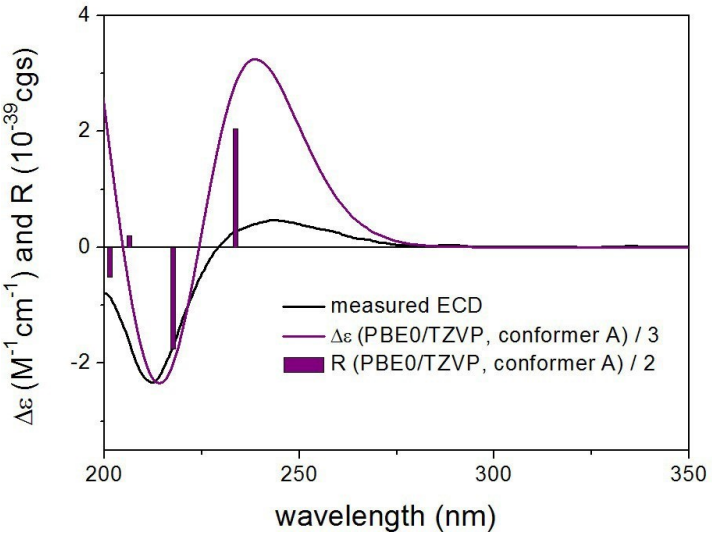

Figure S36. Experimental ECD spectrum of **13** in MeCN compared with the lowest-energy PBE0/TZVP PCM/MeCN ECD spectrum of (1*R*,5*R*,9*R*,17*S*)-**13**. Level of optimization: ωB97X/TZVP PCM/MeCN. Bars represent the rotatory strength values of the lowest-energy conformer.

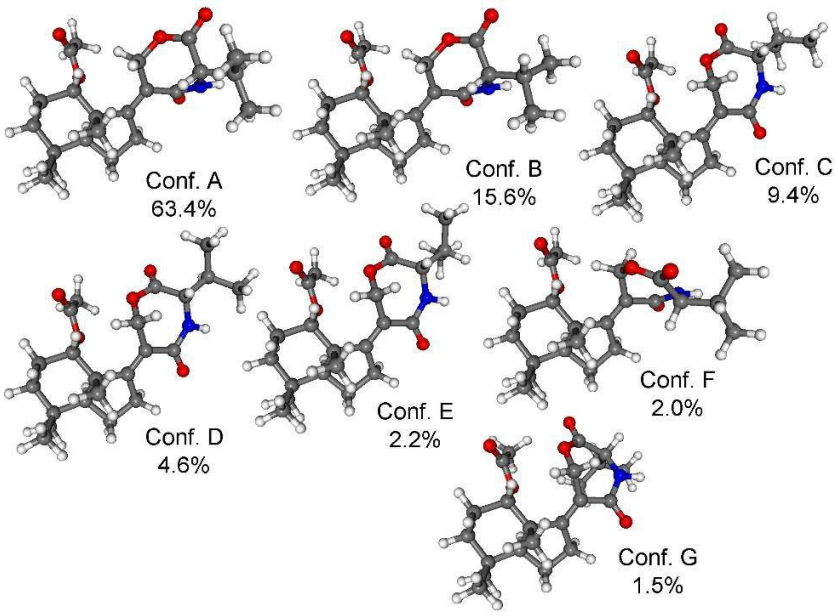

Figure S37. Structure and population of the low-energy SOGGA11-X/TZVP SMD/MeCN conformers (>1%) of (1*S*,5*S*,9*S*,17*S*)-**13**.

38

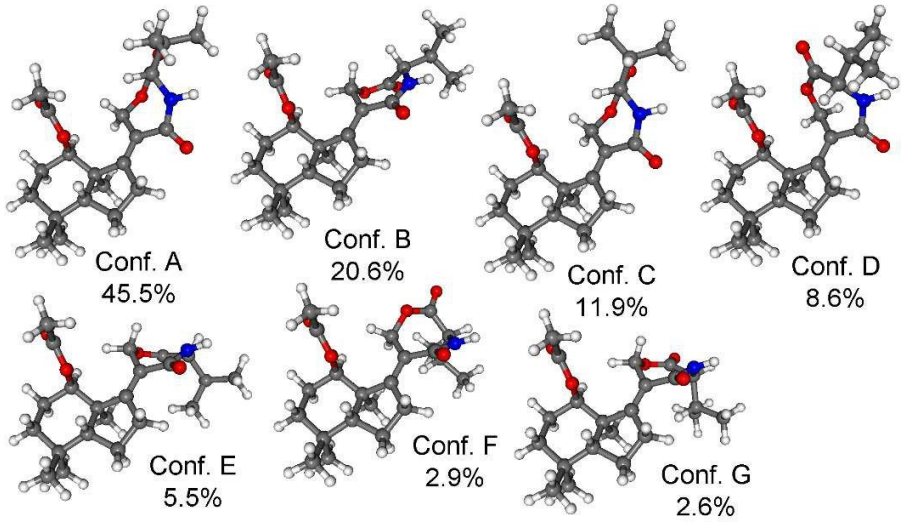

Figure S38. Structure and population of the low-energy SOGGA11-X/TZVP SMD/MeCN conformers (>1%) of (1*R*,5*R*,9*R*,17*S*)-**13**.

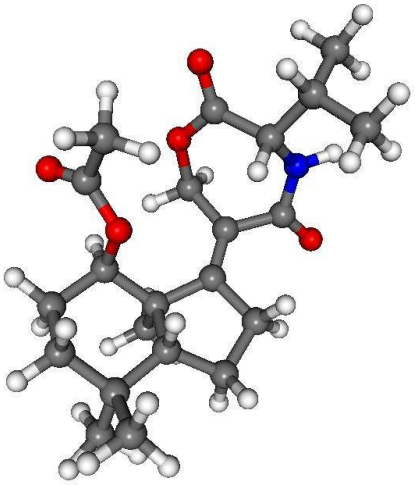

Figure S39. Structure and population of the lowest-energy (24.5%) ωB97X/TZVP PCM/MeCN conformer of (1*R*,5*R*,9*R*,17*S*)-**13** giving moderate normal agreement with the experimental spectrum.

40

Table S1. Boltzmann populations and specific optical rotations of the low-energy conformers of (1*S*,5*S*,9*S*,17*S*)-**13** computed at various levels for the CAM-B3LYP/TZVP PCM/MeOH conformers.

Conformer	Boltzmann population	B3LYP/TZVP	BH&HLYP/TZVP	CAM-B3LYP/TZVP	PBE0/TZVP
Conf. A	40.93	-187.33	-147.95	-162.42	-186.18
Conf. B	19.22	-151.15	-125.76	-134.37	-147.79
Conf. C	11.88	-121.90	-103.53	-108.98	-120.47
Conf. D	10.01	-203.98	-158.23	-176.23	-200.78
Conf. E	6.80	-103.16	-83.91	-90.43	-99.13
Conf. F	4.68	150.48	108.11	116.47	149.72
Conf. G	2.39	-191.12	-146.17	-162.36	-188.44
Conf. H	1.38	-36.76	-13.57	-23.89	-31.78
Conf. I	1.14	-83.09	-50.83	-62.13	-77.51
Average	N/A	-148.95	-119.64	-130.55	-146.88

Table S2. Boltzmann populations and specific optical rotations of the low-energy conformers of (1*R*,5*R*,9*R*,17*S*)-**13** computed at various levels for the CAM-B3LYP/TZVP PCM/MeOH conformers.

Conformer	Boltzmann population	B3LYP/TZVP	BH&HLYP/TZVP	CAM-B3LYP/TZVP	PBE0/TZVP
Conf. A	27.71	-232.94	-173.86	-189.03	-233.36
Conf. B	26.26	-226.28	-179.97	-188.62	-224.40
Conf. C	17.71	61.33	36.20	45.85	57.12
Conf. D	7.84	-109.95	-74.11	-82.49	-109.60
Conf. E	6.68	-215.93	-157.75	-171.23	-216.53
Conf. F	6.16	-156.34	-113.01	-121.56	-155.20
Conf. G	2.44	45.40	27.45	38.13	42.88
Conf. H	1.78	61.30	38.97	49.17	57.60
Conf. I	1.72	57.21	33.29	42.28	47.30
Conf. J	1.38	165.66	128.77	143.60	162.51
Average	N/A	-140.76	-108.97	-115.04	-141.41

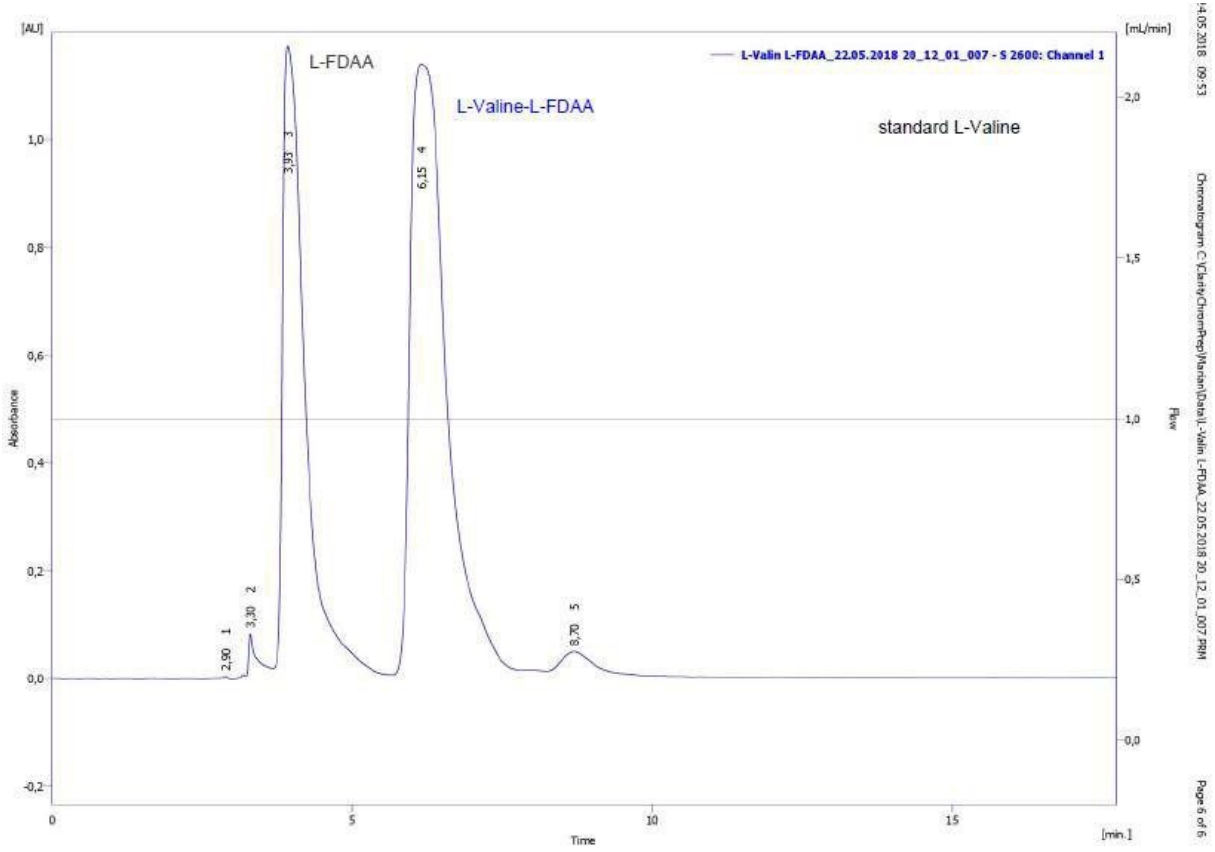

Figure S40. The HPLC chromatogram of L-Valin L-FDAA for Marfey's method

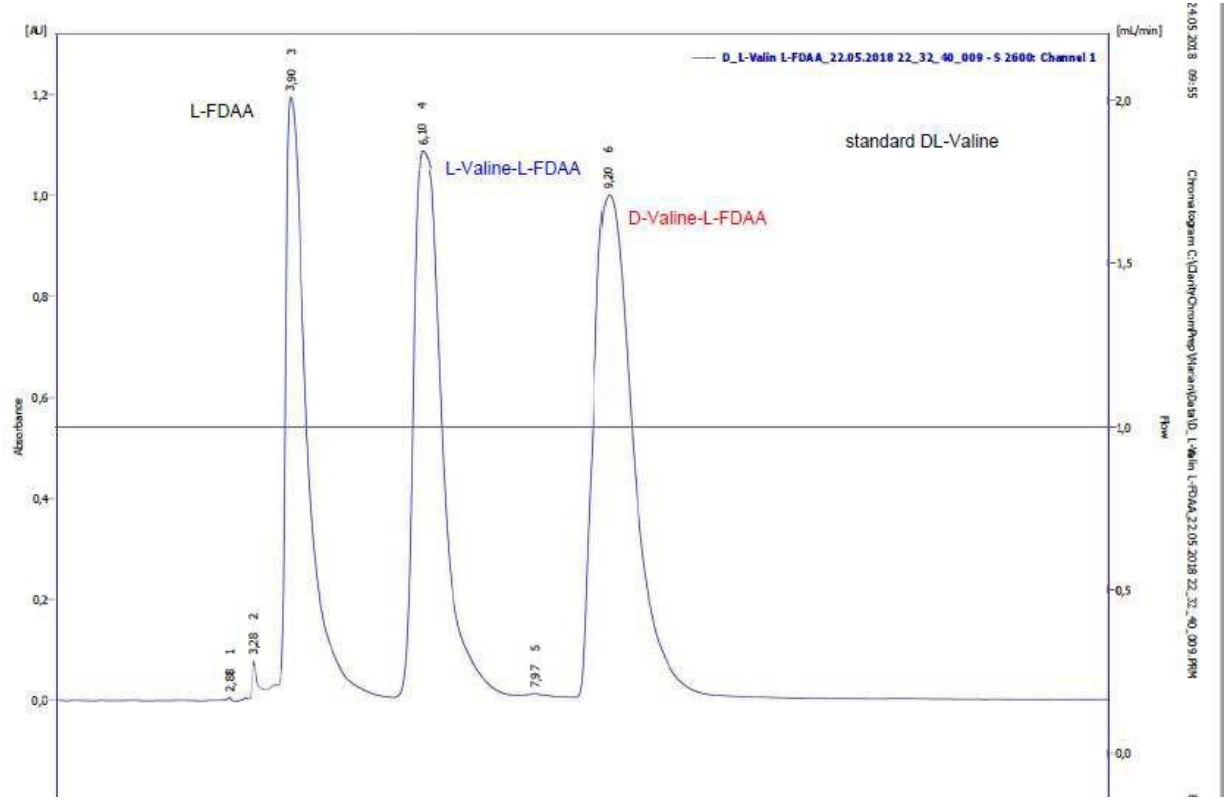

Figure S41. The HPLC chromatogram of DL-Valin L-FDAA for Marfey's method

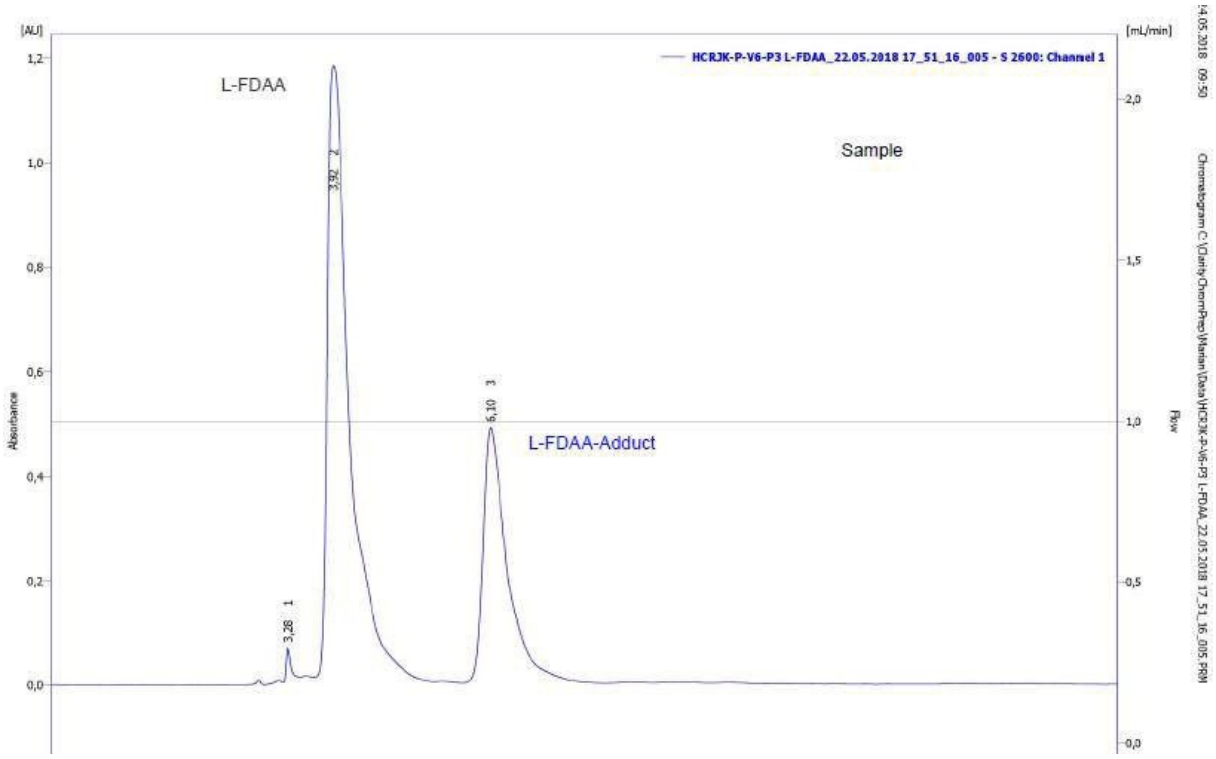

Figure S42. The HPLC chromatogram of compound **13** with L-FDAA for Marfey's method

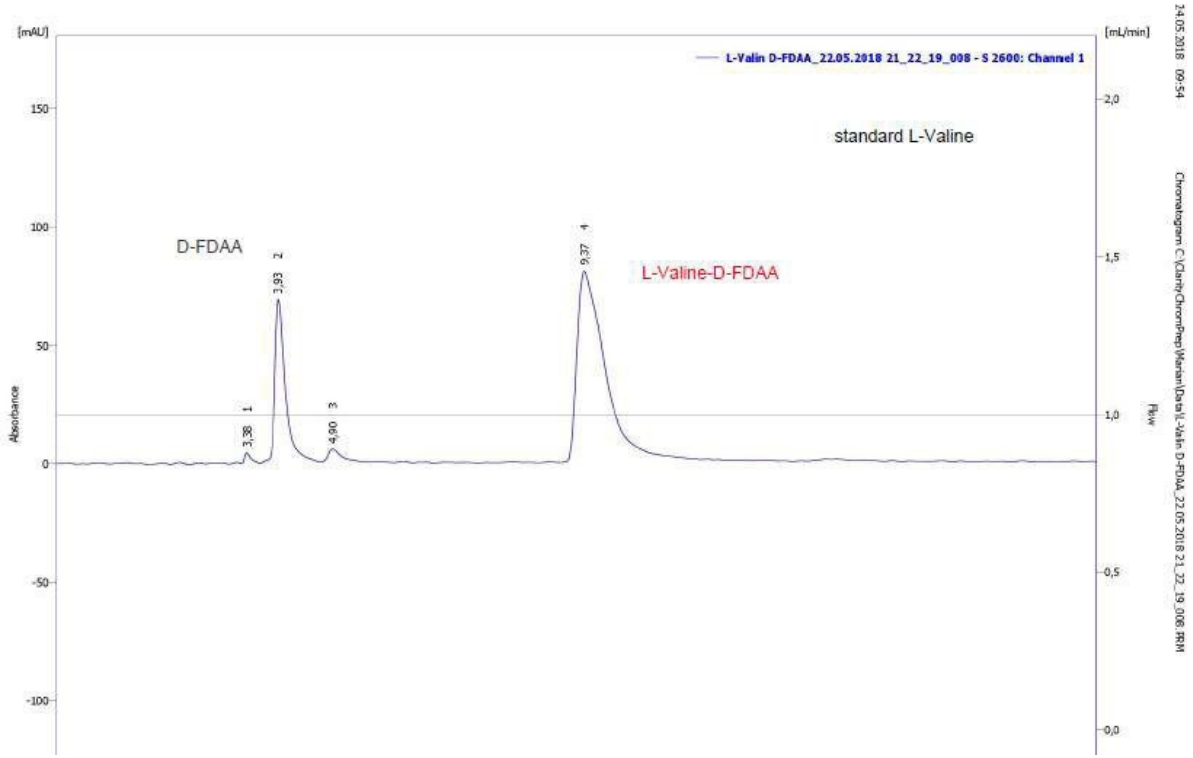

Figure S43. The HPLC chromatogram of L-Valin D-FDAA for Marfey's method

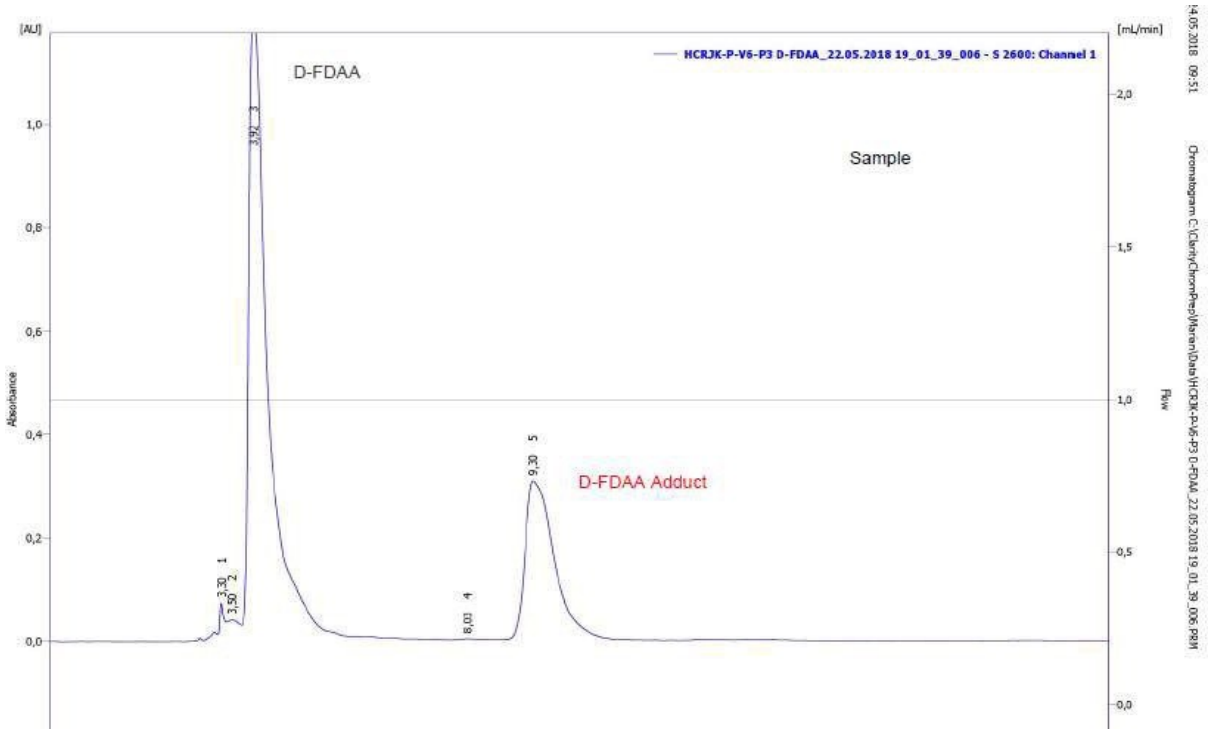

Figure S44. The HPLC chromatogram of compound **13** with D-FDAA for Marfey's method

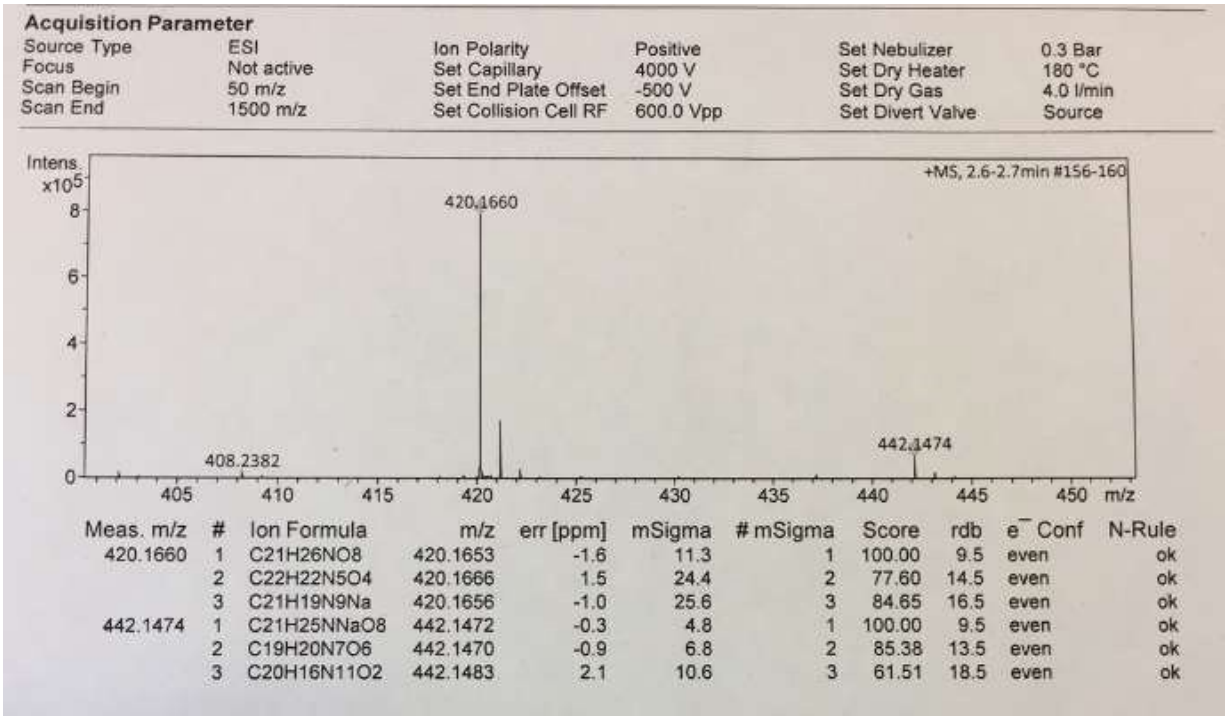

Meas. m/z	#	Ion Formula	m/z	err [ppm]	mSigma	# mSigma	Score	rdb	e⁻ Conf	N-Rule
420.1660	1	C21H26NO8	420.1653	-1.6	11.3	1	100.00	9.5	even	ok
	2	C22H22N5O4	420.1666	1.5	24.4	2	77.60	14.5	even	ok
	3	C21H19N9Na	420.1656	-1.0	25.6	3	84.65	16.5	even	ok
442.1474	1	C21H25NNaO8	442.1472	-0.3	4.8	1	100.00	9.5	even	ok
	2	C19H20N7O6	442.1470	-0.9	6.8	2	85.38	13.5	even	ok
	3	C20H16N11O2	442.1483	2.1	10.6	3	61.51	18.5	even	ok

Figure S45. The HRESIMS of compound **15**

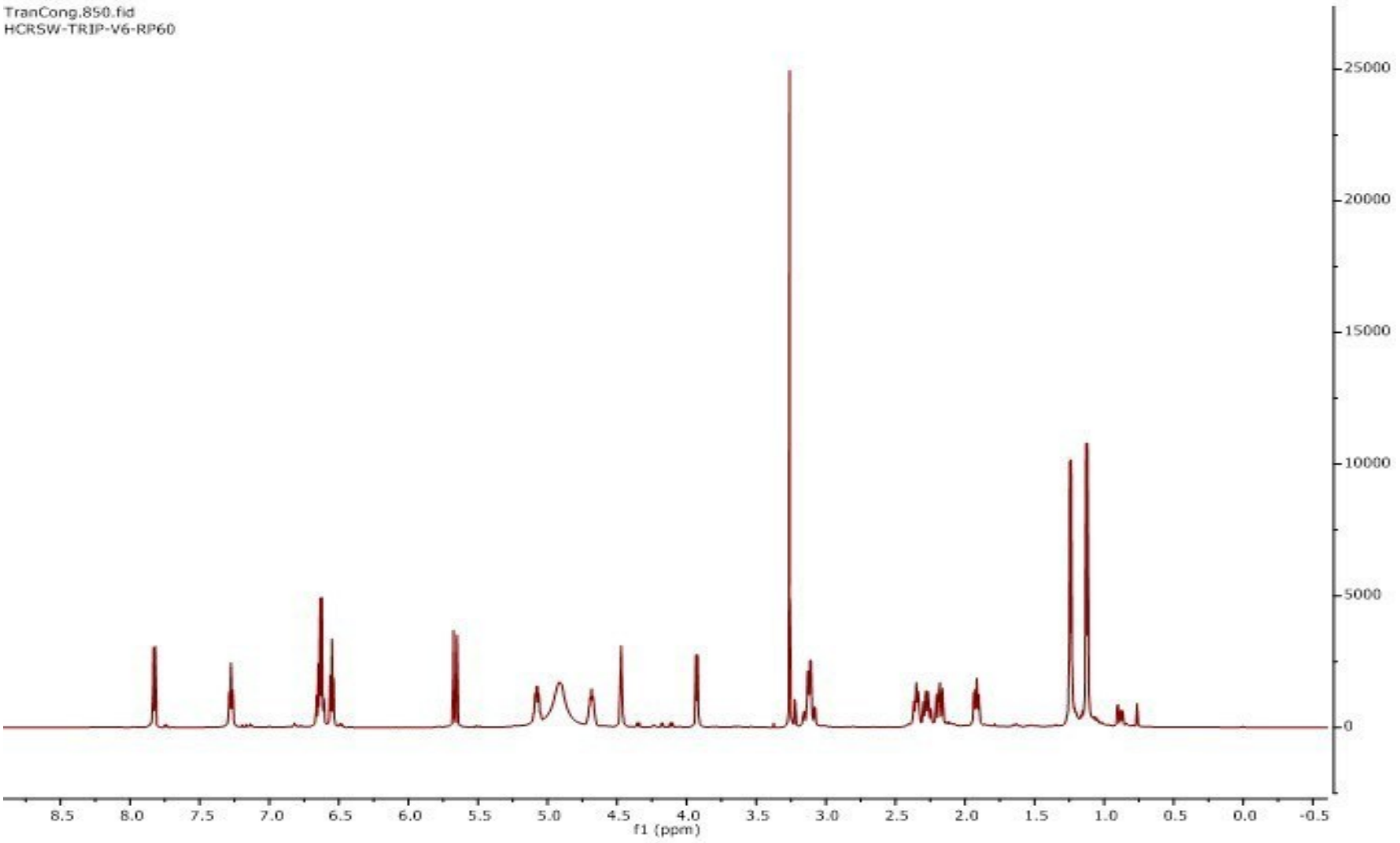

Figure S46. The ^{1}H NMR (600 MHz, CD_3OD) of compound **15**

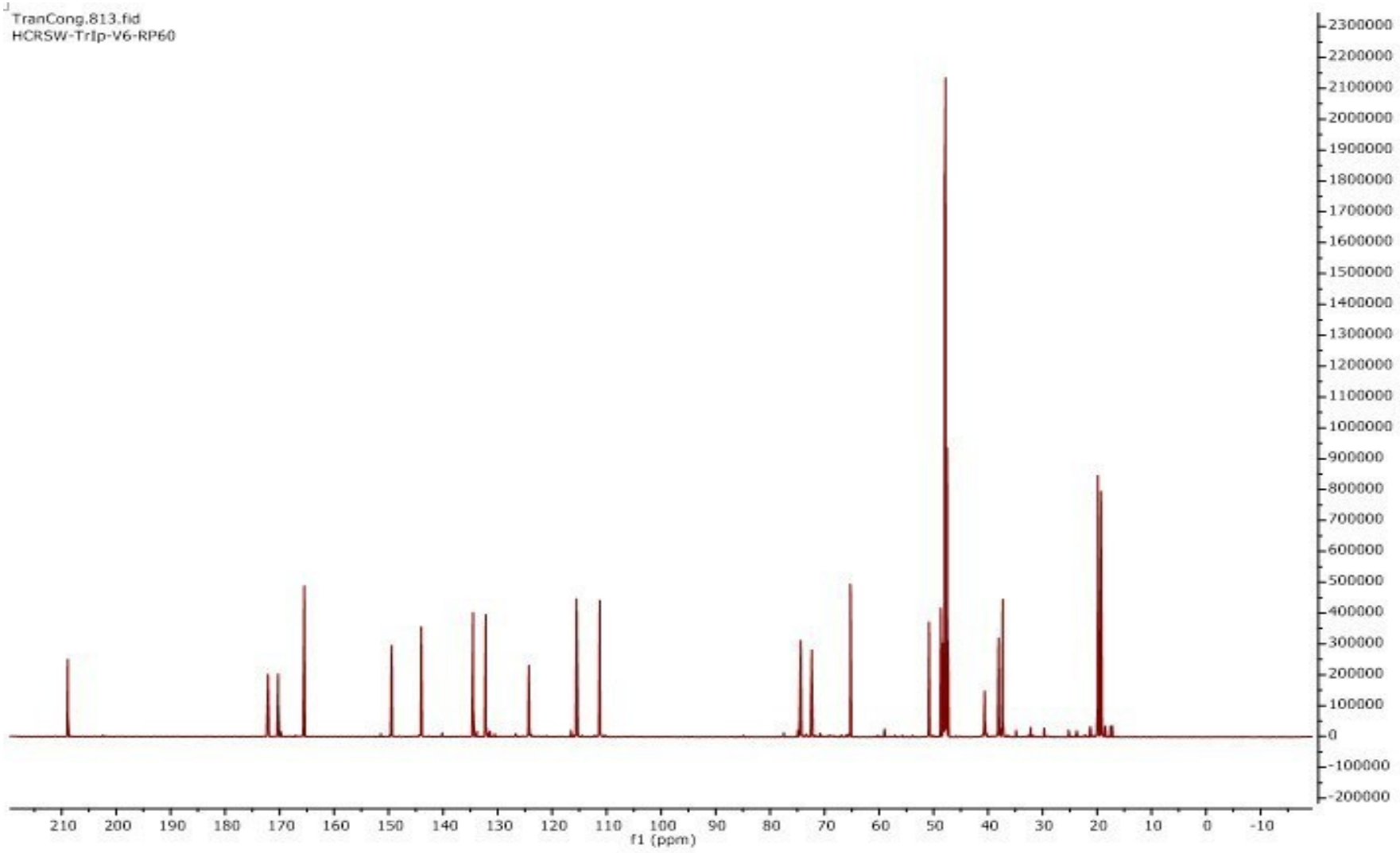

Figure S47. The ^{13}C NMR (150 MHz, CD_3OD) of compound **15** 49

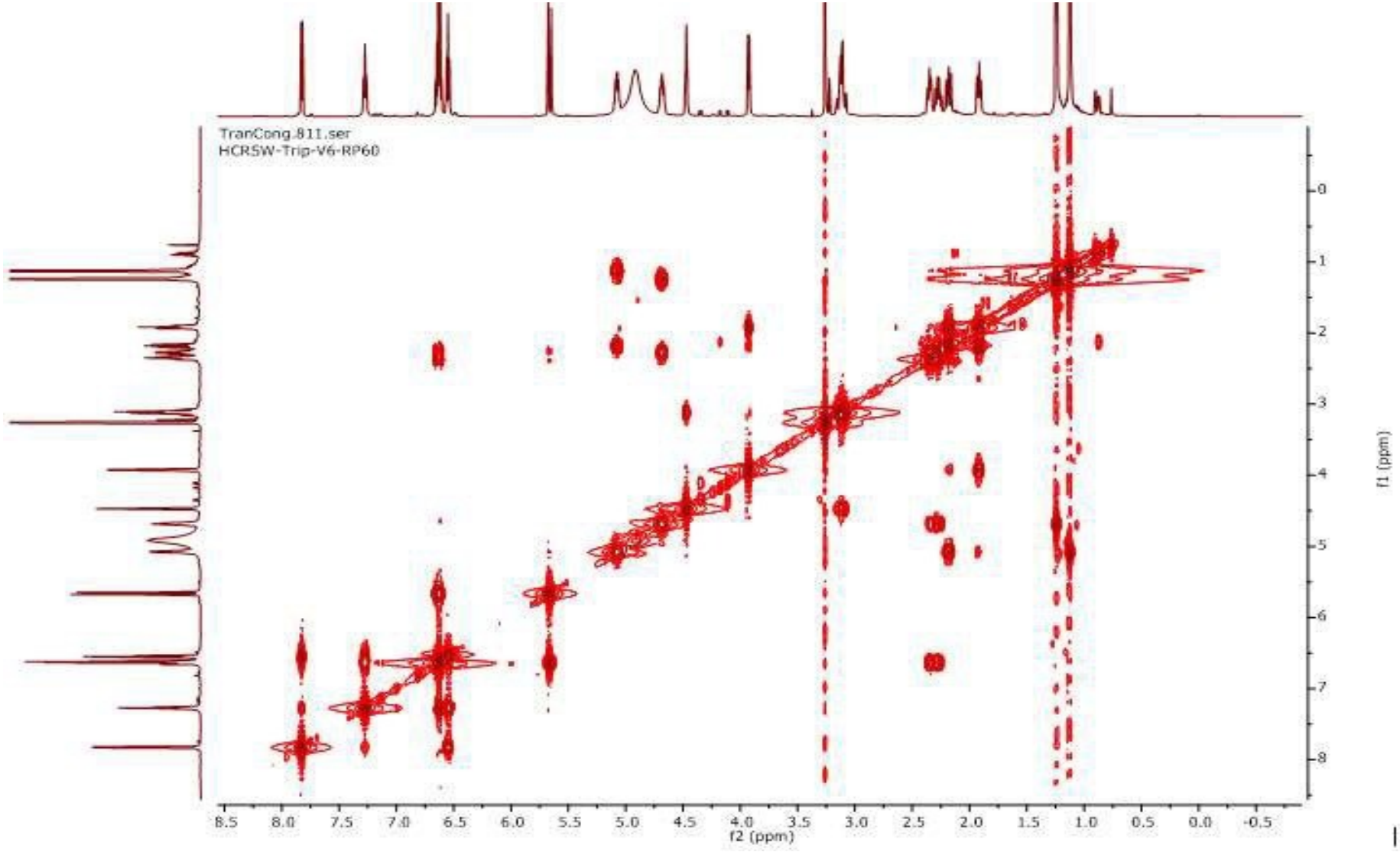

Figure S48. The COSY (600 MHz, CD_3OD) of compound **15**

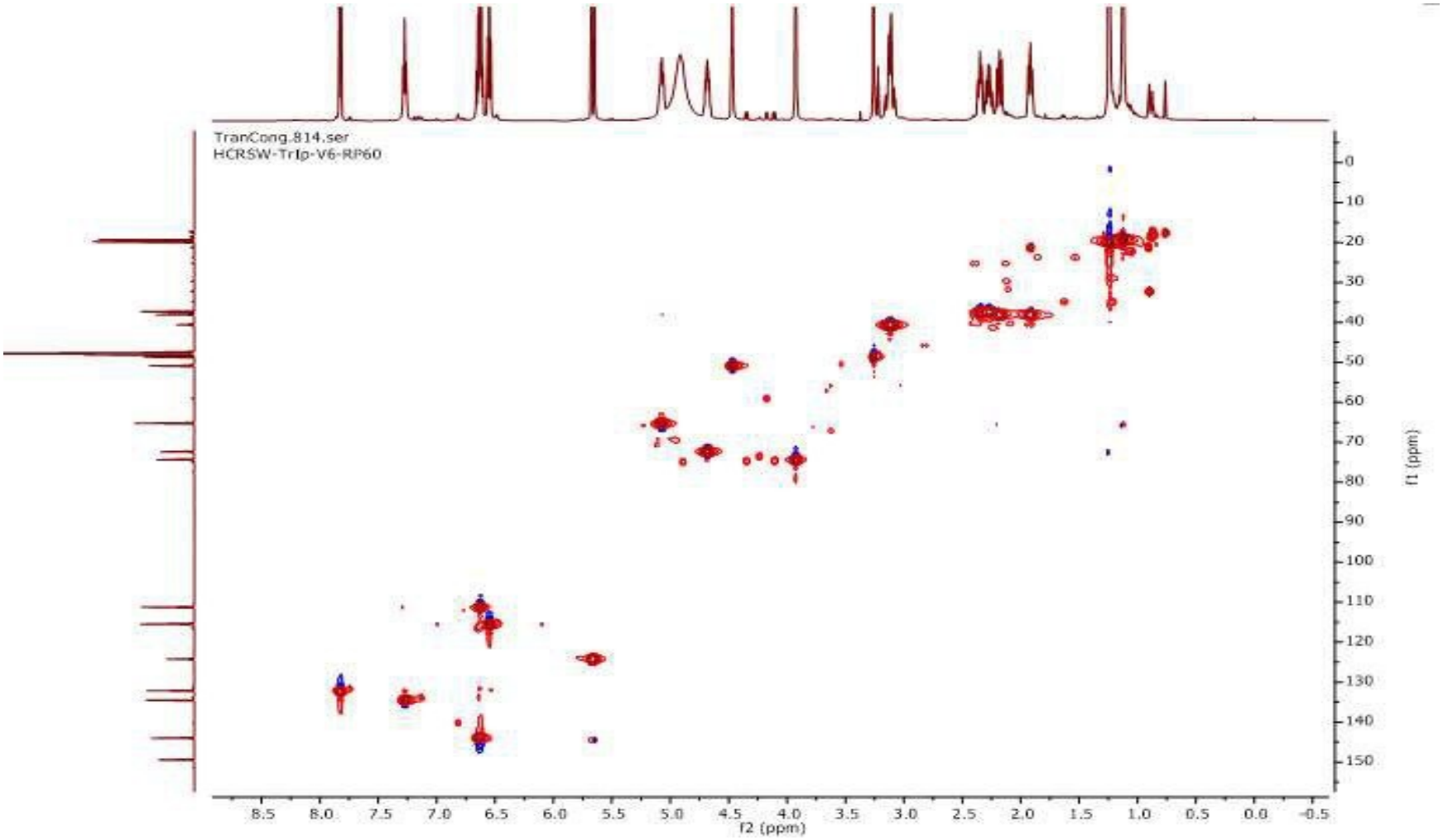

Figure S49. The HSQC (600 MHz, CD_3OD) of compound **15**

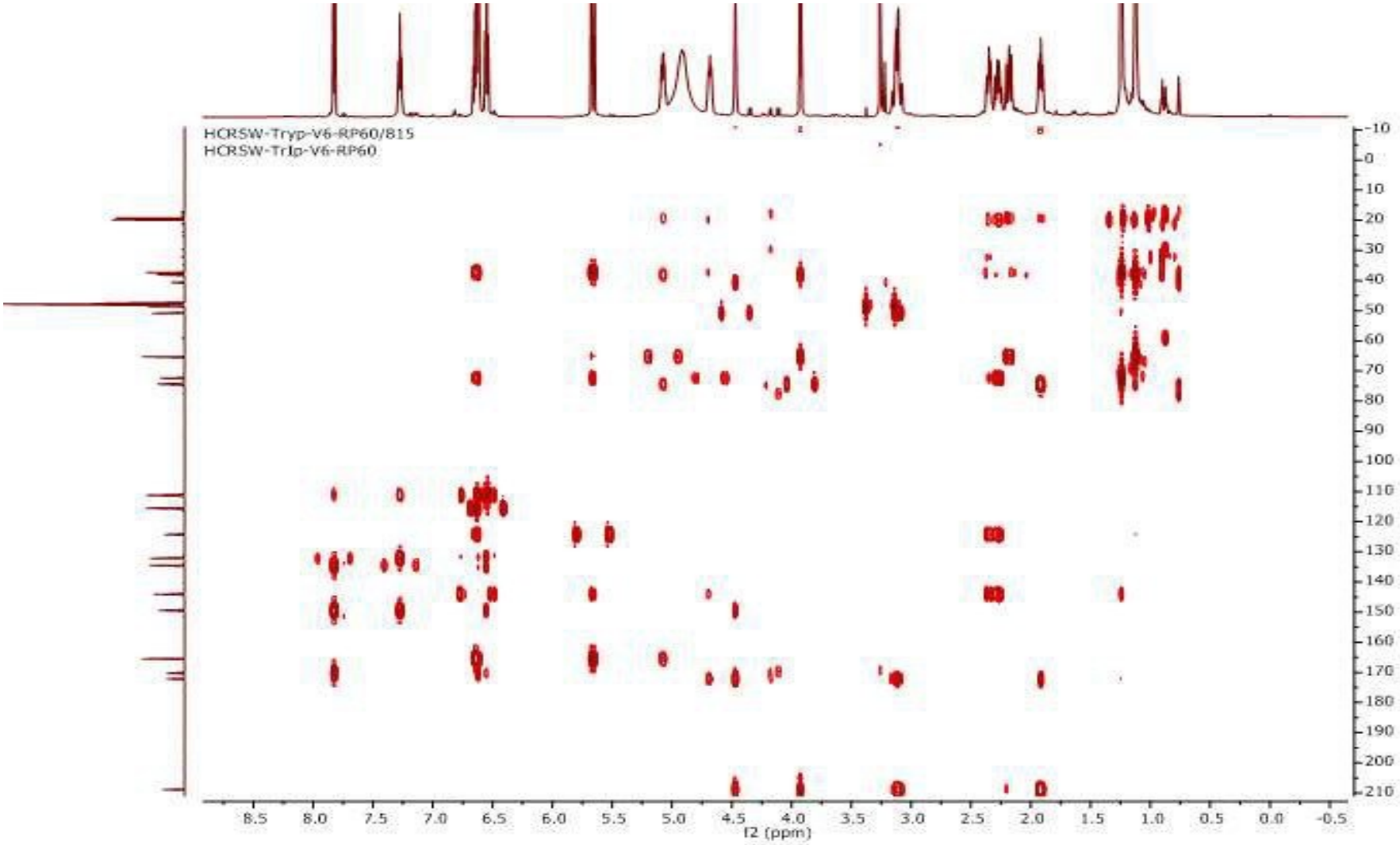

Figure S50. The HMBC (600 MHz, CD_3OD) of compound **15** 52

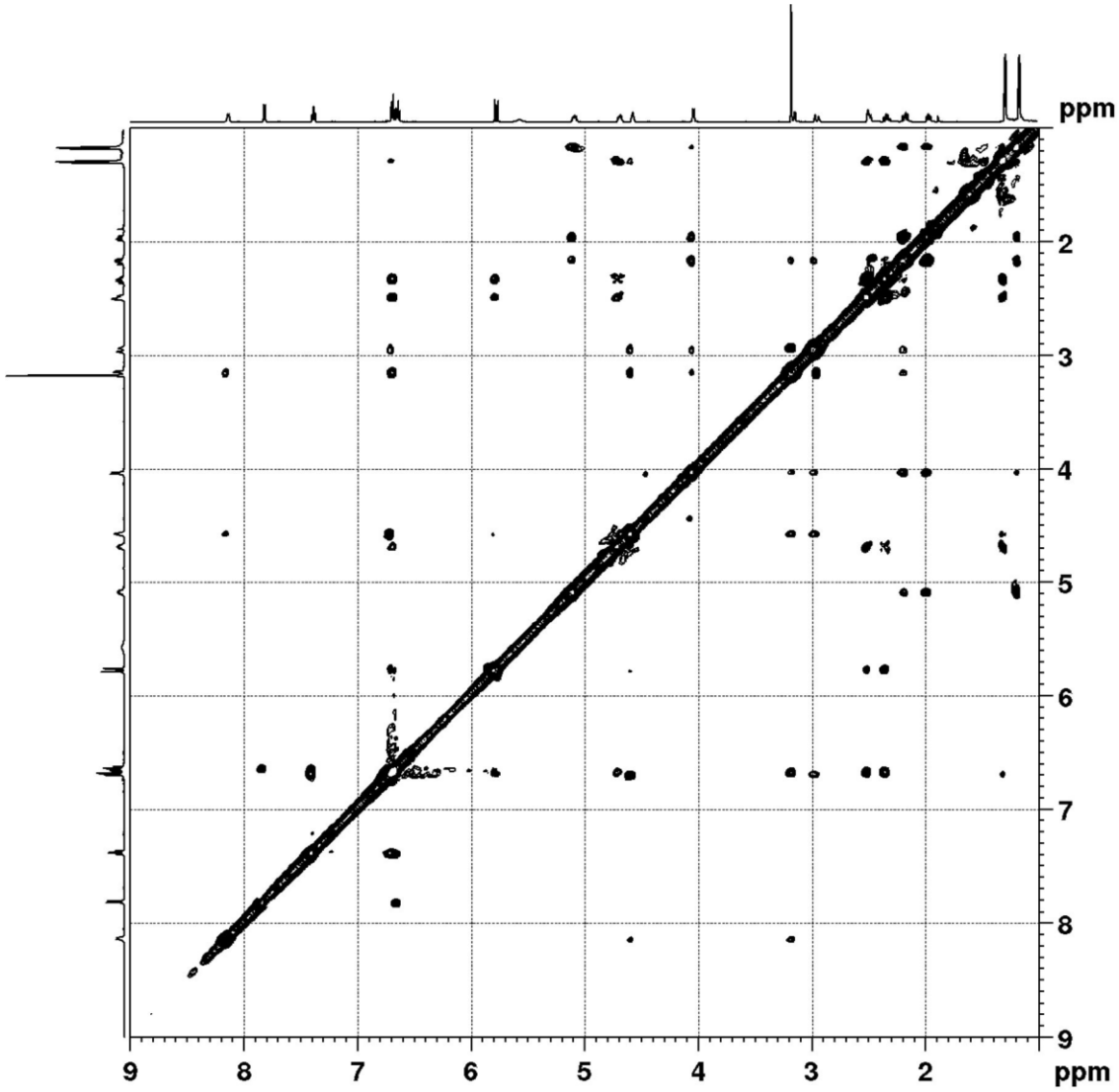

Figure S51. The ROESY (600 MHz, CD_3OD) of compound **15**

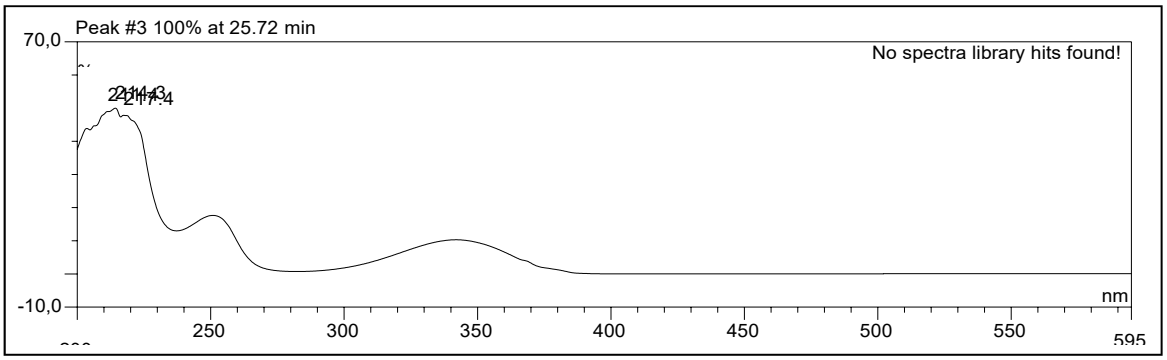

Figure S52. The UV spectrum of compound **15**

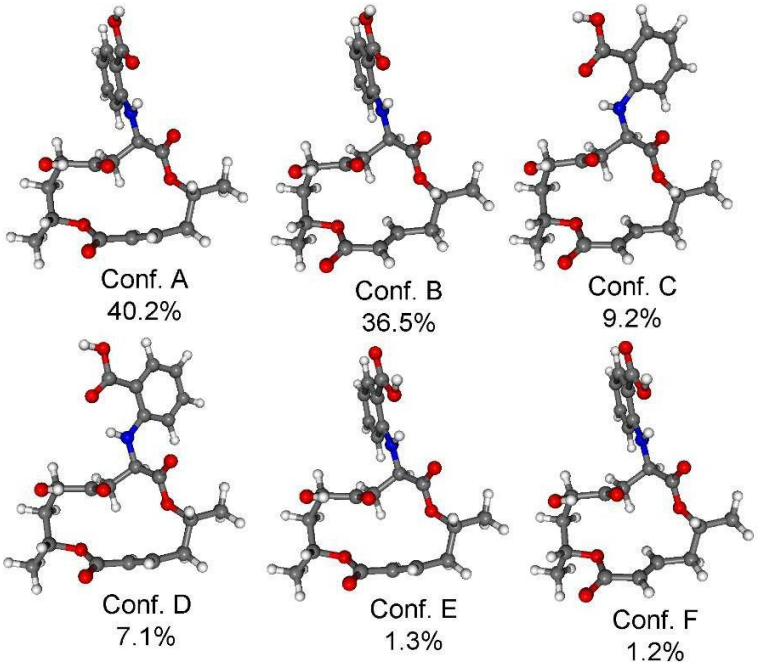

Figure S53. Structure and population of the low-energy ωB97X/TZVP PCM/MeCN conformers (>1%) of (2*R*,8*R*,10*R*,13*R*)-**15**.

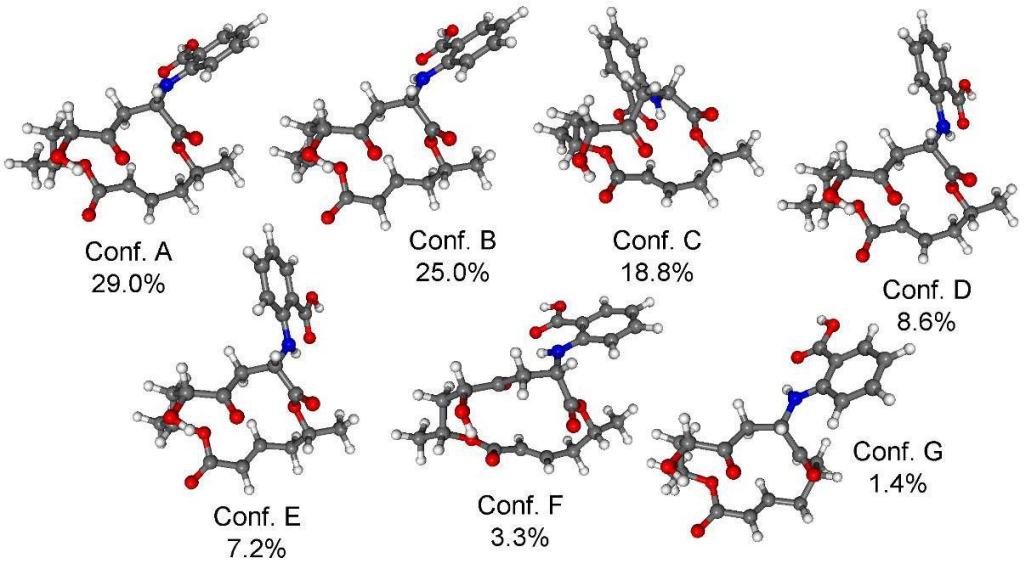

Figure S54. Structure and population of the low-energy ωB97X/TZVP PCM/MeCN conformers (>1%) of (2*R*,8*R*,10*R*,13*S*)-**15**.

Table S3. Comparison of the experimental and the mPW1PW91/6-311+(2d,p) // mPW1PW91/6-311+(2d,p) ^{13}C NMR data of (2*R*,8*R*,10*R*,13*R*)-**15** and (2*R*,8*R*,10*R*,13*S*)-**15**. For a better comparison Δδ values over 2.5 were marked with yellow and those over 5.0 with red.

Carbon	Exp.	calcd (2*R*,8*R*,10*R*,13*R*)-**15**	calcd (2*R*,8*R*,10*R*,13*S*)-**15**	Δδ (2*R*,8*R*,10*R*,13*R*)-**15**	Δδ (2*R*,8*R*,10*R*,13*S*)-**15**
C-2	71.2	72.60	75.77	1.40	4.57
C-3	37.1	40.37	41.11	3.27	4.01
C-4	143.6	151.29	153.11	7.69	9.51
C-5	125.1	125.68	127.42	0.58	2.32
C-6	164.5	165.97	168.99	1.47	4.49
C-8	65.2	64.45	68.31	0.75	3.11
C-9	38.4	39.82	41.32	1.42	2.92
C-10	73.0	76.04	77.86	3.04	4.86
C-11	209.1	212.93	216.57	3.83	7.47
C-12	41.8	41.47	43.92	0.33	2.12
C-13	49.8	50.90	55.79	1.10	5.99
C-14	172.3	172.06	173.68	0.24	1.38
C-15	20.0	19.89	20.31	0.11	0.31
C-16	20.5	20.06	20.72	0.44	0.22
C-17	149.2	149.65	152.29	0.45	3.09
C-18	111.4	109.11	113.10	2.29	1.70
C-19	134.5	136.70	139.34	2.20	4.84
C-20	115.5	113.53	116.62	1.97	1.12
C-21	131.9	133.99	135.79	2.09	3.89
C-22	111.2	106.80	109.53	4.40	1.67
C-23	169.7	168.29	172.23	1.41	2.53
CMAE	N/A	N/A	N/A	1.95	3.48

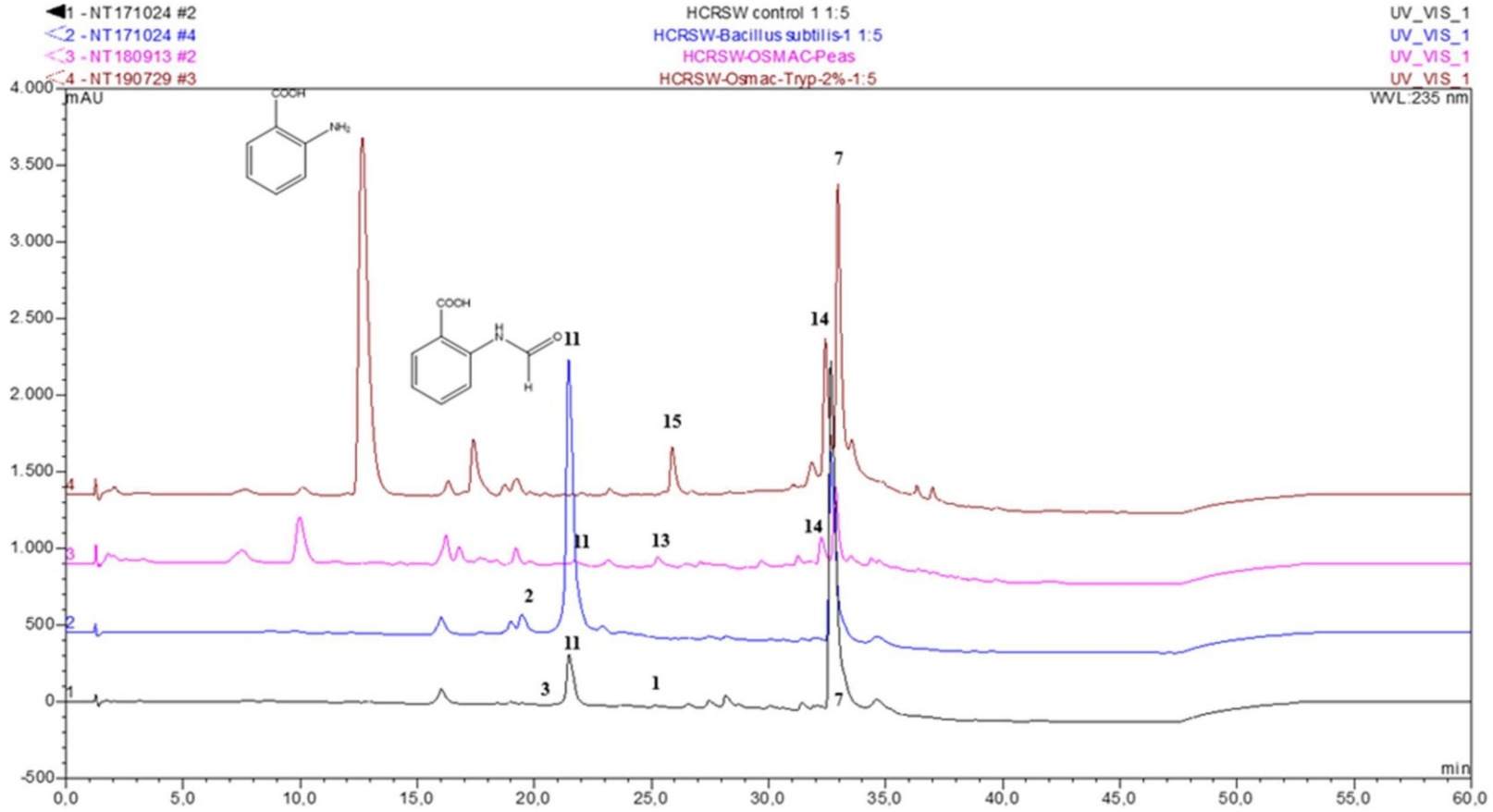

Figure S55. HPLC overlays of the crude extracts.

Table S7. Yield (mg/flask) of compound **11** in axenic fungal control and in coculture with *Bacillus subtilis*.

flask number	Control	Coculture
1	13.4	72.3
2	1.8	65.1
3	1.9	51.5
4	14.0	74.7
5	2.3	76.8
$\bar{x}$	6.7 ± 5.8	68.1 ± 9.2

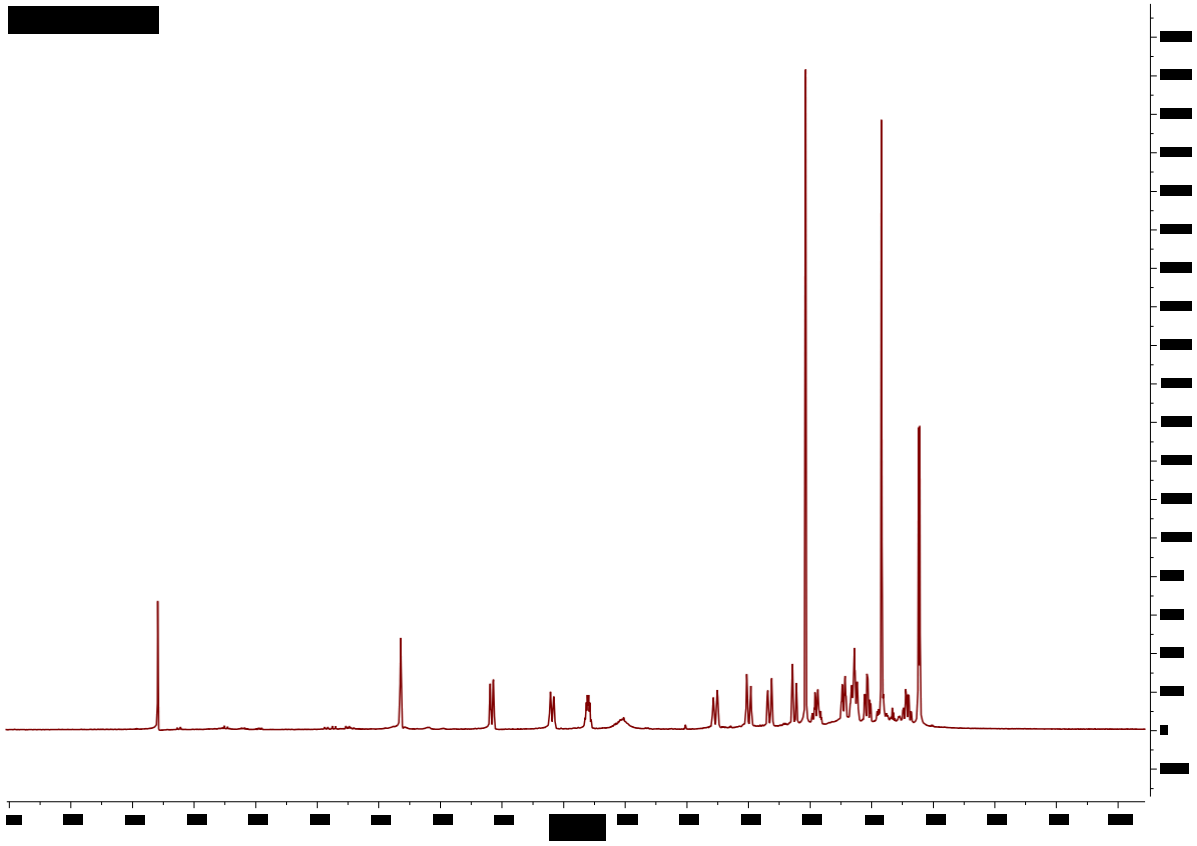

Figure S56. The ^{1}H NMR (600 MHz, CD_3Cl) spectrum of compound **2** after storage in EtOAc.

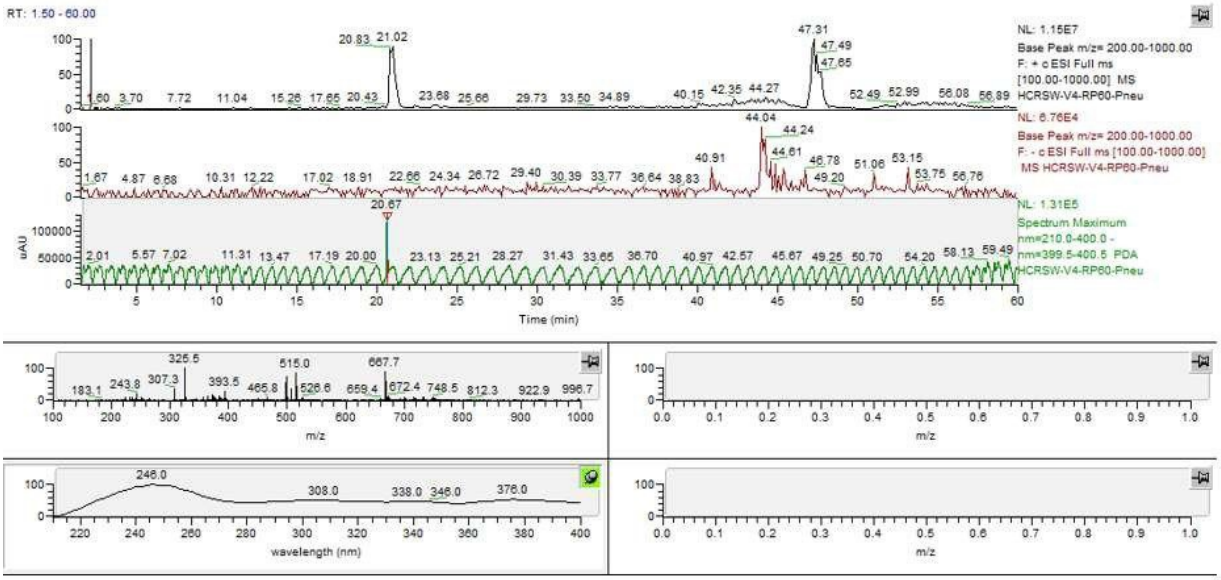

Figure S57. LCMS of compound **2** after storage in EtOAc.

Table S8. Raw data of compound **7** against the L51178Y mouse lymphoma cell line.

Blank						Mean	Mean-Blank	Growth in %	Growth Inhibition in %	Cons. (µg/ml)	SD
0.039	0.039	0.039	0.024	0.039	0.015						
0.197	0.483	0.498	0.391	0.451	0.406	0.446	0.249	100.0	0.0	0	0.05
0.204	0.358	0.351	0.328	0.418	0.379	0.367	0.163	65.4	34.6	0.1	0.03
0.205	0.203	0.206	0.196	0.207	0.187	0.200	-0.005	-2.1	102.1	0.3	0.01
0.2	0.209	0.187	0.197	0.187	0.201	0.196	-0.004	-1.5	101.5	1	0.01
0.23	0.238	0.211	0.228	0.204	0.23	0.222	-0.008	-3.1	103.1	3	0.01
0.367	0.358	0.343	0.36	0.352	0.351	0.353	-0.014	-5.7	105.7	10	0.01
0.039	0.039	0.026	0.039	0.011	0.037			IC_{50} 0.14 µg/mL			

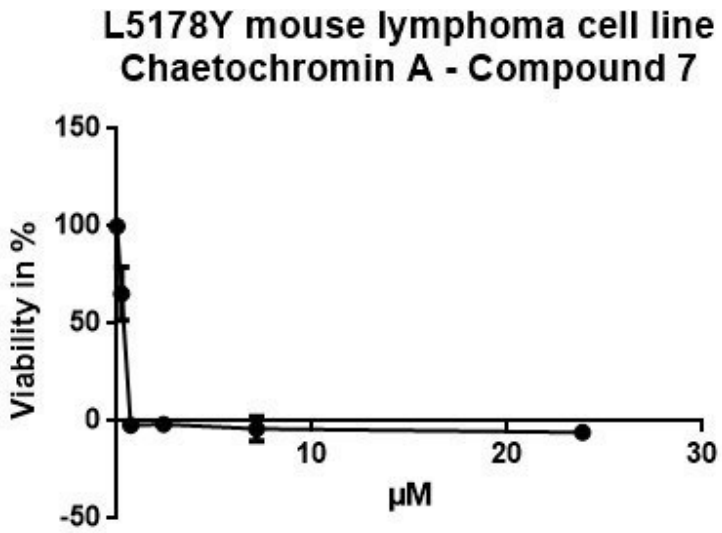

Figure S58. Dose-dependence curve of compound **7** against the L5178Y mouse lymphoma cell line.

Table S9. Raw data of compound **11** against the L51178Y mouse lymphoma cell line.

Blank						Mean	Mean-Blank	Growth in %	Growth Inhibition in %	Cons. (µg/ml)	SD
0.038	0.012	0.006	0.034	0.034	0.068						
0.153	0.709	0.65	0.749	0.637	0.831	0.715	0.563	100.0	0.0	0	0.08
0.164	0.342	0.357	0.563	0.559	0.63	0.490	0.326	58.0	42.0	0.1	0.13
0.15	0.153	0.176	0.24	0.278	0.31	0.231	0.081	14.5	85.5	0.3	0.07
0.146	0.112	0.149	0.169	0.264	0.272	0.193	0.047	8.4	91.6	1	0.07
0.14	0.149	0.157	0.168	0.294	0.276	0.209	0.069	12.2	87.8	3	0.07
0.153	0.236		0.177	0.309	0.279	0.250	0.098	17.3	82.7	10	0.06
0.03	0.035	0.005	0.001	0.073	0.062			IC_{50} 0.14 µg/mL			

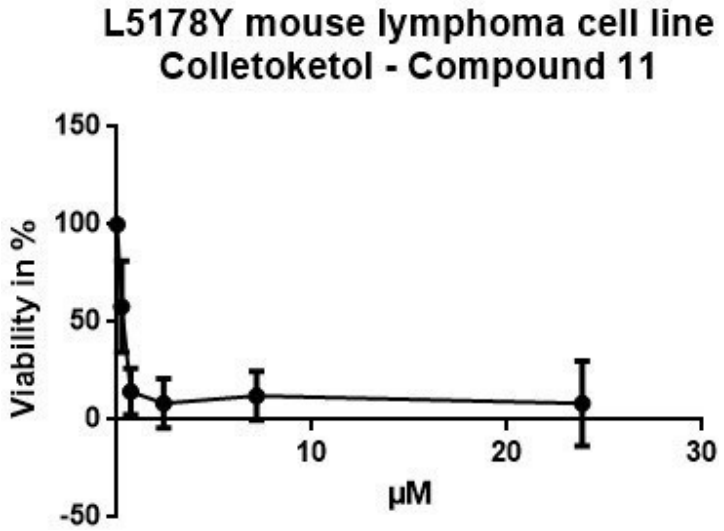

Figure S59. Dose-dependence curve of compound **11** against the L5178Y mouse lymphoma cell line.

Table S10. Raw data of compound **15** against the L51178Y mouse lymphoma cell line.

Blank						Mean	Mean-Blank	Growth in %	Growth Inhibition in %	Cons. (µg/ml)	SD
0.206	0.075	0.204	0.181	0.283	0.264						
0.521	0.695	0.925	0.933	1.043	1.045	0.928	0.407	100.0	0.0	0	0.14
0.5		0.539	0.578	0.639	0.659	0.604	0.104	25.5	74.5	0.1	0.06
0.539	0.312	0.427	0.463	0.542	0.57	0.463	-0.076	-18.7	118.7	0.3	0.10
0.513	0.338	0.414	0.505	0.534	0.611	0.480	-0.033	-8.0	108.0	1	0.11
0.488	0.365	0.38	0.481	0.497	0.589	0.462	-0.026	-6.3	106.3	3	0.09
0.526	0.444	0.391	0.912	0.527	0.604	0.576	0.050	12.2	87.8	10	0.20
0.266	0.15	0.134	0.252	0.232	0.292			IC_{50} 0.065 µg/mL			

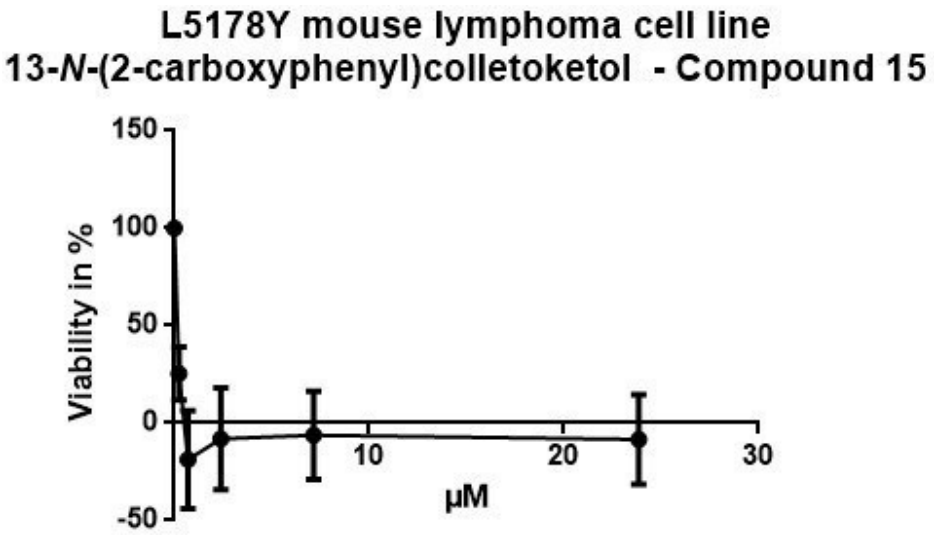

Figure S60. Dose-dependence curve of compound **15** against the L5178Y mouse lymphoma cell line.

6. Publication 3 - Furoic Acid Derivatives from the Endophytic Fungus *Coniothyrium* sp.

Nam Michael Tran-Cong [a] Attila Mándi[b], Kurtán Tibor[b], Wenhan Lin [c], Zhen Liu [a,*], Peter Proksch [a,*]

Published in Chirality

[a]Institute of Pharmaceutical Biology and Biotechnology, Heinrich Heine University Düsseldorf, Universitätsstrasse 1, 40225 Düsseldorf, Germany

[b]Department of Organic Chemistry, University of Debrecen, P. O. Box 400, H-4002 Debrecen, Hungary

[c]State Key Laboratory of Natural and Biomimetic Drugs, Peking University, Beijing 100191, China

Tran-Cong, NM, Mándi, A, Király, SB, et al. Furoic acid derivatives from the endophytic fungus Coniothyrium sp. Chirality. 2020; 1– 6. https://doi.org/10.1002/chir.23209

Received: 17 November 2019 | Revised: 19 January 2020 | Accepted: 17 February 2020
DOI: 10.1002/chir.23209

WILEY

SPECIAL ISSUE ARTICLE

Furoic acid derivatives from the endophytic fungus *Coniothyrium* sp.

Nam Michael Tran-Cong[1] | **Attila Mándi**[2] | **Sándor Balázs Király**[2] | **Tibor Kurtán**[2] | **Wenhan Lin**[3] | **Zhen Liu**[1] | **Peter Proksch**[1]

[1]Institute of Pharmaceutical Biology and Biotechnology, Heinrich Heine University Düsseldorf, Düsseldorf, Germany

[2]Department of Organic Chemistry, University of Debrecen, Debrecen, Hungary

[3]State Key Laboratory of Natural and Biomimetic Drugs, Peking University, Beijing, China

Correspondence
Zhen Liu and Peter Proksch, Institute of Pharmaceutical Biology and Biotechnology, Heinrich Heine University Düsseldorf, Universitätsstrasse 1, 40225 Düsseldorf, Germany.
Email: zhenfeizi0@sina.com; proksch@hhu.de

Funding information
Deutsche Forschungsgemeinschaft, Grant/Award Numbers: 270650915, GRK 2158, 270650915, GRK 2158; National Research, Development and Innovation Office, Grant/Award Number: K120181; Hungarian Academy of Sciences; Manchot Foundation

Abstract

The endophytic fungus *Coniothyrium* sp. was isolated from leaves of *Quercus robur*. Fermentation of this fungus on solid rice medium yielded two new furoic acid derivatives (**1** and **2**) and two additional known compounds. The structures of the new compounds were determined by extensive analysis of 1D and 2D nuclear magnetic resonance spectra as well as high-resolution mass spectrometry data. Compound **1**, containing three aromatic chromophores attached by rotatable sigma bonds and a chirality center in benzylic position, was found to be a scalemic mixture with an excess of the (S) enantiomer, the absolute configuration of which was elucidated as by the solution time-dependent density functional theory-electronic circular dichroism approach. The ωB97X/TZVP PCM/MeCN and SOGGA11-X/TZVP SMD/MeCN methods were used for geometry reoptimization to reproduce the solution conformational ensemble. All isolated compounds were tested for their cytotoxicity but proved to be inactive.

KEYWORDS

Coniothyrium sp, electronic circular dichroism, furoic acid derivatives, TDDFT-ECD calculation

1 | INTRODUCTION

Endophytic fungi are a prominent source for the discovery of new compounds.[1,2] There are an estimated 1.5 million fungal species on Earth, of which only about 70 000 are currently described.[3] Some endophytic fungal genera such as *Aspergillus* and *Penicillium* are well investigated, and their metabolic patterns are well known, even though new compounds are still reported.[4-6] In this study, the endophytic fungus *Coniothyrium* sp. was isolated from leaves of the deciduous tree *Quercus robur*. Literature search for natural products from *Coniothyrium* species revealed several bioactive compounds. Conioimide that was isolated from the Baltic sea alga-derived fungus *Coniothyrium cereale* showed prominent and selective inhibitory activity towards the protease human leukocyte elastase with an IC_{50} value of 0.2 μg/mL.[7] Coniosclerodorolide, a phenalenone derivative, displayed antibacterial activity against *Staphylococcus aureus* SG511 with an MIC value of 24 μM.[8] Coniothyrione, a chlorocyclopentandienylbenzopyrone, was shown to be

a bacterial protein synthesis inhibitor and was isolated from *Coniothyrium cerealis* MF7209.[9]

In this study, fermentation of *Coniothyrium* sp. on solid rice medium yielded two new furoic acid derivatives (**1** and **2**) and two additional known compounds 2,3-dihydroxy-2,4-diphenylcyclopent-4-en-1-one (**3**)[10] and 2-anhydromevalonic acid (**4**).[11] The structure elucidation of the new compounds and the results of cytotoxicity assay are described in this paper (Figure 1).

2 | MATERIALS AND METHODS

2.1 | General experimental procedures

Optical rotations were measured on a PerkinElmer-241 MC polarimeter. 1D and 2D nuclear magnetic resonance (NMR) spectra were recorded with Bruker ARX 300 or AVANCE DMX 600 NMR spectrometers. Mass spectra were obtained from a Finnigan LCQ Deca XP mass spectrometer, while high-resolution mass spectra were recorded by a FTHRMS-Orbitrap (Thermo-Finnigan) mass spectrometer. A Dionex P580 system was used for high-performance liquid chromatography (HPLC) separations in combination with a diode array detector (UVD340S) and an Eurosphere 10 C_{18} column (125 × 4 mm). Semipreparative HPLC was conducted on a Lachrom-Merck Hitachi system (pump L7100, ultraviolet (UV) detector L7400, Eurosphere 100 C_{18} column, 300 × 8 mm, Knauer Germany). Merck MN silica gel 60M (0.04-0.063 mm) was used as stationary phase for column chromatography. TLC plates precoated with silica gel 60 F254 were used for monitoring separation. UV and electronic circular dichroism (ECD) spectra were recorded on a J-810 spectropolarimeter. The HRESIMS, UV, and NMR spectra were included in the Supporting Information.

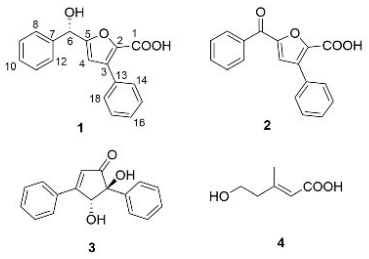

FIGURE 1 Structures of compounds isolated from *Coniothyrium* sp

2.2 | Fungal material and fermentation

Leaves of *Quercus robur* were collected in 2017 in Juelich, Germany. The fresh sample was washed by sterilized water, surface sterilized with 70% ethanol for 1 minute, and cut into small pieces (around 1 × 1 × 1 cm^3) using a flame sterilized blade. These pieces were put on malt agar plates (15 g/L malt extract, 15 g/L agar, and 0.2 g/L chloramphenicol in distilled water, pH 7.4-7.8), and then incubated at room temperature for several days. The purified fungus was later transferred to solid rice medium for fermentation. All steps were conducted in an aseptic environment. The identification of the fungus was done using a molecular protocol as described previously.[12] Sequence data were submitted to GenBank with the accession number MN043344. A voucher strain (2BEY) is kept in the Institute of Pharmaceutical Biology and Biotechnology, Heinrich-Heine University, Düsseldorf, Germany.

Large-scale fermentation of this fungus was conducted in five Erlenmeyer flasks on solid rice medium (100 g rice in 110-mL water and autoclaved) at 20°C under static condition. After 20 days, every flask was treated with 600-mL EtOAc and left overnight. Then the EtOAc extract was evaporated under vacuum to obtain the crude extract.

2.3 | Isolation of compounds

The crude extract (11.65 g) was subjected to silica gel vacuum liquid chromatography (VLC) using a step gradient of *n*-hexane/EtOAc and CH_2Cl_2/MeOH to give 11 fractions (V1-V11). Fraction V4 was further fractionated with RP18-VLC using a gradient of MeOH/H_2O to yield 10 subfractions (V4-1 to V4-10). Compound **3** (6.4 mg) was isolated from subfraction V4-3 by semipreparative HPLC with 30% MeOH/H_2O as mobile phase. Fraction V8 was further subjected to RP18-VLC using a step gradient of MeOH/H_2O to give 10 subfractions (V8-1 to V8-10). Subfraction V8-1 was purified by semipreparative HPLC using 10% MeOH/H_2O to yield **4** (2.1 mg), while subfraction V8-4 was further purified with semipreparative HPLC using 40% MeOH/H_2O to give **1** (1.2 mg) and **2** (2.4 mg).

Coniofuroic acid A (**1**): white amorphous solid; $[\alpha]_D^{20}$ = -4 (*c* = 0.2 in $CHCl_3$); UV (MeCN) λmax (log ε) 263 (3.41), 221 (3.82) nm; ECD (MeCN, λ [nm] (Δε), c 0.212 mM): 264 (−0.36), 214 (+0.39); ^1H and ^{13}C NMR see Table 1; high-resolution mass spectrometry (HRMS) (ESI, *m/z*): $[M-H]^-$ calcd for $C_{18}H_{13}O_4$, 293.0814; found 293.0820.

TABLE 1 ^{1}H and ^{13}C NMR data of compounds **1** and **2**

	1[a]		2[a]	
No.	δ_c Type[b]	δ_H (*J* in Hz)	δ_c Type[b]	δ_H (*J* in Hz)
1	n.d.		n.d.	
2	141.0, C		144.7, C	
3	135.5, C		134.9, C	
4	112.1, CH	6.41, s	123.4, CH	7.49, s
5	160.8, C		152.8, C	
6	70.9, CH	5.81, s	184.0, C	
7	142.3, C		137.8, C	
8,12	127.9, CH	7.49, d (8.0)	130.7, CH	8.11, d (8.1)
9,11	129.5, CH	7.38, t (8.0)	129.8, CH	7.58, t (8.1)
10	129.0, CH	7.32, t (8.0)	134.4, CH	7.69, t (8.1)
13	133.8, C		132.7, C	
14,18	130.4, CH	7.56, d (7.8)	130.5, CH	7.66, d (7.9)
15,17	128.9, CH	7.35, t (7.8)	129.2, CH	7.42, t (7.9)
16	129.1, CH	7.31, t (7.8)	129.4, CH	7.38, t (7.9)

Abbreviations: HMBC: heteronuclear multiple bond correlation; HSQC: heteronuclear single-quantum correlation; n.d.: not detected; NMR: nuclear magnetic resonance.

[a]Recorded at 600 MHz (^{1}H) and 150 MHz (^{13}C) in CD_3OD.

[b]Data were extracted from HSQC and HMBC spectra.

Coniofuroic acid B (**2**): white amorphous solid; ^{1}H and ^{13}C NMR see Table 1; HRMS (ESI, *m/z*): $[M - H]^-$ calcd for $C_{18}H_{11}O_4$, 291.0657; found 291.0664.

2.4 | Cytotoxicity assay

Cytotoxicity against the L5178Y mouse lymphoma cell line was measured using the MTT assay.[13] Kahalalide F and 0.1% ethylene glycol monomethyl ether in DMSO were used as positive and negative control, respectively.

2.5 | Computational methods

Mixed torsional/low-mode conformational searches were carried out by means of the Macromodel 10.8.011 software[14] using the Merck Molecular Force Field (MMFF) with an implicit solvent model for $CHCl_3$ applying a 21 kJ/mol energy window. Geometry reoptimizations of the resultant conformers [ωB97X/TZVP[15] with PCM solvent model for MeCN and SOGGA11-X/TZVP[16] with SMD solvent model for MeCN] and time-dependent density functional theory (TDDFT) calculations were performed with Gaussian 09[17] using various functionals (B3LYP, BH&HLYP, CAM-B3LYP, and PBE0), the TZVP basis set, and the same solvent model as applied in the preceding DFT reoptimization step. ECD spectra were generated as the sum of Gaussians[18] with 3000 cm^{-1} half-height width, using dipole-velocity-computed rotational strengths. Boltzmann distributions were estimated from the ωB97X and the SOGGA11-X energies. The MOLEKEL software package was used for visualization of the results.[19]

3 | RESULTS AND DISCUSSION

Compound **1** was isolated as a white amorphous solid. Its molecular formula was determined as $C_{18}H_{14}O_4$ by HRMS, containing 12° of unsaturation. The ^{1}H NMR data of **1** showed 11 aromatic protons at δ_H 7.56 (d, H-14 and H-18), 7.49 (d, H-8 and H-12), 7.38 (t, H-9 and H-11), 7.35 (t, H-15 and H-17), 7.32 (t, H-10), 7.31 (t, H-16), and 6.41 (s, H-4) as well as one oxygenated methine at δ_H 5.81 (s, H-6) (Table 1). Two monosubstituted benzene rings were assembled by correlation spectroscopy (COSY) correlations between H-8(12)/H-9(11)/H-10 and between H-14(18)/H-15(17)/H-16 together with heteronuclear multiple bond correlation (HMBC) correlations from H-8 to C-10 and C-12, from H-9 to C-7 and C-11, from H-10 to C-8(12), from H-14 to C-16 and C-18, from H-15 to C-13 and C-17, and from H-16 to C-14(18) (Figure 2). The attachment of an oxygenated methine at C-7 was deduced from HMBC correlations from H-6 to C-7 and C-8(12). In addition, HMBC correlations from H-4 to C-2 (δ_C 141.0), C-3 (δ_C 135.5), C-5 (δ_C 160.8), and C-13; from H-6 to C-4 and C-5 (δ_C 112.1); and from H-14(18) to C-3 indicated the presence of a furan ring and the linkages between C-5/C-6 and C-3/C-13. The location of a carboxy group at C-2 was suggested by the molecular formula of **1**. Thus, the planar structure of **1** was elucidated for which the trivial name coniofuroic acid A is suggested.

For the configurational assignment of **1**, the solution TDDFT-ECD method was applied on the arbitrarily chosen (*S*) stereoisomer.[20,21] Since **1** is conformationally flexible and the relative orientation of the three aromatic chromophores produced by rotation along the C-3-C-13 biaryl axis and the sigma bonds of the C-6 chirality center

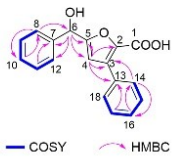

FIGURE 2 Correlation spectroscopy (COSY) and key heteronuclear multiple bond correlation (HMBC) correlations of compound **1**

is expected to be fundamental for the sign and shape of the ECD transitions, a thorough conformational search is inevitable.[22-25] Consequently, the initial 37 MMFF conformers of (*S*)-**1** were reoptimized at both the ωB97X/TZVP[15] PCM/MeCN and the SOGGA11-X/TZVP[16] SMD/MeCN levels of theory.[26,27] (see Supporting Information) ECD calculations were performed for both sets of conformers at the B3LYP/TZVP, BH&HLYP/TZVP, CAM-B3LYP/TZVP, and the PBE0/TZVP levels with the same solvent model as applied for the preceding DFT reoptimization level. Although as expected the individual conformers gave rather diverse ECD spectra, the Boltzmann-averaged spectra obtained at all applied combinations of levels reproduced well the experimental ECD allowing elucidation of the absolute configuration as (*S*) with high confidence (Figures 3 and 4). The low-energy conformers could be classified into six groups (Figure 5) according to the relative orientation of the three aromatic chromophores, ie, by rotation around the C-3-C-13, C-5-C-6, and C-6-C-7 bonds. The contribution of conformer ingroups A and C with a sum Boltzmann population of 56.6% at the SOGGA11-X/TZVP SMD/MeCN level reproduced already the overall shape of the experimental spectrum (Figure 4). It is also worth to note that the averaged computed ECD spectra obtained at any combinations were much more intense than the experimental one. The experimental ECD spectrum had to be multiplied by 20 to be comparable with the calculated ECD spectra, which implies about more than one order of magnitude difference. This indicated that the sample is probably a scalemic mixture with slight excess

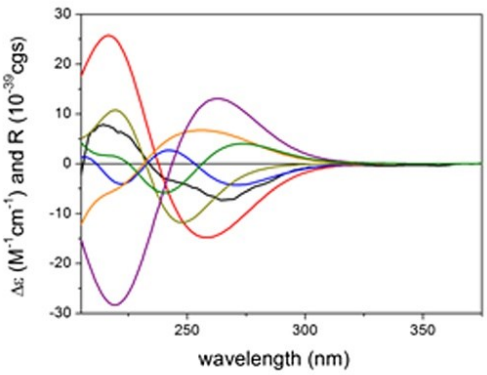

FIGURE 4 Comparison of the experimental electronic circular dichroism spectrum of **1** (black curve) with the PBE0/TZVP SMD/MeCN spectra of the lowest-energy representative conformers of the six conformational ensembles of (*S*)-**1** (level of optimization: SOGGA11-X/TZVP SMD/MeCN). (red: conf. A, blue: conf. B, olive: conf. G, orange: conf. H, purple: conf. O, green: conf. P.) Sum conformational ensembles were found as group A: 43.3% with conformers A, C, D, F, L, Q, and T; group B: 24.0% with conformers B, E, K, and M; group C: 13.3% with conformers G, I, N, and U; group D: 10.4% with conformers H and J; group E: 3.2% with conformers O and R; group F: 3.1% with conformers P and S

of the (*S*) stereoisome.[28-30] Partial racemization of the chirality center is certainly aided by the benzylic position, since the C-6 chirality center is α position to both a

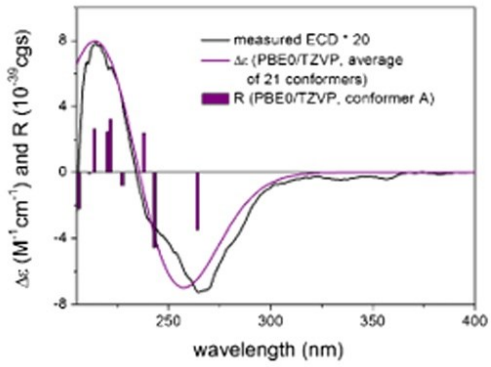

FIGURE 3 Comparison of the experimental electronic circular dichroism (ECD) spectrum of **1** measured in MeCN (multiplied by 20) with the PBE0/TZVP SMD/MeCN spectrum of (*S*)-**1** (level of optimization: SOGGA11-X/TZVP SMD/MeCN). The bars represent the rotational strength values of the lowest energy conformer

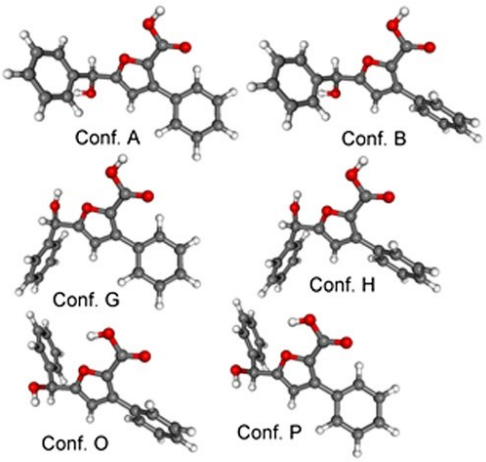

FIGURE 5 Lowest-energy representatives of the 6 conformer groups of (*S*)-**1**

benzene and a furan ring. For the (*S*) enantiomer of **1**, a relatively strong negative Cotton effect is expected at ~215 nm and a strong positive one at around 265 nm. Although separation of the enantiomers on various chiral HPLC columns was attempted, no successful separation could be achieved with the tested conditions.

The molecular formula of **2** was determined as $C_{18}H_{12}O_4$ based on the HRMS data, lacking two protons when compared to **1**. The ^{1}H NMR data of **2** were similar to those of **1** except for the disappearance of the oxygenated methine in **2** (Table 1). In addition, H-4 (δ_H 7.49) and H-8(12) (δ_H 8.11) in **2** were deshielded (δ_H 6.41 and 7.49, respectively in **1**). The above data suggested that the oxygenated methine was replaced by a ketone group in **2**, which was further confirmed by HMBC correlations from H-8(12) to the carbon of this ketone group (δ_C 184.0). Detailed analysis of 2D NMR spectra of **2** revealed that the remaining substructures of **2** were identical to that of **1**. The trivial name coniofuroic acid B is given to compound **2**.

All isolated compounds were submitted for bioassay against the L5178Y mouse lymphoma cell line but proved to be inactive when tested at an initial concentration of 10 μM.

ACKNOWLEDGEMENTS

This project was funded by the Deutsche Forschungsgemeinschaft (project number 270650915, GRK 2158). Further support by the Manchot Foundation to P. P. is gratefully acknowledged. T. K. was supported by the National Research, Development and Innovation Office (K120181) and A. M. by the János Bolyai Research Scholarship of the Hungarian Academy of Sciences. The Governmental Information-Technology Development Agency (KIFÜ) is acknowledged for CPU time.

ORCID

Attila Mándi https://orcid.org/0000-0002-7867-7084
Tibor Kurtán https://orcid.org/0000-0002-8831-8499
Zhen Liu https://orcid.org/0000-0003-3314-7853

REFERENCES

1. Aly AH, Debbab A, Kjer J, Proksch P. Fungal endophytes from higher plants: a prolific source of phytochemicals and other bioactive natural products. *Fungal Diversity*. 2010;41:1-16.
2. Strobel GA. Endophytes as sources of bioactive products. *Microbes Infect*. 2003;5(6):535-544.
3. Hawksworth DL, Rossman AY. Where are all the undescribed fungi? *Phytopathology*. 1997;87(9):888-891.
4. Frank M, Özkaya FC, Müller WEG, et al. Cryptic secondary metabolites from the sponge-associated fungus *Aspergillus ochraceus*. *Mar Drugs*. 2019;17:99.
5. Abdel-Wahab NM, Scharf S, Özkaya FC, et al. Induction of secondary metabolites from the marine-derived fungus *Aspergillus versicolor* through co-cultivation with *Bacillus subtilis*. *Planta Med*. 2019;85(6):503-512.
6. Abdelwahab MF, Fouad MA, Kamel MS, et al. Tanzawaic acid derivatives from freshwater sediment-derived fungus *Penicillium* sp. *Fitoterapia*. 2018;128:258-264.
7. Elsebai MF, Nazir M, Kehraus S, et al. Polyketide skeletons from the marine alga-derived fungus *Coniothyrium cereale*. *Eur J Org Chem*. 2012;2012:6197-6203.
8. Elsebai MF, Kehraus S, Lindequist U, et al. Antimicrobial phenalenone derivatives from the marine-derived fungus *Coniothyrium cereale*. *Org Biomol Chem*. 2011;9(3):802-808.
9. Ondeyka JG, Zink D, Basilio A, et al. Coniothyrione, a chlorocyclopentandienylbenzopyrone as a bacterial protein synthesis inhibitor discovered by antisense technology. *J Nat Prod*. 2007;70(4):668-670.
10. Schüffler A, Liermann JC, Opatz T, Anke T. Elucidation of the biosynthesis and degradation of allantofuranone by isotopic labelling and fermentation of modified precursors. *ChemBioChem*. 2011;12(1):148-154.
11. Xu J, Aly AH, Wray V, Proksch P. Polyketide derivatives of endophytic fungus *Pestalotiopsis* sp. isolated from the Chinese mangrove plant *Rhizophora mucronata*. *Tetrahedron Lett*. 2011;52:21-25.
12. Kjer J, Debbab A, Aly AH, Proksch P. Methods for isolation of marine-derived endophytic fungi and their bioactive secondary products. *Nat Protoc*. 2010;5(3):479-490.
13. Ashour M, Edrada R, Ebel R, et al. Kahalalide derivatives from the Indian sacoglossan mollusk *Elysia grandifolia*. *J Nat Prod*. 2006;69(11):1547-1553.
14. MacroModel. Schrödinger LLC, 2015. http://www.schrodinger.com/MacroModel.
15. Chai JD, Head-Gordon M. Systematic optimization of long-range corrected hybrid density functionals. *J Chem Phys*. 2008;128:084106.
16. Peverati R, Truhlar DG. Communication: A global hybrid generalized gradient approximation to the exchange-correlation functional that satisfies the second-order density-gradient constraint and has broad applicability in chemistry. *J Chem Phys*. 2011;135:191102.
17. Frisch MJ, Trucks GW, Schlegel HB, et al. *Gaussian 09, Revision E.01*. Gaussian Inc: Wallingford CT; 2013.
18. Stephens PJ, Harada N. ECD cotton effect approximated by the Gaussian curve and other methods. *Chirality*. 2010;22(2):229-233.
19. Varetto U. Molekel 5.4. 0.8. Swiss National Supercomputing Centre, Manno, Switzerland 2009.
20. Superchi S, Scafato P, Gorecki M, Pescitelli G. Absolute configuration determination by quantum mechanical calculation of chiroptical spectra: basics and applications to fungal metabolites. *Curr Med Chem*. 2018;25:287-320.
21. Mándi A, Kurtán T. Applications of OR/ECD/VCD to the structure elucidation of natural products. *Nat Prod Rep*. 2019;36:889-918.
22. Pescitelli G, Bruhn T. Good computational practice in the assignment of absolute configurations by TDDFT calculations of ECD spectra. *Chirality*. 2016;28(6):466-474.

23. Grauso L, Teta R, Esposito G, Menna M, Mangoni A. Computational prediction of chiroptical properties in structure elucidation of natural products. *Nat Prod. Rep.* 2019;36(7):1005-1030.
24. Sun P, Xu DX, Mándi A, et al. Structure, absolute configuration, and conformational study of 12-membered macrolides from the fungus *Dendrodochium* sp. associated with the sea cucumber *Holothuria nobilis* Selenka. *J Org Chem*. 2013;78:7030-7047.
25. Mándi A, Swamy MMM, Taniguchi T, Anetai M, Monde K. Reducing molecular flexibility by cyclization for elucidation of absolute configuration by CD calculations: daurichromenic acid. *Chirality*. 2016;28:453-459.
26. Brémond É, Savarese M, Su NQ, et al. Benchmarking density functionals on structural parameters of small-/medium-sized organic molecules. *J Chem Theory Comput*. 2016;12:459-465.
27. Tran-Cong NM, Mándi A, Kurtán T, et al. Induction of cryptic metabolites of the endophytic fungus *Trichocladium* sp. through OSMAC and co-cultivation. *RSC Adv*. 2019;9:27279-27288.
28. Batista ANL, dos Santos FM Jr, Batista JM Jr, Cass QB. Enantiomeric mixtures in natural product chemistry: separation and absolute configuration assignment. *Molecules*. 2018;23:492.
29. Tóth B, Liktor-Busa E, Kúsz N, et al. Phenanthrenes from *Juncus inflexus* with antimicrobial activity against methicillin-resistant *Staphylococcus aureus*. *J Nat Prod*. 2016;79:2814-2823.
30. Ancheeva E, Mándi A, Király SB, et al. Chaetolines A and B, pyrano [3,2-f] isoquinoline alkaloids from cultivation of *Chaetomium* sp. in the presence of autoclaved *Pseudomonas aeruginosa*. *J Nat Prod*. 2018;81(11):2392-2398.

SUPPORTING INFORMATION

Additional supporting information may be found online in the Supporting Information section at the end of this article.

How to cite this article: Tran-Cong NM, Mándi A, Király SB, et al. Furoic acid derivatives from the endophytic fungus *Coniothyrium* sp.. *Chirality*. 2020;1–6. https://doi.org/10.1002/chir.23209

Supporting information

Furoic Acid Derivatives from the Endophytic Fungus *Coniothyrium* sp.

Nam Michael Tran-Cong,[a] Attila Mándi,[b] Sándor Balázs Király,[b] Tibor Kurtán,[b] Wenhan Lin,[c] Zhen Liu,*[a] Peter Proksch,*[a]

[a] Institute of Pharmaceutical Biology and Biotechnology, Heinrich Heine University Düsseldorf, Universitätsstrasse 1, 40225 Düsseldorf, Germany, E-mail: zhenfeizi0@sina.com, proksch@hhu.de

[b] Department of Organic Chemistry, University of Debrecen, Egyetem tér 1, Debrecen 4032 Hungary

[c] State Key Laboratory of Natural and Biomimetic Drugs, Peking University, Beijing 100191, China

Contents

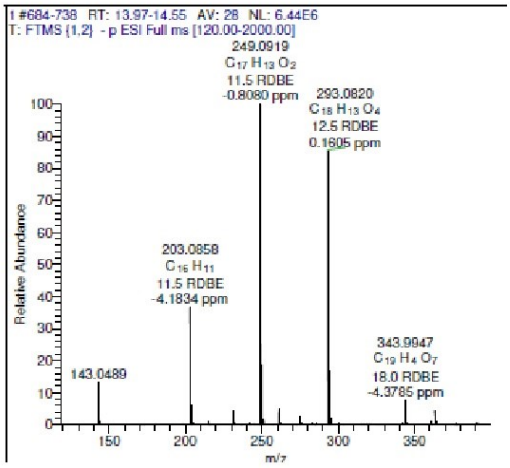

Figure S1. HRESIMS of compound **1**

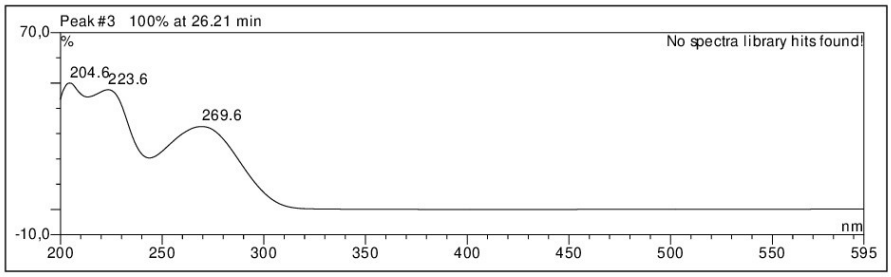

Figure S2. UV spectrum of compound **1**

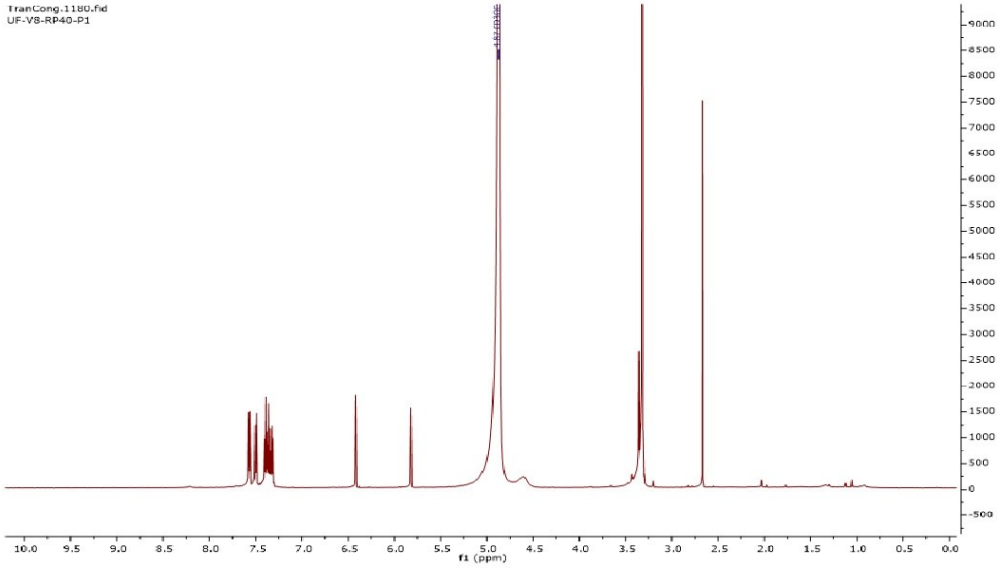

Figure S3. ^{1}H NMR spectrum (600 MHz, CD_3OD) of compound **1**

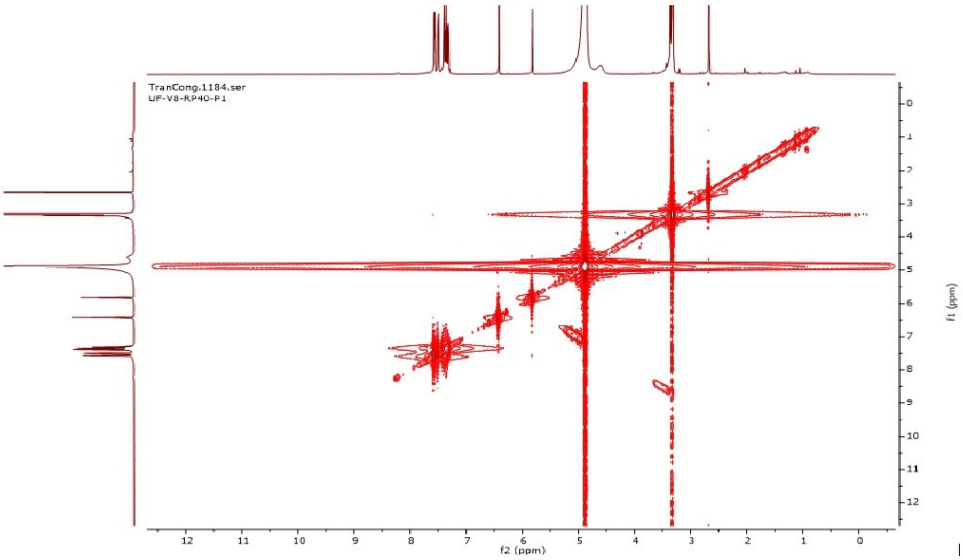

Figure S4. COSY spectrum (600 MHz, CD_3OD) of compound **1**

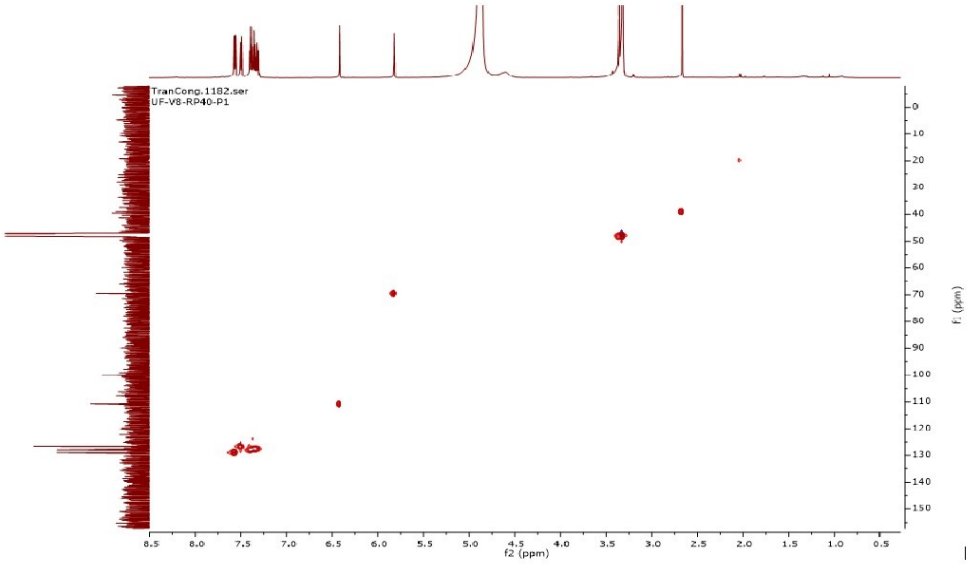

Figure S5. HSQC spectrum (600 MHz, CD_3OD) of compound **1**

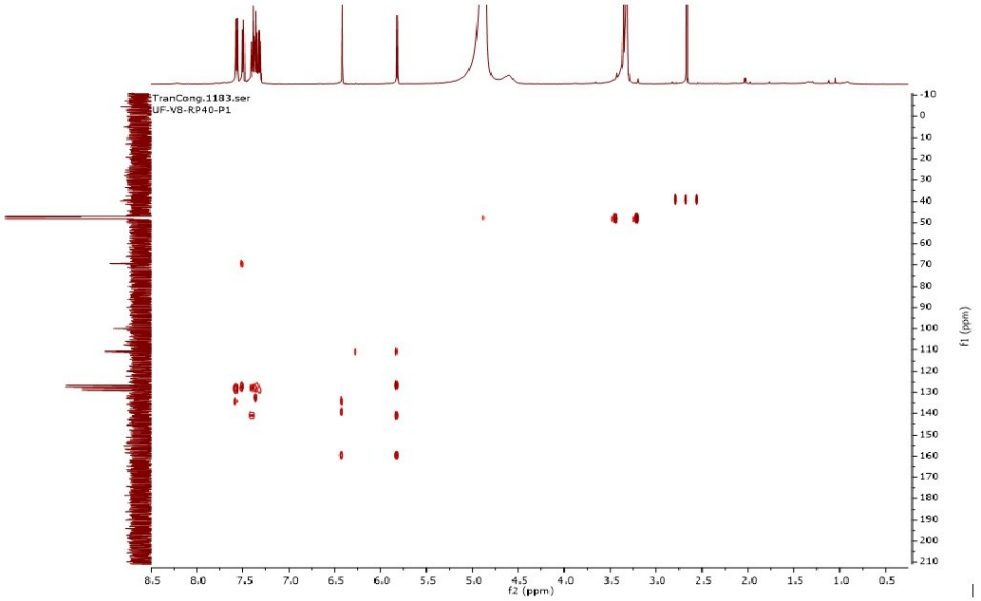

Figure S6. HMBC spectrum (600 MHz, CD_3OD) of compound **1**

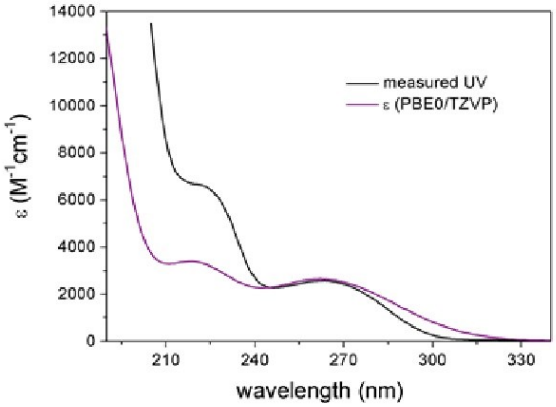

Figure S7. Experimental UV spectrum (black curve) of **1** in acetonitrile compared with the Boltzmann-weighted PBE0/TZVP SMD/MeCN ECD spectrum of 21 SOGGA11-X/TZVP SMD/MeCN conformers of (*S*)-**1** (purple curve). The computed intensity was scaled to the experimental value.

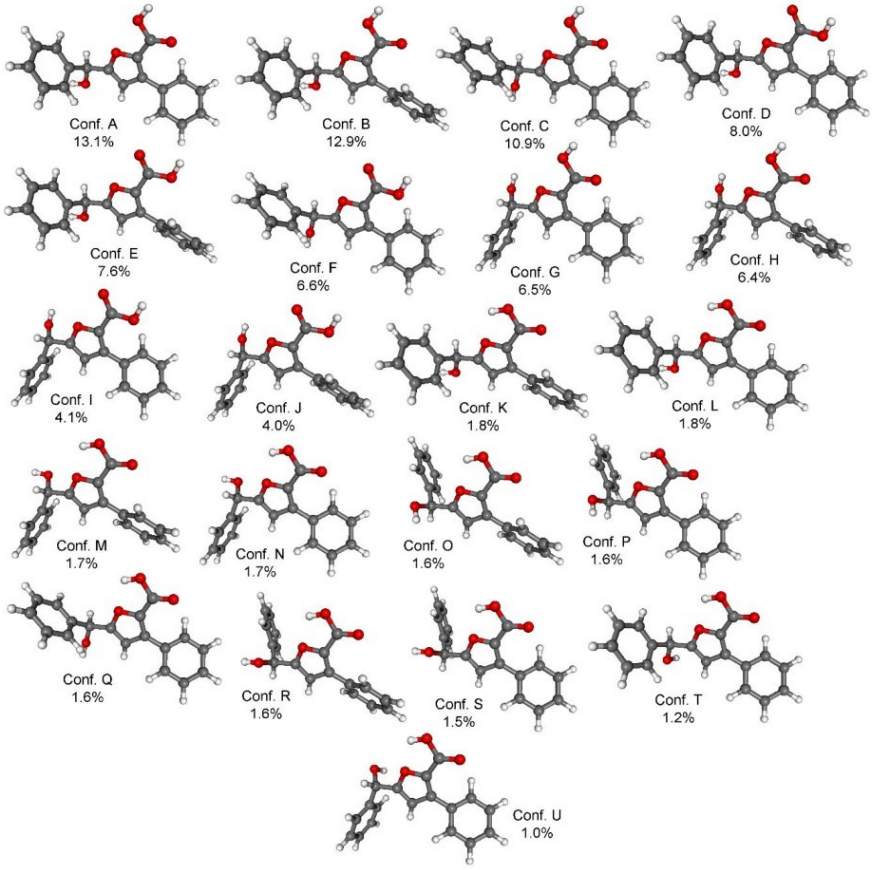

Figure S8. Structure and population of the low-energy SOGGA11-X/TZVP SMD/MeCN conformers (≥ 1%) of (*S*)-**1**.

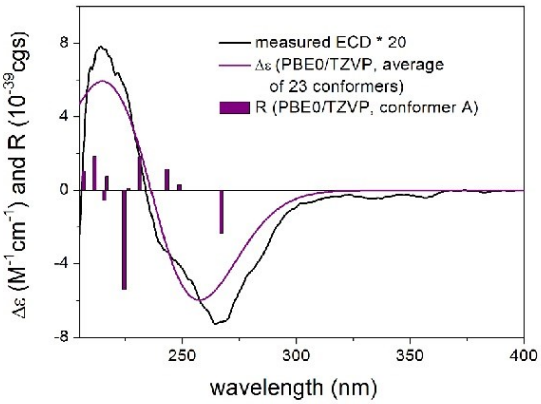

Figure S9. Comparison of the experimental ECD spectrum of **1** measured in MeCN with the PBE0/TZVP PCM/MeCN spectrum of (*S*)-**1** (level of optimization: ωB97X/TZVP PCM/MeCN). The bars represent the rotational strength values of the lowest energy conformer.

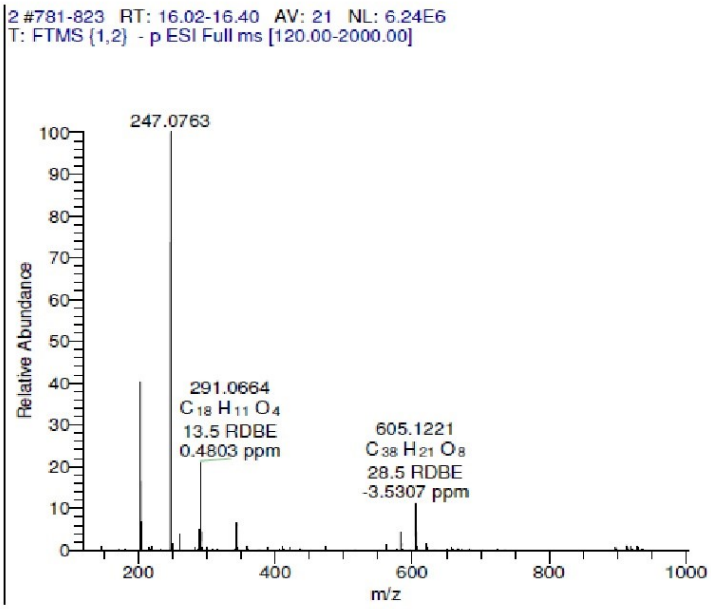

Figure S10. HRESIMS of compound **2**

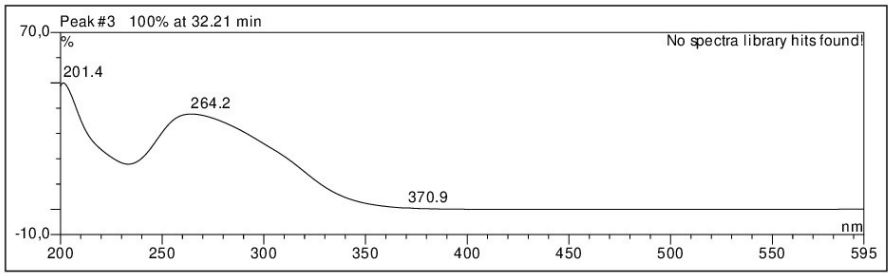

Figure S11. UV spectrum of compound **2**

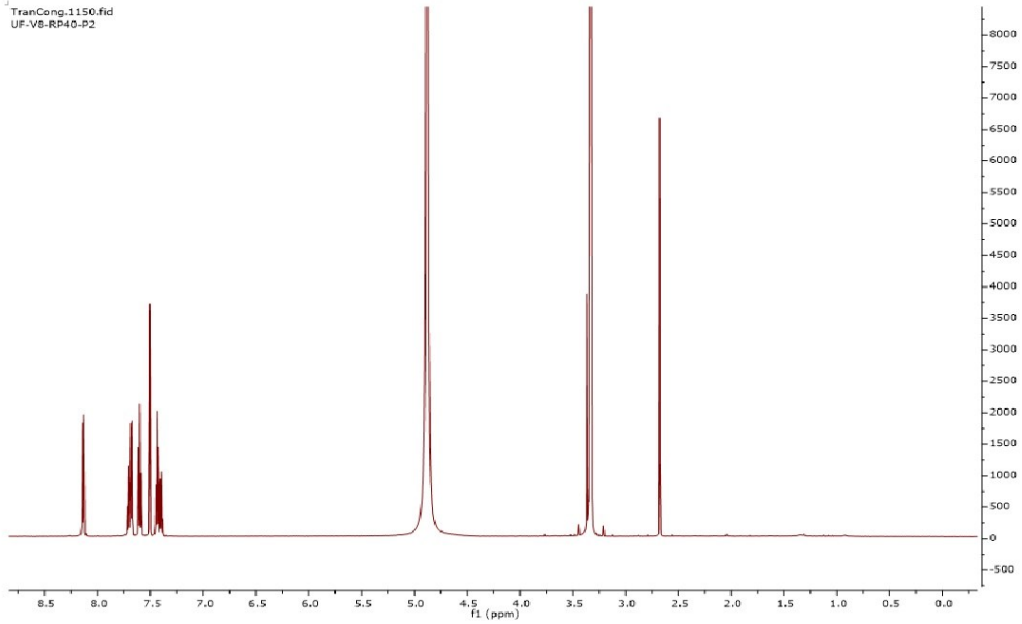

Figure S12. ^{1}H NMR spectrum (600 MHz, CD_3OD) of compound **2**

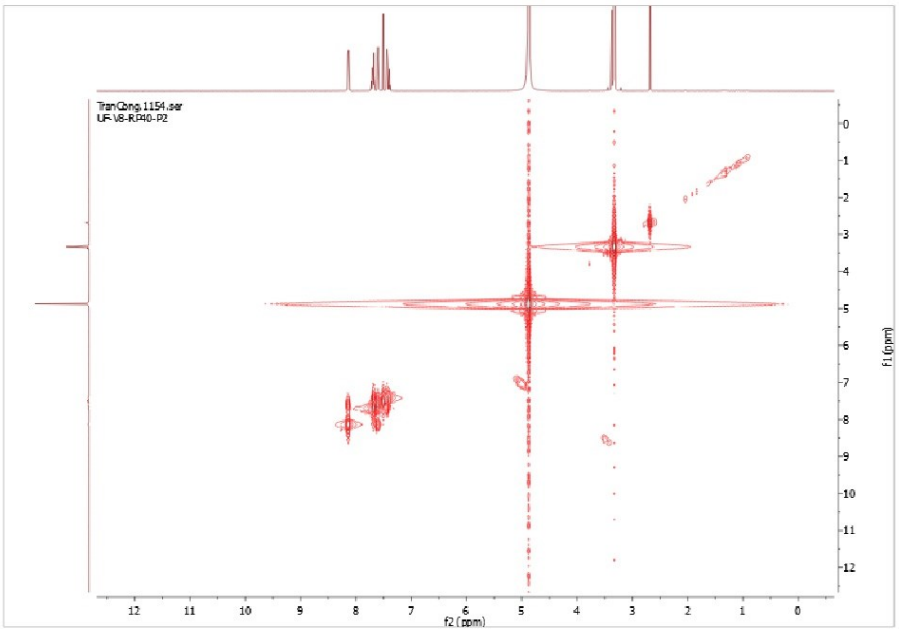

Figure S13. COSY spectrum (600 MHz, CD_3OD) of compound **2**

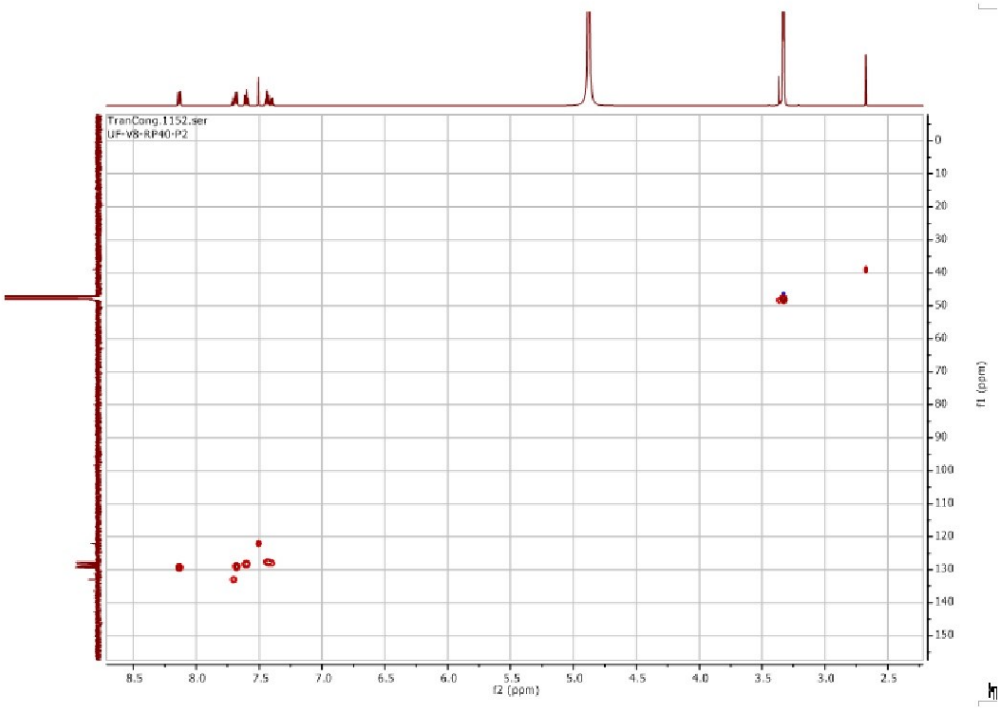

Figure S14. HSQC spectrum (600 MHz, CD_3OD) of compound **2**

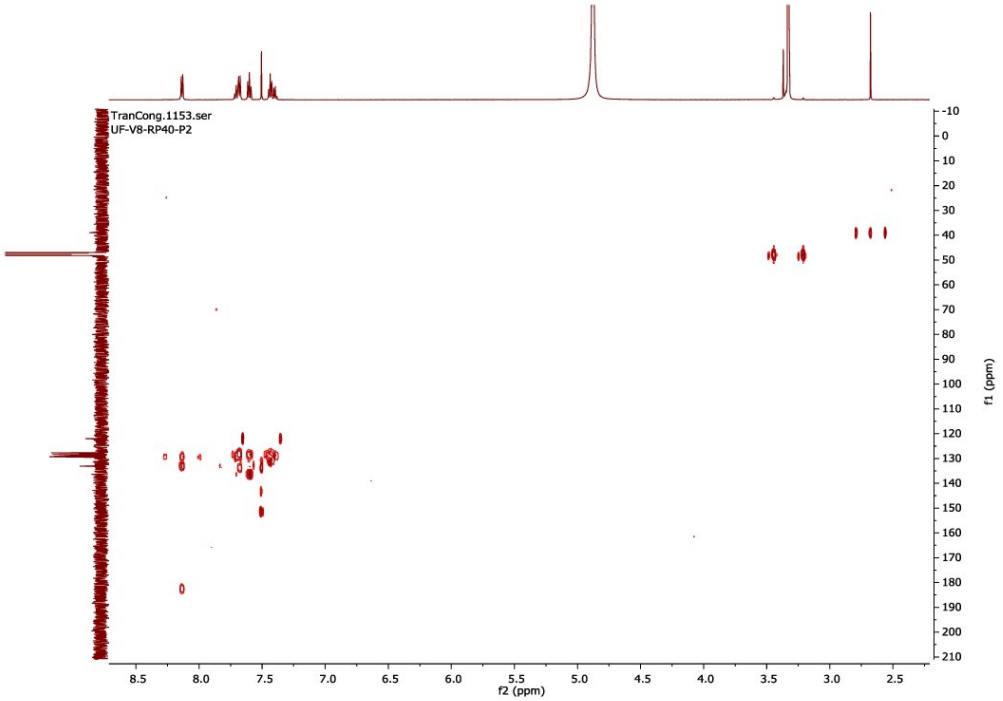

Figure S15. HMBC spectrum (600 MHz, CD_3OD) of compound **2**

8. Discussion

8.1 Fungal metabolites as a promising source for drug discovery

Fungal metabolites are an interesting source for drug discovery and offer a huge diversity of compounds possessing various functions such as virulence factors, defense compounds, or as cross talk metabolites. (Möbius, Hertweck, 2009, Schulz et al., 1999, Sheridan et al., 2014) These metabolites can be isolated using a standardized cultivation protocol such as fermentation on rice medium. However, because more than 70% of secondary metabolite gene cluster remain silent under standard cultivation procedures, OSMAC approaches can be applied to activate silent gene clusters. (Chiang et al., 2011, Özkaya et al., 2018, Pan et al., 2019, Ren et al., 2017) Thereafter, the isolated compounds are analyzed structurally, subjected to various bioassays and in case of active compounds subjected to computational methods with the aim for target finding.

8.2. Expanding the metabolic profile of the endophytic fungus *Trichocladium* sp. by applying OSMAC approaches

Implementing OSMAC approaches on the endophytic fungus *Trichocladium* sp. isolated from the traditional medicinal herb *Houttuynia cordata* (Sauraceae), which has been described in this dissertation, yielded several new natural products. (Tran-Cong et al., 2019)

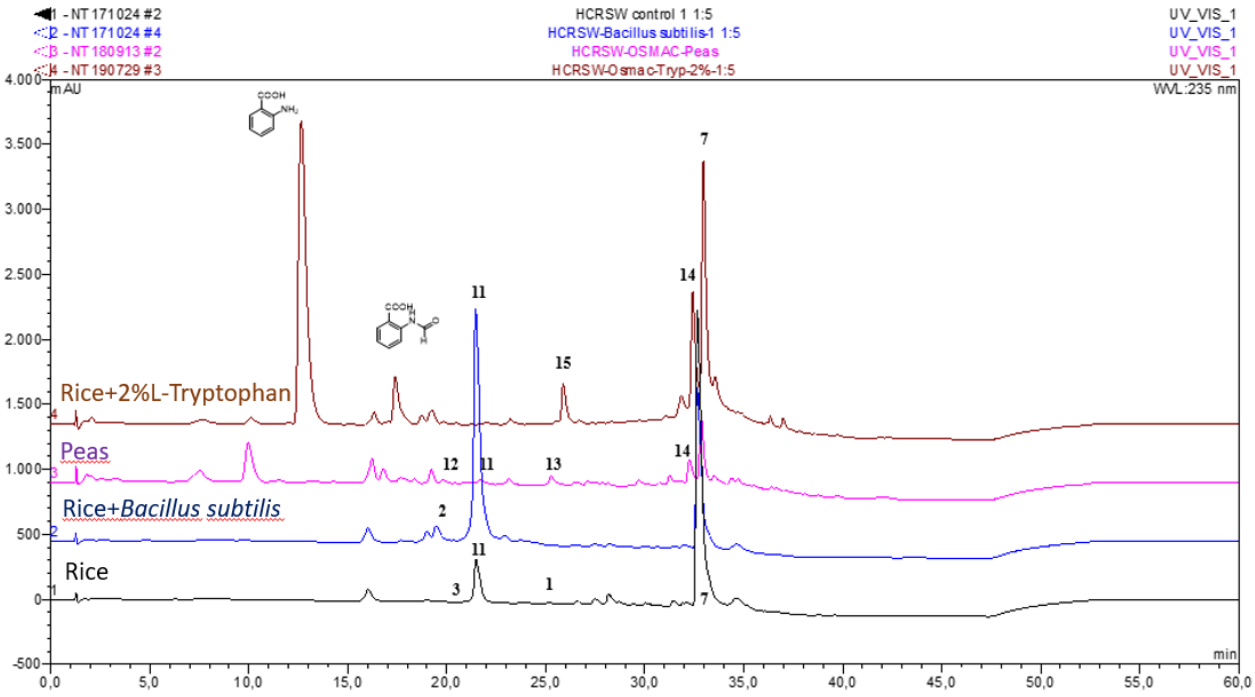

Figure 6 HPLC analysis of different crude extracts obtained from different fermentations of *Trichocladium* sp. Figure is modified after (Tran-Cong et al., 2019)

When the fungus was cultured on peas medium, the yield of the crude extract was much lower than the yield obtained from cultivation on rice medium. A feeding experiment where L-tryptophan (2g per flask) had been added to solid rice medium in order to mimic the higher tryptophan content of peas compared to rice led to an approximately equal crude extract yield when compared to the rice medium. Eventually, this experiment resulted in the isolation of tryptophan derivatives such as anthranilic acid and n-formylanthranilic acid (see **figure 7a+b)** which can be interpreted as catabolic products resulting from metabolism of added tryptophan.

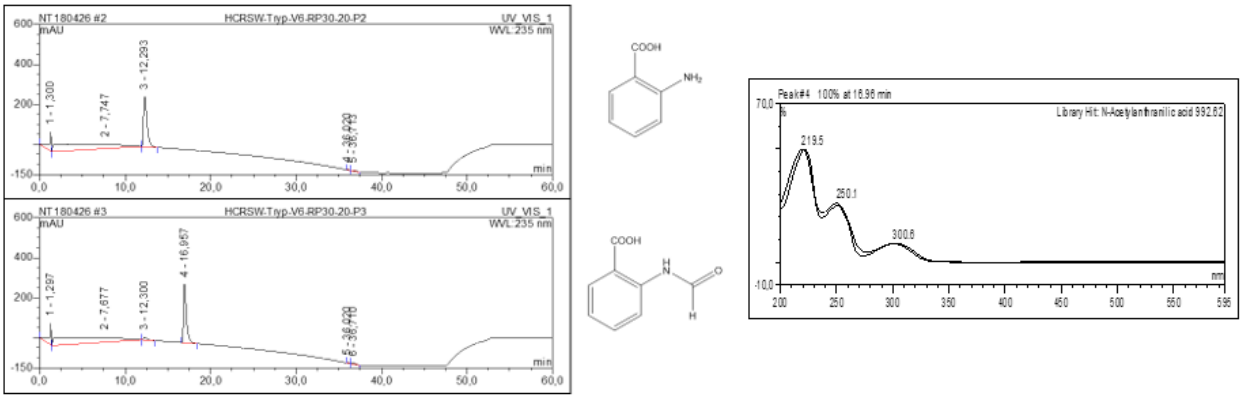

a) b)

Figure 7 a) HPLC – Chromatograms of peaks at 12.293 min and 16.957 min. **b)** Typical UV spectrum of anthranilic acid which is directly identified by comparison to the in house UV-library of the Chromeleon HPLC system.

Interestingly, these two L-tryptophan metabolites were not detectable when the fungus was fermented on solid rice or on peas. The L-tryptophan crude extract showed one peak with a retention time of 25 min exhibited a UV spectrum similar to that of anthranilic acid. Structure elucidation of the metabolite using 1D/2D NMR and HRESIMS analyses indicated the compound to be a new natural product. The new compound was named 13-*N*-(2-carboxyphenyl) colletoketol **(15).** This compound is a derivative of the co-isolated compound colletoketol **(12).** (Tran-Cong et al., 2019) Like for anthranilic acid and *N*-anthranilic acid the origin of the anthranilic acid moiety of compound **15** is probably tryptophan.

In fungi the pyrrole ring of the tryptophan moiety is cleaved and kynurenine is formed by L-tryptophan oxygenase and formamidase. (Wat, Towers, 1979) In the next step kynurenine is metabolized by kynureninase yielding anthranilic acid. Basically, there are two types of kynureninase enzymes. One is involved in the catabolism of tryptophan and it is inducible by tryptophan and the other one is involved in the biosynthesis of NAD from tryptophan but this enzyme is not inducible. (Soda, Tanizawa, 1979).

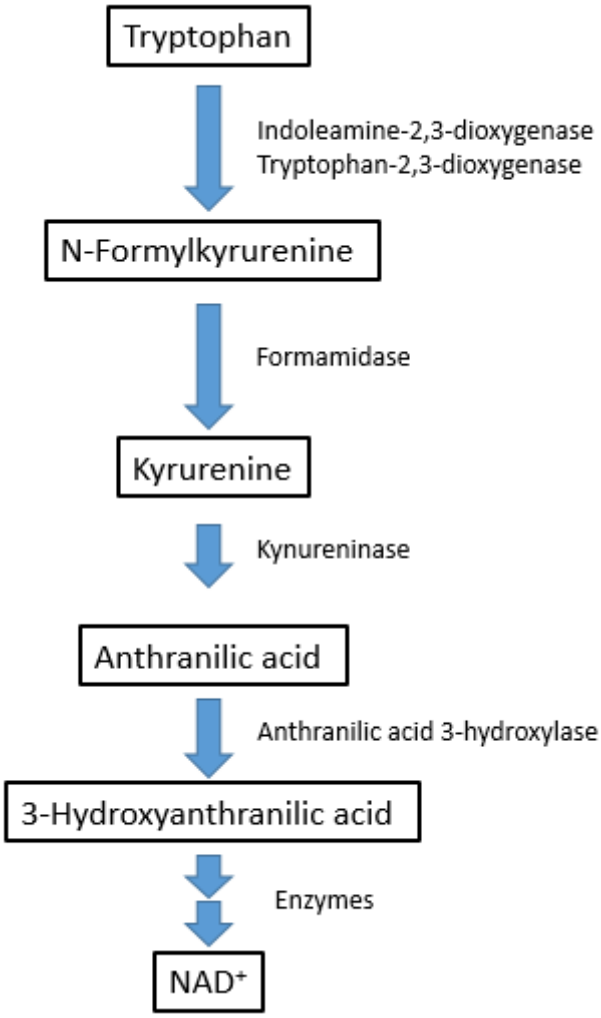

Figure 8 L-Tryptophan catabolic pathway modified after Wat et al. (Wat, Towers, 1979)

When the enzyme kynureninase is upregulated this will lead to an accumulation of anthranilic acid. The main reason for the upregulation of this enzyme may be the potential toxicity of indole derivatives such as tryptophan derivatives which inhibit fungal growth. (Kamath, Vaidyanathan, 1990). In particular, the upregulation of the PKS-NRPS pathway can be considered as a way to dispose L-tryptophan in the form of anthranilic acid derivatives.

8.2.1 Bioactivity of anthranilic acid derivatives

Many bioactive natural products bearing the anthranilic acid moiety have been described in the literature. (Li et al., 2013, Peng et al., 2014, Teponno et al., 2017b) For example, from the endophytic fungus *Dendrothyrium variisporum* isolated from the Algerian plant *Globularia alypum,* three new anthranilic acid derivatives werereported. One of these compounds is 2-phenylethyl 3-hydroxyanthranilate which exhibited cytotoxic activity against KB3.1 cancer cells with an IC_{50} value of 0.07 µM. (Teponno et al., 2017a) In addition, five new anthranilic acid derivatives were isolated from the liquid culture medium of the marine fungus, *Penicillium paneum*. The new compounds possess an amidine moiety due the linkage of anthranilic acid with an enamine. Two new anthranilic acid

derivatives, namely penipacid A and E exhibited cytotoxic activity against the RKO cell line with IC_{50} values of 8.4 and 9.7 µM, respectively. However, antimicrobial screening showed that none of the compounds exhibited activity against S. *aureus* or E. *coli*. (Li et al., 2013) Collectively these findings emphasize that fungi are able to incorporate L-tryptophan or anthranilic acid into natural products.

Comparison of the bioactivity of the reported anthranilic acid derivatives from *Trichoderma* sp with the new 13-*N*-(2-carboxyphenyl) colletoketol-derivative **(15)**, from *Trichocladium* sp. fermented on rice medium with added L-tryptophan, indicated that these compounds exhibited strong cytotoxicity against the mouse lymphoma cells. Additional cytotoxicity assays of compound **15** showed moderate to strong activity also against human Ramos and Jurkat cancer cell lines with IC_{50} values of 30 µM and 22 µM, respectively. However, when incubated for a longer period such as 72h, IC_{50} values against the latter two cell lines were even lower at 10 µM and 6 µM, respectively.

For determining whether the cytotoxicity of the new compound (**15**) was caused through apoptosis or necrosis, further experiments were conducted to explain the mode of action. The results of these experiments are shown in the following figure.

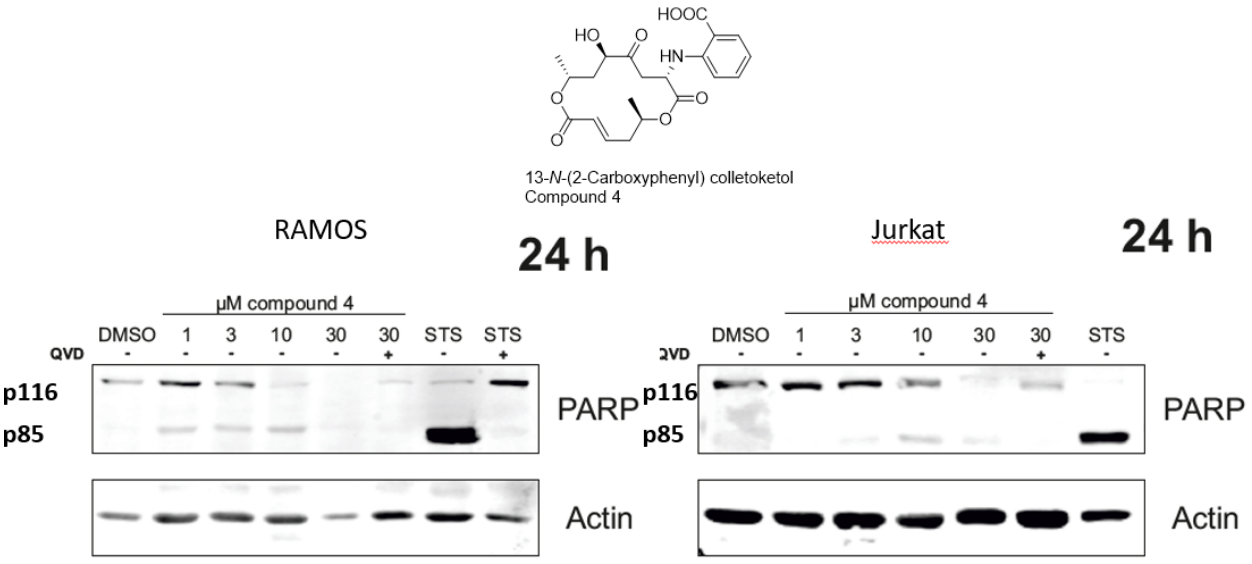

Figure 9 Western Blot results of 24h of incubating RAMOS and Jurkat cell lines with the new compound **15** (in the figure it is labeled as **4**) , DMSO as control, added staurosporine (STS) as positive control. Actin is a house keeping protein serving as a proof for equal protein concentrations. PARP is a substrate of the effector caspase 3. P116 is the uncleaved PARP. Activation of caspase 3 cleaves PARP. Cleaved PARP is in this plot a marker for apoptosis. P85 is the cleaved PARP. A longer incubation time such as 48h led to no activity of caspase 3 because all cells were already dead.

Compound **15** induced activation of caspase 3 with increasing concentration in Ramos as well as Jurkat cell lines. However, in Ramos cell lines the Western Blot shows weak actin bands, especially when 30 µM of compound **15** was used, indicating intensively damaged cells possibly caused by necrotic processes. To conclude, compound **15** is an inducer of apoptosis but in comparison to the used

control staurosporine (2.5 µM), compound **15** is a weak inducer of apoptosis and probably also induces cell necrosis.

Using OSMAC to expand the diversity of secondary metabolites is a promising tool which should not be neglected. Not only the media can be changed but also adding inorganic salts such as sodium nitrite to the media can result in an interesting upregulation of cryptic compounds. From a solid rice fermentation of the endophytic fungus *Aspergillus aculeatus* one new compound exhibiting a L-tryptophan-L-phenyllactic acid moiety was obtained. In addition, an OSMAC approach was conducted for the same fungus by adding 3.5% sodium nitrite to rice medium. This OSMAC approach yielded 10 new substituted L-tryptophan-L-phenyllactic acid conjugates. (Wang et al., 2018)

8.2.2 Michael addition in natural products

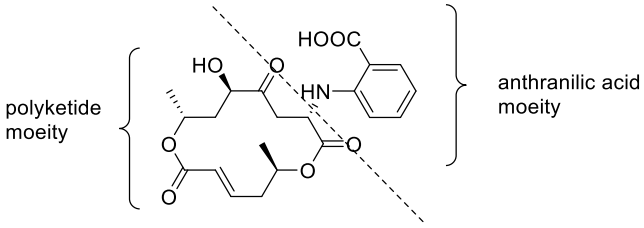

Figure 10 Structure of compound **15** exhibiting two different moieties

The new compound **15** is a derivative of the known compounds colletoketol **(11)** (Gurusiddaiah, Ronald, 1981a) and colletodiol **(12)**. (Keck et al., 1989) Based on the proposed biosynthesis of compound **11** and **12,** a plausible biosynthesis can be suggested (see figure **11**). (O'Neill et al., 1993, Simpson, Stevenson, 1985)

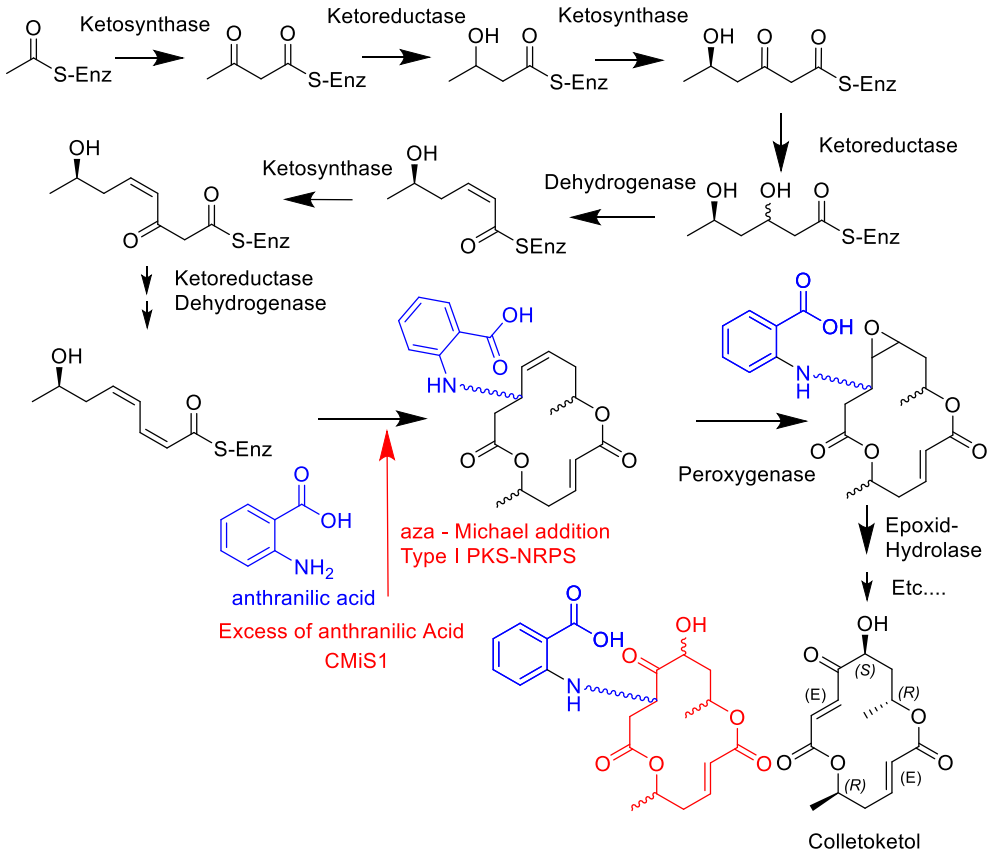

Figure 11 Proposed biosynthesis of the new compound (15) Red : Colletoketol (11 moiety The anthranilic acid moiety is shown in blue.

The anthranilic acid moiety was possibly conjugated by the enzyme complex Type I – Polyketide synthase-non ribosomal protein synthase via *N*-aza Michael addition. (Miyanaga, 2019) Typically, Michael additions occur under basic conditions. (Bergmann et al., 2011) The main enzymes responsible for Michael additions in biosynthesis of natural products are PKS/Polyketide Synthases. (Miyanaga, 2019) Michael addition is not selective, these reactions are able to form diastereomers due to two possibilities of nucleophilic attack. (Bergmann et al., 2011)

In order to exclude the possibility of the occurrence of other Michael-products, the L-tryptophan crude extract was screened but no further products or side products were detected verifying that the new compound **15** is a new natural product possibly derived from PKS-synthase type I on the basis of a *N*-aza Michael addition described for organic synthesis. (Kang, Kim, 2014)

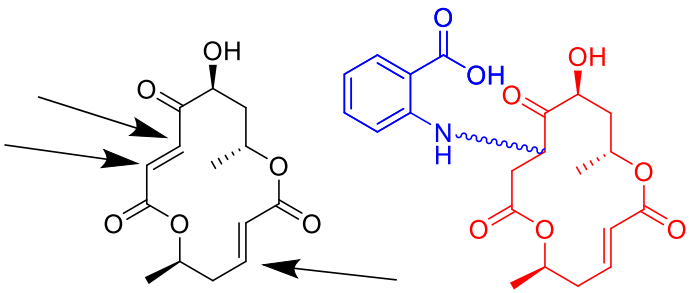

Compound **11**
Colletoketol

Compound **15**
new natural product

Figure 12 Possible location for a nucleophilic attack at an α-β-unsaturated carbonyl function. Three possible locations are shown. Due the nature of Michael addition, the number of possible Michael reaction products can be calculated as at least six different diastereomers. Blue : Anthranilic acid moiety , red : Colletoketol moiety.

Many other natural products exhibiting an anthranilic acid moiety such as auranthine, isolated from *Aspergillus clavatus*, were described in the literature. The carboxylic group of anthranilic acid can be connected with an amino function and the amino function of the anthranilic acid moiety forms an enamine. (Penn et al., 1992) Further feeding studies with radio labeled anthranilic acid revealed that the fed anthranilic acid was incorporated into auranthine (Penn, 1992) demonstrating that fungi were able to directly incorporate anthranilic acid into a natural product .

A culture of *Penicillium cyclopium* fed with radiolabeled tryptophan, mevalonic acid and acetate led to biosynthesis of a known compound, namely alpha-cyclopiazonic acid. During this biosynthesis, tryptophan was connected with two acetate units. Moreover, the biosynthetic gene cluster was elucidated and determined as CpaA PKS-NRPS including nonfunctional PKS domains. Firstly, the carboxylic acid group of tryptophan was connected to the peptidyl carrier protein forming a thioester intermediate. Secondly, the amino function of tryptophan acts as a nucleophile attacking the thioester carbonyl atom of the polyketide carried by the acyl carrier protein.(Seshime et al., 2009) The obtained results suggested that addition of L-tryptophan or of anthranilic acid to a growing fungal culture is a promising OSMAC tool for enhancing silent gene clusters in order to obtain bioactive secondary metabolites such as those that result from activating PKS-NRPS.

8.3. Co-cultivation

Co-cultivation of fungi with different bacteria can be considered as another approach to activate silent gene clusters**.** In general, soil-derived bacteria such as *Bacillus subtilis*, *Streptomyces lividans or Streptomyces coelicolor* can be used for co-cultivation with fungi. (Bentley et al., 2002, Graham, Istock, 1978, van Dijl, Hecker, 2013) (Wellington et al., 1990) Due to their ubiquitous occurrence, these bacteria are good model organisms for co-cultivation with fungi.

When the endophytic fungus *Trichocladium* sp. was co-cultured with *Streptomyces lividans* or with *Streptomyces coelicolor,* no changes in the fungal metabolite pattern could be observed. However, culturing *Trichocladium* sp. with *Bacillus subtilis* led to a change in the metabolite profile of the fungus.

One of the upregulated compounds that were detected following upon co-cultivating the fungus with *Bacillus subtilis* was colleketol (**11)**. This macrolide is a weak broad spectrum antibiotic. Its IC_{50} value against *Bacillus subtilis* was determined as 28.4 µM (Gurusiddaiah, Ronald, 1981b). The upregulation of colleketol **(11)** and its high yield (1.5 g/per flask) provided proof that the fungus reacted to the presence of *Bacillus subtilis*. On the other hand, *Bacillus subtilis* is also known as a producer of antifungal drugs (Landy et al., 1948, Singh, Deverall, 1984) showing that co-cultivation is a tool to simulate natural competition. (Marmann et al., 2014)

When the marine endophyte, *Pestalotia* sp., isolated from the surface of the alga *Rosenvingea* sp. was cultured together with a gram negative unicellular bacterium CNJ-328, this co-cultivation approach led to the isolation of thenew antibiotic pestalone. (Cueto et al., 2001) This example also demonstrated that cultivation of a fungus with another microorganism is a promising tool to induce silent gene clusters.

8.4. Drug discovery - antiplatelet compounds from the endophytic fungus *Talaromyces* sp.

One chapter of this dissertation is devoted to the investigation of antiplatelet compounds from the endophytic fungus *Talaromyces* sp. isolated from the traditional Vietnamese medicinal herb *Houttuynia cordata* (Saururaceae). Twelve compounds were isolated and identified as known natural products with all of them bearing a hydroxyl benzoyl moiety. Target finding approaches using docking experiments and information obtained from a patent (Lavecchia, Di Giovanni, 2015, Luiz Antonio Soares RomeiroCarolyn CumminsLilia Magomedova. Ppar modulators) showed that altenusin, one of the isolated compounds, possesses binding affinity to the peroxisomal proliferated receptor (PPAR) indicating PPAR as one of the promising targets in platelets that may be addressed by altenusin. Zheng et al. however, reported that altenusin is also a farsenoid X receptor modulator. (Zheng et al., 2017)

Farsenoid X receptors and PPARs can also be found in human platelets. (Moraes et al., 2016, Shih, Chou, 2012, Spinelli et al., 2008). Farsenoid X receptors belong to the same receptor class like peroxisomal proliferated activated receptors (PPARs). They are ligand activated transcription factors. (Wang et al., 2008) Due to the fact that platelets have no nucleus, PPAR and FXR exhibit also non genomic effects on platelets regulating their functions such as inhibiting platelet aggregation. (Unsworth et al., 2018)

Generally, PPARs are linked with pain and inflammation providing a suitable target for future analgesics or anti – inflammatory drugs. (Daynes, Jones, 2002, Maeda, Kishioka, 2009) Analgesics as well as anti-platelet agents are widely used drugs. (Melnikova, 2010) Analgesics are drugs which are used to treat long lasting pain or to stop the feeling of pain. Inflammation is a process causing tissue to

swell due to the migration of immune cells and release of inflammatory cytokines as well as vasodilators mediators.

It is worth to mention that inhibiting platelet functions may reduce the possibility to get cancer. (Yuri Gasparyan et al., 2011, Zarbock et al., 2007) Furthermore, constant inflammation may also lead to cancer (Rakoff-Nahoum, 2006) pointing out the importance of anti-inflammatory compounds in prevention of cancer (Aggarwal et al., 2009) and reducing the probability for tumor progression. Pro-inflammatory transmitters such as TNF-α activate NF-κB which is then translocated into the nucleus leading to an increase of the transcription of pro – inflammatory – proteins. By blocking one of the steps of the TNF-α induced pathway of NF-κB activation, inflammation can be reduced as well as a decreased feeling of pain is achieved.

So far, not many fungal derived compounds have been isolated and proven to possess analgesic and anti-platelet activities. Further investigations are still needed to find lead structures for potential anti-inflammatory, anti – platelet or for analgesic drugs. Particularly, secondary metabolites obtained from some fungi are reported to exhibit interesting analgesic properties.

For example, the endophytic fungus *Phomopsis* sp., isolated from the medicinal plant *Erythrina crista galli*, when fermented in 1 L of KGA medium yielded the new compound phomol, which exhibits a polyketide moiety with hydroxyl-functions. Phomol was able to inhibit induced mouse edema by 53.2 % while the known anti-inflammatory compound indomethacin reduced this inflammation by 66 %. (Weber et al., 2004) Interestingly a study demonstrated that the water extract of *Erythrina crista galli* likewise exhibited anti-inflammatory properties. (Mino et al., 2002)

From an ethanolic extract of the fungus *Schizophyllum commune,* five phenolic acid derivatives were obtained. An animal pain model revealed that compounds with phenolic acid moieties inhibit volted gated sodium channels. (YAO et al., 2016) Interestingly, inhibition of these channels results in interrupting the signal transduction with the effect of local anesthetization and pain perception reduction. (Wood et al., 2004)

In summary, in the search for analgesic and anti-inflammatory drugs, secondary metabolites obtained from fungi can be promising candidates for future drug discovery.

9. Conclusion

In the search for anticancer and antibacterial metabolites from endophytic fungi derived from medicinal plants, OSMAC approaches andco-cultivation experiments were carried out in order to expand the chemical diversity of these fungi. The results obtained from the three projects conducted in this dissertation, demonstrated that fermentation of endophytic fungi on solid rice media as well as cultivation on different media as carried out in OSMAC experiments has a high impact on the chemical diversity of secondary metabolites including the induction of new metabolites. The same is true for co-cultvaton of fungi with bacteria which likewise induces silent biogentic gene clusters. Natural product discovery from endophytic fungi is still a promising field to obtain new natural product derived active pharmaceutical ingredients especially when new methods of fermentation that aim at inducing silent biogenetic gene clusters are enrolled.

References

Abe, F.; Hiraki, T. Mechanistic role of ergosterol in membrane rigidity and cycloheximide resistance in *Saccharomyces cerevisiae*. *Biochimica et Biophysica Acta (BBA) - Biomembranes* [Online] **2009,** *1788* (3), 743–752. http://www.sciencedirect.com/science/article/pii/S0005273608003945.

Abrantes-Metz, R. M.; Adams, C.; Metz, A. D. Pharmaceutical Development Phases: A Duration Analysis. *SSRN Journal* [Online] **2004**.

Acred, P.; Brown, D. M.; Turner, D. H.; Wilson, M. J. Pharmacology and chemotherapy of ampicillin—a new broad-spectrum penicillin. *British journal of pharmacology and chemotherapy* **1962,** *18* (2), 356–369.

Adams, C. P.; van Brantner, V. Estimating The Cost Of New Drug Development: Is It Really $802 Million? *Health Affairs* **2006,** *25* (2), 420–428. DOI: 10.1377/hlthaff.25.2.420.

Aggarwal, B. B.; Vijayalekshmi, R. V.; Sung, B. Targeting inflammatory pathways for prevention and therapy of cancer: short-term friend, long-term foe. *Clinical cancer research : an official journal of the American Association for Cancer Research* **2009,** *15* (2), 425–430.

Akone, S. H.; Mándi, A.; Kurtán, T.; Hartmann, R.; Lin, W.; Daletos, G.; Proksch, P. Inducing secondary metabolite production by the endophytic fungus *Chaetomium* sp. through fungal–bacterial co-culture and epigenetic modification. *Tetrahedron* [Online] **2016,** *72* (41), 6340–6347. http://www.sciencedirect.com/science/article/pii/S0040402016307876.

Akram, M. Citric Acid Cycle and Role of its Intermediates in Metabolism. *Cell Biochemistry and Biophysics* [Online] **2014,** *68* (3), 475–478. https://doi.org/10.1007/s12013-013-9750-1.

Baldwin, J. E.; Abraham, E. The biosynthesis of penicillins and cephalosporins. *Natural product reports* **1988,** *5* (2), 129–145.

Bennett, J. W.; Chung, K.-T. Alexander Fleming and the discovery of penicillin. *Advances in Applied Microbiology*; Academic Press, 2001; pp 163–184. DOI: 10.1016/S0065-2164(01)49013-7.

Bentley, S. D.; Chater, K. F.; Cerdeño-Tárraga, A.-M.; Challis, G. L.; Thomson, N. R.; James, K. D.; Harris, D. E.; Quail, M. A.; Kieser, H.; Harper, D.; Bateman, A.; Brown, S.; Chandra, G.; Chen, C. W.; Collins, M.; Cronin, A.; Fraser, A.; Goble, A.; Hidalgo, J.; Hornsby, T.; Howarth, S.; Huang, C.-H.; Kieser, T.; Larke, L.; Murphy, L.; Oliver, K.; O'Neil, S.; Rabbinowitsch, E.; Rajandream, M.-A.; Rutherford, K.; Rutter, S.; Seeger, K.; Saunders, D.; Sharp, S.; Squares, R.; Squares, S.; Taylor, K.; Warren, T.; Wietzorrek, A.; Woodward, J.; Barrell, B. G.; Parkhill, J.; Hopwood, D. A. Complete genome sequence of the model actinomycete Streptomyces coelicolor A3(2). *Nature* [Online] **2002,** *417* (6885), 141–147. https://doi.org/10.1038/417141a.

Bergmann, E. D.; Ginsburg, D.; Pappo, R. *The Michael Reaction * This cooperative study was begun when the three authors were working at the Weizmann Institute of Science, Rehovoth*; Major Reference Works, 2011.

Bertrand, S.; Bohni, N.; Schnee, S.; Schumpp, O.; Gindro, K.; Wolfender, J.-L. Metabolite induction via microorganism co-culture: a potential way to enhance chemical diversity for drug discovery. *Biotechnology advances* **2014,** *32* (6), 1180–1204. DOI: 10.1016/j.biotechadv.2014.03.001.

Blackwell, M. The fungi: 1, 2, 3 … 5.1 million species? *American journal of botany* **2011,** *98* (3), 426–438. DOI: 10.3732/ajb.1000298.

Bode, H. B.; Walker, M.; ZEECK, A. Structure and Biosynthesis of Mutolide, a Novel Macrolide from a UV Mutant of the Fungus F-24′707. *Eur. J. Org. Chem.* **2000,** *2000* (8), 1451–1456. DOI: 10.1002/(SICI)1099-0690(200004)2000:8<1451:AID-EJOC1451>3.0.CO;2-F.

Bunch, Robert L., Mcguire, James M. *Erythromycin, its salts, and method of preparation;* Google Patents, 1953.

Burstein, C.; Cohn, M.; Kepes, A.; Monod, J. Rôle du lactose et de ses produits métaboliques dans l'induction de l'opéron lactose chez *Escherichia coli*. *Biochimica et Biophysica Acta (BBA) - Nucleic Acids and Protein Synthesis* [Online] **1965,** *95* (4), 634–639. http://www.sciencedirect.com/science/article/pii/0005278765905174.

Butler, M. S.; Robertson, A. A. B.; Cooper, M. A. Natural product and natural product derived drugs in clinical trials. *Natural product reports* [Online] **2014,** *31* (11), 1612–1661. http://dx.doi.org/10.1039/C4NP00064A.

Chiang, Y.-M.; Chang, S.-L.; Oakley, B. R.; Wang, C. C. C. Recent advances in awakening silent biosynthetic gene clusters and linking orphan clusters to natural products in microorganisms. *Current opinion in chemical biology* **2011,** *15* (1), 137–143.

Christensen, M. A View of Fungal Ecology. *Mycologia* **1989,** *81* (1), 1–19. DOI: 10.1080/00275514.1989.12025620.

Collie, J. N. CLXXI.—Derivatives of the multiple keten group. *Journal of the Chemical Society, Transactions* **1907,** *91*, 1806–1813.

Cragg, G. M.; Newman, D. J. Natural Product Drug Discovery in the Next Millennium. *Pharmaceutical Biology* **2001,** *39* (sup1), 8–17. DOI: 10.1076/phbi.39.s1.8.0009.

Cross, J. B.; Thompson, D. C.; Rai, B. K.; Baber, J. C.; Fan, K. Y.; Hu, Y.; Humblet, C. Comparison of several molecular docking programs: pose prediction and virtual screening accuracy. *Journal of chemical information and modeling* **2009,** *49* (6), 1455–1474.

Crowfoot, D.; Bunn, C. W.; Rogers-Low, B. W.; Turner-Jones, A. The X-ray crystallographic investigation of the structure of penicillin. *The Chemistry of Penicillin* [Online] **2015**.

Cueto, M.; Jensen, P. R.; Kauffman, C.; Fenical, W.; Lobkovsky, E.; Clardy, J. Pestalone, a New Antibiotic Produced by a Marine Fungus in Response to Bacterial Challenge. *Journal of natural products* **2001,** *64* (11), 1444–1446. DOI: 10.1021/np0102713.

Microbial coculture and OSMAC approach as strategies to induce cryptic fungal biogenetic gene clusters.; Daletos, G., Ebrahim, W., Ancheeva, E., El-Neketi, M., Lin, WH., Proksch, P., Ed.; Chemical biology of natural products, 2017.

Daynes, R. A.; Jones, D. C. Emerging roles of PPARS in inflammation and immunity. *Nature Reviews Immunology* [Online] **2002,** *2* (10), 748–759. https://doi.org/10.1038/nri912.

Dempsey, M. E. Regulation of steroid biosynthesis. *Annual review of biochemistry* **1974,** *43* (1), 967–990.

DiMasi, J. A.; Hansen, R. W.; Grabowski, H. G. The price of innovation: new estimates of drug development costs. *Journal of Health Economics* [Online] **2003,** *22* (2), 151–185. http://www.sciencedirect.com/science/article/pii/S0167629602001261.

Dischler, N. M.; Xu, L.; Li, Y.; Nichols, C. B.; Alspaugh, J. A.; Bills, G. F.; Gloer, J. B. Wortmannin and Wortmannine Analogues from an Undescribed *Niesslia* sp. *Journal of natural products* **2019,** *82* (3), 532–538. DOI: 10.1021/acs.jnatprod.8b00923.

Du, L.; Feng, T.; Zhao, B.; Li, D.; Cai, S.; Zhu, T.; Wang, F.; Xiao, X.; Gu, Q. Alkaloids from a deep ocean sediment-derived fungus Penicillium sp. and their antitumor activities. *J. Antibiot.* [Online] **2010,** *63*, 165 EP -. https://doi.org/10.1038/ja.2010.11.

Ernst, Brandl, Hans, Margreiter. *Acid-stable penicillins;* Google Patents, 1956.

Evidente, A.; Maddau, L.; Spanu, E.; Franceschini, A.; Lazzaroni, S.; Motta, A. Diplopyrone, a New Phytotoxic Tetrahydropyranpyran-2-one Produced by *Diplodia mutila*, a Fungus Pathogen of Cork Oak. *Journal of natural products* **2003,** *66* (2), 313–315. DOI: 10.1021/np020367c.

Fleming, A. On the Antibacterial Action of Cultures of a Penicillium, with Special Reference to their Use in the Isolation of B. *influenzæ*. *British journal of experimental pathology* [Online] **1929,** *10* (3), 226–236. https://www.ncbi.nlm.nih.gov/pmc/articles/PMC2048009/.

Frisvad, J. C.; Andersen, B.; Thrane, U. The use of secondary metabolite profiling in chemotaxonomy of filamentous fungi. *Mycological research* **2008,** *112* (Pt 2), 231–240. DOI: 10.1016/j.mycres.2007.08.018.

Fuchser, J.; ZEECK, A. Secondary Metabolites by Chemical Screening, 34. – Aspinolides and Aspinonene/Aspyrone Co-Metabolites, New Pentaketides Produced by *Aspergillus ochraceus*. *Liebigs Ann./Recl.* **1997,** *1997* (1), 87–95. DOI: 10.1002/jlac.199719970114.

Glusker, J. P. Dorothy Crowfoot Hodgkin (1910-1994). *Protein science : a publication of the Protein Society* **1994,** *3* (12), 2465–2469. DOI: 10.1002/pro.5560031233.

Graham, J. B.; Istock, C. A. Genetic exchange in *Bacillus subtilis* in soil. *Molecular and General Genetics MGG* [Online] **1978,** *166* (3), 287–290. https://doi.org/10.1007/BF00267620.

Grimaldi, B.; Coiro, P.; Filetici, P.; Berge, E.; Dobosy, J. R.; Freitag, M.; Selker, E. U.; Ballario, P. The *Neurospora crassa* White Collar-1 dependent blue light response requires acetylation of histone H3 lysine 14 by NGF-1. *Molecular biology of the cell* [Online] **2006,** *17* (10), 4576–4583. https://www.ncbi.nlm.nih.gov/pubmed/16914525.

Gurusiddaiah, S.; Ronald, R. C. Grahamimycins: antibiotics from *Cytospora* sp. Ehrenb. W.F.P.L. 13A. *Antimicrobial agents and chemotherapy* **1981a,** *19* (1), 153–165. DOI: 10.1128/aac.19.1.153.

Gurusiddaiah, S.; Ronald, R. C. Grahamimycins: antibiotics from *Cytospora* sp. Ehrenb. WFPL 13A. *Antimicrobial agents and chemotherapy* **1981b,** *19* (1), 153–165.

Harrison, P. J.; Dunn, T. M.; Campopiano, D. J. Sphingolipid biosynthesis in man and microbes. *Natural product reports* **2018,** *35* (9), 921–954.

Harvey, A. L. Natural products in drug discovery. *Drug discovery today* **2008,** *13* (19-20), 894–901.

Hegnauer, R. Phytochemistry and plant taxonomy — an essay on the chemotaxonomy of higher plants. *Phytochemistry* **1986,** *25* (7), 1519–1535. DOI: 10.1016/S0031-9422(00)81204-2.

Hemphill, C. F. P.; Sureechatchaiyan, P.; Kassack, M. U.; Orfali, R. S.; Lin, W.; Daletos, G.; Proksch, P. OSMAC approach leads to new fusarielin metabolites from *Fusarium tricinctum*. *J. Antibiot.* [Online] **2017,** *70*, 726 EP -. https://doi.org/10.1038/ja.2017.21.

Hertweck, C. Die biosynthetische Grundlage der Polyketid-Vielfalt. *Angewandte Chemie* **2009,** *121* (26), 4782–4811.

Hopwood, D. A. Genetic Contributions to Understanding Polyketide Synthases. *Chemical Reviews* **1997,** *97* (7), 2465–2498. DOI: 10.1021/cr960034i.

Hoshino, M.; Yanaihara, C.; Hong, Y.-M.; Kishida, S.; Katsumaru, Y.; Vandermeers, A.; Vandermeers-Piret, M.-C.; Robberecht, P.; Christophe, J.; Yanaihara, N. Primary structure of

helodermin, a VIP-secretin-like peptide isolated from Gila monster venom. *FEBS letters* **1984,** *178* (2), 233–239.

The classes of natural product and their isolation; J.R. Hanson, Ed. 17; Royal Society of Chemistry: Cambridge, 2003.

Jain, M. K. Role of Cholesterol in Biomembranes and Related Systems. In *Current Topics in Membranes and Transport*; Bronner, F., Kleinzeller, A., Eds.; Academic Press, 1975; pp 1–57. DOI: 10.1016/S0070-2161(08)60101-X.

Kamath, A. V.; Vaidyanathan, C. S. New pathway for the biodegradation of indole in *Aspergillus niger*. *Applied and Environmental Microbiology* **1990,** *56* (1), 275.

Kang, K.-T.; Kim, S.-G. One-Pot Catalytic Enantioselective Synthesis of Functionalized Tetrahydroquinolines by Aza-Michael/Michael Cascade Reactions of N-Protected 2-Aminophenyl α,β-Unsaturated Esters with Nitroolefins. *Synthesis* **2014,** *46* (24), 3365–3373. DOI: 10.1055/s-0034-1379044.

Kappos, L.; Radue, E.-W.; O'Connor, P.; Polman, C.; Hohlfeld, R.; Calabresi, P.; Selmaj, K.; Agoropoulou, C.; Leyk, M.; Zhang-Auberson, L. A placebo-controlled trial of oral fingolimod in relapsing multiple sclerosis. *New England Journal of Medicine* **2010,** *362* (5), 387–401.

Katz, L.; Baltz, R. H. Natural product discovery: past, present, and future. *Journal of industrial microbiology & biotechnology* **2016,** *43* (2-3), 155–176. DOI: 10.1007/s10295-015-1723-5.

Keck, G. E.; Boden, E. P.; Wiley, M. R. Total synthesis of (+)-colletodiol: new methodology for the synthesis of macrolactones. *J. Org. Chem.* **1989,** *54* (4), 896–906. DOI: 10.1021/jo00265a033.

Kitchen, D. B.; Decornez, H.; Furr, J. R.; Bajorath, J. Docking and scoring in virtual screening for drug discovery: methods and applications. *Nature reviews. Drug discovery* **2004,** *3* (11), 935–949. DOI: 10.1038/nrd1549.

Kowalski, T.; Bartnik, C. *Cryptosporiopsis radicicola* sp. nov. from roots of *Quercus robur*. *Mycological research* **1995,** *99* (6), 663–666.

Landy, M.; Warren, G. H.; RosenmanM, S. B.; Colio, L. G. Bacillomycin: an antibiotic from *Bacillus subtilis* active against pathogenic fungi. *Proceedings of the Society for Experimental Biology and Medicine* **1948,** *67* (4), 539–541.

Lavecchia, A.; Di Giovanni, C. Amorfrutins are efficient modulators of peroxisome proliferator-activated receptor gamma (PPARγ) with potent antidiabetic and anticancer properties: a patent evaluation of WO2014177593 A1. *Expert Opinion on Therapeutic Patents* **2015,** *25* (11), 1341–1347.

Li, C.-S.; Li, X.-M.; Gao, S.-S.; Lu, Y.-H.; Wang, B.-G. Cytotoxic anthranilic acid derivatives from deep sea sediment-derived fungus *Penicillium paneum* SD-44. *Marine drugs* **2013,** *11* (8), 3068–3076. DOI: 10.3390/md11083068.

Luiz Antonio Soares RomeiroCarolyn CumminsLilia Magomedova. Ppar modulators.

Brock Mikrobiologie. *Brock biology of microorganism*. S.320; M.T. Madigan, T. D. Brock, Ed., 13th ed.; Pearson Higher Education: München, 2013.

Maeda, T.; Kishioka, S. Chapter 13 PPAR and Pain. *International Review of Neurobiology*; Academic Press, 2009; pp 165–177. DOI: 10.1016/S0074-7742(09)85013-7.

Marmann, A.; Aly, A. H.; Lin, W.; Wang, B.; Proksch, P. Co-cultivation--a powerful emerging tool for enhancing the chemical diversity of microorganisms. *Marine drugs* **2014,** *12* (2), 1043–1065. DOI: 10.3390/md12021043.

Melnikova, I. Pain market. *Nature Reviews Drug Discovery* [Online] **2010,** *9*, 589 EP -. https://doi.org/10.1038/nrd3226.

Meng, L.-H.; Li, X.-M.; Lv, C.-T.; Huang, C.-G.; Wang, B.-G. Brocazines A–F, Cytotoxic Bisthiodiketopiperazine Derivatives from *Penicillium brocae* MA-231, an Endophytic Fungus Derived from the Marine Mangrove Plant *Avicennia marina*. *Journal of natural products* **2014,** *77* (8), 1921–1927. DOI: 10.1021/np500382k.

Meng, L.-H.; Wang, C.-Y.; Mándi, A.; Li, X.-M.; Hu, X.-Y.; Kassack, M. U.; Kurtán, T.; Wang, B.-G. Three Diketopiperazine Alkaloids with Spirocyclic Skeletons and One Bisthiodiketopiperazine Derivative from the Mangrove-Derived Endophytic Fungus *Penicillium brocae* MA-231. *Organic Letters* **2016,** *18* (20), 5304–5307. DOI: 10.1021/acs.orglett.6b02620.

Mino, J.; Gorzalczany, S.; Moscatelli, V.; Ferraro, G.; Acevedo, C.; Hnatyszyn, O. Actividad antinociceptiva y antiinflamatoria de *Erythrina crista-galli* L.(" Ceibo"). *Acta Farmaceútica Bonaerense* **2002,** *21* (2), 93–98.

Miyanaga, A. Michael additions in polyketide biosynthesis. *Natural product reports* **2019,** *36* (3), 531–547.

Möbius, N.; Hertweck, C. Fungal phytotoxins as mediators of virulence. *Current opinion in plant biology* **2009,** *12* (4), 390–398.

Moraes, L. A.; Unsworth, A. J.; Vaiyapuri, S.; Ali, M. S.; Sasikumar, P.; Sage, T.; Flora, G. D.; Bye, A. P.; Kriek, N.; Dorchies, E. Farnesoid X receptor and its ligands inhibit the function of platelets. *Arteriosclerosis, thrombosis, and vascular biology* **2016,** *36* (12), 2324–2333.

Mullard, A. Parsing clinical success rates. *Nature Reviews Drug Discovery* [Online] **2016,** *15*, 447 EP -. https://doi.org/10.1038/nrd.2016.136.

Netzker, T.; Fischer, J.; Weber, J.; Mattern, D. J.; König, C. C.; Valiante, V.; Schroeckh, V.; Brakhage, A. A. Microbial communication leading to the activation of silent fungal secondary metabolite gene clusters. *Frontiers in microbiology* **2015,** *6*, 299. DOI: 10.3389/fmicb.2015.00299.

Nierman, W. C.; Pain, A.; Anderson, M. J.; Wortman, J. R.; Kim, H. S.; Arroyo, J.; Berriman, M.; Abe, K.; Archer, D. B.; Bermejo, C.; Bennett, J.; Bowyer, P.; Chen, D.; Collins, M.; Coulsen, R.; Davies, R.; Dyer, P. S.; Farman, M.; Fedorova, N.; Fedorova, N.; Feldblyum, T. V.; Fischer, R.; Fosker, N.; Fraser, A.; García, J. L.; García, M. J.; Goble, A.; Goldman, G. H.; Gomi, K.; Griffith-Jones, S.; Gwilliam, R.; Haas, B.; Haas, H.; Harris, D.; Horiuchi, H.; Huang, J.; Humphray, S.; Jiménez, J.; Keller, N.; Khouri, H.; Kitamoto, K.; Kobayashi, T.; Konzack, S.; Kulkarni, R.; Kumagai, T.; Lafon, A.; Lafton, A.; Latgé, J.-P.; Li, W.; Lord, A.; Lu, C.; Majoros, W. H.; May, G. S.; Miller, B. L.; Mohamoud, Y.; Molina, M.; Monod, M.; Mouyna, I.; Mulligan, S.; Murphy, L.; O'Neil, S.; Paulsen, I.; Peñalva, M. A.; Pertea, M.; Price, C.; Pritchard, B. L.; Quail, M. A.; Rabbinowitsch, E.; Rawlins, N.; Rajandream, M.-A.; Reichard, U.; Renauld, H.; Robson, G. D.; Rodriguez de Córdoba, S.; Rodríguez-Peña, J. M.; Ronning, C. M.; Rutter, S.; Salzberg, S. L.; Sanchez, M.; Sánchez-Ferrero, J. C.; Saunders, D.; Seeger, K.; Squares, R.; Squares, S.; Takeuchi, M.; Tekaia, F.; Turner, G.; Vazquez de Aldana, C. R.; Weidman, J.; White, O.; Woodward, J.; Yu, J.-H.; Fraser, C.; Galagan, J. E.; Asai, K.; Machida, M.; Hall, N.; Barrell, B.; Denning, D. W. Genomic sequence of the pathogenic and allergenic filamentous fungus *Aspergillus fumigatus*. *Nature* **2005,** *438* (7071), 1151–1156. DOI: 10.1038/nature04332.

Norn, S.; Kruse, P. R.; Kruse, E. History of opium poppy and morphine. *Dansk medicinhistorisk arbog* **2005,** *33*, 171–184.

Oldfield, E.; Lin, F.-Y. Terpene Biosynthesis: Modularity Rules. *Angew. Chem. Int. Ed.* **2012,** *51* (5), 1124–1137. DOI: 10.1002/anie.201103110.

Olivera, B.; Gray, W.; Zeikus, R.; McIntosh, J.; Varga, J.; Rivier, J.; Santos, V. de; Cruz, L. Peptide neurotoxins from fish-hunting cone snails. *Science* **1985,** *230* (4732), 1338–1343. DOI: 10.1126/science.4071055.

Oliynyk, M.; Samborskyy, M.; Lester, J. B.; Mironenko, T.; Scott, N.; Dickens, S.; Haydock, S. F.; Leadlay, P. F. Complete genome sequence of the erythromycin-producing bacterium *Saccharopolyspora erythraea* NRRL23338. *Nature Biotechnology* [Online] **2007,** *25*, 447 EP -. https://doi.org/10.1038/nbt1297.

O'Neill, J. A.; Simpson, T. J.; Willis, C. L. Biosynthesis of collectodiol and related polyketide macrodiolides in *Cytospora* sp. ATTCC 20502: synthesis and metabolism of advanced intermediates. *Journal of the Chemical Society, Chemical Communications* **1993,** No. 9, 738–740. DOI: 10.1039/C39930000738.

Opal, S. M.; Fisher, C. J.; Dhainaut, J.-F. A.; Vincent, J.-L.; Brase, R.; Lowry, S. F.; Sadoff, J. C.; Slotman, G. J.; Levy, H.; Balk, R. A. Confirmatory interleukin-1 receptor antagonist trial in severe sepsis: a phase III, randomized, doubleblind, placebo-controlled, multicenter trial. *Critical care medicine* **1997,** *25* (7), 1115–1124.

Özkaya, F. C.; Ebrahim, W.; El-Neketi, M.; Tanrıkul, T. T.; Kalscheuer, R.; Müller, W. E. G.; Guo, Z.; Zou, K.; Liu, Z.; Proksch, P. Induction of new metabolites from sponge-associated fungus Aspergillus carneus by OSMAC approach. *Fitoterapia* **2018,** *131*, 9–14.

Pan, R.; Bai, X.; Chen, J.; Zhang, H.; Wang, H. Exploring Structural Diversity of Microbe Secondary Metabolites Using OSMAC Strategy: A Literature Review. *Front. Microbiol.* [Online] **2019,** *10*, 294. https://www.frontiersin.org/articles/10.3389/fmicb.2019.00294/pdf.

Paranagama, P. A.; Wijeratne, E. M. K.; Gunatilaka, A. A. L. Uncovering biosynthetic potential of plant-associated fungi: effect of culture conditions on metabolite production by *Paraphaeosphaeria quadriseptata* and *Chaetomium chiversii*. *Journal of natural products* **2007,** *70* (12), 1939–1945. DOI: 10.1021/np070504b.

Pascolutti, M.; Quinn, R. J. Natural products as lead structures: chemical transformations to create lead-like libraries. *Drug discovery today* **2014,** *19* (3), 215–221.

Patridge, E.; Gareiss, P.; Kinch, M. S.; Hoyer, D. An analysis of FDA-approved drugs: natural products and their derivatives. *Drug discovery today* **2016,** *21* (2), 204–207. DOI: 10.1016/j.drudis.2015.01.009.

Peng, J.; Gao, H.; Zhang, X.; Wang, S.; Wu, C.; Gu, Q.; Guo, P.; Zhu, T.; Li, D. Psychrophilins E-H and versicotide C, cyclic peptides from the marine-derived fungus Aspergillus versicolor ZLN-60. *Journal of natural products* **2014,** *77* (10), 2218–2223. DOI: 10.1021/np500469b.

Penn, J. Biosynthesis of glyantrypine by *Aspergillus clavatus*. *FEMS Microbiology Letters* **1992,** *92* (3), 229–233. DOI: 10.1016/0378-1097(92)90714-Y.

Penn, J.; Mantle, P. G.; Bilton, J. N.; Sheppard, R. N. Glyantrypine, a novel anthranilic acid-containing metabolite of *Aspergillus clavatus*. *Journal of the Chemical Society, Perkin Transactions 1* [Online] **1992,** No. 12, 1495–1496.

Rakoff-Nahoum, S. Cancer Issue: Why cancer and inflammation? *The Yale journal of biology and medicine* **2006,** *79* (3-4), 123.

Reilly, M.; Miller, R. M.; Thomson, M. H.; Patris, V.; Ryle, P.; McLoughlin, L.; Mutch, P.; Gilboy, P.; Miller, C.; Broekema, M. Randomized, double-blind, placebo-controlled, dose-escalating phase I, healthy subjects study of intravenous OPN-305, a humanized anti-TLR2 antibody. *Clinical Pharmacology & Therapeutics* **2013,** *94* (5), 593–600.

Ren, H.; Wang, B.; Zhao, H. Breaking the silence: new strategies for discovering novel natural products. *Current opinion in biotechnology* **2017,** *48*, 21–27.

Roberts, D. T. Oral therapeutic agents in fungal nail disease. *Journal of the American Academy of Dermatology* **1994,** *31* (3), S78-S81.

Rodriguez, R. J.; White, J. F.; Arnold, A. E.; Redman, R. S. Fungal endophytes: diversity and functional roles. *The New phytologist* **2009,** *182* (2), 314–330. DOI: 10.1111/j.1469-8137.2009.02773.x.

SCHIEWE, H.-J.; ZEECK, A. Cineromycins, .GAMMA.-Butyrolactones and Ansamycins by Analysis of the Secondary Metabolite Pattern Created by a Single Strain of *Strepomycest*. *J. Antibiot.* **1999,** *52* (7), 635–642. DOI: 10.7164/antibiotics.52.635.

Schmidt-Dannert, C. Biosynthesis of Terpenoid Natural Products in Fungi. In *Biotechnology of Isoprenoids*; Schrader, J., Bohlmann, J., Eds.; Springer International Publishing: Cham, 2015; pp 19–61. DOI: 10.1007/10_2014_283.

Schulz, B.; Römmert, A.-K.; Dammann, U.; Aust, H.-J.; Strack, D. The endophyte-host interaction: a balanced antagonism? *Mycological research* **1999,** *103* (10), 1275–1283.

Seshime, Y.; Juvvadi, P. R.; Tokuoka, M.; Koyama, Y.; Kitamoto, K.; Ebizuka, Y.; Fujii, I. Functional expression of the *Aspergillus flavus* PKS–NRPS hybrid CpaA involved in the biosynthesis of cyclopiazonic acid. *Bioorganic & Medicinal Chemistry Letters* [Online] **2009,** *19* (12), 3288–3292. http://www.sciencedirect.com/science/article/pii/S0960894X09005678.

Sheridan, K. J.; Dolan, S. K.; Doyle, S. Endogenous cross-talk of fungal metabolites. *Front. Microbiol.* **2014,** *5*, 732. DOI: 10.3389/fmicb.2014.00732.

Shih, C.-Y.; Chou, T.-C. The antiplatelet activity of magnolol is mediated by PPAR-β/γ. *Biochemical Pharmacology* [Online] **2012,** *84* (6), 793–803. http://www.sciencedirect.com/science/article/pii/S0006295212004200.

Shoichet, B. K. Virtual screening of chemical libraries. *Nature* [Online] **2004,** *432* (7019), 862–865. https://doi.org/10.1038/nature03197.

Simon, R. Optimal two-stage designs for phase II clinical trials. *Controlled clinical trials* **1989,** *10* (1), 1–10.

Simpson, T. J.; Stevenson, G. I. Studies of polyketide chain-assembly processes: origins of the hydrogen and oxygen atoms in colletodiol. *Journal of the Chemical Society, Chemical Communications* **1985,** No. 24, 1822–1824. DOI: 10.1039/C39850001822.

Singh, V.; Deverall, B. J. *Bacillus subtilis* as a control agent against fungal pathogens of citrus fruit. *Transactions of the British Mycological Society* **1984,** *83* (3), 487–490.

Soda, K.; Tanizawa, K. *Kynureninases: Enzymological Properties and Regulation Mechanism*; Advances in Enzymology - and Related Areas of Molecular Biology, 1979.

Spinelli, S. L.; O'brien, J. J.; Bancos, S.; Lehmann, G. M.; Springer, D. L.; Blumberg, N.; Francis, C. W.; Taubman, M. B.; Phipps, R. P. The PPAR-platelet connection: modulators of inflammation and potential cardiovascular effects. *PPAR research* **2008,** *2008*.

Stone, M. J.; Williams, D. H. On the evolution of functional secondary metabolites (natural products). *Molecular Microbiology* **1992,** *6* (1), 29–34. DOI: 10.1111/j.1365-2958.1992.tb00834.x.

Sukthankar, A. Syphilis. *Medicine* **2014,** *42* (7), 394–398.

Suvarna, V. Phase IV of drug development. *Perspectives in clinical research* **2010,** *1* (2), 57.

Tedersoo, L.; Bahram, M.; P??lme, S.; K??ljalg, U.; Yorou, N. S.; Wijesundera, R.; Ruiz, L. V.; Vasco-Palacios, A.??d. M.; Thu, P. Q.; Suija, A.; Smith, M. E.; Sharp, C.; Saluveer, E.; Saitta, A.; Rosas, M.; Riit, T.; Ratkowsky, D.; Pritsch, K.; P??ldmaa, K.; Piepenbring, M.; Phosri, C.; Peterson, M.; Parts, K.; P??rtel, K.; Otsing, E.; Nouhra, E.; Njouonkou, A. L.; Nilsson, R. H.; Morgado, L. N.; Mayor, J.; May, T. W.; Majuakim, L.; Lodge, D. J.; Lee, S. S.; Larsson, K.-H.; Kohout, P.; Hosaka, K.; Hiiesalu, I.; Henkel, T. W.; Harend, H.; Guo, L.-d.; Greslebin, A.; Grelet, G.; Geml, J.; Gates, G.; Dunstan, W.; Dunk, C.; Drenkhan, R.; Dearnaley, J.; Kesel, A. de; Dang, T.; Chen, X.; Buegger, F.; Brearley, F. Q.; Bonito, G.; Anslan, S.; Abell, S.; Abarenkov, K. Global diversity and geography of soil fungi. *Science* **2014,** *346* (6213), 1256688. DOI: 10.1126/science.1256688.

Teponno, R.; Noumeur, S.; Helaly, S.; Hüttel, S.; Harzallah, D.; Stadler, M. Furanones and anthranilic acid derivatives from the endophytic fungus *Dendrothyrium variisporum*. *Molecules* **2017a,** *22* (10), 1674.

Teponno, R. B.; Noumeur, S. R.; Helaly, S. E.; Hüttel, S.; Harzallah, D.; Stadler, M. Furanones and Anthranilic Acid Derivatives from the Endophytic Fungus Dendrothyrium variisporum. *Molecules (Basel, Switzerland)* **2017b,** *22* (10). DOI: 10.3390/molecules22101674.

Tholl, D. Biosynthesis and Biological Functions of Terpenoids in Plants. In *Biotechnology of Isoprenoids*; Schrader, J., Bohlmann, J., Eds.; Springer International Publishing: Cham, 2015; pp 63–106. DOI: 10.1007/10_2014_295.

Tollenaere, J. P. The role of structure-based ligand design and molecular modelling in drug discovery. *Pharmacy World and Science* [Online] **1996,** *18* (2), 56–62. https://doi.org/10.1007/BF00579706.

Tran-Cong, N. M.; Mándi, A.; Király, S. B.; Kurtán, T.; Lin, W.; Liu, Z.; Proksch, P. Furoic acid derivatives from the endophytic fungus Coniothyrium sp. *Chirality* [Online] **2020**.

Tran-Cong, N. M.; Mándi, A.; Kurtán, T.; Müller, W. E. G.; Kalscheuer, R.; Lin, W.; Liu, Z.; Proksch, P. Induction of cryptic metabolites of the endophytic fungus *Trichocladium* sp. through OSMAC and co-cultivation. *RSC Adv.* **2019,** *9* (47), 27279–27288.

Traxler, M. F.; Kolter, R. Natural products in soil microbe interactions and evolution. *Natural product reports* **2015,** *32* (7), 956–970.

Tvrzicka, E.; Kremmyda, L.-S.; Stankova, B.; Zak, A. FATTY ACIDS AS BIOCOMPOUNDS: THEIR ROLE IN HUMAN METABOLISM, HEALTH AND DISEASE-A REVIEW. PART 1: CLASSIFICATION, DIETARY SOURCES AND BIOLOGICAL FUNCTIONS. *Biomedical Papers of the Medical Faculty of Palacky University in Olomouc* **2011,** *155* (2).

Unsworth, A. J.; Flora, G. D.; Gibbins, J. M. Non-genomic effects of nuclear receptors: insights from the anucleate platelet. *Cardiovascular research* **2018,** *114* (5), 645–655.

van Dijl, JanMaarten, Hecker, Michael. *Bacillus subtilis: from soil bacterium to super-secreting cell factory;* BioMed Central, 2013.

Vardar, F.; Lilly, M. D. Effect of cycling dissolved oxygen concentrations on product formation in penicillin fermentations. *European journal of applied microbiology and biotechnology* [Online] **1982,** *14* (4), 203–211. https://doi.org/10.1007/BF00498464.

Venoms to Drugs: Venom as a Source for the Development of Human Therapeutics; The Royal Society of Chemistry, 2015.

Walker, SR; Walker, S. R. *Trends and changes in drug research and development;* Springer, 2012.

Wang, G.; Tang, W.; Bidigare, R. R. Terpenoids As Therapeutic Drugs and Pharmaceutical Agents. In *Natural Products: Drug Discovery and Therapeutic Medicine*; Zhang, L., Demain, A. L., Eds.; Humana Press: Totowa, NJ, 2005; pp 197–227. DOI: 10.1007/978-1-59259-976-9_9.

Wang, H.; Eze, P. M.; Höfert, S.-P.; Janiak, C.; Hartmann, R.; Okoye, F. B. C.; Esimone, C. O.; Orfali, R. S.; Dai, H.; Liu, Z.; Proksch, P. Substituted l -tryptophan- l -phenyllactic acid conjugates produced by an endophytic fungus *Aspergillus aculeatus* using an OSMAC approach. *RSC Adv.* **2018,** *8* (14), 7863–7872. DOI: 10.1039/C8RA00200B.

Wang, Y.-D.; Chen, W.-D.; Moore, D. D.; Huang, W. FXR: a metabolic regulator and cell protector. *Cell Research* [Online] **2008,** *18*, 1087 EP -. https://doi.org/10.1038/cr.2008.289.

Wat, C.-K.; Towers, G. H. N. Metabolism of the Aromatic Amino Acids by Fungi. In *Biochemistry of Plant Phenolics*; Swain, T., Harbone, J. B., van Sumere, C. F., Eds.; Springer US: Boston, MA, 1979; pp 371–432. DOI: 10.1007/978-1-4684-3372-2_12.

Weber, D.; Sterner, O.; Anke, T.; Gorzalczancy, S.; Martino, V.; Acevedo, C. Phomol, a new antiinflammatory metabolite from an endophyte of the medicinal plant *Erythrina crista-galli*. *J. Antibiot.* **2004,** *57* (9), 559–563.

Wellington, E. M. H.; Cresswell, N.; Herron, P. R.; Clewlow, L. J.; Saunders, V. A.; Wipat, A. Gene transfer between streptomycetes in soil. *Bacterial Genetics in Natural Environments*; Springer, 1990; pp 216–230.

Wille, H.; Schönhöfer, P. S. Arzneimittelsicherheit und NachmarktkontrolleEntwicklungen seit der Reform des Arzneimittelgesetzes im Jahr 1978. *Der Internist* [Online] **2002,** *43* (4), 469–481. https://doi.org/10.1007/s00108-002-0575-z.

William Fenical,Paul R. Jensen,Xing C. Cheng. Halimide, a cytotoxic marine natural product, and derivatives thereof. US6069146A.

Williams, R. B.; Henrikson, J. C.; Hoover, A. R.; Lee, A. E.; Cichewicz, R. H. Epigenetic remodeling of the fungal secondary metabolome. *Organic & biomolecular chemistry* **2008,** *6* (11), 1895–1897. DOI: 10.1039/b804701d.

Wood, J. N.; Boorman, J. P.; Okuse, K.; Baker, M. D. Voltage-gated sodium channels and pain pathways. *J. Neurobiol.* **2004,** *61* (1), 55–71. DOI: 10.1002/neu.20094.

YAO, H.-M.; WANG, G.; LIU, Y.-P.; RONG, M.-Q.; SHEN, C.-B.; YAN, X.-W.; LUO, X.-D.; LAI, R. Phenolic acids isolated from the fungus *Schizophyllum commune* exert analgesic activity by inhibiting voltage-gated sodium channels. *Chinese Journal of Natural Medicines* [Online] **2016,** *14* (9), 661–670. http://www.sciencedirect.com/science/article/pii/S1875536416300784.

Yuri Gasparyan, A.; Ayvazyan, L.; P Mikhailidis, D.; D Kitas, G. Mean platelet volume: a link between thrombosis and inflammation? *Current pharmaceutical design* **2011,** *17* (1), 47–58.

Zarbock, A.; Polanowska-Grabowska, R. K.; Ley, K. Platelet-neutrophil-interactions: linking hemostasis and inflammation. *Blood reviews* **2007,** *21* (2), 99–111.

Zheng, Z.; Zhao, Z.; Li, S.; Lu, X.; Jiang, M.; Lin, J.; An, Y.; Xie, Y.; Xu, M.; Shen, W. Altenusin, a nonsteroidal microbial metabolite, attenuates nonalcoholic fatty liver disease by activating the farnesoid X receptor. *Molecular pharmacology* **2017,** *92* (4), 425–436.

Ziegler, J.; Facchini, P. J. Alkaloid Biosynthesis: Metabolism and Trafficking. *Annual Review of Plant Biology* **2008,** *59* (1), 735–769. DOI: 10.1146/annurev.arplant.59.032607.092730.

Zmijewski, Milton J., Jr.; Briggs, B. Biosynthesis of vancomycin: identification of TDP-glucose: aglycosyl-vancomycin glucosyltransferase from Amycolatopsis orientalis. *femsle* **1989,** *59* (1-2), 129–133. DOI: 10.1111/j.1574-6968.1989.tb03096.x.

List of abbreviations

$[\alpha]_D$	Specific rotation at the sodium D-line
5-AC	5-Azacytidine
Å	Ångström
amu	Atomic mass unit
BGCs	Biosynthetic gene clusters
br	Broad
CD3OD	Deuterated methanol
CDCl3	Deuterated chloroform
CH2Cl2,	DCM Dichloromethane
$CH3COONH_4$	Ammonium acetate
COSY	Correlation spectroscopy
d	Doublet
dd	Doublet of doublet signal
ddd	Doublet of doublet of doublet signal
DMAPP	Dimethylallyl pyrophosphate
DMSO	Dimethyl sulfoxide
DNA	Deoxyribonucleic acid
DNMT	DNA methyltransferase
e. g.	Exempli gratia (for the sake of example)
EMA	European Medical Agency
et al. et	altera (and others)
EtOAc	Ethyl acetate
FDA	United States Food and Drug Administration
FDAA	1-fluoro-2-4-dinitrophenyl-5-L-alanine amide
FXR	Farnesoid X receptor
g	Gram
h	hour
HCl	Hydrochloric acid
HDAC	Histone deacetylase
HMBC	Heteronuclear multiple bond connectivity
HMG-CoA	3-Hydroxy-3-methyl-glutaryl-CoA
HPLC	High performance liquid chromatography
HRESIMS	High resolution electrospray ionisation mass
HSQC	Heteronuclear single quantum coherence spectroscopy
HSQC	Heteronuclear single quantum coherence
Hz	Hertz
IC_{50}	Half maximal inhibitory concentration
ITS	Iternal transcriber spacers
L	Liter
LC-MS	Liquid chromatography-mass spectrometry
m	Multiplet signal
M	Mole
m/z	Mass per charge
MeOH	Methanol
mg	Milligram
MHz	Mega Herz
MIC	Minimum inhibitory concentration
min	Minute
mL	Milliliter
mm	Millimeter
MS	Mass spectrometry
MTT	3-(4,5-Dimethylthiazol-2-yl)-2,5-diphenyltetrazolium bromide
MW	Molecular weight
NaOH	Sodium hydroxide
nm	Nanometer
NMR	nuclear magnetic resonance spectrometry
NMR	nitrogen metabolite repression
NOE	Nuclear Overhauser effect
OSMAC	One Strain MAny Compounds

PDB	Potato dextrose broth
PKS-NRPS	Polyketide synthases - Non-ribosomal peptide
PPAR	Peroxisome proliferator-activated receptor
ppm	Parts per million
ROESY	Rotating frame overhauser effect spectroscopy
RP	18 Reversed phase C18
s	Singlet signal
SAHA	Suberoylanilide hydroxamic acid
SAR	Structure and activity relationship
sp.	Species
t	Triplet signal
TFA	Trifluoroacetic acid
TLC	Thin layer chromatography
Trp	Tryptophan
TSA	Trichostatin A
UV	Ultra-violet
VLC	Vacuum liquid chromatography
μM	Micromolar

Research contributions

Publications

(1) **Nam Michael Tran-Cong**, Thomas Hohlfeld, Michele Bonus, Marian Frank, Holger Gohlke, Wenhan Lin, Liu Zhen and Peter Proksch (2019) The mycotoxin altenusin is a platelet aggregation inhibitor, manuscript in preparation for submission
The first author contributed 50% to this publication. The first author's work involved all laboratory work including compound isolation, structure elucidation, and manuscript preparation

(2) **Nam Michael Tran-Cong**, Attila Mándi, Tibor Kurtán, Werner E. G. Müller, Rainer Kalscheuer, Wenhan Lin, Zhen Liu and Peter Proksch (2019) Induction of cryptic metabolites of the endophytic fungus Trichocladium sp. through OSMAC and co-cultivation, Royal Society of Chemistry Advances., 2019, 9, 27279-27288
The first author contributed 60% to this publication. The first author's work involved part of laboratory work including compound isolation, structure elucidation that derived from OSMAC approach and manuscript preparation.

(3) **Nam Michael Tran-Cong**, Attila Mándi, Tibor Kurtán, Wenhan Lin, Zhen Liu, Peter Proksch (2019) Furoic Acid Derivatives from the Endophytic Fungus *Coniothyrium* sp., manuscript in preparation for submission
The first author contributed 60% to this publication. The first author's work involved part of laboratory work including compound isolation, structure elucidation and manuscript preparation.

Declaration of academic honesty/Erklärung

Ich versichere an Eides Statt, dass die Dissertation**, „Secondary Metabolites from Endophytic fungi derived from Traditional Medicinal Herbs: Drug Discovery, Diversity Enhancement, Structure Elucidation and Bioactivity“**, von mir selbständig und ohne unzulässige fremde Hilfe unter Beachtung der „Grundsätze zur Sicherung guter wissenschaftlicher Praxis an der Heinrich-Heine-Universität Düsseldorf“ erstellt worden ist. Außer den angegebenen Quellen und Hilfsmitteln wurden keine weiteren verwendet. Diese Dissertation wurde weder in gleicher noch in abgewandelter Form in einem anderen Prüfungsverfahren vorgelegt. Weiterhin erkläre ich, dass ich früher weder akademische Grade erworben habe, noch dies versucht habe.

Düsseldorf, den 28.10.2019

Nam Michael Tran-Cong

Acknowledgments

Firstly, I would like to express my deepest appreciation to Prof. Dr. Dres. h.c. Peter Proksch as my doctorate father and for giving me the opportunity to make my own research in fungal secondary metabolites. As my doctorate father, he taught me in the ways of scientific work and collaboration. Secondly, my deepest thanks for his guidance and giving me the opportunity to join the research training group GRK2158 and of course providing me the excellent working conditions and facilities. Thirdly, I am very grateful for his guidance, helpful suggestions and discussions as well as his constructive critics regarding my work. Nevertheless, I am appreciating him as a person as well.

In addition, I would like to thank him for giving me the opportunity of spending a one month stay at Peking University under the guidance of Professor Wenhan Lin. This stay broadened my horizon, fortifying my understanding of the Chinese culture and people and for providing me my unforgettable stay in Peking. I learned a lot from him and from the Chinese colleagues, lastly allowing myself to develop further.

I would like to thank Prof. Dr. Rainer Kalscheuer for the antibiotic assay as well the fruitful discussions and as my second referee.

I would like to express my gratitude to Prof. Dr. Thomas Hohlfeld for his support, suggestions and ideas for the antiplatelet topics. I would also like to thank his co-worker, Kirsten Bartkowski as well and of course for the pleasant and fruitful coffee breaks at the medical department.

I appreciate Dr. Zhen Liu for his help on structure elucidations and manuscript preparations as well as his suggestions on my experiments. Moreover, I would like to thank Dr. Marian Frank for the manuscript preparations, the inspiring discussions, the fruitful teamwork during practical students courses and of course the personal relationship making the time less exhausting. I would like to thank Dr. Elena Ancheeva and Dr. Georgios Daletos for them advises and suggestions.

My deep thanks to Prof. Dr. Werner E.G. Müller for the cytotoxicity test and to I would like to thank Prof. Dr. Holger Gohlke and Mr. Michele Bonus for their help and support for the docking studies. I am thanking Prof. Dr. Claus Paßreiter for the safety introduction and the various interesting discussions.

My special thanks and a special goose hug to my lab mates Dr. Yang Liu, Mr. Haiqian Yu and Ms. Flaminia Mazzone for staying and enjoying the lab time together. In addition, I would like to thank Mr. Haiqian Yu for having a very good time together while visiting conferences in Naples and Beijing and for spending the time as well as travelling in China.

I would also like thank Mrs. Dina Hassouna for her help in various situation as well as sharing a pleasant time together and especially for bringing sunshine.

I would like to thank Mrs. Claudia Eckelskemper for her help in administration and the technicians Ms. Simone Miljanovic, Ms. Waltraud Schlag, Mrs. Katja Friedrich, Ms. Maryam Masrouri, Ms. Simone Mönninghoff-Pützer, Ms. Eva Müller, Ms. Linda Wiegand, and Ms. Heike Goldbach-Gecke for their support and their encouragement regarding my work

I would like to express my deep thanks to my colleagues and friends Ms. Anna-Lene Kiffe-Delf, Dr. Amin Mokhlesi, Ms. Arta Kuci, Dr. Catalina Perez Hemphill, Ms. Chenyin Wang, Mr. Dieter Meier, Ms. Dina Elkashef. Mr.Feng Pan, Mr. Mr. Haiqian Yu, Prof. Han Xiao, Mr. Harwoko, Dr. Huiqin Chen, Ms. Imke Form, Ms. Julia Werner, Mr. Lasse van Geelen, Mr. Lei Wang, Mr. Lin Wang, Ms. Mariam Moussa, Ms. Miada Sakr, Ms. Mi-Yong Chung, Ms. Nada Mohamed, Ms. Nihal Aktas, Ms. Ni Putu Ariantari, Dr. Peter Eze, Dr. Rini Muharini, Dr. Rudiyansyah, Dr. Shuai Liu, Mr. Tino Seidemann, Mr. Viktor Simons, Mr. Steffen Schindler, Ms. Xiaoqin Yu, Ms. Ying Gao, Ms. Yvonne Gröner for their help and assistance, as well as the shared time together.

Last but not least, I would like to express my thanks to my parents, Thi Hoa and Tam Tran-Cong and my siblings, Danh and Son, for their continuous support in everything and encouragement for me to finish my PhD. I would like to thank my passed grandparents who shaped me in my childhood and for being patient with me. I would like to thank and give a special hug to my girlfriend Ms. Kim Thao Le, my beloved Hibo, for spending and enjoying the various stays in the institute as well as enduring our practical courses. She has put a lot of effort in backing me up and without my family and her help I would not be the person who I have been. Thank you for supporting me and for elevating my morale.